



## City Research Online

### City, University of London Institutional Repository

---

**Citation:** Ahmed Al-Ani, A. S. (1987). Dispersion of chemical and natural materials to produce composites with commercially useful properties.. (Unpublished Doctoral thesis, The City University)

This is the draft version of the paper.

This version of the publication may differ from the final published version.

---

**Permanent repository link:** <https://openaccess.city.ac.uk/id/eprint/34275/>

**Link to published version:**

**Copyright:** City Research Online aims to make research outputs of City, University of London available to a wider audience. Copyright and Moral Rights remain with the author(s) and/or copyright holders. URLs from City Research Online may be freely distributed and linked to.

**Reuse:** Copies of full items can be used for personal research or study, educational, or not-for-profit purposes without prior permission or charge. Provided that the authors, title and full bibliographic details are credited, a hyperlink and/or URL is given for the original metadata page and the content is not changed in any way.

---

---

---

City Research Online:

<http://openaccess.city.ac.uk/>

[publications@city.ac.uk](mailto:publications@city.ac.uk)

---

DISPERSION OF CHEMICAL AND  
NATURAL MATERIALS TO PRODUCE  
COMPOSITES WITH COMMERCIALY  
USEFUL PROPERTIES

A thesis submitted for the degree of Doctor  
of Philosophy in the Faculty of Science,  
The City University, London.

by

AMAL SHEHAB AHMED AL-ANI

Department of Chemistry,  
The City University,  
Northampton Square,  
London EC1V 0HB

1987

## IMAGING SERVICES NORTH

Boston Spa, Wetherby

West Yorkshire, LS23 7BQ

[www.bl.uk](http://www.bl.uk)

**VOLUME CONTAINS  
CLEAR OVERLAYS**

**TO  
MY FATHER  
AND  
MOHAMED**

### Acknowledgements

First of all I would like to thank my supervisor, Professor J.D. Donaldson for his help, encouragement and guidance throughout the course of his work.

I wish to thank also Dr. S.J. Clark for his helpful advice and his useful discussion throughout the period of this work.

My grateful thanks are also due to Dr. A. Holding, Dr. S.M. Grimes and Dr. P.J. Baldry.

My special thanks go to Mr. A.H. Jones of the Civil Engineering Department for his help, and his expert advice with my work. I would also like to acknowledge the help I have received from all the technical staff in that department and especially Mr. A.B. Bonomini.

I should also like to convey my thanks for the help and support of friends, colleagues and the technical staff of the Chemistry Department.

I would also like to thank the Physics Department for their kind assistance in permitting me to use their X-ray facilities.

I would also like to mention [REDACTED] [REDACTED] to whom I am indebted for his excellent photographs featured in this thesis.

I would also like to thank [REDACTED] [REDACTED] for the excellent quality of the typing of this thesis.

I wish to thank also the IRAQI MINISTRY OF HIGHER EDUCATION AND SCIENTIFIC RESEARCH for the financial support they have given me.

Finally, I would like to express my gratitude to my family for their continuous encouragement and support throughout the years I have spent studying and to my husband [REDACTED] for his encouragement - without his help this thesis would not have reached its final stage.

## ABSTRACT

Polymer composites are manufactured for various purposes. Three aspects of dispersion of materials are studied in this work viz:

- (1) Dispersion of metals and semi-conducting material to obtain electrically conducting composites.
- (2) Dispersion of natural fibres in polymers, cement and ceramic to strengthen the product.
- (3) Dispersion of reagents in matrix to increase active shelf life.

Two types of polymer matrix were investigated in the conducting composite studies - thermoplastics (polyethene, polyvinyl chloride, polyvinyl acetate and polystyrene) and thermosetting polymers (phenolic resin - BAKELITE resin R-17620 and VARCUM 29-112). The conducting materials dispersed in the polymers included: antimony tin oxide, indium tin oxide, carbon black, tin (II) oxide, caesium tin tribromide and tin "suboxide". Attempts were also made to prepare new semiconducting oxide phases. The properties of the final composites are found to be improved by (1) the addition of coupling agents to improve the dispersant-polymer bonds and (2) by blending conducting oxides with inert white filler materials.

The tensile strength and Young's modulus data are obtained for composites of polymers, cement and ceramic when natural fibres are used as strengthening agents. The hair fibre used in this work was in the form of either chopped or powdered hair. It was found that (1) The tensile strengths of the composites increase with increasing the load of the fibre. (2) The Young's moduli of the composites increase with increasing the load of the fibre except that for cement when a decrease in the compressive strength occurs with increasing the load of the fibre. (3) The tensile strengths and the Young's moduli of the polymer composites can be improved by the addition of coupling agents.

It was also found that tin (II) sulphate dispersion in methane sulphonic acid and *p*-toluene sulphonic acid has a longer shelf life and is simpler to manufacture than tin (II) methane sulphonate or tin (II)*p*-toluene sulphonate.

## CONTENTS

	<u>PAGE</u>	
CHAPTER ONE	Introduction	1
CHAPTER TWO	Conductive materials dispersed in polymer systems	8
CHAPTER THREE	Mixed metal oxide semi-conductors	55
CHAPTER FOUR	Natural fibres reinforced thermo- plastics	101
CHAPTER FIVE	Natural fibres reinforced cement and ceramics materials	156
CHAPTER SIX	Tin (II) methane sulphonate, tin (II) $\rho$ -toluene sulphonate and dispersion of tin (II) sulphate in benzene sulphonic acid, $\rho$ - toluene sulphonic acid and methane sulphonic acid	187

## CONTENTS

<u>CHAPTER ONE: INTRODUCTION</u>	<u>PAGE</u>
1.1 Introduction	1
1.2 Range of Equipment Available	2
1.3 The Three Stages of the Dispersion Process	4
1.4 References	7

## CHAPTER ONE

### INTRODUCTION

#### 1.1 Introduction

The term dispersion is used here to refer to the complete process of incorporating a solid into a fluid medium such that the final product consists of fine particles distributed throughout the medium. This is an important process in a number of industries including adhesives, ceramics, chemicals, paint, paper, pharmaceuticals, pigments/dyestuffs, plastics, printing inks, rubber etc. although there are considerable differences in the nature and the technological requirements of the dispersions for each industry. Frequently the fluid dispersion itself is involved at an intermediate stage in a process. Thus a liquid paint or printing ink provides a means by which a thin film of a solid pigmented polymer may be deposited upon a substrate, the final product being the dry film or coating. In such cases, the degree of dispersion required is governed by the requirements of the end use. For example there should be no pigment aggregates or agglomerates sufficiently large to cause irregularities in the surface of a dried paint film and thus reduce the gloss or spoil some other needed surface characteristic, and the particles should be sufficiently well dispersed to attain the required

opacity. The dispersion stability must also be sufficient to give long storage stability without excessive settlement, and to enable the coloured pigments present in the mixture to maintain the desired colour of the surface coating.

In the pharmaceutical industry, uniformity of dispersion and long-term stability are required to attain accurate dose rates, and considerable attention has been paid to the degree of dispersion of pharmaceutical materials in relation to assimilation rates of drugs. In other industries such as ceramics and foodstuffs, dispersions may be used soon after production, so that long-term stability is not so important.

## 1.2 Range of Equipment Available

Within the last 15-20 years a number of new techniques have been developed, proved, modified and established. The types of equipment described below represent the four basic concepts of dispersion equipment design. Development in the equipment used for preparing dispersions have occurred within these four groups.

### 1. Low shear rate equipment:-

This category includes all equipment employing slow speed mixing at high viscosity or high solid concentration

and are considered in order of power requirement. The basic principle of operation of low shear rate equipment is to formulate the dispersion base to give the maximum resistance to the movement of the blades within the capabilities of the unit. The motor power is transmitted to the batch through blades which present a large working surface to the batch, and the energy so transmitted is used at high shear stress in the normally fairly cohesive mass at extremely low shear stress rates. In all cases the blades pass close to the walls of the container to ensure complete intermixing and to impart additional shear at this point.

## 2. High shear rate equipment:-

This type of equipment is typified by the use of impellers moving at high peripheral speeds. These generate high shear rates and high rates of interparticle shear by virtue of careful control of dispersion base rheology, or by the use of a variety of different shear rate control baffle arrangements.

## 3. Ball mills:-

This classification covers all types of equipment in which the energies transmitted are applied to the dispersion by use of free-moving members irrespective of size, shape or means of activation.

#### 4. Roll mills:-

The equipment in this category uses one or more rollers designed to carry the dispersion base under pressure between either two rollers or a roller and a blade at a closely controlled gap.

### 1.3 THE THREE STAGES OF THE DISPERSION PROCESS:

The dispersion process can be considered in terms of the following three stages:

(i) **WETTING OF THE POWDER:**

In the dry state the powder usually contains some aggregates of primary particles and these may be attached to other aggregates or primary particles forming agglomerates. It is necessary for the dispersing medium not only to wet the external surfaces but it must also displace air from the internal surfaces between the particles in the clusters.

(ii) **BREAKING UP THE CLUSTERS TO FORM COLLOIDAL PARTICLES:**

Aggregates may require considerable mechanical energy to break them down completely to the point when the surface of each primary particle is available to the wetting medium.

(iii) **FLOCCULATION OF THE DISPERSION:**

Conditions are established such that undesired flocculation of the dispersed particles is prevented or minimised. There are attractive forces between fine particles in an unstabilised dispersion which would normally lead to flocculation. Stabilisation occurs as a result of interactions occurring at the solid-liquid interface, (such as the adsorption of molecules or ions from solution) which modify the attractive potential between the particles by introducing a repulsive electric charge or by preventing the close approach of particles into the region of strong attractive forces by entropic repulsion. The work described in this thesis is concerned with the following aspects of dispersion.

- (1) Dispersion of conducting powders in polymers.
- (2) Dispersion of natural fibres in polymers.
- (3) Dispersion of natural fibres in cement and ceramics.
- (4) Dispersion of tin-containing reagents to increase the active life of the reagent.
- (5) The use of dispersing agents and aids to improve the properties of dispersions.

These topics are discussed at various stages in this thesis. This introductory chapter is followed by a chapter dealing with the dispersion of known conducting oxides and carbon black in a number of polymer systems. Then follows a chapter dealing with attempts that were made to produce cheaper alternative conducting oxide phases for dispersion in polymers. Chapters four and five deal with the dispersion of natural fibres in polymers and cement or ceramic materials respectively, while chapter six describes the work done on the dispersion of reagents. The thesis thus contains a description of research work designed to produce:

- (a) materials with antistatic properties
- (b) materials strengthened by natural fibres
- (c) dust-free reagents with increased shelf life

1-4 References

1. G.D. Parfitt, "Dispersion of powders in liquid", second edition, 1973.

## CONTENTS

<u>CHAPTER TWO:</u>	<u>Conductive materials dispersed in polymer systems</u>	PAGE
2.1	Introduction	9
2.2.	Band theory of a solid	10
2.3	Effect on conductivity of polymers by dispersing conducting materials	16
2.4	The application of conductive polymers	16
2.5	Experimental	17
2.5.1	Preparation of composites	17
2.5.2	Source of the conducting powders used in the preparation of the composites	24
2.5.3	The preparation of tin (II) oxide	25
2.5.4	The preparation of caesium tin tribromide	26
2.6	Electrical conductivity measurements	26
2.7	Optical density measurements	30
2.8	Results	30
2.8.1	Study of the effect of dispersing conducting powders on the electrical conductivity properties of polymers	30
2.8.2	Electrical conductivity measurements	31
2.8.3	Optical density measurements	46
2.9	Study of the effects of dispersing coupling agent additives on the electrical conductivity of the composites	46
2.10	Conclusion	53
2.11	References	54

## CHAPTER TWO

### Conductive materials dispersed in polymer systems

#### 2.1 Introduction<sup>1</sup>

The main aim of the work described in this chapter is to study the preparation and effectiveness of conducting composites that contain electrically conducting materials in essentially non-conducting polymer matrices.

Most polymers are insulating materials but conductive fillers can be added to them to transform them from electrical insulators to conductors. In the work described in this thesis two kinds of polymer matrices are considered: thermoplastics, (such as polyethene, polyvinyl chloride, polyvinyl acetate and polystyrene) and thermosetting polymers, [such as phenolic resin-BAKELITE resin R-17620 and phenolic resin-VARCUM 29-112].

A great deal of work has been carried out on the dispersion of metal powders and flakes to produce conducting polymers. The work described in this thesis is, however, concerned mainly with the addition of non-metallic conducting powders to the polymers. The powders used were the commercially available antimony tin oxide, indium tin oxide, carbon black and the compounds: tin (II) oxide, caesium tin tribromide, and tin "suboxide" all of which are known to have conducting properties. The results from these are compared with those from dispersed tin powder.

## 2.2 Band theory of a solid<sup>2,3,4,5,6</sup>

The band theory of a solid considers that electrons of isolated atoms occupy only specific orbitals or energy levels and that gaps exist between these levels. In effect, the electrons establish standing waves around an atom. This is also found in the inner or subvalence electrons of metals; however, the outer or valence electrons are delocalized. As a result the valence orbitals form a band, and the standing waves are influenced by every atom which is involved. A consequence of this fact is that a band possesses as many discrete energy levels as there are atoms in the system. In order to treat large numbers of electrons it is necessary to use Fermi-Dirac statistics, which take account of the discrete energy levels required by the quantum theory, and the Pauli principle which states that only two electrons may occupy the same orbital level [and these two must be of opposite spin].

Electrical conduction occurs by movement of electrons or holes within the bands of the crystal. The dependence of this conductivity on the band structure of a crystal gives rise to three classes of solids:

- (a) Conductors or metals, which have high electrical

conductivities of the order of  $10^4$ - $10^6$  ohm<sup>-1</sup> cm<sup>-1</sup> at room temperature and in which conductivity decreases with increasing temperature.

- (b) Insulators, which have low conductivities lying in the range of  $10^{-14}$  to  $10^{-22}$  ohm<sup>-1</sup> cm<sup>-1</sup> at room temperature.
- (c) Semiconductors - these have conductivities that are intermediate between those of metals and insulators and which increase with increasing temperature.

In conductors (Fig. 1a) there is either a partly filled valence band such as in sodium where the first valence band is only half-filled or a filled valence band overlapping an empty band. The latter case occurs for magnesium, which has two valence electrons per atom, which will fill the first valence band but in which this filled band overlaps the next band which is empty.

In silicon, the four valence electrons per atom completely fill the first two valence bands and there is an energy gap between this band and the next available empty band. Silicon, therefore, is not a metallic conductor ( $\rho_{Si} = 0.2 \times 10^6$  ohm cm). It behaves as a semiconductor because its energy gap is of such size that a few highly energized electrons are able to jump the gap and gain momentum in the

conduction band. If the band gap is such that some electrons have sufficient thermal energy ( $KT$ ) to cross it, then the crystal is an intrinsic semiconductor (Fig. 1b) The energy gap in silicon,  $E_g = 1.1 \text{ eV}$  is of the correct order to permit some electron promotion. At absolute zero all intrinsic semiconductors would behave as insulators. Examples of intrinsic semiconductors include B, Si, Ge, PbS, GaAs, InSb and  $\text{Fe}_3\text{O}_4$ .

In an insulator the large energy gap between the highest filled valence band and the lowest empty conduction band is such that the forbidden gap is inaccessible to thermal electrons (Fig. 1c) e.g. diamond,  $E_g = 5.4 \text{ eV}$ .

A number of insulators become semiconductors by introducing impurities into their lattices, they are then called extrinsic semiconductors. Examples of extrinsic semiconductors are doped Si, doped Ge, doped ZnO, doped  $\text{TiO}_2$  and doped  $\text{Mn}_3\text{O}_4$ .

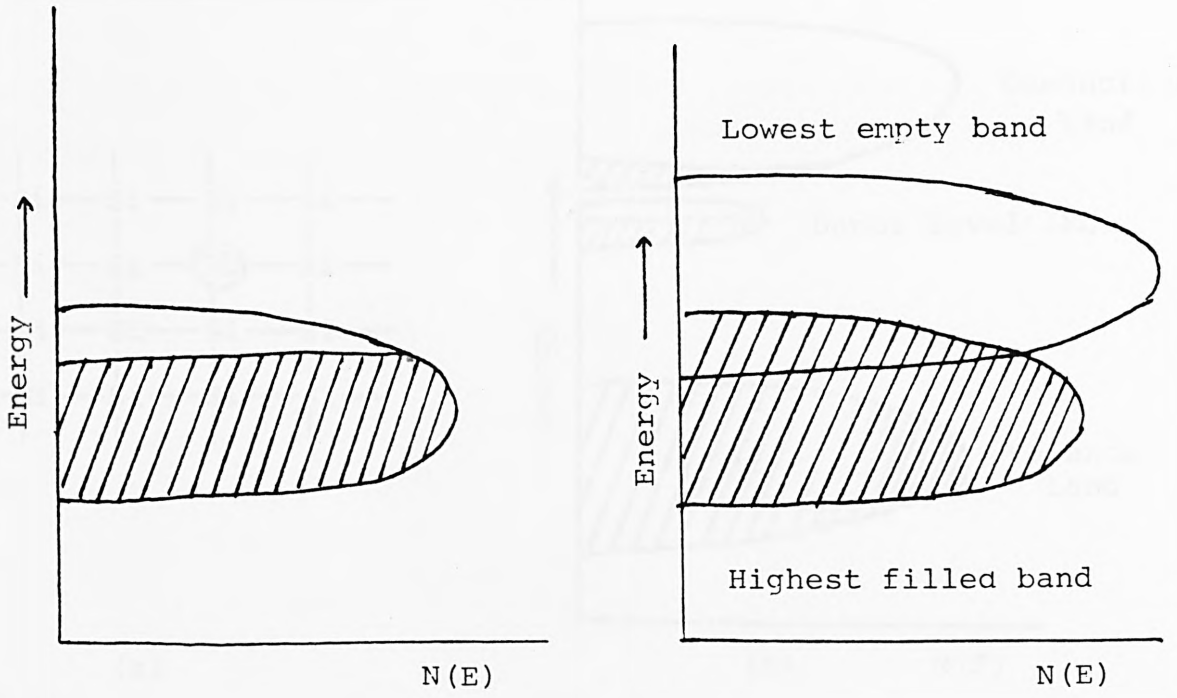
### N-type semiconductors

Impurities alter the semiconducting characteristics of materials by introducing excess electrons or excess electron holes. This can be illustrated by considering silicon containing an atom of antimony. Antimony has five valence electrons rather than the four found with Silicon

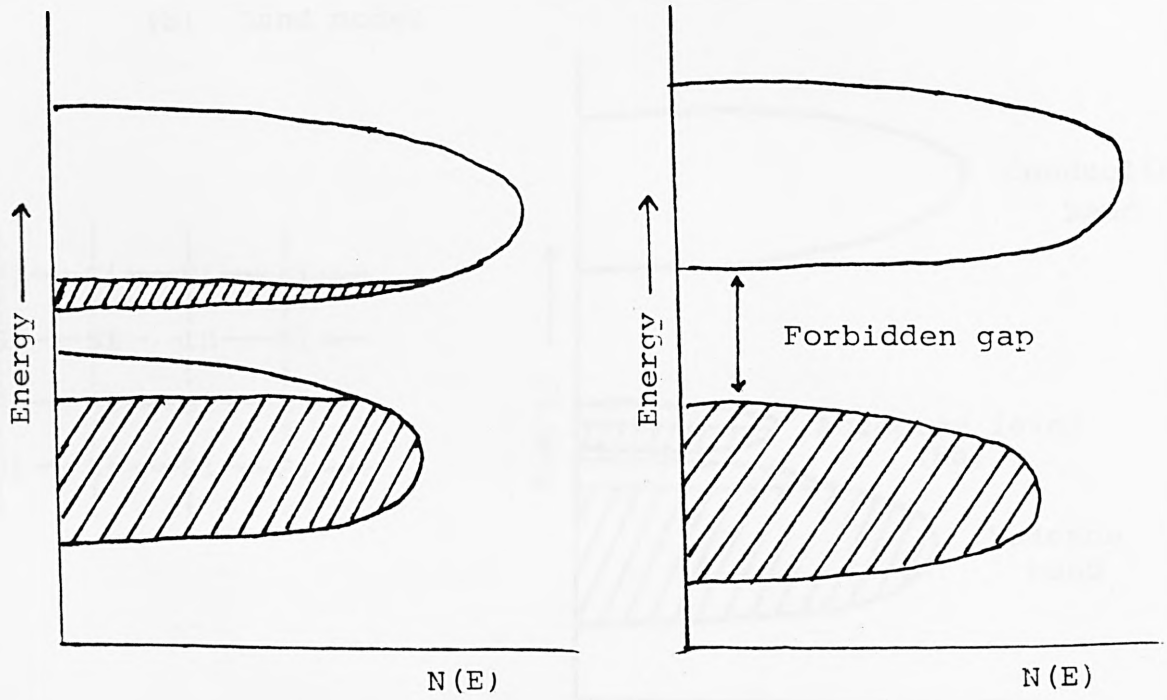
(Fig. 2 a). The extra electron is present independently of the electron pairs which serve as bonds between neighbouring atoms. The extra electron which cannot reside in the valence band because it is already full, is located near the top of the energy gap (Fig. 2 b). In this position it forms a donor level ( $E_d$ ) from which the extra electron can easily be activated into the conduction band. Group V [N, P, As and Sb] of the periodic table can supply negative or n-type charge carriers to semiconductors.

### P-type semiconductors

Group III elements (B, Al, Ga and In) have only three valence electrons. Therefore, when indium atom is added to silicon crystal as an impurity (Fig. 3 a) each indium atom can accept one electron. The indium atom therefore creates an acceptor level in the solid that can be populated from the valence band. The band model (Fig. 3 b) shows that the energy difference for electrons from the valence band to the acceptor level, ( $E_a$ ), is much less than the full energy gap. The electron holes remaining in the valence band are available as positive carriers for p-type semiconduction.



(a)



(b)

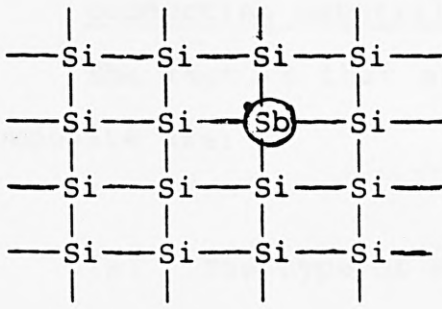
(c)

Fig. (1) Energy band diagrams

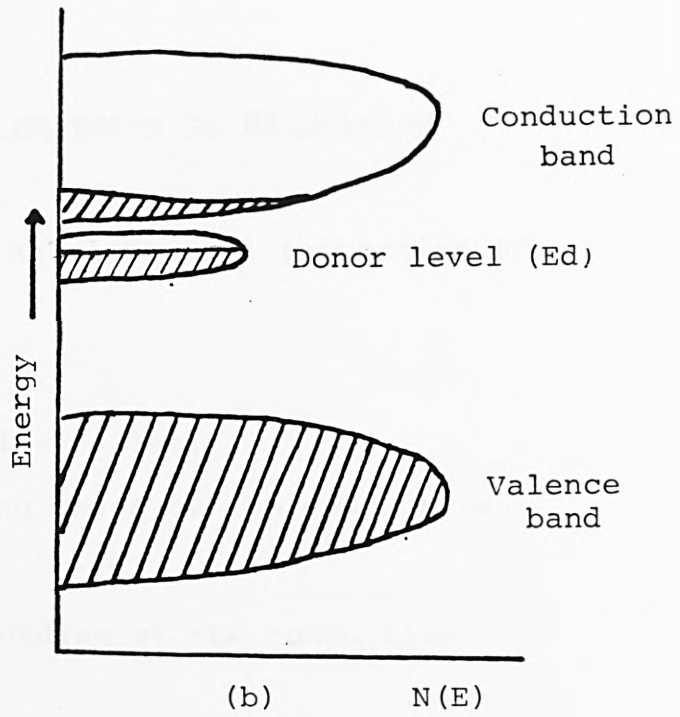
(a) Conductor

(b) Intrinsic semiconductor

(c) Insulator



(a)

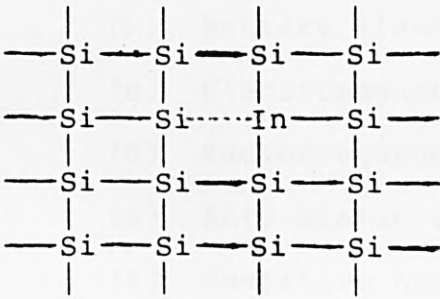


(b)

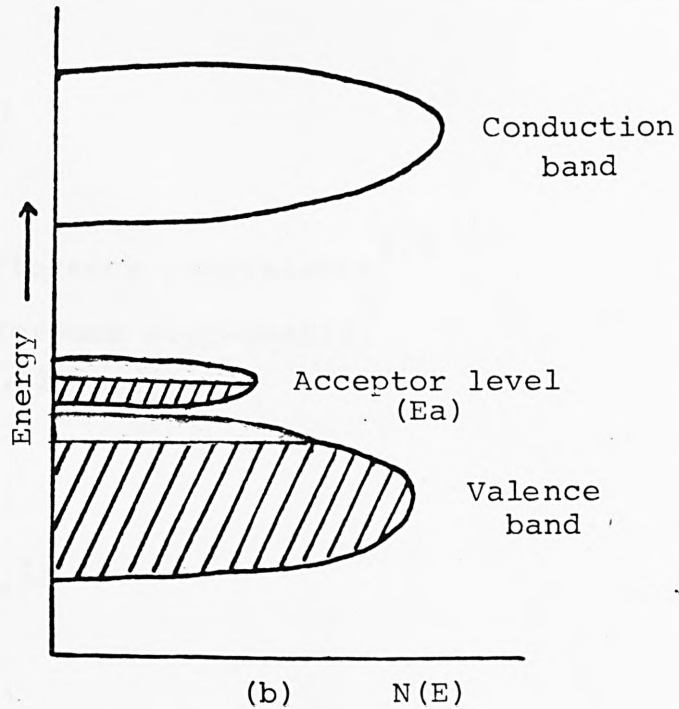
Fig. ( 2 ) Extrinsic semiconductors (n-type)

(a) An n-type impurity

(b) Band model



(a)



(b)

Fig.( 3 ) Extrinsic semiconductors (p-type)

(a) A p-type impurity

(b) Band model

### 2.3 Effect on conductivity of polymers by dispersing conducting materials

The factors that affect the electrical properties of a composite are:-

- (a) The type of conductive filler.
- (b) The particle size and shape of the conductive filler.
- (c) The concentration loading of the conductive filler.

### 2.4 The application of conductive polymers

The possible application of conductive polymers include:-

- (a) Conductive adhesives.<sup>7</sup>
- (b) Battery electrodes.
- (c) Electromagnetic interference suppressors.<sup>8,9</sup>
- (d) Radiofrequency interference suppressors.<sup>9</sup>
- (e) Anti-static fibres.<sup>10,11</sup>
- (f) Resistive heating.<sup>12</sup>
- (g) Thermal dissipation.<sup>12</sup>
- (h) Liquid crystal optics.<sup>13</sup>
- (i) Electrophotographics.

## 2.5 Experimental

### 2.5.1 Preparation of Composites:

Composites of the commercially available powders such as antimony tin oxide, indium tin oxide, tin "suboxide", carbon black and tin powder, and the laboratory-prepared conducting powders such as tin(II)oxide and caesium tin tribromide with the selected polymer systems such as polyethene, polyvinyl chloride, polystyrene, polyvinyl acetate and phenolic resin systems were prepared by the following method:

#### (a) Polyethene systems

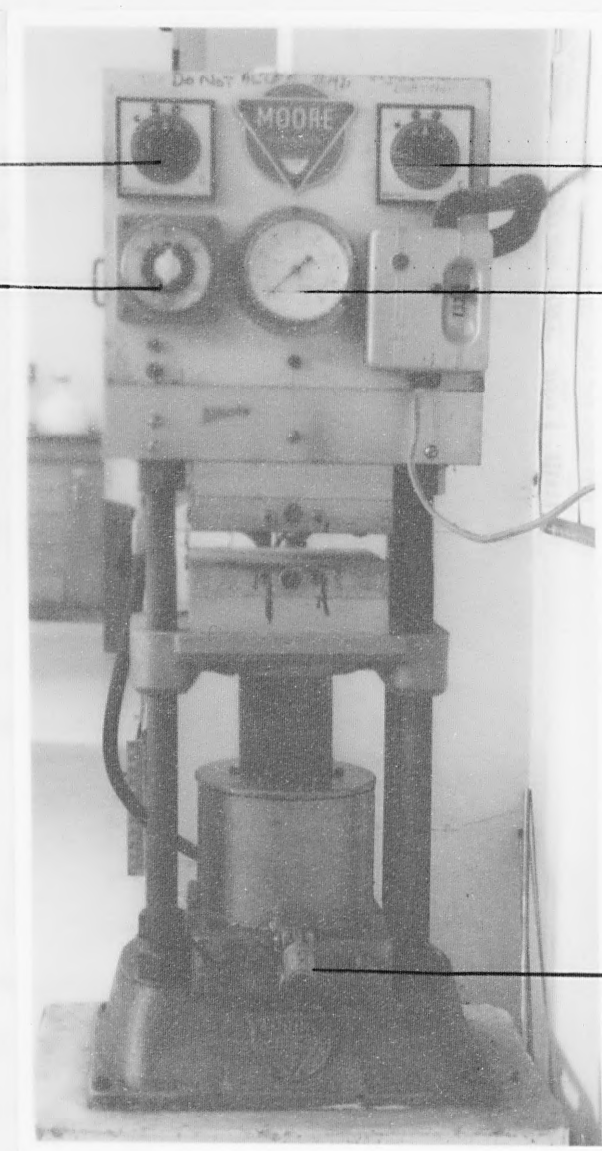
A range of samples of low density polyethene- [MW<200,000] based composite materials were prepared. A mixture of the appropriate weight ratio of polyethene and conducting powder was ball-milled for one hour with approximately 50 ml of propan-2-ol to achieve a homogeneous mix. The alcohol was then allowed to evaporate and composite samples were prepared by pressing the mixture between clean glass plates in a heated hydraulic press (Fig. 4) at temperatures between 130°C and 180°C. As the fraction of conducting powder was increased the polymer was found to become less flexible until at over 80% conducting powder it

Temp. meter for  
top plate (C°)

Time meter (min)

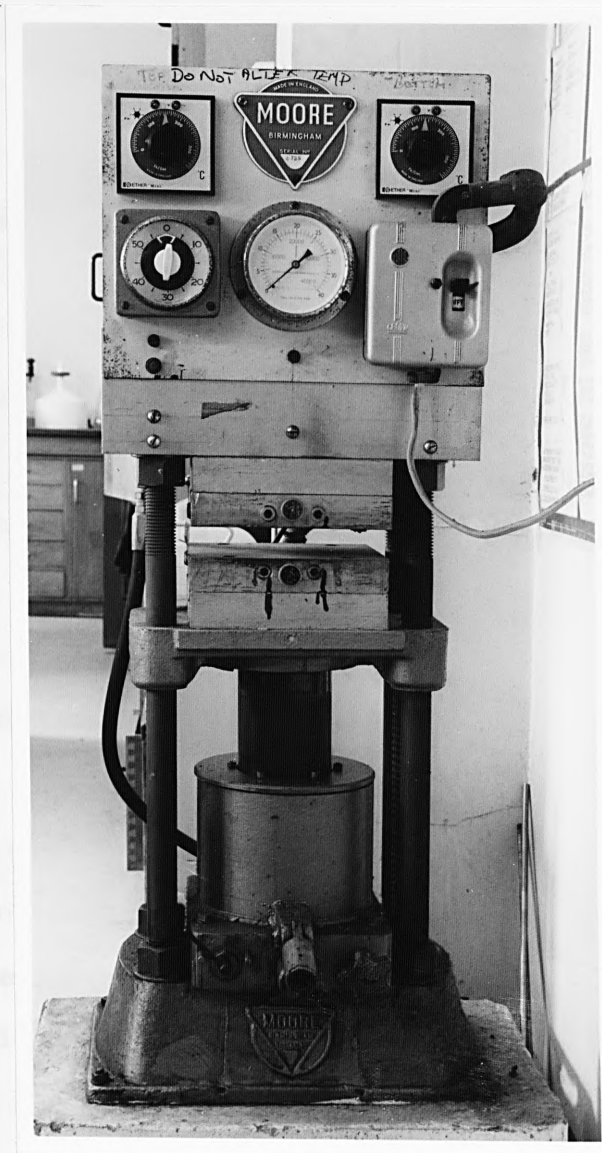
Temp. meter for  
bottom plate (C°)

Compression meter  
(tonnes)



Handle

Figure (4) Heated hydraulic press



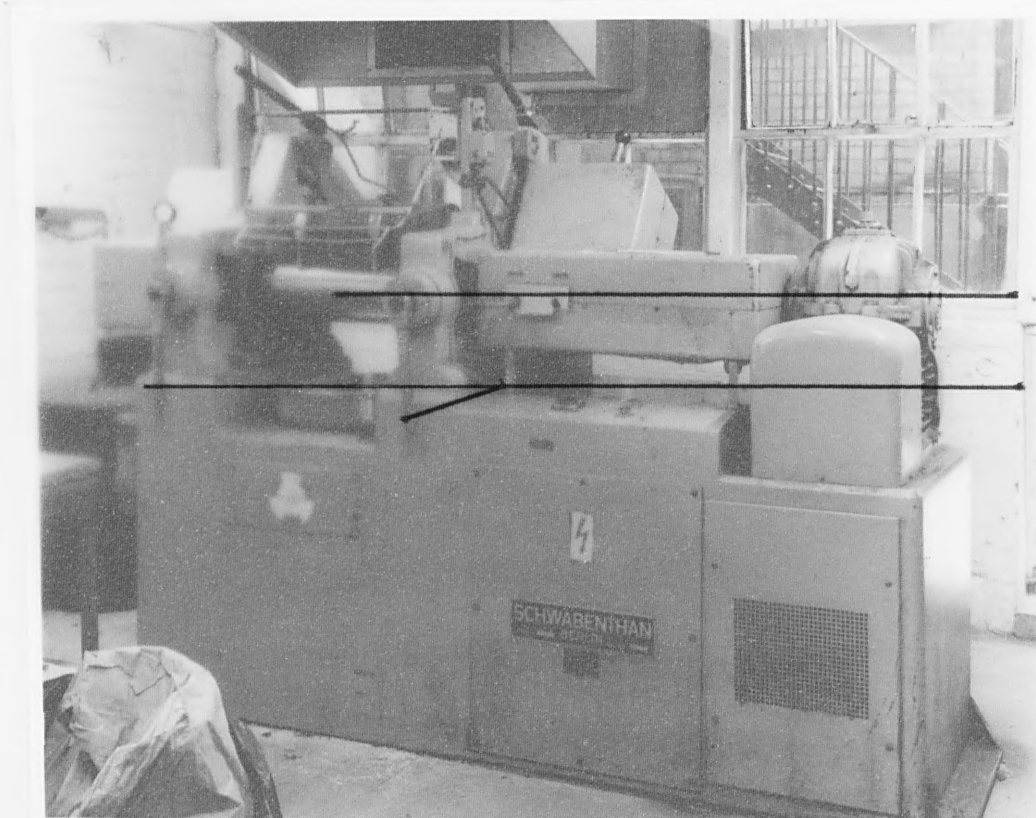
proved impossible to form the composite.

Attempts were made to prepare thin films of polyethene conducting powder composite by dipping or spraying techniques but these are unsuccessful because of shrinkage and surface fracture of the film on drying.

(b) Polyvinyl chloride systems:

Sheets of (PVC) were made using an electrically heated two-roll mill Fig.(5). In order to form good, crack-free sheets of PVC, it was necessary to add the plasticiser di-iso-octyl-phthalate and a stabilizer (basic lead carbonate).

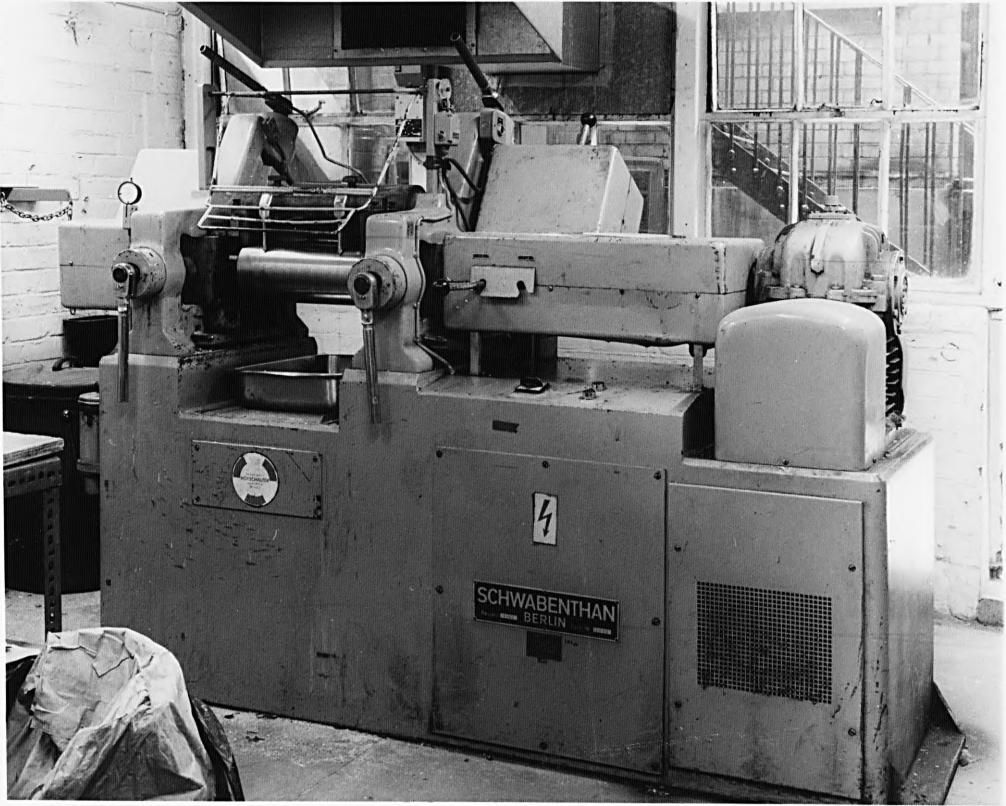
The mixture of PVC and 20-40 per hundred resin (phr) plasticiser and 1-2 (phr) of stabilizer were mixed with the oxide and then blended on the two-roll mill. The front and rear rollers of the mill were set at 110°C and 115°C respectively and the mixture was milled until a homogeneous crepe was formed. This crepe was then removed from the mill and sandwiched between two "Milinex" sheets and placed in a stainless steel mould of dimensions 0.3 x 15.2 x 15.2 cm. The mould was then placed in a press Fig(6) and heated to 140°C for one minute at ambient pressure before being pressed at  $5.5 \times 10^6$  Pa for a further two minutes. The mould was then removed and placed in a fly press Fig.(7) to keep the polymer flat as it cooled.



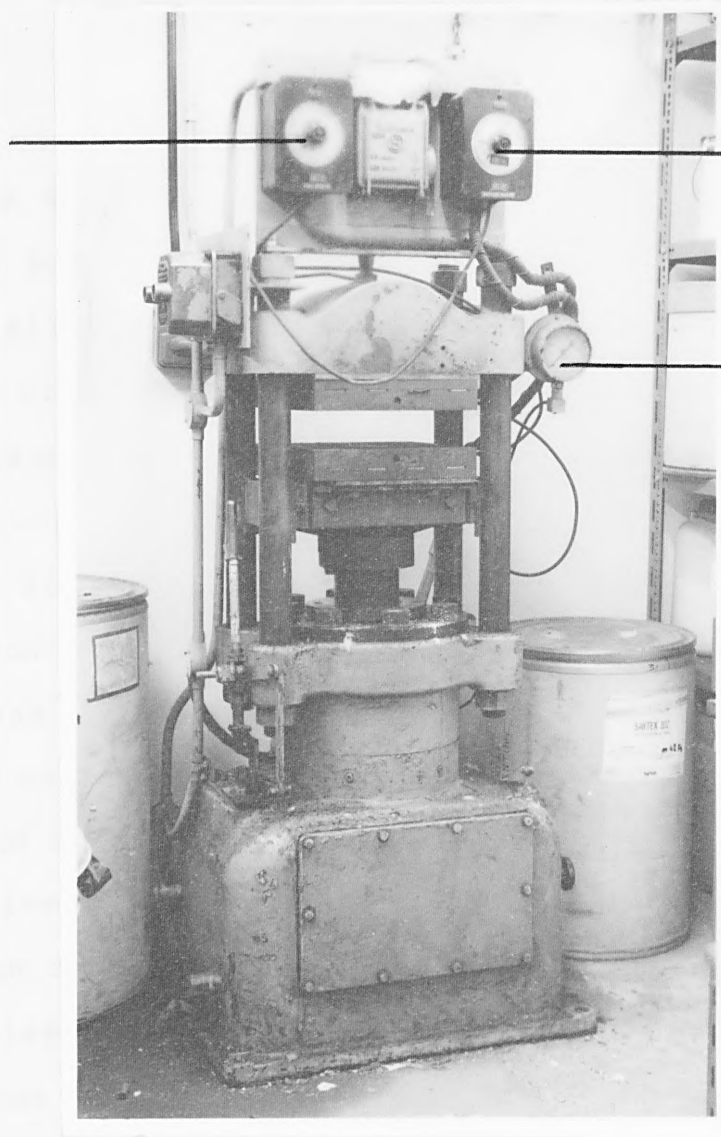
Rollers

Handles

Figure (5) Two-roll mill



Temp. meter  
for top plate  
(C°)



Temp. meter for  
bottom plate (C°)

Compression meter

Figure (6) Heated press

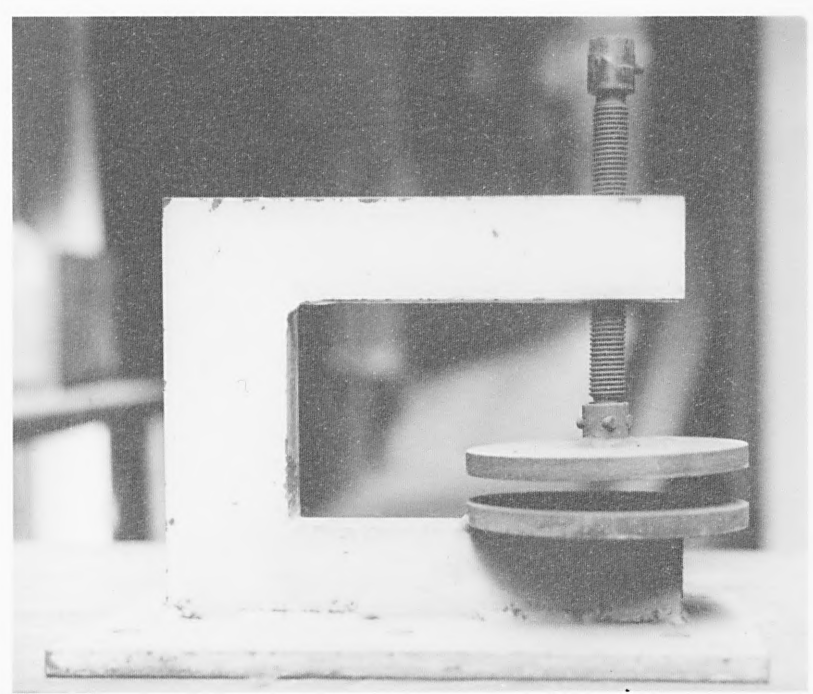
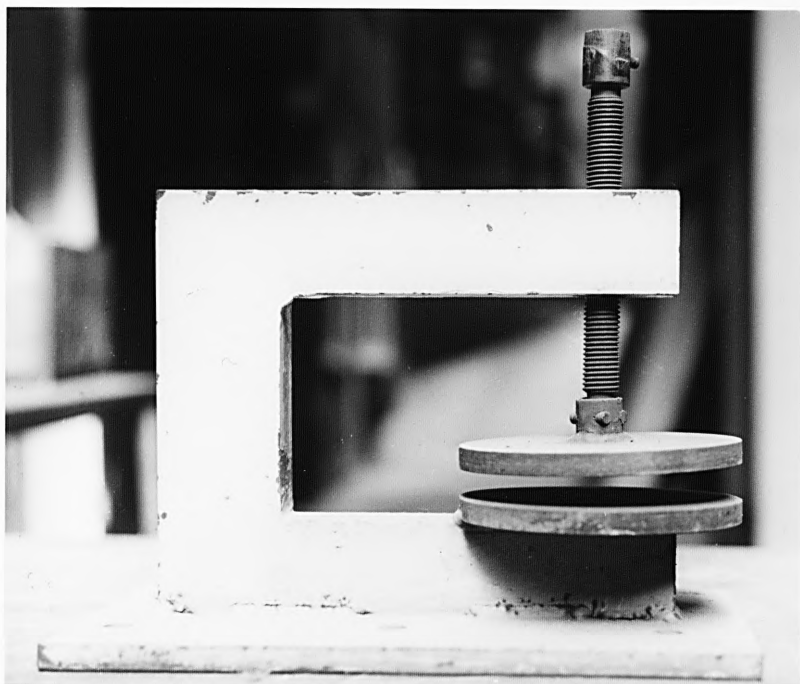
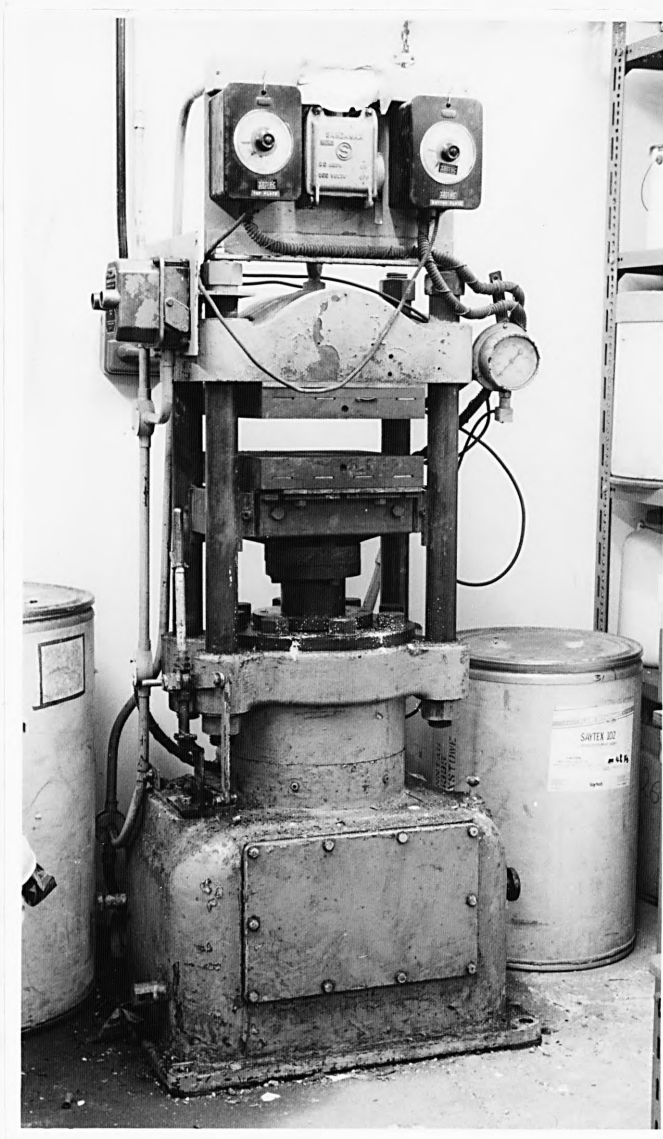


Figure (7) Fly press



As well as measurements made on PVC sheets, films of PVC were successfully made by the spraying and dipping method. All spraying was carried out using a commercially available glass spray chosen for its resistance to chemical attack and ease of cleaning. In order to obtain even films which showed no streaking, it was necessary to use highly volatile solvents. The best solvent for PVC film preparation was found to be tetrahydrofuran (THF). The polymer was dissolved in an appropriate solvent and a known weight of conducting powder added along with 1-2% wt of the basic lead carbonate to prevent scorching. The mixture was then ball-milled for one hour to produce a homogeneous suspension of the conducting powder in the polymer solution. To minimise any settling out of the conducting powder, the mixture was sprayed as soon as possible after milling.

Since the films were easily removed from their substrates it was possible to check their composition by burning off the polymer in air in a thermo-balance. The results obtained were in good agreement with the weight fraction of the conducting powder used.

(c) Polystyrene and Polyvinyl acetate systems:

As attempts to prepare polystyrene and PVA films by pressing using a heated hydraulic press proved unsuccessful,

they were prepared by the dip method. The polymer was dissolved in benzene then ball milled for one hour with an appropriate weight of conducting powder. The composite films were then made by dipping microscope slides in these mixtures, and allowing the solvent to evaporate from the slides.

(d) Phenolic Resin systems:

Composites were prepared with the thermosetting polymers B.P. "BAKELITE" Resin R.17620 and VARCUM 29-112. Early experiments carried out using spray deposition gave poor results and so the dip method was used to produce composite phenolic resin films.

The resins chosen were selected for their high solubility in most solvents and their low stoving temperatures. After some trial preparations, methanol and butan-2-ol were found to be the best solvents for BAKELITE and VARCUM respectively. The resin was dissolved in a suitable solvent, ball-milled for one hour with an appropriate weight of the conducting powder. Clean glass slides were then dipped into the suspension and withdrawn evenly. The solvent was allowed to evaporate and the slides hung in the oven to stove under the following conditions:

Polymer	Solvent	Stoving	
		Time	Temp
BAKELITE Resin R.17620	Methanol	30-40 min	160°C
VARCUM 29-112	Butan-2-OL	60 min	65°C

After stoving the previously blue-grey film became much clearer and green in colour. Since the resins are yellow and the conducting powder is blue, this must be due to the inclusion of conducting powder particles within the resin layer and is therefore a sign of an even distribution of the conducting powder.

#### 2.5.2 Source of the conducting powders used in the preparation of the composites

The conducting powders used in this work are:

1. Commercial conducting powders such as:
  - Antimony tin oxide KW175 supplied by Keeling and Walker.
  - Antimony tin oxide KW375 supplied by Keeling and Walker.

- Antimony tin oxides TA/5/1, TA/5/3 and TA/5 supplied by Keeling and Walker
- Tin "suboxide" KW3 supplied by Keeling and Walker
- Tin powder
- Carbon black supplied by Twin Star Chemicals Ltd.
- Indium tin oxide supplied by Keeling and Walker

2. Laboratory-prepared conducting powders such as:

- Tin(II) oxide ( $\text{SnO}$ )
- Caesium tin tribromide ( $\text{CsSnBr}_3$ )

### 2.5.3 The preparation of tin(II) oxide

Blue-black tin(II) oxide was prepared as follows:

60 gram of "Analar" copper sulphate ( $\text{CuSO}_4$ ) and 400 ml 2N  $\text{H}_2\text{SO}_4$  refluxed with excess of granulated tin (about 70g). The solution was boiled under oxygen-free nitrogen. The copper in the solution was replaced by tin and the solution eventually became colourless and the deposit of copper turned grey, due to the re-deposition of tin on its surface. The re-deposition of tin is a better indication of the completeness of the reaction than is the disappearance of the colour of the cupric ion. At this point the solution was filtered rapidly under oxygen-free nitrogen. To the filtrate, 40% NaOH was added (about 150 ml) until the phenylphthalein indicator present turned pink. The solution was then boiled until the tin(II) oxide crystallised out. The

blue-black product of tin(II) oxide was then filtered and washed with acetone and oven dried at 100°C.

#### 2.5.4 The preparation of-caesium tin tribromide

Caesium tin tribromide was prepared from solutions containing the stoichiometric proportions of the caesium bromide and tin(II) bromide in the minimum amount of water and 50:50 HBr(48%) respectively. The black product was then crystallised out by heating the mixture under an atmosphere of nitrogen. When not in use, the sample was stored in vacuo over potassium hydroxide pellets.

#### 2.6 Electrical conductivity measurements<sup>14</sup>

The electrical conductivity of a particular sample was obtained from the relationship:

$$\sigma_s = \frac{It}{VA}$$

where:

t = thickness of the sample in centimeters  
determined using a micrometer screw gauge

I = provided the current in amperes

V = the potential drop in volts

A = the area of contacts in cm<sup>2</sup>

$\sigma_s$  = electrical conductivity of the sample ( $\text{ohm}^{-1}\text{cm}^{-1}$ )

V = IR Ohm's Law

Then:

$$\sigma_s = \frac{t}{R_s A}$$

where:

$R_s$  = the resistance of the sample (Ohm)

To measure the bulk electrical conductivity of the composites prepared in this work, samples of  $1.5 \text{ cm}^2$  were taken. To ensure a good electrical contact, a small amount of silver conducting paint was placed on each face of the sample taking care to ensure there was no contact between the two layers of silver. The sample was then inserted into the sample holder, (Fig. 8), and the copper electrodes held on to the sample contacts by a spring assembly. The sample holder was then attached to a Keithley Model 616 electrometer using coaxial cable.

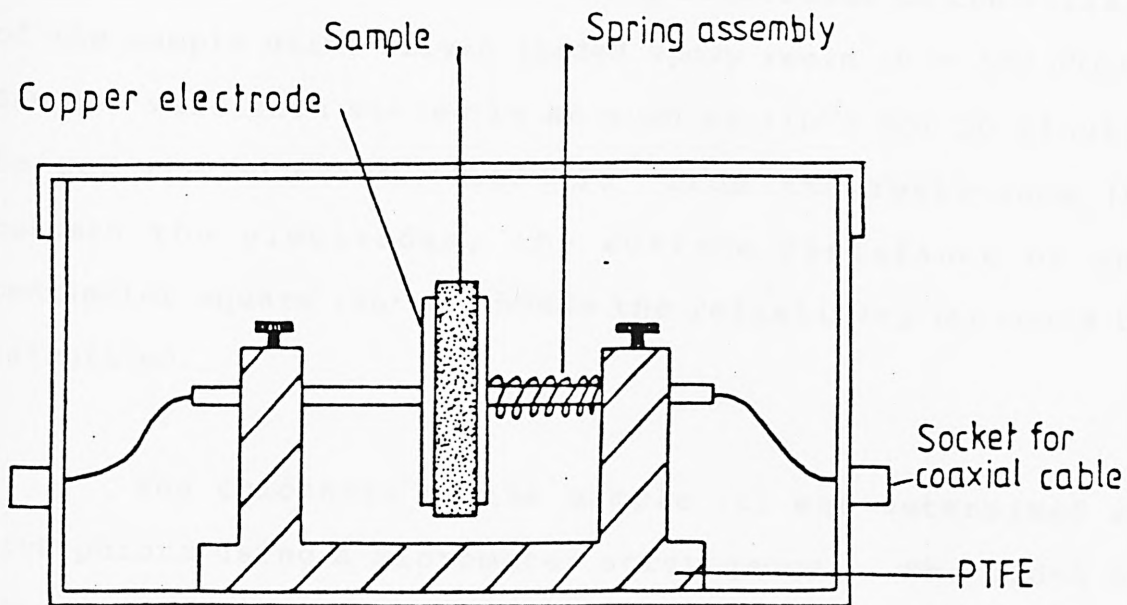


Fig. (8) Sample holder used for electrical conductivity measurements.

This study was extended to measure the surface conductivity of the composites prepared in this work. Samples of a microscope slide size were taken. The electrical properties of the sample were measured by attaching two copper or brass strip electrodes on the surface of the sample using silver loaded epoxy resin ( $\rho = 500 \mu\Omega \text{cm}$ ). Samples were then stoved in an oven at  $110^\circ\text{C}$  for 30 minutes to set the adhesive, (Fig. 9 ). From the resistance (R) between the electrodes, the surface resistance of one centimeter square ( $R_o$ ) and hence the resistivity ( $\rho$ ) could be calculated.

The thickness of the sample (t) was determined at five points using a micrometer screw gauge. The width of the sample ( $\omega$ ) and the electrode separation ( $\ell$ ) were determined using a vernier.

For the thin film:

$$\begin{aligned}
 \text{By definition: } R_o &= \frac{\rho}{t} \\
 \sigma &= \frac{\ell}{AR} = \frac{1}{\rho} \\
 \therefore R_o &= \frac{AR}{\ell t} \\
 \therefore A &= \omega t \\
 \therefore R_o &= \frac{\omega R}{\ell}
 \end{aligned}$$

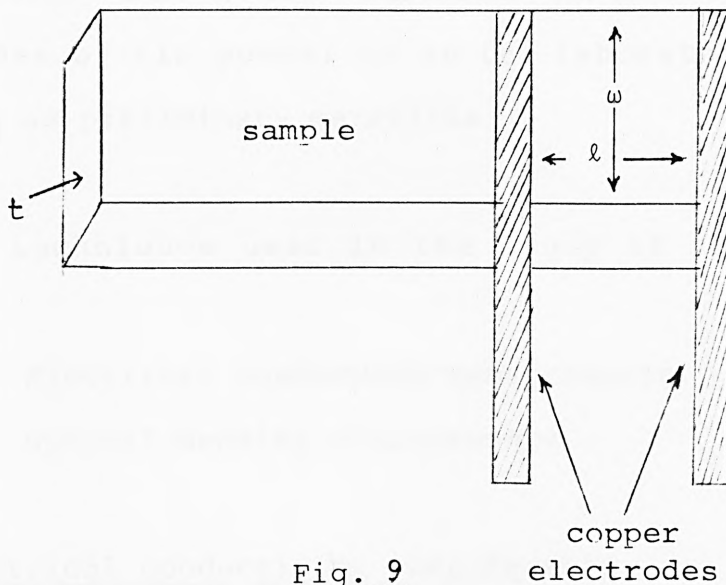


Fig. 9

## 2.7 Optical density measurements

The light transmission of the films was measured on an EEL densitometer using an uncoated glass slide as a reference.

## 2.8 Results

### 2.8.1 Study of the effect of dispersing conducting powders on the electrical conductivity properties of polymers

This section deals with the results obtained from the comprehensive study of the electrical conductivity properties of a number of polymer systems such as PVC, PE, PVA, polystyrene and phenolic resins, with (a) commercial

conducting powders such as antimony tin oxide (KW), indium tin oxide, carbon black, tin "suboxide" (KW<sub>3</sub>) and commercial reagent grades of tin powder or as (b) laboratory prepared SnO, CsSnBr<sub>3</sub> as preliminary materials.

The techniques used in the study of the mixtures were:-

Electrical conductivity measurements.

Optical density measurements .

### 2.8.2 Electrical conductivity measurements

The electrical conductivities of the composites was measured using the method described in Section 2.6.

#### Polyethene system

The results from electrical conductivity analysis of polyethene composites are shown in Tables 1 and 2. (Figs. 10, 11 and 12, show the electrical conductivities obtained from polyethene sheets plotted against % wt oxide at 130°C, 150°C and 180°C respectively.

An electrical conductivity of  $10^{-2}$  ohm<sup>-1</sup> cm<sup>-1</sup> was achieved with 70-80% wt of antimony tin oxide KW175 and of  $10^{-4}$  ohm<sup>-1</sup> cm<sup>-1</sup> was achieved with 60% of antimony tin oxide KW375 and of  $10^{-3}$  ohm<sup>-1</sup> cm<sup>-1</sup> with 70% wt of indium tin oxide

Table I

poly- ethylene gram	KW175 gram	press- ing time min	press tempera- ture C <sup>o</sup>	R ohm	$\sigma$ ohm <sup>-1</sup> cm <sup>-1</sup>	-log $\sigma$
50	50	10	130	$3.3 \times 10^3$	$2.5 \times 10^{-5}$	4.6
50	50	10	150	$7.85 \times 10^2$	$9 \times 10^{-5}$	4.05
50	50	3	180	$1.3 \times 10^3$	$2 \times 10^{-5}$	4.7
45	55	10	150	$4.16 \times 10^2$	$13 \times 10^{-5}$	3.9
40	60	30	130	$2 \times 10^2$	$4 \times 10^{-4}$	3.4
40	60	10	150	$10^2$	$7.5 \times 10^{-4}$	3.1
40	60	3	180	$10^2$	$6 \times 10^{-4}$	3.2
35	65	30	150	16	$3.6 \times 10^{-3}$	2.4
30	70	30	130	8	$10^{-2}$	2
30	70	30	140	17	$5.1 \times 10^{-3}$	2.3
30	70	30	150	6	$1.7 \times 10^{-2}$	1.77
30	70	30	160	14	$6.2 \times 10^{-3}$	2.2
30	70	15	170	15	$3.6 \times 10^{-3}$	2.4
30	70	10	180	9	$5 \times 10^{-3}$	2.30
25	75	20	150	5	$14.5 \times 10^{-3}$	1.8
20	80	70	130	2.2	$3 \times 10^{-2}$	1.5
20	80	50	150	1	$9.9 \times 10^{-2}$	1
20	80	15	180	2.1	$4 \times 10^{-2}$	1.4
15	85		150	it doesn't work		

Table 2

poly-ethylene gram	indium-tin oxide[90:10] gram	KW375 gram	pressing time min.	press temperature C <sup>o</sup>	R ohm	$\sigma$ ohm <sup>-1</sup> cm <sup>-1</sup>
50	-	50	10	150	$3.3 \times 10^4$	$1.6 \times 10^{-6}$
40	-	60	10	150	$2.8 \times 10^2$	$1.6 \times 10^{-4}$
45	55	-	15	150	$1.7 \times 10^5$	$2 \times 10^{-7}$
30	70	-	15	150	13	$3 \times 10^{-3}$

Table 3

pvc gram	KW375 gram	% oxide	R ohm	$\sigma$ ohm <sup>-1</sup> cm <sup>-1</sup>	-log $\sigma$
30	70	49.3	$10^{11}$	$1.6 \times 10^{-13}$	12.8
30	75	51	$4.5 \times 10^{11}$	$4 \times 10^{-13}$	12.4
30	80	52.6	$1.05 \times 10^9$	$1.8 \times 10^{-10}$	9.7
15	50	58.14	$1.75 \times 10^{10}$	$10^{-11}$	11
10	55	63.95	$3.3 \times 10^7$	$4 \times 10^{-9}$	8.4
10	65	67.7	$3.05 \times 10^6$	$5 \times 10^{-8}$	7.3
10	70	69.3	$9.4 \times 10^5$	$1.8 \times 10^{-7}$	6.7

Fig.10

-log conductivity v. composition of polyethene/  
KW 175 phases at 130°C

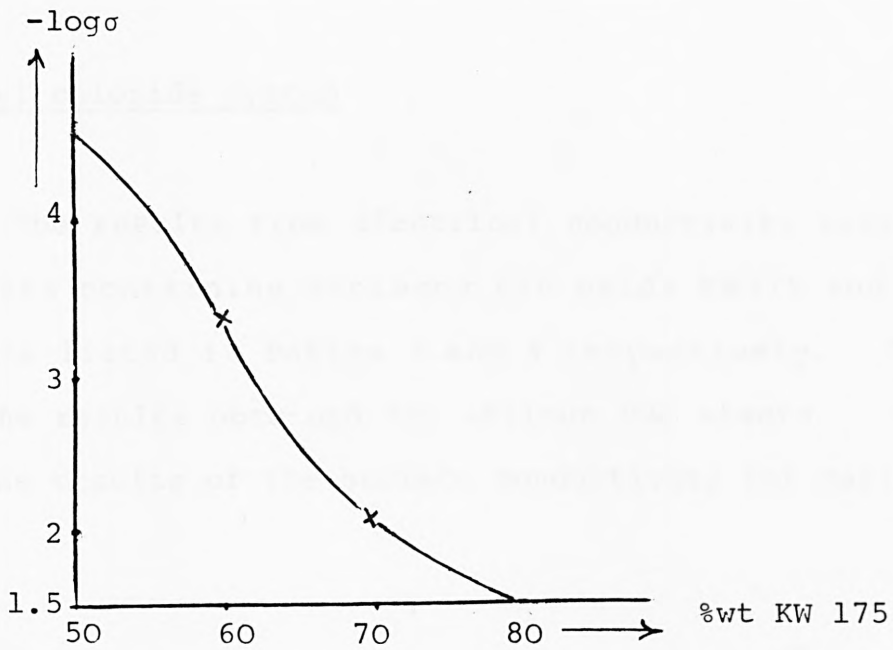
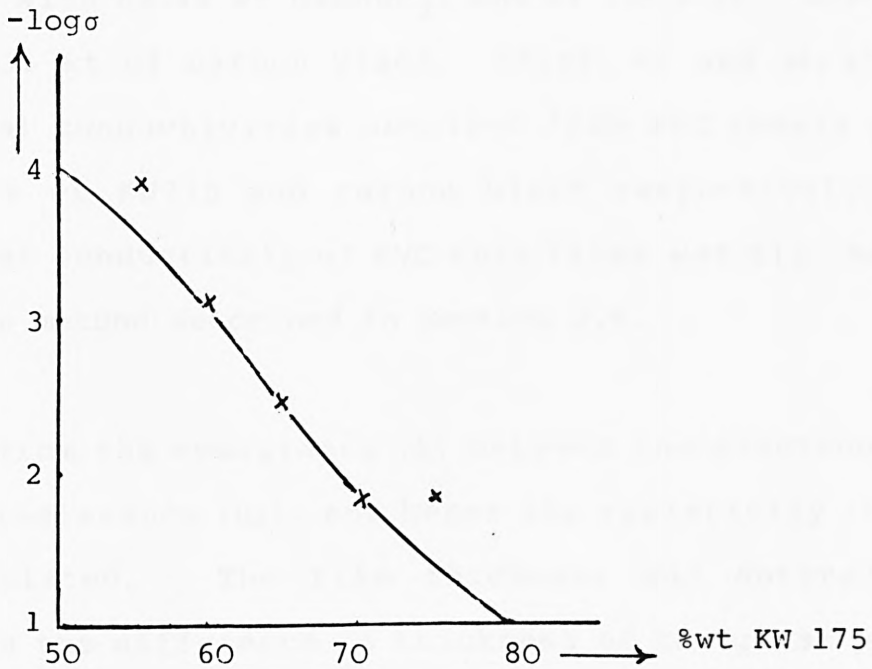


Fig.11

-log conductivity v. composition of polyethene/  
KW 175 phases at 150°C



(90:10).

### Polyvinyl chloride system

The results from electrical conductivity analysis of PVC sheets containing antimony tin oxide KW375 and carbon black are listed in Tables 3 and 4 respectively. Table 5 lists the results obtained for various PVC sheets. Table 6 lists the results of the surface conductivity for various PVC sheets.

An electrical conductivity of  $1.8 \times 10^{-7} \text{ ohm}^{-1} \text{ cm}^{-1}$  was achieved with 69.3% wt of antimony tin oxide KW375 and of  $4.5 \times 10^{-9} \text{ ohm}^{-1} \text{ cm}^{-1}$  with 60% wt of antimony tin oxide KW175. Electrical conductivity of  $6.8 \times 10^{-9} \text{ ohm}^{-1} \text{ cm}^{-1}$  was achieved with 64.4% wt  $\text{CsSnBr}_3$ , and of  $7.9 \times 10^{-7} \text{ ohm}^{-1} \text{ cm}^{-1}$  with 32.3% wt of carbon black. (Figs. 13 and 14) show the electrical conductivities obtained from PVC sheets plotted against % wt KW375 and carbon black respectively. The electrical conductivity of PVC thin films was also measured using the method described in Section 2.6.

From the resistance (R) between the electrodes, the surface resistance ( $R_0$ ), and hence the resistivity ( $\rho$ ) could be calculated. The film thickness was determined by measuring the difference in thickness of the glass plate at five points before and after coating. Table 7 shows the

Fig.12 -log conductivity v. composition of polyethene/  
KW 175 phases at 180°C

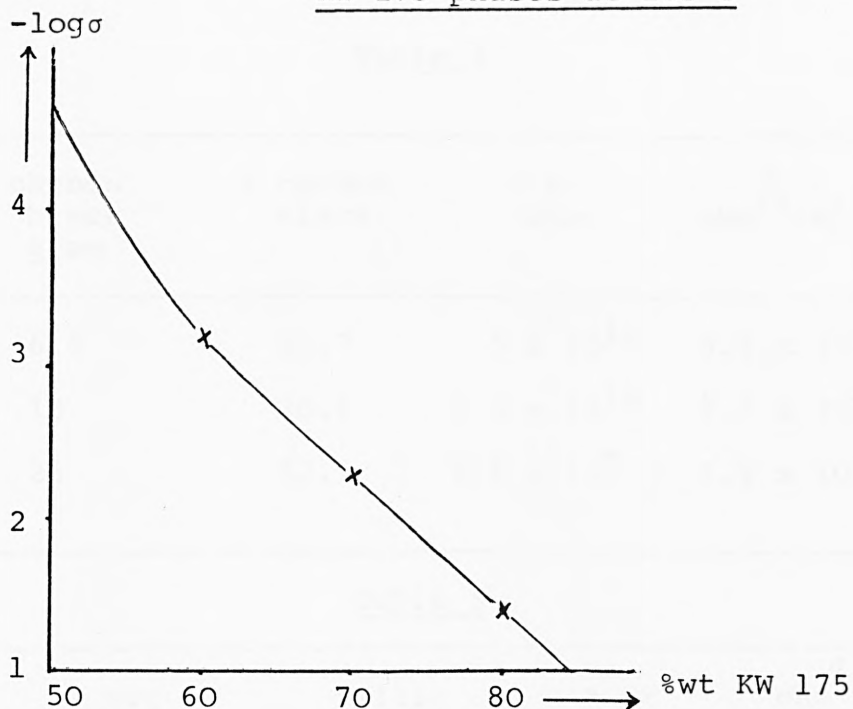


Fig.13 -log conductivity v. composition of PVC/KW 375

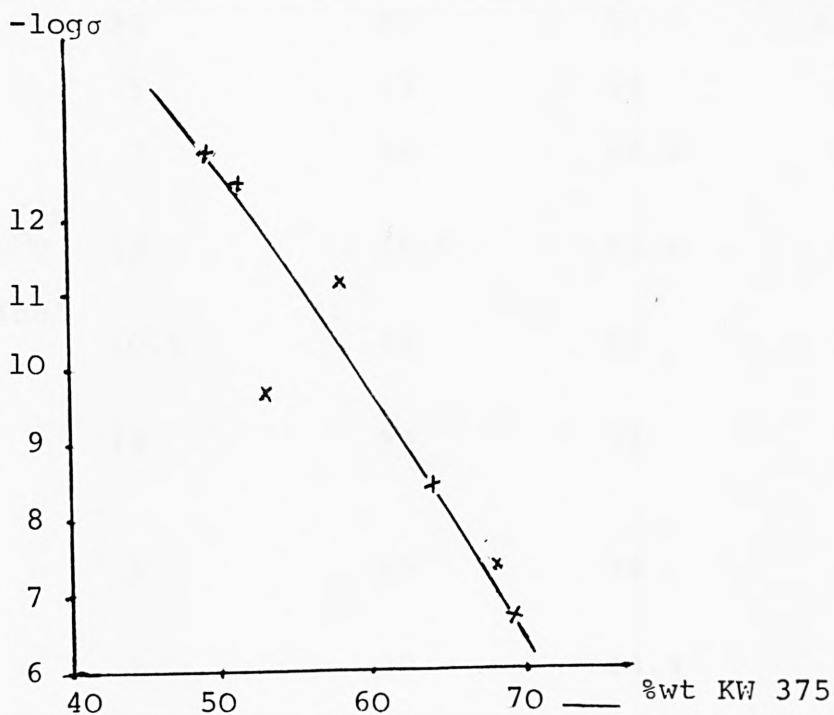


Table 4

pvc gram	carbon black gram	% carbon black	R ohm	$\sigma$ $\text{ohm}^{-1}\text{cm}^{-1}$	$-\log \sigma$
34	6.5	10.7	$5 \times 10^{11}$	$5.5 \times 10^{-13}$	12.3
34	13	20.8	$9.3 \times 10^{10}$	$2.2 \times 10^{-12}$	11.7
34	26	32.3	$2.6 \times 10^5$	$7.9 \times 10^{-7}$	6.1

Table 5

filler	pvc gram	filler gram	% wt filler	$\sigma$ $\text{ohm}^{-1}\text{cm}^{-1}$ $\times 10^{-10}$
KW175	28	60	60	45
TA/5/1	30	80	52.6	0.018
TA/5/3	30	80	52.6	0.26
TA/5	30	80	52.6	0.031
SnO	5	23	59	0.29
SnO	3	30	69.8	0.31
SnO heated for 1 hr at 500°C	10	66.5	69.6	0.18
tin"sub oxide" KW <sub>3</sub>	10.5	70	67	0.14
tin powder (commercial grade)	14	90	72	0.12
tin powder (reagent grade)	5	55	78	7.1
CsSnBr <sub>3</sub>	5	28	64.4	68

Table 6

filler	pvc gram	filler gram	% wt filler	surface conductivity $\text{ohm}^{-1} \text{cm}^{-1} \times 10^{-10}$
KW375	30	70	49.3	0.0125
	30	75	51	0.1
	30	80	52.6	7.5
	15	50	58.1	0.54
	10	55	64	34
	10	65	67.7	61
	10	70	69.3	82
KW175	28	60	60	29
TA/5/1	30	80	52.6	0.055
TA/5/3	30	80	52.6	19
TA/5	30	80	52.6	0.03
SnO	5	23	59	0.198
tin"sub oxide" KW <sub>3</sub>	10.5	70	67	0.09
tin powder (reagent grade)	5	55	78	2.35
CsSnBr <sub>3</sub>	5	28	64.4	11.2

Fig. 14 -log conductivity v. composition of PVC/  
carbon black phases

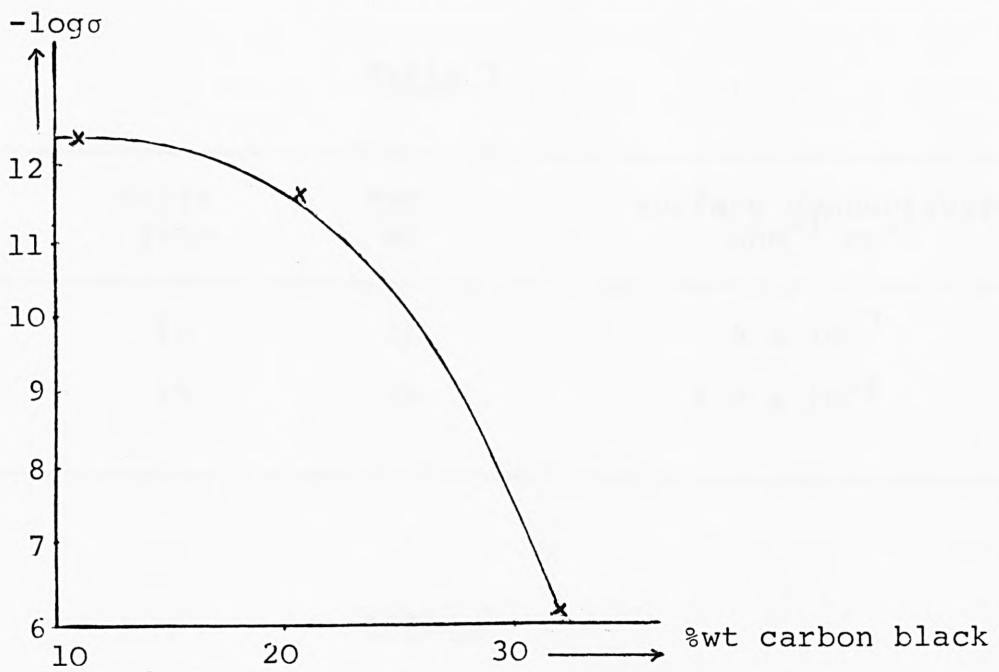


Fig. 15 -log conductivity v. composition of polystyrene/  
KW 375 phases

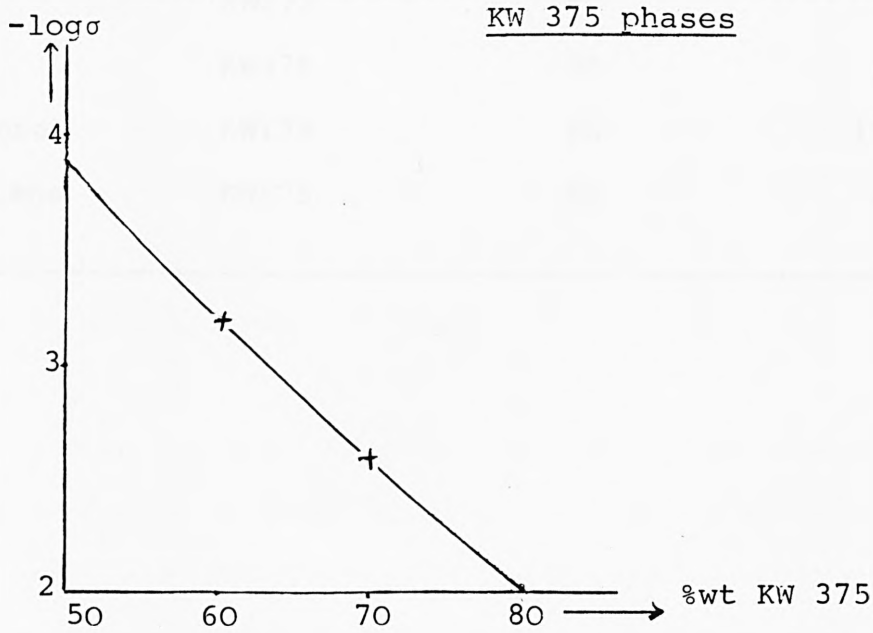


Table 7

PVC gram	KW175 gram	THF ml	surface conductivity $\text{ohm}^{-1} \text{cm}^{-1}$
10	10	50	$9 \times 10^{-7}$
10	15	50	$1.8 \times 10^{-6}$

Table 8

polymer	oxide	% oxide	optical density %
PVC	KW175	25	8.5
PVC	KW175	50	20
PVC	KW375	40	12
PVC	KW375	50	16
polyethylene	KW175	50	17.5
polystyrene	KW175	50	40

results obtained from the surface conductivity of PVC films containing antimony tin oxide KW175. A surface conductivity of  $1.8 \times 10^{-6} \text{ ohm}^{-1} \text{ cm}^{-1}$  was achieved with 60% wt KW175.

#### Polyvinyl acetate and polystyrene

The results from the electrical conductivity analysis of PVA and polystyrene thin films containing antimony tin oxide KW375 are listed in Tables 9 and 10 respectively. Electrical surface conductivities of  $10^{-2} \text{ ohm}^{-1} \text{ cm}^{-1}$  and  $10^{-3} \text{ ohm}^{-1} \text{ cm}^{-1}$  were achieved with 80% wt of KW375 for polystyrene and PVA respectively. (Figs. 15 and 16) show the electrical surface conductivity plotted against % wt of KW375 for polystyrene and PVA respectively.

#### Phenolic resins

The results from the electrical conductivity analysis of BP BAKELITE Resin R.17620 and VARCUM 29-112 thin films containing antimony tin oxides KW375 and KW175 are listed in Tables 11 and 12 respectively.

(Figs. 17 and 18) show the electrical conductivity of BAKELITE resin R.17620 plotted against % wt of KW175 and KW375 respectively. (Fig. 19) shows the electrical conductivity of VARCUM 29-112 plotted against % wt KW375.

Table 9

polystyrene gram	KW375 gram	% oxide	$\sigma$ $\text{ohm}^{-1}\text{cm}^{-1}$	$-\log \sigma$
10	10	50	$1.2 \times 10^{-4}$	3.92
10	15	60	$4.6 \times 10^{-4}$	3.2
10	24	70.6	$2.5 \times 10^{-3}$	2.6
10	40	80	$1.1 \times 10^{-2}$	1.96

Table 10

PVA gram	KW375 gram	% oxide	$\sigma$ $\text{ohm}^{-1}\text{cm}^{-1}$	$-\log \sigma$
10	10	50	$2.5 \times 10^{-6}$	5.6
10	15	60	$1.1 \times 10^{-4}$	3.96
10	24	70.6	$7 \times 10^{-4}$	3.15
10	40	80	$10^{-3}$	3.0

Fig. 16 -log conductivity v. composition PVA/KW 375 phases

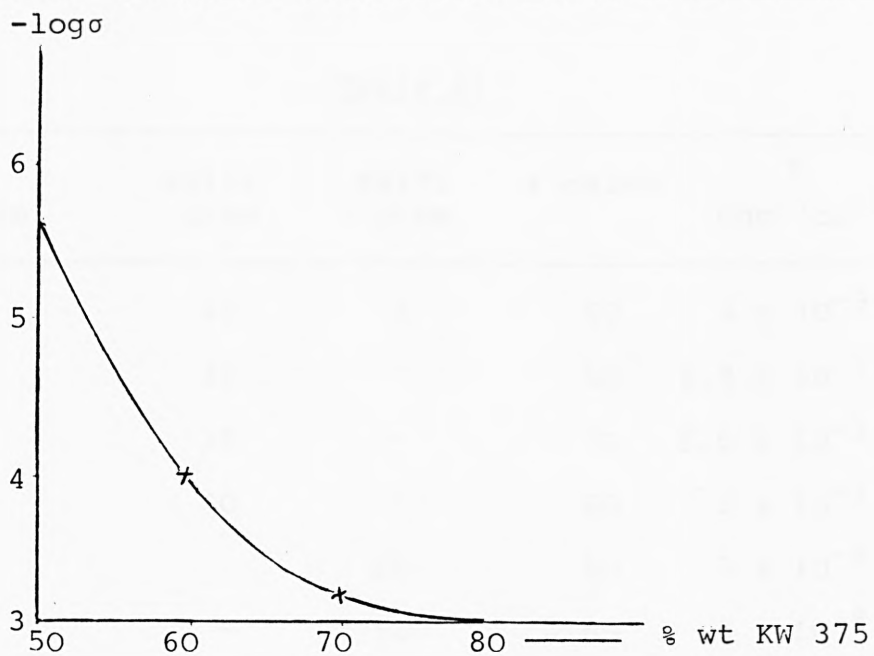


Fig. 17 -log conductivity v. composition BAKELITE  
R.17620/KW 175 phases

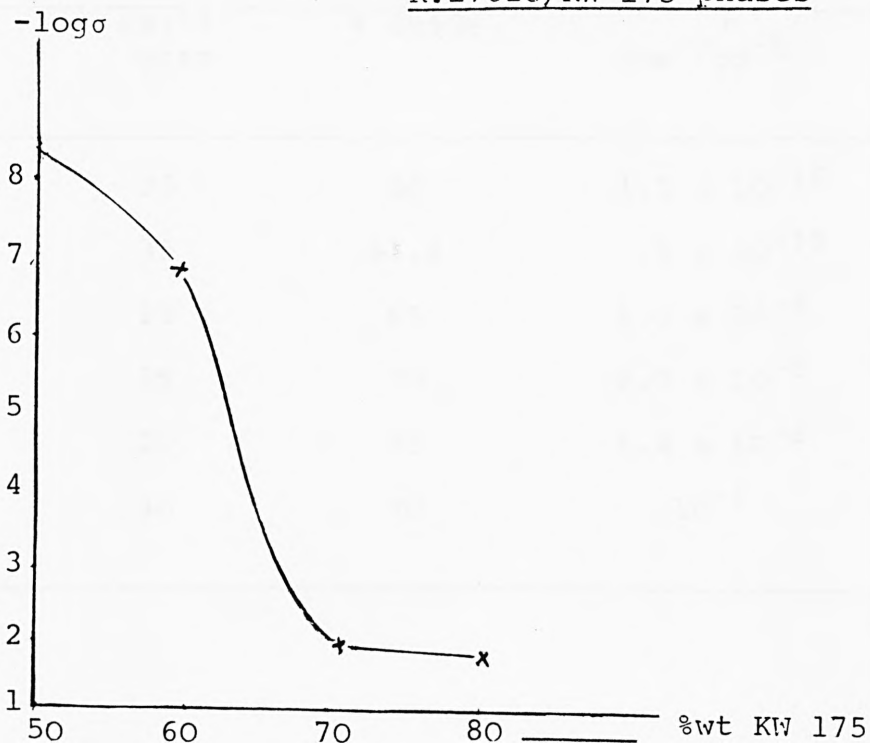


Table 11

BAKELITE R-17620 gram	KW175 gram	KW375 gram	% oxide	$\sigma$ ohm <sup>-1</sup> cm <sup>-1</sup>	-log $\sigma$
20	20	-	50	$4 \times 10^{-9}$	8.4
20	30	-	60	$1.4 \times 10^{-7}$	6.85
15	35	-	70	$8.6 \times 10^{-3}$	2.06
10	40	-	80	$2 \times 10^{-2}$	1.70
20	-	20	50	$3 \times 10^{-9}$	8.5
20	-	30	60	$3 \times 10^{-8}$	7.52
15	-	35	70	$1.7 \times 10^{-2}$	1.77
10	-	40	80	$4.5 \times 10^{-2}$	1.34

Table 12

VARCUM 29-112 gram	KW375 gram	% oxide	$\sigma$ ohm <sup>-1</sup> cm <sup>-1</sup>	-log $\sigma$
35	35	50	$1.5 \times 10^{-10}$	9.8
22	35	61.4	$5 \times 10^{-10}$	9.3
7	13	65	$1.7 \times 10^{-9}$	8.77
15	35	70	$2.7 \times 10^{-5}$	4.57
7	21	75	$1.4 \times 10^{-3}$	2.85
10	40	80	$10^{-1}$	1.0

Fig. 18  $-\log$  conductivity v. composition BAKELITE  
R.17620/KW 375 phases

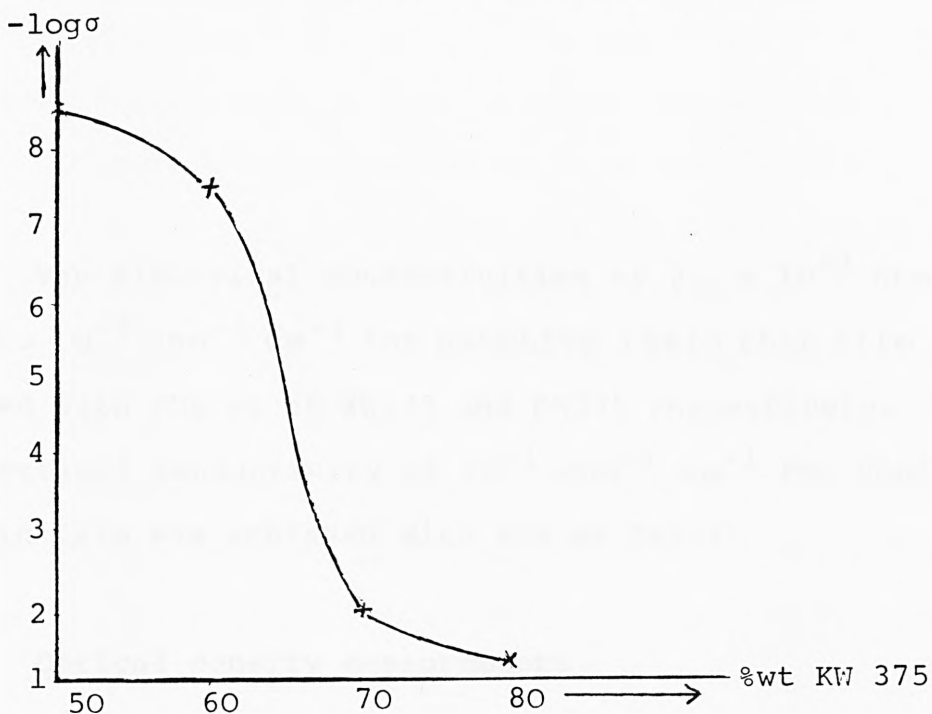
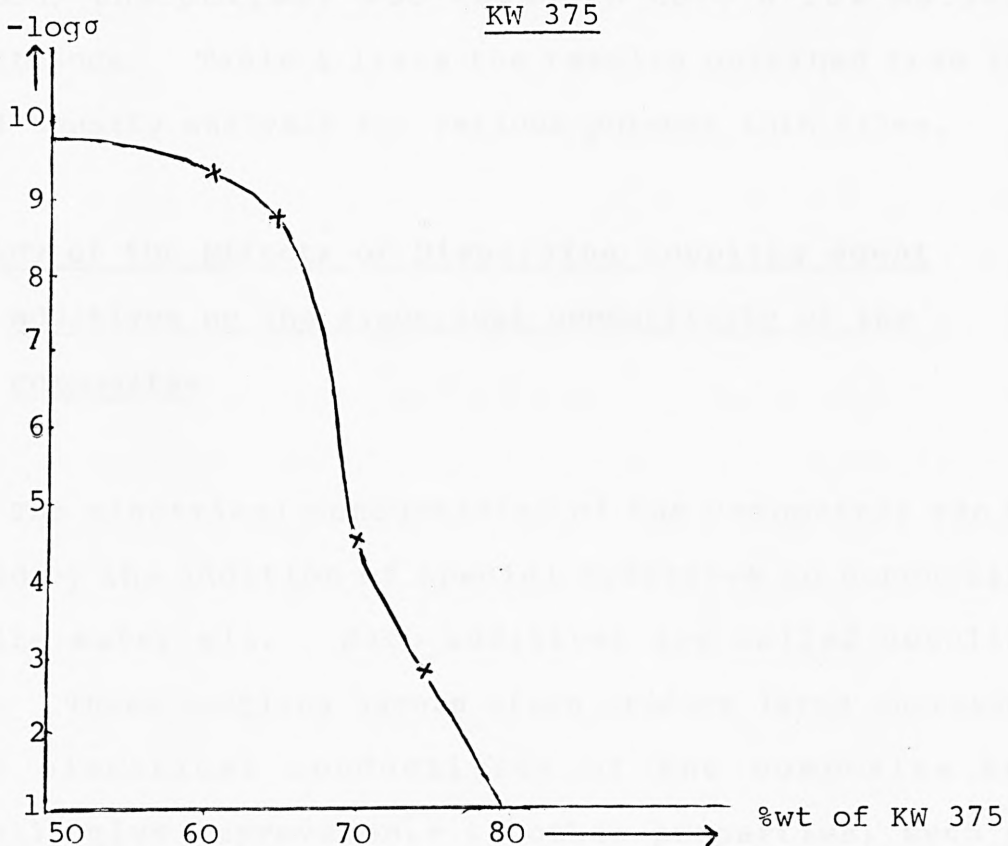


Fig. 19  $-\log$  conductivity v. composition VARCUM 29-112/  
KW 375



The electrical conductivities of  $2 \times 10^{-2} \text{ ohm}^{-1} \text{ cm}^{-1}$  and  $4.5 \times 10^{-2} \text{ ohm}^{-1} \text{ cm}^{-1}$  for BAKELITE resin thin film were achieved with 80% wt of KW175 and KW375 respectively. While an electrical conductivity of  $10^{-1} \text{ ohm}^{-1} \text{ cm}^{-1}$  for VARCUM 29-112 thin film was achieved with 80% wt KW375.

### 2.8.3 Optical density measurements

The optical density of polymer thin films considered in this work was measured using the method described in Section 2.7. As the fraction of the conducting powders was increased, the polymer was found to have a low optical transmittance. Table 8 lists the results obtained from the optical density analysis for various polymer thin films.

### 2.9 Study of the Effects of Dispersing coupling agent additives on the electrical conductivity of the composites

The electrical conductivity of the composites can be improved by the addition of special additives to conducting composite materials. Such additives are called coupling agents. These coupling agents often produce large increases in the electrical conductivity of the composite and frequently give improvements in other properties, such as

hydrophobicity, stability, flexibility and dispersion leading to improved performance. The coupling agents need only to be added in small quantities, often less than 1%, to provide the improvements and therefore are potentially able to provide superior materials with high cost advantages. The simplest coupling agents are the fatty acids (e.g. stearic acid) and some of their salts (e.g. sodium stearate) but other agents such as HALLCOMID products which are the unique series of N,N-Dimethyl Amides can also be used. It has been suggested that the coupling agents work by reacting with polymer surface protons at the inorganic interface with the formation of matrix compatible/reactive organic monomolecular layers on the inorganic surface.

In the present work, composites were prepared containing between 0 to 0.25 parts of coupling agent to 10 parts PVC and 55 parts KW 375 (64% KW 375). A maximum electrical conductivity of  $10^{-7}$  was obtained for a sample containing 0.03 parts of the coupling agent compared with  $10^{-9}$  for the same material without the coupling agent. The electrical conductivity of the composites was measured using the method described in (Section 2.6) and Tables (13) and (14) contain the results obtained for PVC/KW 375 with stearic acid and sodium stearate respectively. Figs. (20) and (21) show electrical conductivity plotted against weight of stearic acid and sodium stearate respectively. Measurements were carried out on samples of PVC/KW 375 which had been prepared

Table 13

PVC gram	KW 375 gram	stearic acid gram	R ohm	$\sigma$ $\text{ohm}^{-1}\text{cm}^{-1}$	$-\log \sigma$
10	55	-	$3.3 \times 10^7$	$4 \times 10^{-9}$	8.40
"	"	0.01	$9.1 \times 10^5$	$1.6 \times 10^{-7}$	6.79
"	"	0.02	$9.8 \times 10^5$	$1.6 \times 10^{-7}$	6.79
"	"	0.03	$6.7 \times 10^5$	$2.3 \times 10^{-7}$	6.64
"	"	0.04	$8 \times 10^5$	$2 \times 10^{-7}$	6.70
"	"	0.05	$9.1 \times 10^5$	$1.8 \times 10^{-7}$	6.74
"	"	0.1	$1.3 \times 10^6$	$1.3 \times 10^{-7}$	6.88
"	"	0.15	$2.1 \times 10^6$	$7.8 \times 10^{-8}$	7.11
"	"	0.2	$1.7 \times 10^6$	$8.7 \times 10^{-8}$	7.06

Table 14

PVC gram	KW 375 gram	sodium stearate gram	R ohm	$\sigma$ $\text{ohm}^{-1}\text{cm}^{-1}$	$-\log \sigma$
10	55	-	$3.3 \times 10^7$	$4 \times 10^{-9}$	8.40
"	"	0.01	$1.3 \times 10^6$	$1.3 \times 10^{-7}$	6.88
"	"	0.02	$1.1 \times 10^6$	$1.4 \times 10^{-7}$	6.85
"	"	0.03	$6 \times 10^5$	$2.5 \times 10^{-7}$	6.60
"	"	0.04	$8.4 \times 10^5$	$2 \times 10^{-7}$	6.70
"	"	0.05	$8 \times 10^5$	$1.8 \times 10^{-7}$	6.74
"	"	0.1	$9.7 \times 10^5$	$1.5 \times 10^{-7}$	6.82
"	"	0.15	$8.1 \times 10^5$	$1.6 \times 10^{-7}$	6.80
"	"	0.2	$1.2 \times 10^6$	$1.5 \times 10^{-7}$	6.82
"	"	0.25	$7.1 \times 10^5$	$2.2 \times 10^{-7}$	6.66
"	"	0.5	$8.5 \times 10^5$	$1.8 \times 10^{-7}$	6.74

Fig. 20  $-\log$  conductivity v. composition 64% KW 375/PVC/  
stearic acid phases

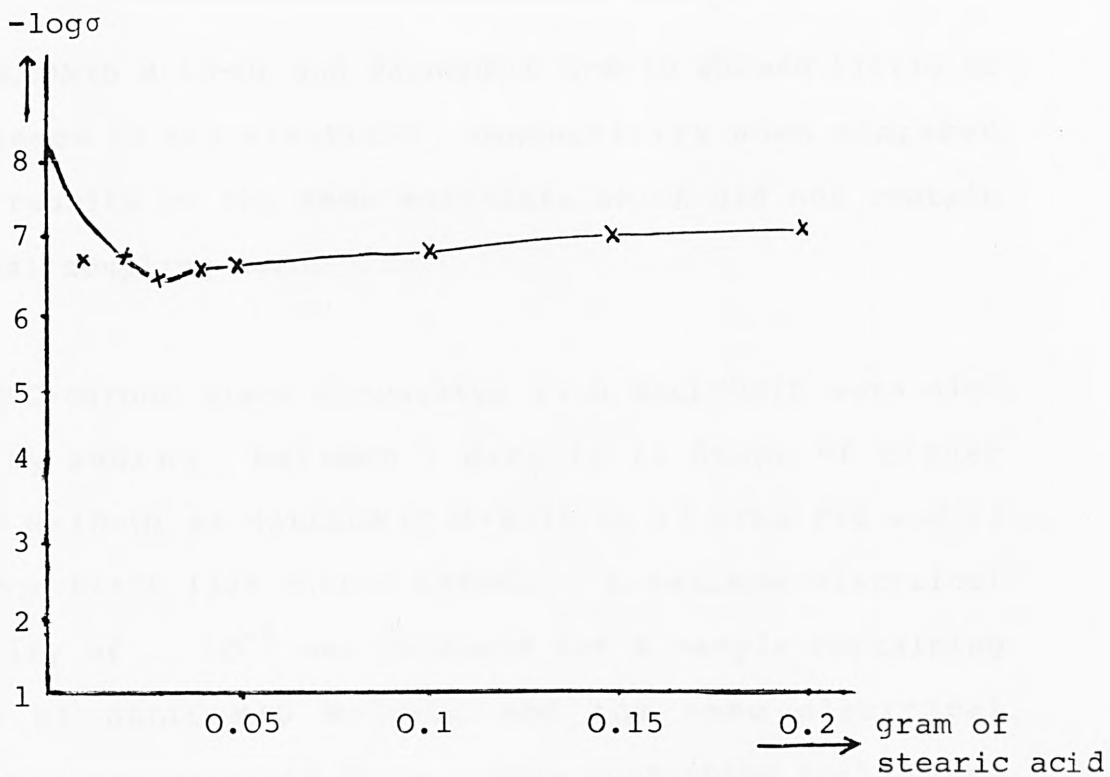
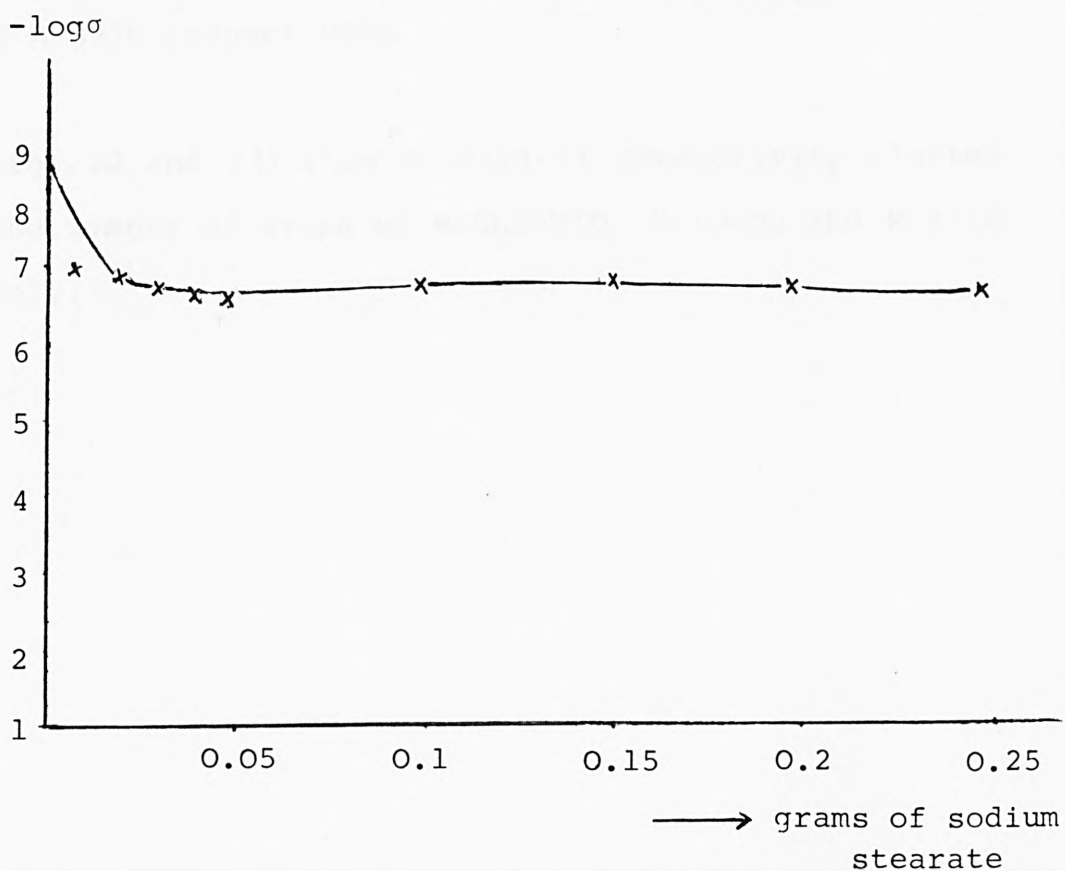


Fig. 21  $-\log$  conductivity v. composition 64% KW 375/PVC/  
sodium stearate phases



using HALLCOMID M-10-OL and HALLCOMID M-8-10 showed little or no difference in the electrical conductivity when compared with the results of the same materials which did not contain a potential coupling agent.

PVC-carbon black composites with HALLCOMID were also prepared by adding between 1 drop to 25 drops of either HALLCOMID M-10-OL or HALLCOMID M-8-10 to 17 gram PVC and 13 gram carbon black (32% carbon black). A maximum electrical conductivity of  $10^{-5}$  was obtained for a sample containing 15 drops of HALLCOMID M-10-OL and the same electrical conductivity was obtained for a sample containing 10-15 drops of HALLCOMID M-8-10 compared with  $7.9 \times 10^{-7}$  for the same material without the coupling agent. Tables (15) and (16) list results obtained for PVC/carbon black with HALLCOMID M-10-OL and M-8-10 respectively.

(Figs. 22 and 23) show electrical conductivity plotted against the number of drops of HALLCOMID M-10-OL and M-8-10 respectively.

Table 15

PVC gram	carbon black gram	HALLCOMID M-10-oL drops	R ohm	$\sigma$ $\text{ohm}^{-1}\text{cm}^{-1}$	$-\log\sigma$
17	13	-	$2.6 \times 10^5$	$7.9 \times 10^{-7}$	6.1
"	"	3	$6.5 \times 10^4$	$3.1 \times 10^{-6}$	5.51
"	"	5	$3.4 \times 10^4$	$7.3 \times 10^{-6}$	5.14
"	"	10	$3.6 \times 10^4$	$8.6 \times 10^{-6}$	5.07
"	"	15	$1.6 \times 10^4$	$1.6 \times 10^{-5}$	4.8
"	"	20	$3.7 \times 10^4$	$6.23 \times 10^{-6}$	5.2
"	"	25	$6.4 \times 10^4$	$4.2 \times 10^{-6}$	5.38

Table 16

PVC gram	carbon black gram	HALLCOMID M-8-10 drops	R ohm	$\sigma$ $\text{ohm}^{-1}\text{cm}^{-1}$	$-\log\sigma$
17	13	-	$2.6 \times 10^5$	$7.9 \times 10^{-7}$	6.1
"	"	1	$1.2 \times 10^5$	$1.9 \times 10^{-6}$	5.72
"	"	2	$1.5 \times 10^5$	$3.2 \times 10^{-6}$	5.49
"	"	3	$4.8 \times 10^4$	$3.7 \times 10^{-6}$	5.43
"	"	5	$3.5 \times 10^4$	$5 \times 10^{-6}$	5.30
"	"	10	$1.5 \times 10^4$	$1.5 \times 10^{-5}$	4.82
"	"	15	$7 \times 10^3$	$2.5 \times 10^{-5}$	4.61
"	"	20	$7 \times 10^4$	$3.3 \times 10^{-6}$	5.48
"	"	25	$1.5 \times 10^5$	$1.2 \times 10^{-6}$	5.92

Fig. (22) -log conductivity v. composition 32% carbon black/

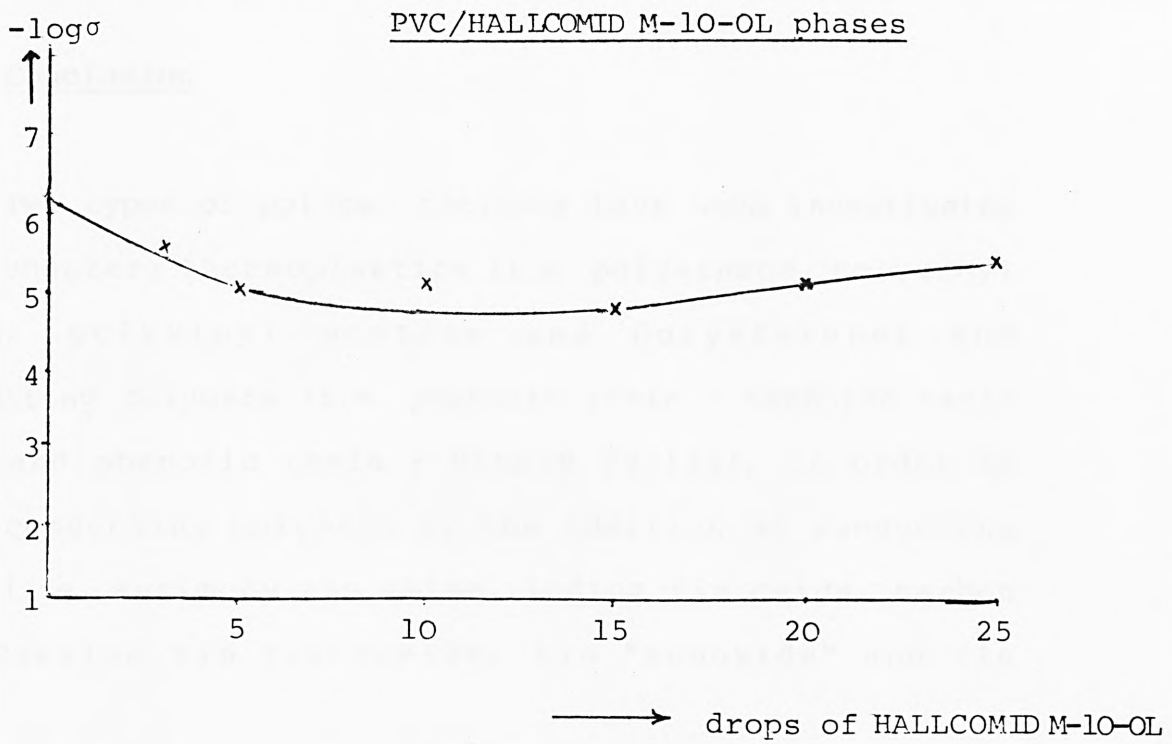
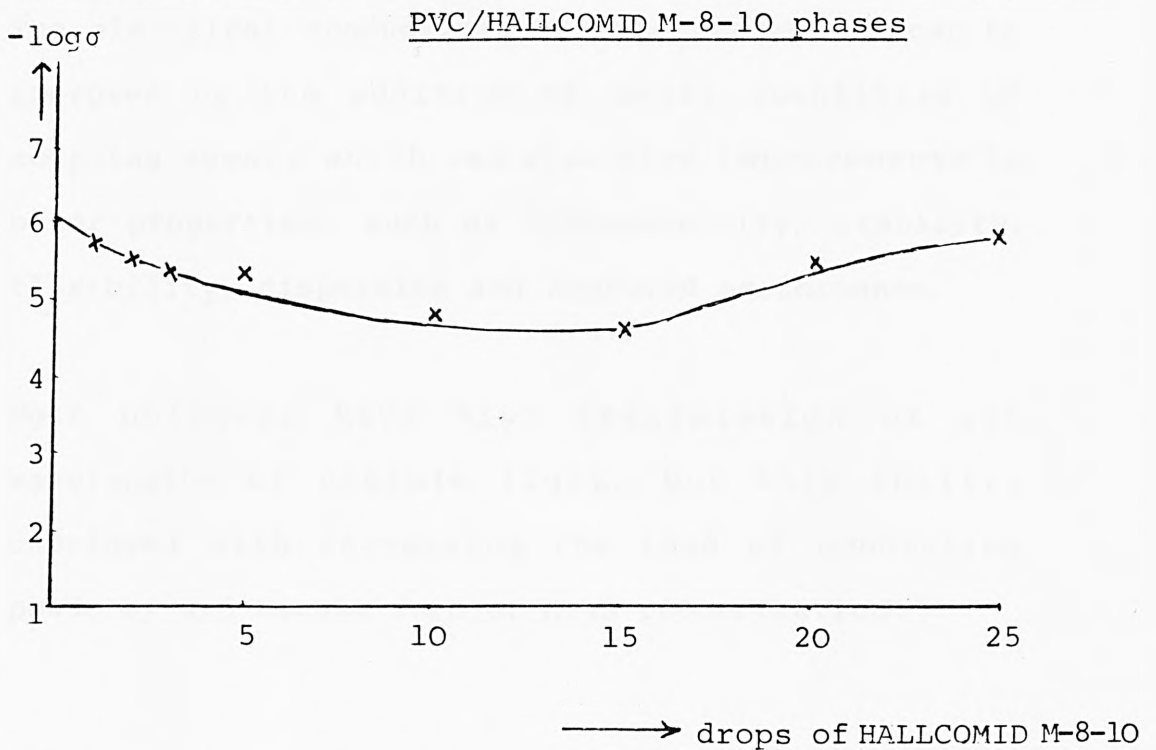


Fig. (23) -log conductivity v. composition 32% carbon black/



## 2.10 Conclusion

Two types of polymer matrices have been investigated in this chapter; thermoplastics (i.e. polyethene, polyvinyl chloride, polyvinyl acetate and polystyrene) and thermosetting polymers (i.e. phenolic resin - BAKELITE resin R-17620 and phenolic resin - VARCUM 29-112), in order to produce conducting polymers by the addition of conducting powders (i.e. antimony tin oxide, indium tin oxide, carbon black, caesium tin tribromide, tin "suboxide" and tin powder).

This work has shown that:

1. The electrical conductivity of the composites increases with increasing the load of the conducting powders.
2. The electrical conductivity of the composites can be improved by the addition of small quantities of coupling agents which can also give improvements in other properties, such as hydrophobicity, stability, flexibility, dispersion and improved performance.
3. Most polymers have high transmission of all wavelengths of visible light, but this ability decreased with increasing the load of conducting powders, and became zero at high concentration.

References

1. "Conductive polymers", R.B. Seynow, Polymer science and technology, Vol.15, (1981).
2. H.J.M. Bowen, "Properties of solids and their atomic structures", U.K., (1967).
3. L.H.V. Vlack, "Elements of materials science and engineering", Third edition, Michigan, (1975).
4. S.J.E. Clark, Ph.D. thesis, London, 1979.
5. C.Kittel, "Introduction to solid state physics", second edition, Berkeley, California, (1956).
6. H.M. Rosenberg, "The solid state", 2nd edition, Oxford, (1978).
7. K & W reprint, ME, (1979), 38.
8. K & W reprint, ME, (1980), 29.
9. K & W reprint, ME, (1982), 37.
10. K & W reprint, Textile Horizons, (1981), Nov., 28.
11. K & W reprint, SAMPE Quarterly, (1982), April, 33.
12. Reference 1, page 49.
13. K & W reprint, ME, (1982), 92.
14. K.L. Horovitz and V.A. Johnson, "Methods of experimental physics", Vol. 6, part 8, (1959).

## CONTENTS

<u>CHAPTER THREE: Mixed Metal Oxide Semiconductors</u>		<u>Page</u>
3.1	Introduction	56
3.2	Analytical techniques	58
3.2.1	Electrical conductivity measurements	58
3.2.2	Particle size analysis	61
3.2.3	Powder X-ray diffraction	63
3.3	Experimental	67
 <u>Section I</u>		
3.3.1	The preparation of mixed metal oxides	67
3.3.1.1	Zirconium dioxide system	67
3.3.1.2	Titanium dioxide system	73
3.3.1.3	Aluminium oxide system	76
3.3.1.4	Zinc oxide system	77
3.3.2	Mixed metal oxides based on zirconium, titanium, aluminium and zinc oxides discussion	84
 <u>Section II</u>		
3.3.3	An investigation into the effects of diluants on the resistivity of antimony tin oxide	91
3.3.4	Results and discussion	93
3.4	Conclusion	98
3.5	References	101

## CHAPTER THREE

### Mixed metal oxide semiconductors

#### 3.1 Introduction

At the present time there are two commercially available conducting mixed oxides containing tin(IV) viz. antimony tin oxide and indium tin oxide. Antimony tin oxide is manufactured by Keeling and Walker as a dark grey/blue powder with a resistivity of around 0.2 ohm cm, depending on the particle size.

The current major commercial use for antimony tin oxide is in the glass manufacturing industry where it is used to make glass melting electrodes for the production of lead crystal glass.

A large potential future market for antimony tin oxide may involve its use as a conductive filler in plastic anti-static coatings. Chapter II of this thesis described results obtained on dispersion of antimony tin oxide in polymer systems. One drawback to the use of antimony tin oxide in this area is its high chromophoricity, a consequence of this being that any plastic doped with this oxide takes on a blue/grey coloration which is undesirable in many uses including tin antimony oxide doped plastics for sprayed anti-

static coatings.

Although indium tin oxide is a considerably more expensive material than antimony tin oxide due to the relative prices of indium and antimony metals, it has the advantage of having a pale green colour and therefore being less chromophoric than antimony tin oxide, for this reason indium tin oxide, apart from its cost, appears to be an ideal material for use in specialised anti-static plastics in place of the highly coloured antimony tin oxide.

The main aim of the work described in this chapter of the thesis is to study a series of mixed metal oxides to try to find conducting oxides cheaper than indium tin oxide and less chromophoric than antimony tin oxide.

The work undertaken in this chapter comprised the two sections outlined below:-

- (i) The first part of the investigation was an attempt to prepare a new semiconducting mixed metal oxide
- (ii) The second part of the investigation was to find an inexpensive, white filler which could be successfully blended with 6.5:93.5 antimony tin oxide to yield a new composite material of low resistivity and chromophoricity.

Three main methods were used to characterise the mixed metal oxides prepared in this work viz. conductivity measurement, particle size analysis and X-ray diffraction. These are described briefly in the following sections:

### 3.2 Analytical techniques

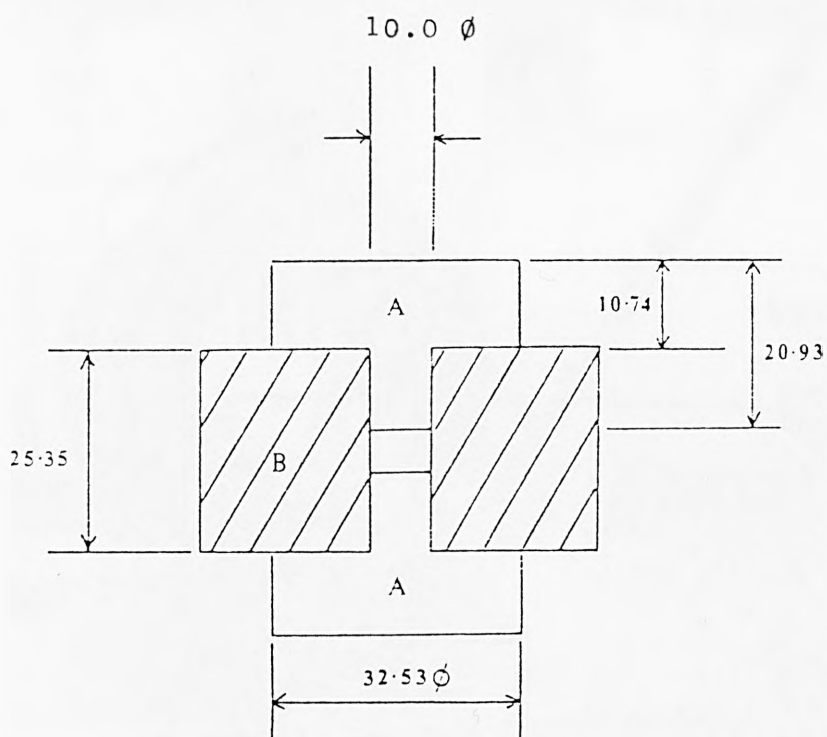
#### 3.2.1 Electrical conductivity measurements:

Powder conductivity measurements were carried out using the specially designed cell shown in Figure (24). The electrode and plugs (A) were constructed from beryllium aluminium alloy (Beral) and the housing (B) from "Nylon". Approximately (0.8g) of the sample was placed into the cell, and the cell was then placed in a Beckman hydraulic press shown in Figure (25). The powder was compressed using a one ton load.

The resistance of the sample in the cell was then measured using a Keithley Model 616 Electrometer (Fig. 25).

The initial decrease in resistivity which is observed on first applying pressure to the sample arises from an improved contact between the electrodes and the particles. The initial increase in pressure also helps to squeeze out the air which fills the interparticular voids and which is responsible for the high resistivity of the powdered material at atmospheric pressure. The measured resistance was converted into resistivity using this equation:-

Figure (24) - The Powder Conductivity Cell



All Dimensions Given in Millimetres

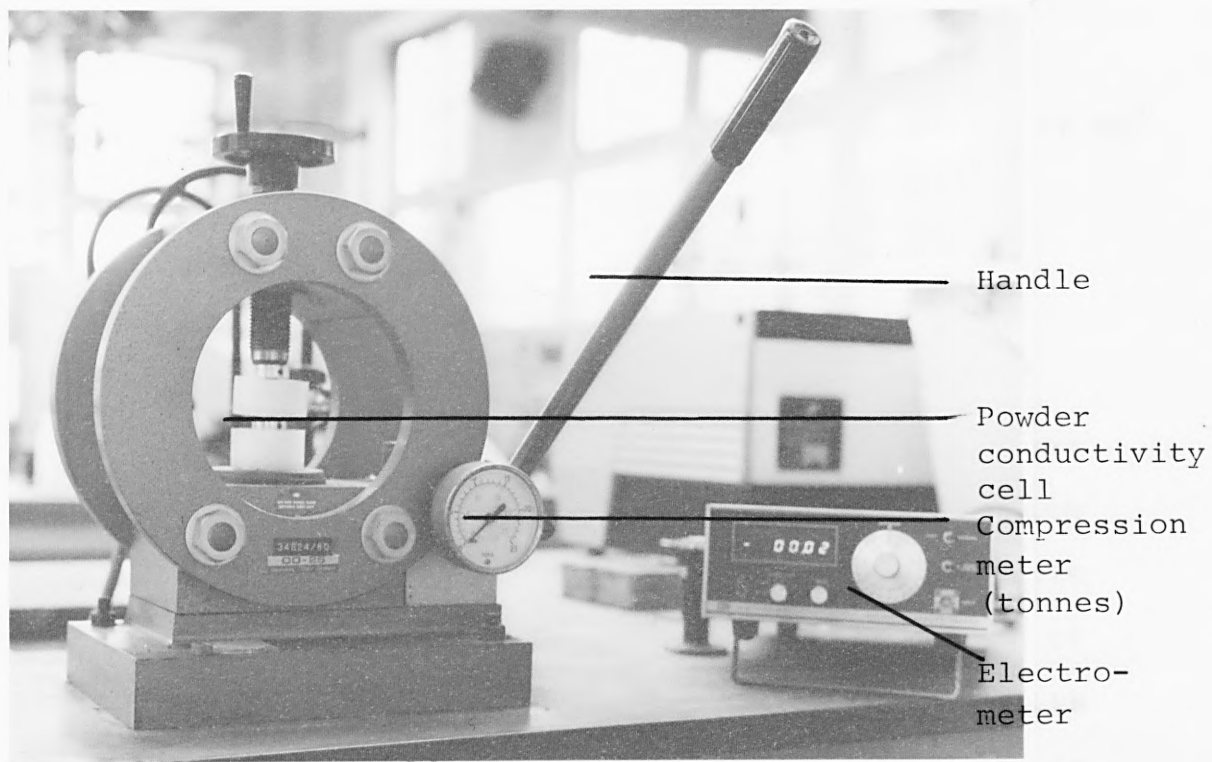
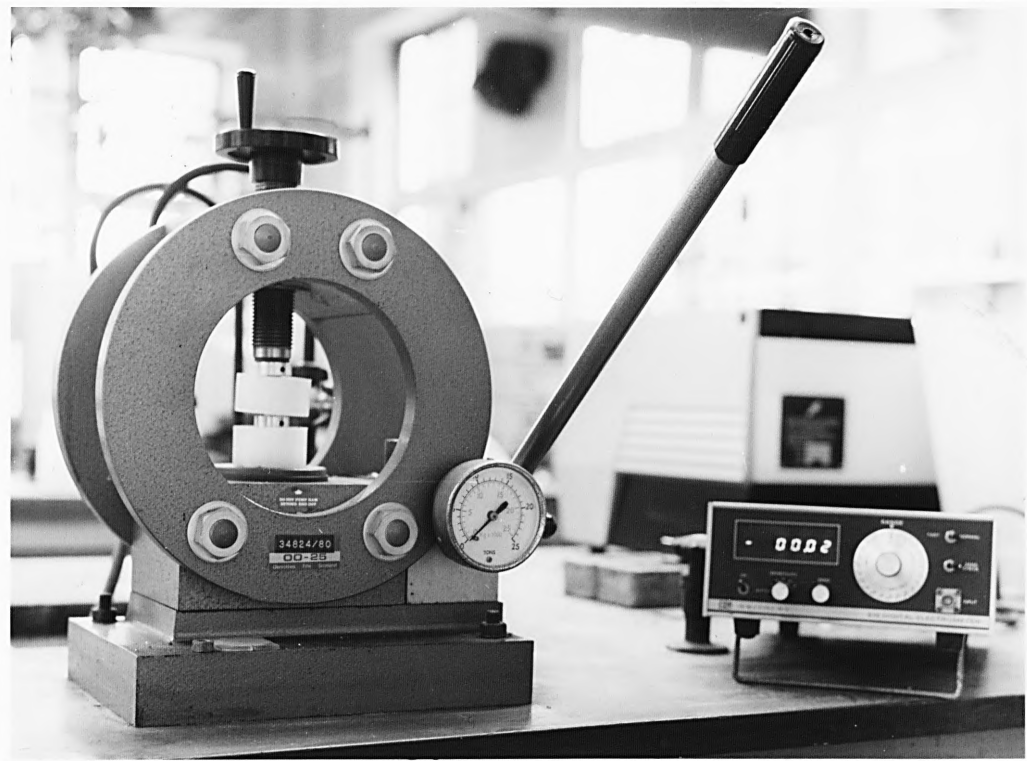


Figure (25) Beckman hydraulic press



$$\rho = \frac{R \times A}{t}$$

where:

$\rho$  = Resistivity in ohm.cm

R = Resistance of powder bed in ohms

A = Cross sectional area of powder bed in  $\text{cm}^2$

t = Thickness of powder bed in cm

### 3.2.2 Particle size analysis<sup>1,2</sup>

In this investigation particle size analysis was carried out using the MALVERN 2600/3600 particle sizer which is a complete measurement tool for the analysis of particle size distribution in the range of 1 to 1800 micron. Use of appropriate sample cell and measurement techniques permits the measurement of size distribution by weight of solid in liquid suspension. In this work the distilled water was used as the dispersion medium. The instrument uses the principle of Fraunhofer Diffraction from the particles, as illustrated in Figure (26).

A low power visible laser transmitter produces a parallel monochromatic beam of light which is arranged to illuminate the particles by use of an appropriate sample

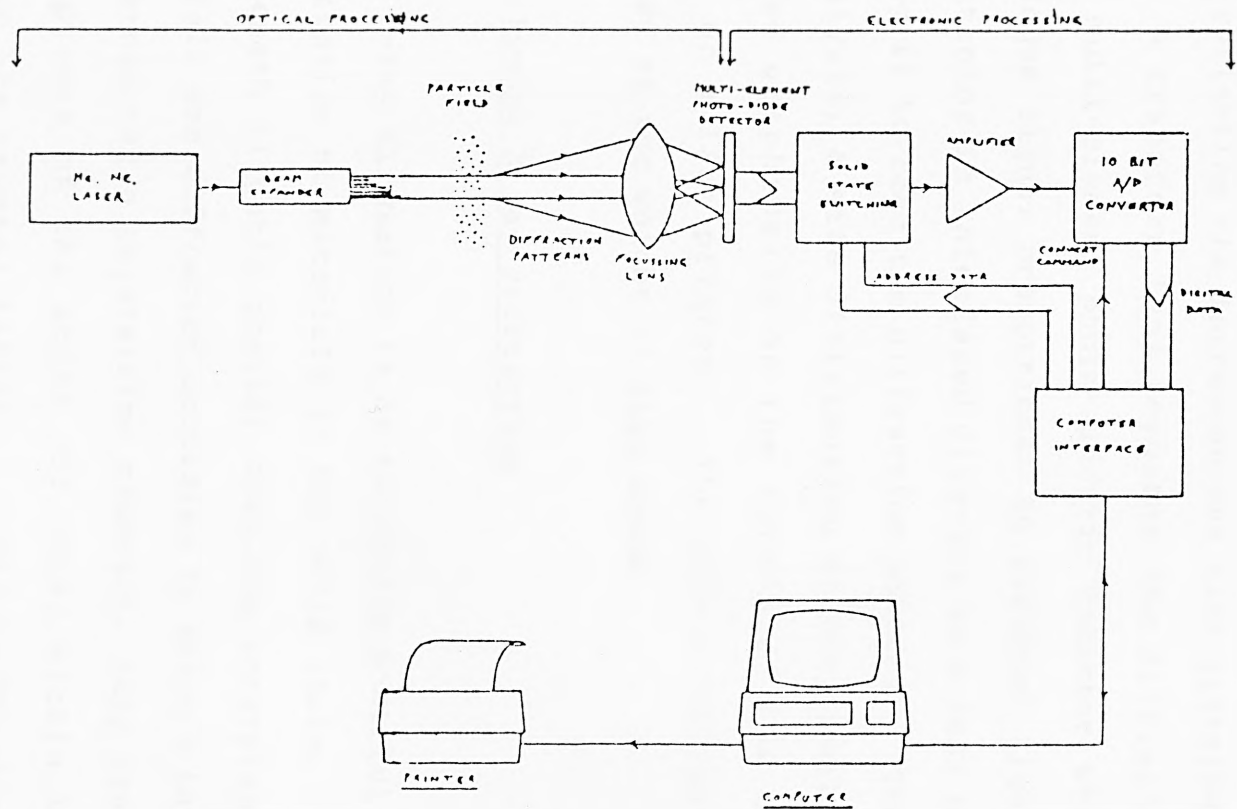


Figure (26) Basic opto-electronic system to obtain particle size and distribution

cell. The incident light is diffracted by the particles illuminated to give a stationary diffraction pattern regardless of particle movement. As particles enter and leave the illuminated area, the diffraction pattern 'evolves' always reflecting the instantaneous size distribution in this area. A transform lens focusses the diffraction pattern onto a multi-element photo-electric detector which produces an analogue signal proportional to received light intensity. This detector is interfaced directly to a desk top computer allowing it to read the diffraction pattern. The results of the analysis, a size distribution of the sample by weight, displayed graphically on the screen of the computer or printed on a line printer. The size distribution can be presented as the weight in size bands.

### 3.2.3 Powder X-ray diffraction

X-ray diffraction is an extremely powerful tool in the identification of materials in the solid state. X-ray with a wavelength slightly greater than the interplanar spacings of crystals are diffracted according to Bragg's Law, when the X-rays encounter a crystalline material, they are diffracted by the planes of the atoms (or ions) within the crystal making up the crystal lattice. Figure(27) shows a set of atomic planes together with a train of X-ray striking them at an angle  $\theta$ . The reflected rays from all planes of the set

take the same direction, and if they are out of phase they will interfere with each other and can be destroyed. Only if the difference in path between rays reflected from successive planes is an integral number of wavelengths, will they reinforce each other and form a reflected beam. From Figure (27) the difference in path between rays reflected from successive planes is  $ef + fg$ .

Furthermore,  $ef = fg = d\sin\theta$ . The condition for successful reflection is given by the Bragg's Law:

$$n\lambda = 2d\sin\theta$$

when the diffraction angle ( $\theta$ ) depends upon the wavelength ( $\lambda$ ) of the X-rays and the distance ( $d$ ) between the planes. The value ( $n$ ) is the integer number of waves which occur in the distance ( $efg$ ).

Two types of method are employed in X-ray crystallography for obtaining measurements of reflected rays from samples, one for single crystals and the other for powders. In this work only the powder method was used. The ideal powder sample consists of an enormous number of minute crystals with completely random orientation. For any set of planes with spacing  $d_{hkl}$ , there are many crystals orientated so that their  $hkl$  planes make the correct Bragg angle ( $\theta$ ) with the primary beam. Since the correctly orientated crystals all have orientations about the primary

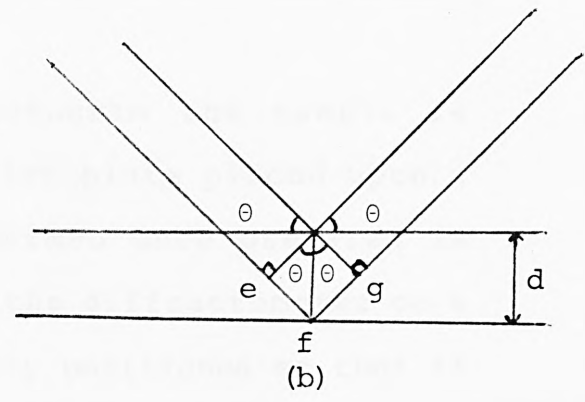
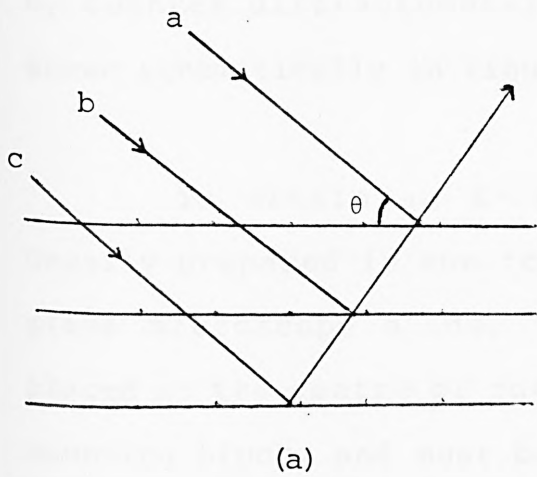


**Figure 27** The Bragg Angle of Reflection

- (a) - Condition for Reflection
- (b) - Path Difference =  $2d\sin\theta$

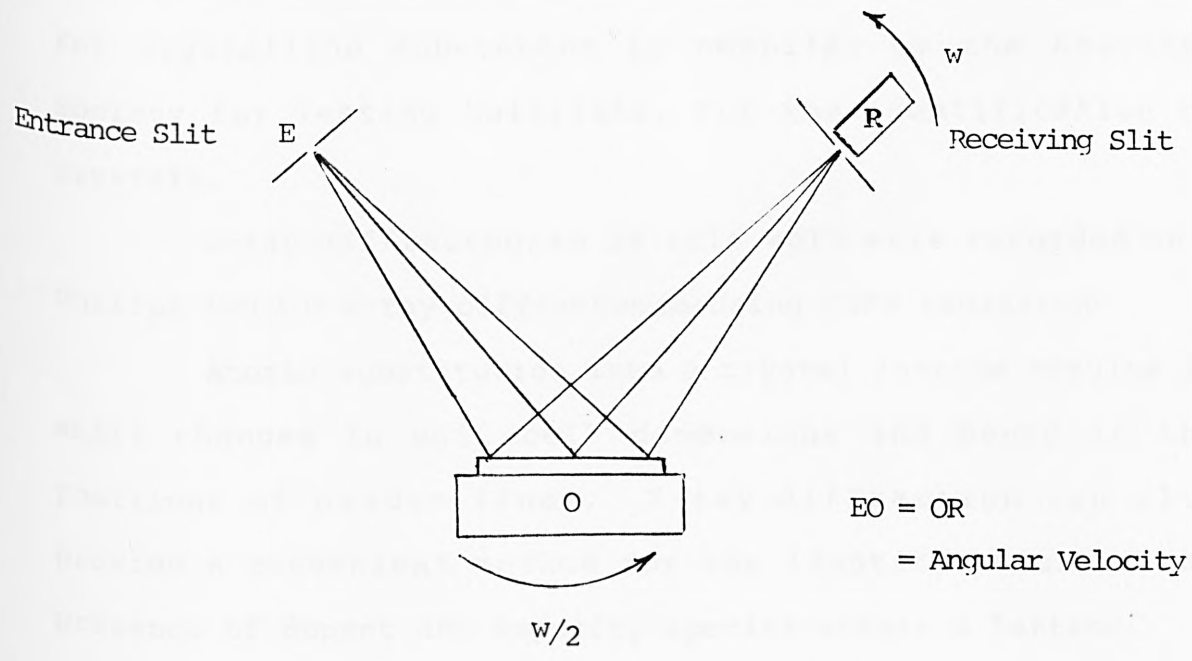


**Figure 28** The Counter Diffractometer

beam, the diffracted beams form a cone of half apex angle ( $2\theta$ ). For each planar spacing  $d_{hkl}$  there is a cone of angle  $2\theta_{hkl}$ . Powder patterns are usually registered by film recording or by counter diffractometer, the diffractometer process is shown schematically in Figure (28).

To obtain an X-ray diffractogram the sample is usually prepared in the form of a flat plate placed upon a glass microscope slide. The specimen once prepared is placed at the centre of rotation of the diffractometer on a mounting block, and must be accurately positioned so that it is tangent and parallel to the diffractometer's axis of rotation. As every crystalline material produces a different X-ray diffractogram, due to variation in cell dimensions and types of atoms within the atomic planes, the immediate use of powder X-ray diffraction data is in material identification. A comprehensive index of powder patterns for crystalline substances is compiled by the American Society for Testing Materials, for the identification of crystals.

X-ray diffractogram in this work were recorded on a Philips PW1010 X-ray diffractometer using  $\text{CuK}\alpha$  radiation.

Atomic substitution into a crystal lattice results in small changes in unit cell dimensions and hence in the positions of powder lines. X-ray diffraction can also provide a convenient method for the identification of the presence of dopant and impurity species within a lattice.

### 3.3 EXPERIMENTAL

#### Section I

##### 3.3.1 The preparation of Mixed Metal Oxides

This work was carried out in an attempt to find a new semiconducting material to replace indium tin oxide and antimony tin oxide. The oxides considered in this work as the main matrix elements are:

zirconium dioxide, titanium dioxide, zinc oxide and  
aluminium oxide

##### 3.3.1.1 Zirconium dioxide system:-

The following systems were studied in this work to investigate the effects of selected dopants on the resistivity of zirconium dioxide.

- Antimony doped zirconium dioxide (using antimony oxide)
- Cadmium doped zirconium dioxide (using cadmium carbonate)
- Vanadium doped zirconium dioxide (using vanadium(III) oxide)
- Indium doped zirconium dioxide (using indium metal)
- Zinc doped zirconium dioxide (using zinc oxide)

- Bismuth doped zirconium dioxide (using bismuth oxy-carbonate)
- Tantalum doped zirconium dioxide (using tantalum(V) chloride)
- Niobium doped zirconium dioxide (using niobium(V) chloride)
- Yttrium doped zirconium dioxide (using yttrium (III) oxide)
- Flourine doped zirconium dioxide (using ammonium flouride)

3

The preparative methods considered in this work were:

1. Co-Precipitation of mixed oxide phases followed by calcining

The experimental procedure adopted was as follows:

Zirconium nitrate  $Zr(NO_3)_4 \cdot 5H_2O$  (70g) was dissolved in acidified distilled water [300 ml water+10 ml nitric acid]. Then a nitric acid solution of the dopant (as the compounds listed) was added to the zirconium nitrate solution. Levels of 1%, 5%, 10% and 15% of dopant were used. Aqueous ammonia solution was then added to the solution of mixed nitrates to co-precipitate the dopant with hydrous zirconium oxide. The resulting precipitate was washed with water by decantation to pH7 and then oven dried at 110°C. The

dried material was ball milled for 15 minutes, and was then divided into two parts. One half was calcined at 700°C for 3 hrs and the other half at 1100°C for 3 hrs to yield samples of doped zirconium oxides. After calcination the two batches of material were kept separate and were both ball milled for a second time for 15 minutes to prepare a homogeneous sample for resistivity analysis. This procedure was used to prepare all the dopant materials except the fluorine doped zirconium dioxide which was prepared as follows:

Zirconium nitrate (70g) was dissolved in acidified distilled water [300 ml water + 10 ml nitric acid]. Aqueous ammonia solution was added to the zirconium nitrate solution to precipitate the hydrous zirconium dioxide. The resulting precipitate was washed with water by decantation until it became free from ammonia and was then centrifuged to give a hydrous oxide paste. Ammonium fluoride was then added to the paste with stirring and then oven dried at 110°C.

Levels of 1%, 5% and 10% of fluorine were prepared. The dried material was ball milled for 15 minutes, and was then divided into two parts. The first was calcined at 700°C while the second part was similarly treated at 1100°C both for 3 hrs to yield fluorine zirconium oxide.

After calcination the two batches were kept separate and were both ball milled for a second time for 15 minutes to prepare a homogeneous sample for resistivity analysis.

A summary of the results obtained, together with the calcination temperature used in this preparation is given in Table (17).

## 2. Direct Milling of Oxide Powders

Yttrium zirconium oxide was also prepared by direct milling to compare the results with those obtained from the co-precipitation method.

Zirconium dioxide (10-x)g was ball milled in ethanolic solution with (xg) yttrium (III) oxide for 90 minutes and the mixture was then dried at 110°C in an oven. The dried material was divided into two parts. The first calcined at 700°C for 3 hrs, while the second was calcined at 1100°C for 3 hrs. After calcination the mixed oxide was cooled, ball milled for a second time for 15 minutes in ethanol and oven dried to prepare a homogeneous sample for resistivity analysis. The measured resistivities of the yttrium doped zirconium oxides are shown in Table (17).

Table (17)

Resistivities of zirconium oxide doped selected doping species

dopant	% wt dopant	% wt ZrO <sub>2</sub>	Resistivity ohm.cm		colour		preparation method
			700°C	1100°C	700°C	1100°C	
Sb	1	99	3x10 <sup>7</sup>	3x10 <sup>3</sup>	white	off white	co-precipitation
	5	95	8x10 <sup>7</sup>	5x10 <sup>6</sup>	off white	off white	
	10	90	5x10 <sup>8</sup>	7x10 <sup>8</sup>	white	off white	
	15	85		6x10 <sup>8</sup>		off white	
Cd	1	99	10 <sup>8</sup>	2x10 <sup>7</sup>	white	off white	co-precipitation
	5	95	4x10 <sup>9</sup>	7x10 <sup>7</sup>	white	beige	
	10	90	5x10 <sup>8</sup>	4x10 <sup>9</sup>	white	brown	
V	1	99	2x10 <sup>8</sup>	2x10 <sup>7</sup>	dk.cream	mustard	co-precipitation
	5	95	2.5x10 <sup>6</sup>	2x10 <sup>7</sup>	mustard	cream/ brown	
	10	90	10 <sup>6</sup>	7x10 <sup>5</sup>	mustard	brown	
	15	85		2x10 <sup>4</sup>		brown	
In	1	99	2x10 <sup>7</sup>	2x10 <sup>7</sup>	cream	off white	co-precipitation
	5	95	10 <sup>8</sup>	6x10 <sup>8</sup>	white	stone grey	
	10	90	5x10 <sup>7</sup>	8x10 <sup>8</sup>	white	grey	
Zn	1	99	3x10 <sup>8</sup>	2x10 <sup>9</sup>	off white	pale grey	co-precipitation
	5	95	2x10 <sup>10</sup>	2x10 <sup>9</sup>	white	stone grey	
	10	90	10 <sup>9</sup>	3x10 <sup>10</sup>	off white	stone grey	

Table (17) Contd.

Resistivities of zirconium oxide doped selected doping species

dopant	% wt dopant	% wt ZrO <sub>2</sub>	Resistivity ohm.cm		colour		preparation method
			700°C	1100°C	700°C	1100°C	
Bi	1	99	7x10 <sup>7</sup>	10 <sup>9</sup>	white	cream	co-precipitation
	5	95	6x10 <sup>8</sup>	10 <sup>8</sup>	cream	dk.cream	
	10	90	2x10 <sup>8</sup>	6x10 <sup>9</sup>	grey	dk.cream	
Ta	1	99	7x10 <sup>8</sup>	2x10 <sup>8</sup>	white	off white	co-precipitation
	5	95	2x10 <sup>8</sup>	10 <sup>8</sup>	white	grey/white	
	10	90	2x10 <sup>7</sup>	10 <sup>8</sup>	white	white	
Nb	1	99	10 <sup>8</sup>	2x10 <sup>6</sup>	white	white	co-precipitation
	5	95	3x10 <sup>8</sup>	7x10 <sup>5</sup>	white	white	
	10	90	5x10 <sup>8</sup>	8x10 <sup>5</sup>	,"	,"	
Y	1	99	3.4x10 <sup>7</sup>	4.3x10 <sup>8</sup>	off white	off white	co-precipitation
				2.6x10 <sup>7</sup>	2.6x10 <sup>7</sup>	off white	off white
	5	95	1.6x10 <sup>6</sup>	2x10 <sup>7</sup>	off white	light grn.	co-precipitation
			1.2x10 <sup>7</sup>	1.1x10 <sup>7</sup>	beige	light grn.	direct milling
F	1	99	9x10 <sup>9</sup>	8x10 <sup>7</sup>	white	white	co-precipitation
	5	95	8x10 <sup>10</sup>	5x10 <sup>8</sup>	white	white	
	10	90	2x10 <sup>11</sup>	10 <sup>9</sup>	white	white	
	0	100	2.7x10 <sup>7</sup>	5.1x10 <sup>7</sup>	white	white	co-precipitation

### 3.3.1.2 Titanium dioxide system:

The following systems were studied in this work to investigate the effects of selected dopants on the resistivity of titanium dioxide.

- Antimony doped titanium dioxide [using antimony chloride]
- Cadmium doped titanium dioxide [using cadmium carbonate]
- Vanadium doped titanium dioxide [using vanadium chloride]
- Indium doped titanium dioxide [using indium metal]
- Bismuth doped titanium dioxide [using bismuth chloride]
- Copper doped titanium dioxide [using copper(I)chloride]
- Niobium doped titanium dioxide [using niobium(V)chloride]
- Yttrium doped titanium dioxide [using yttrium (III) oxide]
- Lithium doped titanium dioxide [using lithium hydroxide  
LiOH.H<sub>2</sub>O]
- Flourine doped titanium dioxide [using ammonium flouride]

All of the samples were prepared by co-precipitation followed by calcination.

#### Co-precipitation of mixed oxide phases followed by calcining

Distilled water (150 ml) was added gradually in small quantities to a dried beaker containing titanium tetrachloride (29 ml) with continuous stirring until the solution became clear.

The compound containing the dopant species was then dissolved in hydrochloric acid and added to the titanium tetrachloride solution.

Levels of 1%, 5% and 10% of dopant were used.

Aqueous ammonia solution was then added to the solution of mixed chlorides to precipitate out the doped hydrous titanium dioxide. The resulting precipitate was washed with water by decantation until it became free from chloride and then oven dried at  $110^{\circ}\text{C}$ . The dried material was ball milled for 15 minutes and was then divided into two parts; one half was calcined at  $700^{\circ}\text{C}$  for 3 hrs, and the other half at  $1100^{\circ}\text{C}$  for 3 hrs to yield doped titanium oxide. The cooled product was ball milled for a second time for 15 minutes to prepare a homogeneous sample for resistivity analysis.

This procedure was used to prepare all of the metal-doped titanium oxide samples (except Li), while the fluorine-doped and lithium-doped titanium oxides were prepared by the following method.

Distilled water (150 ml) was added gradually to a dried beaker containing titanium tetrachloride (29 ml) in small quantities with continuous stirring until the solution became clear. Aqueous ammonia solution was added to the titanium tetrachloride solution to precipitate

Table (18)

Resistivities of titanium oxide doped selected doping species

dopant	% wt dopant	% wt TiO <sub>2</sub>	Resistivity ohm.cm		colour	
			700°C	1100°C	700°C	1100°C
Sb	1	99	$9 \times 10^7$	$2 \times 10^8$	light grey	light grey
	5	95	$6 \times 10^6$	$6 \times 10^7$	light cream	light grey
	10	90	$9 \times 10^5$	$6 \times 10^7$	pale yellow	light grey
Cd	1	99	$3 \times 10^7$	$4 \times 10^8$	white	cream
	5	95	$4 \times 10^7$	$8 \times 10^9$	white	pale cream
	10	90	$3 \times 10^7$	$4 \times 10^8$	off white	cream
V	1	99	$10^6$	$8 \times 10^7$	light green	brown
	5	95	$2 \times 10^6$	$5 \times 10^6$	dark brown	dark brown
	10	90	$2 \times 10^6$	$6 \times 10^5$	dark brown	mid brown
In	1	99	$2 \times 10^8$	$2 \times 10^9$	white	light yellow
	5	95	$10^{10}$	$3 \times 10^9$	white	light yellow
	10	90	$10^9$	$2 \times 10^9$	pale yellow	lemon
Bi	1	99	$9 \times 10^8$	$10^9$	off white	grey
	5	95	$4 \times 10^8$	$6 \times 10^9$	off white	mid grey
	10	90	$2 \times 10^9$	$8 \times 10^9$	off white	light grey
Cu	1	99	$5 \times 10^9$	$2 \times 10^9$	dark brown	green brown
	5	95	$4 \times 10^9$	$5 \times 10^8$	dark brown	grey brown
	10	90	$10^8$	$8 \times 10^8$	dark brown	grey brown
Nb	1	99	$4 \times 10^6$	$10^7$	off white	light grey
	5	95	$2 \times 10^6$	$10^7$	yellow	light grey
	10	90	$4 \times 10^8$	$8 \times 10^8$	yellow	mid grey
Y	1	99	$2.2 \times 10^9$	$2.4 \times 10^9$	off white	light green
	5	95	$2.1 \times 10^9$	$1.6 \times 10^9$	off white	light green
Li	1	99	$2 \times 10^7$	$6 \times 10^7$	white	grey
	5	95	$10^7$	$3 \times 10^7$	white	off white
	10	90	$9 \times 10^8$	$10^8$	white	white
F	1	99	$3 \times 10^7$	$2 \times 10^8$	off white	light grey
	5	95	$3 \times 10^7$	$3 \times 10^7$	off white	light grey
	10	90	$5 \times 10^9$	$4 \times 10^6$	off white	mid grey
	0	100	$1.5 \times 10^7$	$2 \times 10^8$	white	white

out the hydrous titanium oxide. The resulting precipitate was washed with water by decantation until it became free from ammonia and chlorine, and was then centrifuged to give a hydrous oxide paste. Then dopant compound [ $\text{NH}_4\text{F}$  or  $\text{Li}(\text{OH})$ ] was then added to the paste with stirring, then oven dried at  $110^\circ\text{C}$ . The dried material was ball milled for 15 minutes and divided into two parts; one half was calcined at  $700^\circ\text{C}$  for 3 hrs and the other half at  $1100^\circ\text{C}$  for 3 hrs to yield the fluorine doped and lithium doped titanium oxides. The cooled products were ball milled for a second time for 15 minutes to prepare homogeneous samples for resistivity analysis. Levels of 1%, 5% and 10% of the dopant were used. A summary of the results obtained, together with the calcination temperature used in this preparation, is given in Table (18).

### 3.3.1.3 Aluminium oxide system

The following samples were studied in this work to investigate the effects of selected dopants on the resistivity of aluminium oxide:

- Tin(IV) doped aluminium oxide [using tin(IV) chloride penta hydrate]
- Copper doped aluminium oxide [using copper(I)chloride]
- Vanadium doped aluminium oxide [using vanadium(III) oxide]
- Antimony doped aluminium oxide [using antimony chloride]

- Magnesium doped aluminium oxide [using magnesium carbonate]
- Silicon doped aluminium oxide [using silicon oxide]

All of the doped species, except the silicon doped aluminium oxide, were prepared by a method similar to that used for the doped zirconium oxide samples in which aluminium nitrate  $\text{Al}(\text{NO}_3)_3 \cdot 9\text{H}_2\text{O}$  (73.6g) was dissolved in [200 ml water + 10 ml  $\text{HNO}_3$ ], and a nitric acid [20 ml water + 10 ml  $\text{HNO}_3$ ] solution of the dopant compound was added.

The silicon doped aluminium oxide was prepared by a method similar to that used to prepare fluorine doped zirconium oxide.

A summary of the results obtained together with the calcination temperature used in this preparation is given in Table (19).

#### 3.3.1.4 Zinc-oxide system

The following samples were studied in this work to investigate the effects of selected dopants on the resistivity of zinc oxide:

Table (19)

Resistivities of aluminium oxide doped selected doping species

dopant	% wt dopant	% wt Al <sub>2</sub> O <sub>3</sub>	Resistivity ohm.cm		colour	
			700°C	1100°C	700°C	1100°C
Sn	1	99	3 x 10 <sup>9</sup>	4 x 10 <sup>7</sup>	cream	white
	5	95	7 x 10 <sup>6</sup>	4 x 10 <sup>7</sup>	cream	white
	10	90	10 <sup>8</sup>	3 x 10 <sup>7</sup>	cream	white
Cu	1	99	4 x 10 <sup>7</sup>	10 <sup>6</sup>	blue/green	green/brown
	5	95	3 x 10 <sup>7</sup>	10 <sup>6</sup>	green	red/brown
	10	90	2 x 10 <sup>8</sup>	2 x 10 <sup>8</sup>	dark green	brown
V	1	99	6 x 10 <sup>10</sup>	9 x 10 <sup>6</sup>	cream	light brown
	5	95	2 x 10 <sup>8</sup>	8 x 10 <sup>6</sup>	mustard	brown
	10	90	4 x 10 <sup>7</sup>	8 x 10 <sup>6</sup>	ochre	dark brown
Sb	1	99	7 x 10 <sup>9</sup>	4 x 10 <sup>9</sup>	white	white
	5	95	3 x 10 <sup>9</sup>	8 x 10 <sup>8</sup>	off white	off white
	10	90	4 x 10 <sup>9</sup>	3 x 10 <sup>12</sup>	off white	off white
Mg	1	99	4 x 10 <sup>11</sup>	1.8 x 10 <sup>11</sup>	white	white
	5	95	8.7 x 10 <sup>11</sup>	1.2 x 10 <sup>11</sup>	white	white
Si	1	99	3.5 x 10 <sup>11</sup>	3.1 x 10 <sup>8</sup>	white	white
	5	95	11.8 x 10 <sup>10</sup>	2.6 x 10 <sup>11</sup>	white	white
	0	100	3.7 x 10 <sup>6</sup>	3.4 x 10 <sup>6</sup>	white	white

- Copper doped zinc oxide [using copper(I) chloride]
- Potassium doped zinc oxide [using potassium carbonate]
- Yttrium doped zinc oxide [using yttrium (III) oxide]
- Aluminium doped zinc oxide [using aluminium nitrate]

All of the doped zinc oxide samples were prepared by a method similar to that used for the doped zirconium oxide samples in which zinc oxide (20g) was dissolved in acidified distilled water [200 ml water + 10 ml HNO<sub>3</sub>] and a nitric acid solution of dopant compound was then added. The potassium doped zinc oxide was prepared by a method similar to that used to prepare fluorine doped zirconium oxide.

A summary of the results obtained, together with the calcination temperature used in this preparation, is given in Table (20).

Three different procedures were considered in this work for the preparation of aluminium doped zinc oxide in addition to the above procedure.

1. The Fuji method<sup>4</sup>

This method was used to prepare 0.05Al<sub>2</sub>O<sub>3</sub>:99.95 ZnO. A mixture of 20g of zinc oxide, 1 ml of 10% aqueous solution of aluminium nitrate and 20 ml of water was converted into a

homogeneous dispersion by treating it in an ultrasonic bath for ten minutes. The paste was oven dried at  $110^{\circ}\text{C}$ . The dried material was calcined at  $700^{\circ}\text{C}$  for 3 hrs and then ball milled for five minutes to prepare a homogeneous sample for resistivity analysis. The measured resistivities of aluminium doped zinc oxide prepared by this method are given in Table (20).

## 2. Thermal decomposition of salts<sup>5</sup>

This method was used to prepare  $0.5\text{Al}_2\text{O}_3:99.5\text{ ZnO}$ . Zinc oxide (50g) was dissolved in acidified distilled water [200 ml water + 10 ml nitric acid] and a nitric acid solution of (1.85g) aluminium nitrate was added and the solution was then allowed to evaporate to dryness to leave the product.

The dried material was ball milled for 15 minutes and was then divided into two parts. The first was calcined at  $700^{\circ}\text{C}$  for 3 hrs and the second part was calcined at  $1100^{\circ}\text{C}$  for 3 hrs. After calcination the two batches of material were kept separate and were both ball milled for a second time for 15 minutes to prepare a homogeneous sample for resistivity analysis.

The measured resistivities of aluminium doped zinc oxide prepared by this method are given in Table (20).

Table (20)

Resistivities of zinc oxide doped selected doping species

dopant	% wt dopant	% wt ZnO	Resistivity ohm.cm		colour		preparation method
			700°C	1100°C	700°C	1100°C	
Cu	1	99	$6 \times 10^5$	$1.5 \times 10^6$	beige	light grn.	co-precipitation
	5	95	$1.4 \times 10^6$	$4.3 \times 10^7$	grey	green	
K	1	99	$2.3 \times 10^6$	$6 \times 10^6$	pale yellow	light green	co-precipitation
	5	95	$5.1 \times 10^6$	$5.1 \times 10^5$	light green	light green	
Y	1	99	$3.4 \times 10^7$	$4.3 \times 10^8$	pale yellow	light green	co-precipitation
	5	95	$1.6 \times 10^6$	$2 \times 10^7$	light green	light green	co-precipitation
Al	1	99	$3 \times 10^7$	$2 \times 10^9$	off white	light grn.	co-precipitation
	5	95	$3 \times 10^8$	$10^7$	off white	light grn.	
	10	90	$2 \times 10^8$	$9 \times 10^6$	off white	light grn.	
	0.05	99.95	$7 \times 10^8$		off white	light grn.	Fuji method
	0.5	99.5	$9.4 \times 10^6$	$4.7 \times 10^6$	off white	light grn.	thermal decomposition
	0.1	99.9	$1.5 \times 10^7$	$11.4 \times 10^6$	off white	yellow )	
	0.25	99.75	$7.6 \times 10^6$	$4.8 \times 10^6$	off white	yellow )	coating on
	0.5	99.5	$3.3 \times 10^6$	$3.9 \times 10^6$	off white	light grn)	oxide surface
	1	99	$5.1 \times 10^6$	$4.1 \times 10^6$	off white	light grn)	
	0	100	$10^8$	$3.6 \times 10^8$	white	white	co-precipitation

### 3.Coating on oxide surface from thick precipitate or gel mixtures

A mixture of (100g) zinc oxide, (100 ml) water and two drops of "teepol" was ball milled for four hours to give a homogeneous dispersion. Zinc oxide paste ( 1g) was taken after each 30 minutes of milling and then oven dried at 110°C. The dried material was ball milled for five minutes to prepare a homogeneous material for particle size analysis. Particle size measurements were carried out on a Malvern 2600/3600 particle sizer described in Section 3.2.2.

The measured particle sizes together with the milling times are given in Table (21) and Figure (29). The particle size analysis showed that the particle size decreased by increasing milling time.

Aluminium nitrate solution containing 0.05g  $Al_2O_3/ml$  was added to (20g) zinc oxide paste to prepare 0.1, 0.25, 0.5 and 1% of aluminium doped zinc oxide samples. The mixture was ball milled for 20 minutes and then oven dried at 110°C. The dried material was divided into two parts, one half was calcined at 700°C for 3 hrs, and the other half at 1100°C for 3 hrs to yield samples of aluminium doped zinc oxide. After calcination the two batches of material were kept separate and were both ball milled for a second time for 15 minutes to prepare homogeneous samples for resistivity analysis. The measured resistivities of aluminium doped zinc oxide prepared by this method are given in Table (20).

**Table (21)**

The effect of the milling time on the particle size of the dried zinc oxide paste

Time of milling (min)	Particle size ( $\mu$ )
0	11.2
30	7.9
60	2.1
90	3.6
120	4.3
150	1.9
180	2.0
210	1.8
240	1.8

Particle size ( $\mu$ )

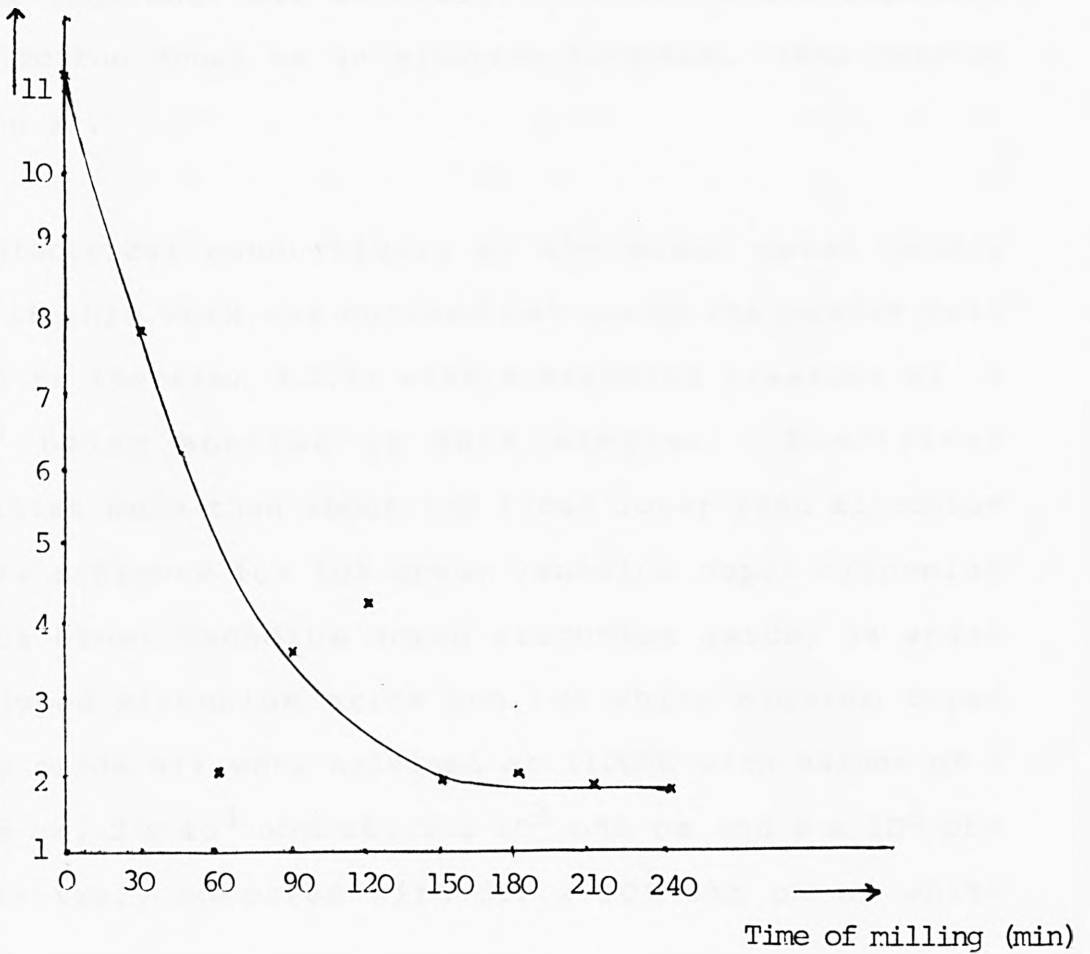


**Figure (29)** The particle size of dried zinc oxide paste against the time

### 3.3.2 Mixed Metal Oxides based on Zirconium, Titanium, Aluminium and Zinc Oxides Discussion

The aim of the present work was to find out if the addition of a dopant species to the oxide matrices zirconium(IV) oxide, titanium oxide, aluminium oxide and zinc oxide could lead to conducting materials with low chromophoricity. The incorporation of an impurity atom in a crystal lattice could be accompanied by the appearance of energy levels in the forbidden energy gap. The presence of these energy levels could then give rise to increase conductivity by creation of either n- or p-type semiconducting behaviour depending on whether the impurity was an electron donar or an electron acceptor. (See Chapter 2, Section 2).

Electrical conductivity of the mixed metal oxides prepared in this work was carried out using the powder cell described in (Section 3.2.1) with a standard pressure of 1 tonne/cm<sup>2</sup> being applied to each sample. Electrical resistivities more than about 100 times lower than zirconium oxide were achieved for 10% brown vanadium doped zirconium oxide, 15% brown vanadium doped zirconium oxide, 5% white niobium doped zirconium oxide and 10% white niobium doped zirconium oxide all were calcined at 1100°C with values of  $7 \times 10^5$  ohm cm,  $2 \times 10^4$  ohm cm,  $7 \times 10^5$  ohm cm and  $8 \times 10^5$  ohm cm respectively compared with  $5.1 \times 10^7$  ohm cm of white

zirconium oxide calcined at 1100°C. Smaller reduction in the resistivity compared with that for zirconium oxide were also found for 5% off white antimony doped zirconium oxide calcined at 1100°C, 5% and 10% mustard vanadium doped zirconium oxide calcined at 700°C, 1% white niobium doped zirconium oxide calcined at 1100°C and 5% off white yttrium doped zirconium oxide calcined at 700°C. None of the resistivities obtained for the doped zirconium oxide phases studied in this work, however, are as low as the 66 ohm cm measured for antimony tin oxide.

Electrical resistivities about two orders of magnitude less than that for titanium oxide were achieved for 10% pale yellow antimony doped titanium oxide calcined at 700°C and 10% mid brown vanadium doped titanium oxide calcined at 1100°C with values of  $9 \times 10^5$  ohm cm and  $6 \times 10^5$  ohm cm respectively, compared with  $1.5 \times 10^7$  ohm cm and  $2 \times 10^8$  ohm cm of white titanium oxide calcined at 700°C and 1100°C respectively. Smaller reductions in the resistivity compared with that for titanium oxide were also found for 5% light cream antimony doped titanium oxide calcined at 700°C, 1% light green and 10% dark brown vanadium doped titanium oxide calcined at 700°C, 5% dark brown vanadium doped titanium oxide calcined at 700°C and 1100°C, 1% off white and 5% yellow niobium doped titanium oxide calcined at 700°C and 5% mid grey fluorine doped titanium oxide calcined at 1100°C.

None of the resistivities obtained for doped titanium oxide phases studied in this work, however, are as low as the 66 ohm cm measured for antimony tin oxide.

The lowest resistivity found for the aluminium oxide samples was  $10^6$  achieved from 1% green brown copper doped aluminium oxide and 5% red/brown copper doped aluminium oxide and both calcined at  $1100^{\circ}\text{C}$  but this is only similar to that of aluminium oxide calcined at  $1100^{\circ}\text{C}$ . ( $3.4 \times 10^6$  ohm cm).

While electrical resistivities more than about 1000 times lower than zinc oxide were achieved from 1% beige copper doped zinc oxide calcined at  $700^{\circ}\text{C}$  and 5% light green potassium doped zinc oxide calcined at  $1100^{\circ}\text{C}$  with values of  $6 \times 10^5$  ohm cm and  $5.1 \times 10^5$  ohm cm respectively compared with  $10^8$  ohm cm and  $3.6 \times 10^8$  ohm cm of white zinc oxide calcined at  $700^{\circ}\text{C}$  and  $1100^{\circ}\text{C}$  respectively, and electrical resistivities more than about 100 times lower than zinc oxide were obtained for most of the doped zinc oxide phases.

None of the resistivities obtained for doped zinc oxide phases studied in this work, however, are as low as the 66 ohm cm measured for antimony tin oxide.

The control samples of zirconium oxide, titanium oxide, aluminium oxide and antimony tin oxide used in this work were prepared by the co-precipitation method.

In order to determine whether any new phases were formed in the systems studied, X-ray powder diffractograms were taken of ZnO, 0.5 Al<sub>2</sub>O<sub>3</sub>:99.5 ZnO and 1 Al<sub>2</sub>O<sub>3</sub>:99ZnO calcined at 700°C at 1100°C. These data provide no evidence for the formation of any new phases since all the lines of the powder patterns can be assigned to ZnO. This is as expected because the 0.5% and 1% concentration of the dopant are at the lower limit for identification by X-ray powder diffraction method. The data given in Table (22) and Figures (30, 31 and 32).

As an alternative, attempts to prepare white mixed metal oxides of low resistivity by adding diluants to the antimony tin oxide were carried out in this work.

The preparative method, together with results, are explained in the following section.

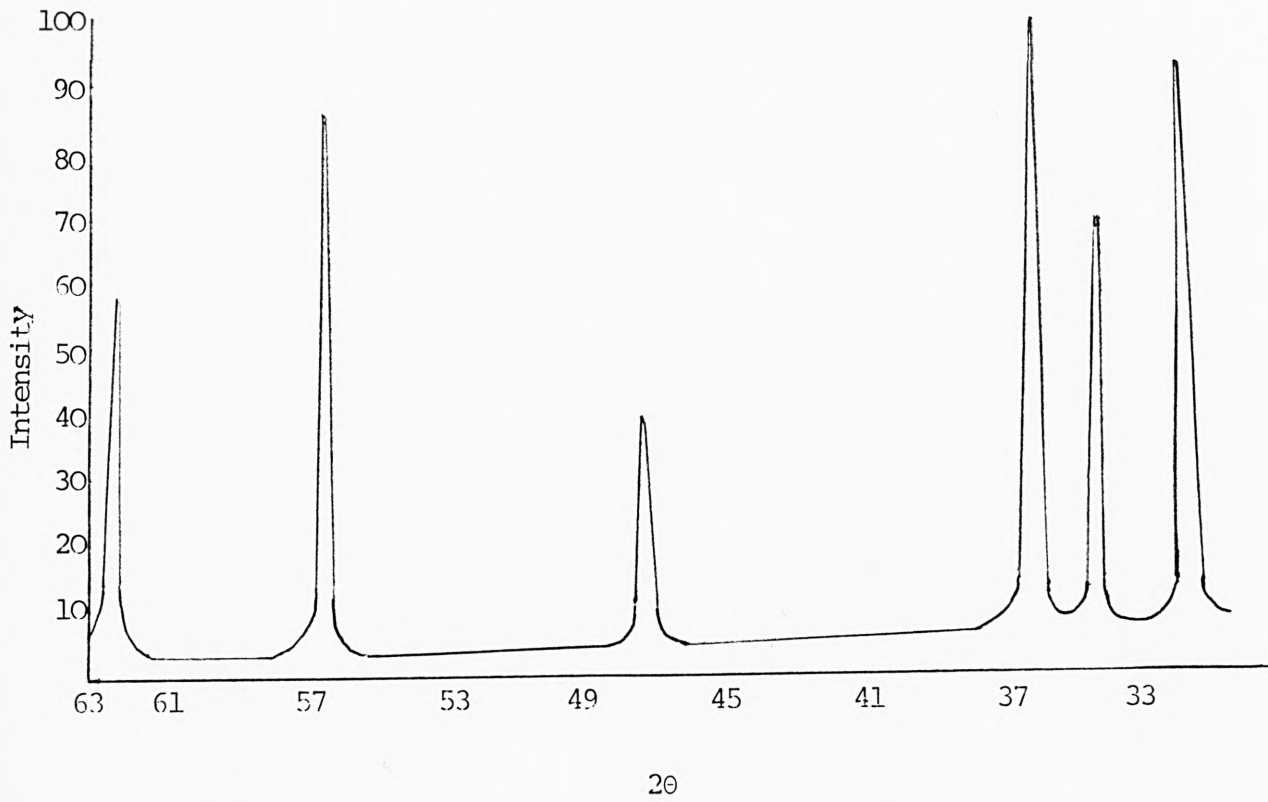


Figure (30) X-ray diffractograms of dried zinc oxide paste  
calcined at 1100°C

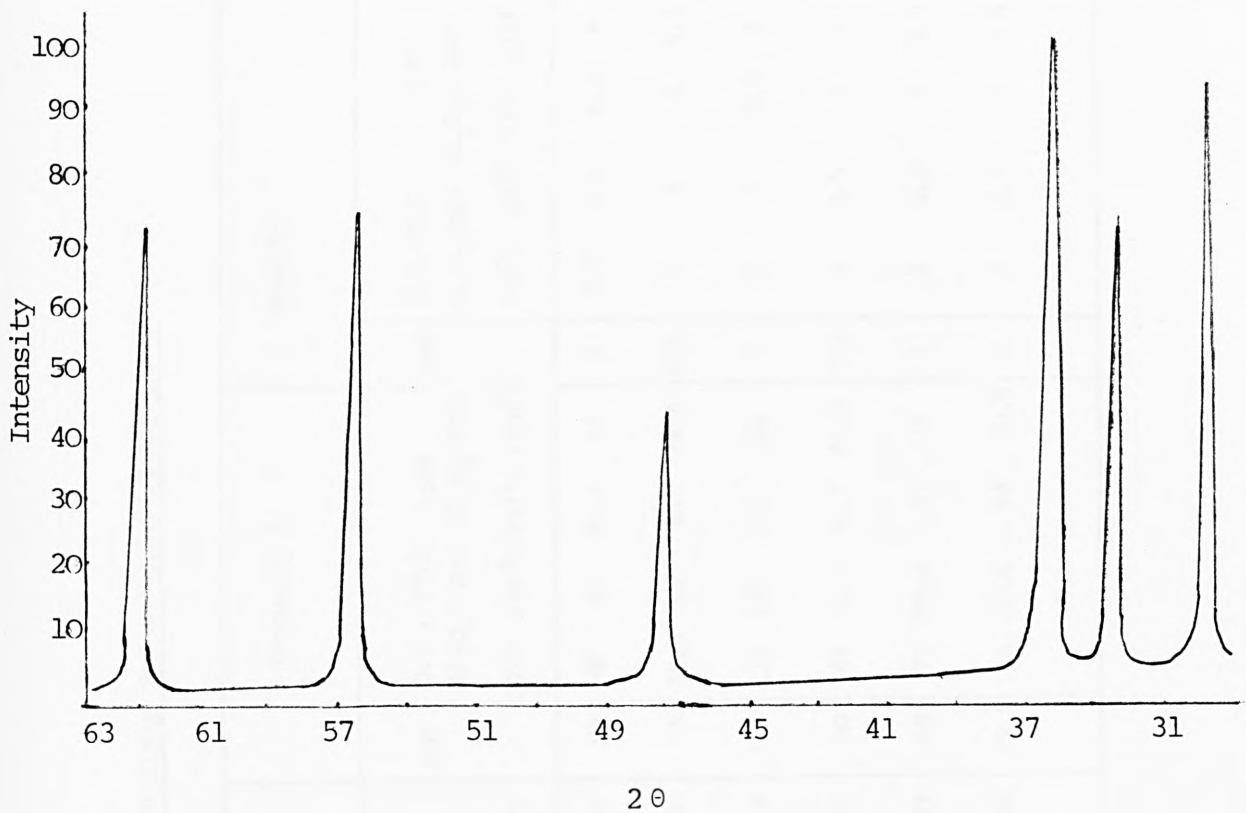


Figure (31) X-ray diffractograms of  $1\text{Al}_2\text{O}_3:99 \text{ ZnO}$  calcined at  $1000^\circ\text{C}$

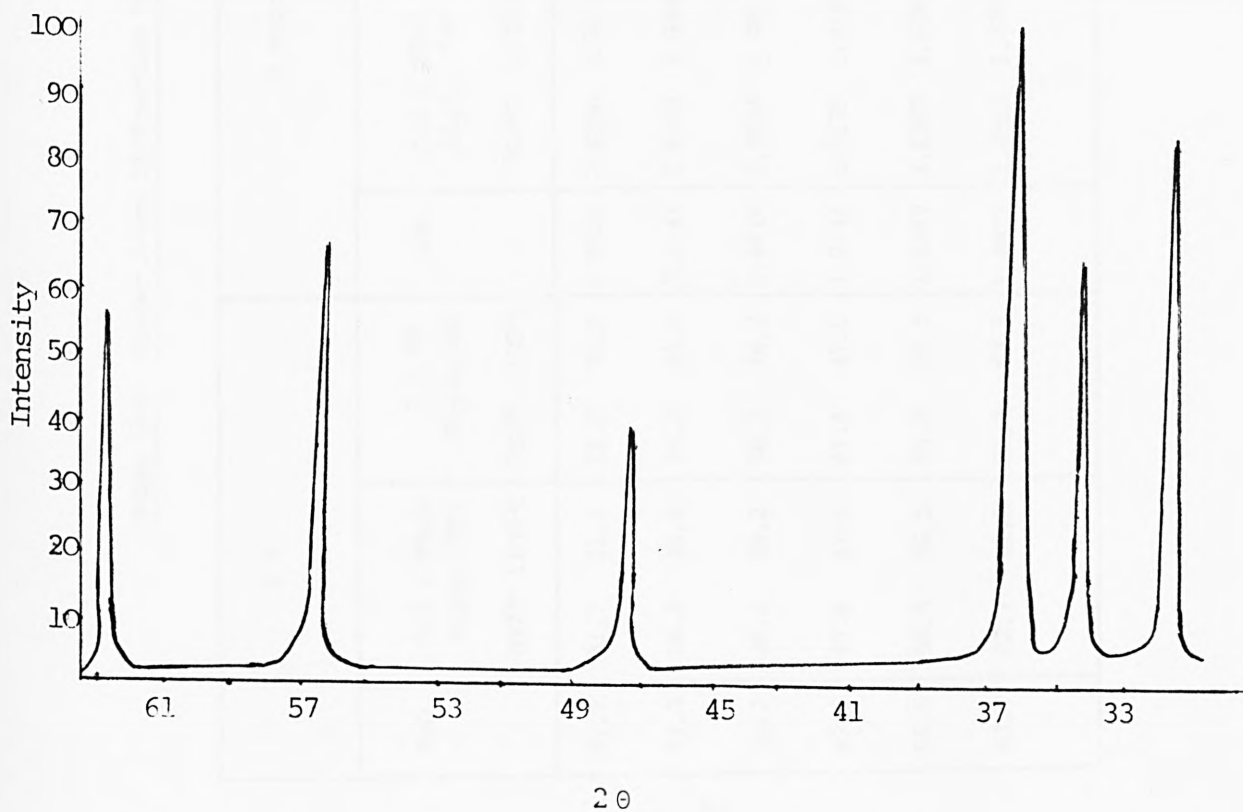


Figure (32) X-ray diffractograms of  $\text{Al}_2\text{O}_3:99.5 \text{ ZnO}$  calcined at  $1000^\circ\text{C}$

Table (22) Powder X-Ray Diffraction Data for ZnO, 1:99 Al<sub>2</sub>O<sub>3</sub>: ZnO and 0.5:99.5 Al<sub>2</sub>O<sub>3</sub>:ZnO

06

2 θ					d spacing					Intensity %					Base (I <sub>0</sub> )				
ZnO	0.5 : 99.5 Al <sub>2</sub> O <sub>3</sub> : ZnO		1 : 99 Al <sub>2</sub> O <sub>3</sub> :ZnO		ZnO	0.5 : 99:5 Al <sub>2</sub> O <sub>3</sub> : ZnO		1 : 99 Al <sub>2</sub> O <sub>3</sub> : ZnO		ZnO	0.5 : 99.5 Al <sub>2</sub> O <sub>3</sub> : ZnO		1:99 Al <sub>2</sub> O <sub>3</sub> :ZnO		ZnO	0.5:99.5 Al <sub>2</sub> O <sub>3</sub> :ZnO		1:99 Al <sub>2</sub> O <sub>3</sub> : ZnO	
	700°C	1100°C	700°C	1100°C		700°C	1100°C	700°C	1100°C		700°C	1100°C	700°C	1100°C		700°C	1100°C	700°C	1100°C
31.7	31.7	31.7	31.7	31.7	2.8226	2.8226	2.8226	2.8226	2.8226	93	89	84	80.4	95	7	5.5	5.5	6.5	6
34.3	34.3	34.4	34.3	34.4	2.6143	2.6143	2.6070	2.6143	2.6070	71	68.5	63	64	74.5	6.5	5	5	5	5.5
36.2	36.2	36.2	36.2	36.2	2.4814	2.4814	2.4814	2.4814	2.4814	132	132	132	132	132	7	5	5	5.5	6
47.5	47.4	47.5	47.4	47.5	1.9141	1.9179	1.9141	1.9179	1.9141	40	44	30.9	30.7	44.5	3.5	2	2.5	3	3
56.5	56.5	56.5	56.5	56.5	1.6287	1.6287	1.6287	1.6287	1.6287	68	75	60.2	67	73	3	2	2.5	2	2.5
62.7	62.7	62.8	62.7	62.8	1.4817	1.4817	1.4796	1.4817	1.4796	59.5	65	50.6	64	60.6	3	2	2.5	2	2.5

## Section II

### 3.3.3 An Investigation into the effects of Diluants on the Resistivity of Antimony Tin Oxide

The aim of this part of the investigation was to find an inexpensive, white filler which could be successfully blended with 6.5:93.5 antimony tin oxide to yield a new composite material of low resistivity.

The materials considered in this work as diluants are: zirconium oxide, titanium oxide, aluminium oxide and clays supplied by English China Clays.

The experimental procedure adopted was as follows: Tin(IV) chloride penta hydrate (20g) was dissolved in acidified distilled water [50 ml water + 10 ml hydrochloric acid]. Antimony chloride (0.935g) was dissolved in [20 ml water + 10 ml hydrochloric acid] and was added to the solution of tin(IV) chloride to give 6.5:93.5 antimony tin oxide. Diluant was then added to the solution of mixed chlorides to give levels of 10, 25 and 50% diluant in the doped antimony tin oxide.

A mixture was then homogenised by stirring for 20 minutes. Sodium hydroxide solution 40% was then added to

the mixture to precipitate out the doped hydrous antimony tin oxide on the diluant particles. The resulting precipitation was washed with water by decantation to  $\text{pH} < 7$  and then oven dried at  $110^{\circ}\text{C}$ . The dried material was ball milled for 15 minutes and calcined at  $750^{\circ}\text{C}$  for 3 hrs.

Resistivity analysis was carried out using the powder conductivity cell described in Section 3.2.1.

Zirconium oxide and aluminium oxide used in these experimental trials were laboratory grade reagent. Titanium oxide used was from either laboratory grade reagent or from several batches of Ti-Oxide Ltd. while the clays used in this work came from several batches of English Clays Lovering Pochin & Co. Ltd.

The control sample of antimony tin oxide used in the above trial was prepared as follows:

Tin(IV) chloride penta hydrate (20g) was dissolved in acidified distilled water [50 ml water + 10 ml hydrochloric acid]. Antimony chloride (0.935g) was dissolved in [20 ml water + 10 ml hydrochloric acid] and was added to the solution of tin(IV) chloride to give 6.5:93.5 antimony tin oxide. Sodium hydroxide solution 40% was then added to the solution of mixed chlorides to precipitate out a mixed antimony hydroxide/hydrous tin(IV) oxide gel. The resulting precipitation was washed with water by decantation to  $\text{pH} < 7$

and then oven dried at 110°C. The dried material was ball milled for 15 minutes and was calcined at 750°C for 3 hrs to give antimony tin oxide as a dark grey/blue powder.

#### 3.3.4 Results and Discussion

Antimony tin oxide prepared in this work was a dark grey/blue powder with resistivity of 66 ohm cm.

Electrical behaviour of antimony doped tin oxide have been investigated by many workers.<sup>6,7,8,9</sup> Herman et. al<sup>6</sup> and Pyke et. al<sup>7</sup> reported that the dark blue crystals of antimony tin oxide represent the phase  $\text{SnO}_2 \cdot n\text{Sb}_2\text{O}_4$ . Pyke, Reid and Tilley<sup>7</sup> reported that the X-ray and analytical evidence showed that the antimony tin oxides are very close in composition to  $\text{SnO}_2$  (pale yellow), but that the dark blue coloration could be explained in terms of a charge transfer between  $\text{Sb}^{3+}$  and  $\text{Sb}^{5+}$  sites in the  $\text{SnO}_2$  matrix rather than to the presence of  $\text{Sn}^{2+}$ . In order that charge transfer of this type should take place, it would be necessary for both the cations to be in similar geometrical sites and in close proximity to each other, this can be achieved by introduction of  $\text{Sb}^{3+}$  and  $\text{Sb}^{5+}$  ions into the  $\text{SnO}_2$  matrix where they could occupy interstitial octahedral sites to form an oxide of composition  $\text{Sb}_x^{3+}\text{Sb}_x^{5+}\text{SnO}_2$  or alternatively substitute into the tin positions to form an oxide of formula  $(\text{Sb}_x^{3+}\text{Sb}_x^{5+})\text{Sn}_{1-2x}\text{O}_2$ . It has been shown that calcination of

the milled mixed oxide samples is necessary to incorporate the dopant species into the host crystals lattice, by a crystal growth mechanism which occurs at elevated temperatures.

Samples before calcination are simple mixtures of host and dopant species, but during the calcination treatment amorphous particles of material anneal together to form a coherent structure. It is only after calcination that the dopant species becomes fully incorporated into the crystal lattice to give semiconducting materials. The work carried out by Herman *et. al*<sup>6</sup> and Portefaix *et. al*<sup>8</sup> however, showed that the calcination temperatures were important and that calcination of homogeneous samples of antimony tin oxide at temperatures in excess of 773°C caused demixing of the oxides and flat sheets of antimony tetraoxide ( $Sb_2O_4$ ) were positively identified in the bulk phase of the material by X-ray crystallographic methods. The best conducting is achieved from materials calcined at about 700-750°C. Material obtained at higher and lower temperatures has poorer conductivity because of antimony oxide precipitation and failure to incorporate the Sb in the oxide lattice respectively.

10

Evidence exists to suggest that the main conducting mechanism in antimony tin oxide is a surface rather than a bulk effect. The main aim of precipitating the antimony tin

Table (23)

Resistivities of Zirconium dioxide, Titanium dioxide and Aluminium oxide doped Antimony tin oxide phases

Dopant	% wt dopant	% wt 6.5:93.5 Sb <sub>2</sub> O <sub>3</sub> :SnO <sub>2</sub>	Resistivity $\Omega$ cm	Colour	Particle size of the dopant ( $\mu$ )
ZrO <sub>2</sub>	0	100	$0.66 \times 10^2$	dark blue	13.8
	10	90	$1.6 \times 10^2$	grey	
	25	75	$2.2 \times 10^4$	grey	
	50	50	$5.2 \times 10^5$	grey	
TiO <sub>2</sub>	10	90	$9.8 \times 10^5$	grey	206
	25	75	$1.2 \times 10^6$	light green	
	50	50	$9 \times 10^5$	light green	
Al <sub>2</sub> O <sub>3</sub>	10	90	$3.9 \times 10^7$	grey	206
	25	75	$6.8 \times 10^7$	light green	
	50	50	$2.5 \times 10^9$	off white	

Table (24)

Resistivities of Titanium dioxide CLD 1769  
doped Antimony Tin oxide phases

Dopant	% wt dopant	% wt 6.5:93.5 Sb <sub>2</sub> O <sub>3</sub> :SnO <sub>2</sub>	Resistivity $\Omega$ cm	Colour	Particle size of the dopant ( $\mu$ )
CLD1769/1	0	100	$0.66 \times 10^2$	dark blue	1.36
	10	90	$3.1 \times 10^2$	grey	
	25	75	$5.2 \times 10^4$	light green	
	50	50	$2.1 \times 10^4$	off white	
CLD1769/2	10	90	$5.5 \times 10^2$	grey	1.22
	25	75	$1.6 \times 10^3$	light green	
	50	50	$3.5 \times 10^4$	off white	
CLD1769/3	10	90	$4.8 \times 10^2$	grey	1.22
	25	75	$3.1 \times 10^3$	grey	
	50	50	$7.7 \times 10^4$	light grey	
CLD1769/4	10	90	$9.1 \times 10^2$	grey	1.22
	25	75	$1.3 \times 10^3$	light grey	
	50	50	$4.7 \times 10^4$	light grey	
CLD1769/5	10	90	$2.4 \times 10^3$	light grey	1.22
	25	75	$1.5 \times 10^3$	light grey	
	50	50	$1 \times 10^4$	light grey	
CLD1769/6	10	90	$2.3 \times 10^3$	grey	1.22
	25	75	$3.9 \times 10^3$	grey	
	50	50	$7.9 \times 10^4$	light grey	
CLD1769/7	10	90	$3.5 \times 10^5$	grey	1.28
	25	75	$5.1 \times 10^5$	grey	
	50	50	$8.1 \times 10^5$	light grey	
CLD1769/8	10	90	$3.6 \times 10^5$	grey	1.28
	25	75	$5.5 \times 10^5$	light grey	
	50	50	$1.4 \times 10^6$	light grey	

**Table (25)**

Resistivities of porous and non-porous materials doped  
Antimony Tin oxide phases

Dopant	% wt Dopant	% wt 6.5:93.5 Sb <sub>2</sub> O <sub>3</sub> :SnO <sub>2</sub>	Resistivity Ω cm	Colour	Particle size of the dopant (μ)
RLO 3311	0	100	0.66 x 10 <sup>2</sup>	dark blue	
porous mullite,	10	90	2.1 x 10 <sup>3</sup>	grey	30.28
surface area	25	75	1.3 x 10 <sup>3</sup>	grey	
3m <sup>2</sup> .g <sup>-1</sup>	50	50	3.4 x 10 <sup>3</sup>	light grey	
RLO 3312	10	90	2 x 10 <sup>4</sup>	grey	67.04
porous mullite,	25	75	1.3 x 10 <sup>5</sup>	grey	
surface area	50	50	1.8 x 10 <sup>5</sup>	off white	
40m <sup>2</sup> .g <sup>-1</sup>					
RLO 3313	10	90	5.2 x 10 <sup>4</sup>	grey	4.58
Alphagloss,	25	75	2 x 10 <sup>5</sup>	grey	
fine American	50	50	1.6 x 10 <sup>6</sup>	grey	
Clay					
RLO 3314	10	90	8.5 x 10 <sup>2</sup>	grey	5.34
SPS, fine	25	75	7.7 x 10 <sup>4</sup>	grey	
English Clay	50	50	3.7 x 10 <sup>5</sup>	light grey	

oxide on diluant particles is therefore to achieve a conducting coating on the inert diluant with the minimum reduction in surface conductivity. A secondary aim is the production of lighter coloured materials because of mixing, the blue antimony tin oxide with the white diluant materials. The results obtained from diluting antimony tin oxide with various levels of zirconium dioxide, titanium dioxide and aluminium oxide are contained in Table(23) and those obtained from a series of titanium dioxide samples with low particle size are in Table (24). The resistivities of antimony tin oxide diluted with porous and non-porous clays are given in Table (25).

The results show that there is always a loss of conductivity of the antimony tin oxide on dilutions but that reasonable resistivity values ( $<10^3$  ohm.cm) can be achieved by dilution with 10%  $ZrO_2$ , 10%  $TiO_2$  and 10% clay (RLO 3314). Doping with higher levels of diluent resulted in increasingly higher resistivities.

### 3.4 Conclusion

The results show that doping antimony tin oxide with a white diluant phases  $ZrO_2$ ,  $TiO_2$ ,  $Al_2O_3$  and clays is a more satisfactory way of achieving low chromophoricity while retaining useful conductivity than doping oxide phases similar to the diluant with other ions. For titanium

dioxide for example the lowest resistivity achieved in doping experiments was  $6 \times 10^5$  ohm.cm while values of  $10^4$ - $10^6$  ohm.cm can be achieved by doping antimony tin oxide with 50%  $TiO_2$ .

The overall conclusion of this part of the work is that dilution of antimony tin oxide can give materials of lower chromophoricity but that loss of conductivity does occur in the process and the doped materials could only be used where resistivities of  $10^2$ - $10^4$  ohm.cm were acceptable.

References

1. 2600/3600 particle size handbook
2. G.D. Parfitt, "Dispersion of powders in liquids", second edition, 1973.
3. S.J.E. Clark, personal communication.
4. U.K. patent, appl. 2,094,013.
5. J.D. Donaldson, personal communication.
6. J.M.J. Herman, J.L. Portefaix, M. Forisser, F. Figueras, P. Pichat, J.Chem.Soc., Faraday Trans.1, 1979, 75(6), 1346.
7. D. Pyke, R. Reid, R.J.D. Tilley, J. Solid State Chem., 1978, 25, 231.
8. J.L. Portefaix, P. Bussiere, J.P. Forisser, J.M. Friedt, J.P. Sanchez, F. Theobald, J.Chem.Soc., Faraday Trans.I, 1980, 76(8), 1952.
9. M.K. Paria, H.S. Maiti, J.Mater.Sci., 1982, 17(11), 3275.
10. S.A. Lawrence, Ph.D. thesis, London, 1984.

## CONTENTS

<u>CHAPTER FOUR:</u>	<u>Natural fibres reinforced thermoplastics</u>	<u>PAGE</u>
4.1	Introduction	102
4.2	The chemical composition of keratins	108
4.3	Strength and the stress-strain curve	110
4.4	Experimental	116
4.4.1	Preparation of composites	116
4.5	Results and discussion	118
4.5.1	Study of the effect of dispersing natural fibre on the physical properties of polymer systems	118
4.5.2	Study of the effects of dispersing coupling agent additives on the physical properties of the composites	130
4.6	Conclusion	154
4.7	References	155

## CHAPTER FOUR

### Natural fibres reinforced thermoplastics

#### 4.1 Introduction<sup>1</sup>

Polymer engineers using thermoplastics often have a requirement for improved properties of the polymers in terms of strength, rigidity, dimensional stability, conductivity etc. One means of altering these properties is to produce a composite material in which an additive is dispersed in the polymer to achieve improvements in properties. The work described in this chapter deals with the use of natural fibres as an additive to improve the tensile and compressive strengths of polymers.

Many combinations of reinforcements and thermoplastics are used in industry to effect a diversity of performance and cost characteristics in materials. Almost any thermoplastic property can be improved or changed to meet desired requirements. Typical resins being commercially used include nylon, polyethene, polypropylene, polycarbonate, polystyrene, ABS, SAN, polyphenylene oxide, polyvinyl chloride, polysulfone and urethane. The most common reinforcements used are glass and asbestos fibres in different forms including glass in continuous roving, chopped

strand glass and milled asbestos. Other materials that have been used include molybdenum disulphide, carbon black, talc, graphite, calcium carbonate and silica flour.

The addition of a fibre to a polymer can have either beneficial or undesirable effects depending upon the circumstances. The reinforcement can cause an increase in hardness and abrasion resistance, and decrease in mould shrinkage, creep and dimensional changes with humidity. Undesirable effects include opacity, occasional fibrous appearance, lower surface gloss and loss of mechanical flexibility.

The polymer and the reinforcing components do not merge completely into each other. Normally the components can be physically identified along with the interface between them. The behaviour and properties of the interfaces formed generally control the properties of the composite. Some of these properties develop gradually with increasing reinforcement, while others change sharply. Properties such as: impact strength and heat distortion temperature also depend very much on the specific thermoplastics.

Since the 1940's when engineered composites or reinforced plastics were first described, fibreglass has continued to be the most widely used ingredient. New type

composites such as graphite, boron, whiskers and natural fibre will provide even more potential for greater advancement in the future.

In some cases the bond between the polymer and reinforcing fibre has been improved by the use of coupling agents. Several different theories have been advanced in order to explain how the coupling agents incorporated into resins improve the reinforcement resin bond. Extensive research since the 1940's has been developed with effective coupling agents for thermosetting resins.

The surface of most fibres, glass, asbestos, silicon carbide, boron, etc. either possesses, or may easily be prepared with surface oxides, which are readily hydrolysed. Polyester resins, for example, do not adhere readily, in particular to fibreglass, where the strength properties are severely reduced by accumulation of water at the interface, a large range of coupling agents has been developed. These are chemical compounds originally designed to link with the oxide, hydroxide, sulphide or other charged surface groups on fibres and provide organic groups to combine with the resin. An extension of this idea is to coat fibres immediately after preparation, a process which reduces abrasion as well as keeping out excessive damp.

Manufacturers have developed coupling agent systems that provide greatly improved properties in specific thermoplastic systems. Various forms of continuous reinforced thermoplastic sheets are available using combinations of the different reinforcements described in this introduction. To date most of the resins used are polyvinyl chlorides and polystyrenes.

These types of sheet materials are relatively new to industry. They are being used principally in captive compression moulding operations. Being thermoplastics, they can be heat-formed into various shapes. Applications include automotive parts, aircraft parts, building panels, storage tanks, containers, electronics and housewares.

The properties of reinforced thermoplastics from various manufacturers can vary because of differences in fibre dispersion, fibre length and fabrication procedure.

A major development in improving properties and lowering costs of reinforced thermoplastics is now in process since these types of materials are recognised as an important part of future composite growth.

The work undertaken in this project involves studies of the mechanical properties of selected reinforced polymers

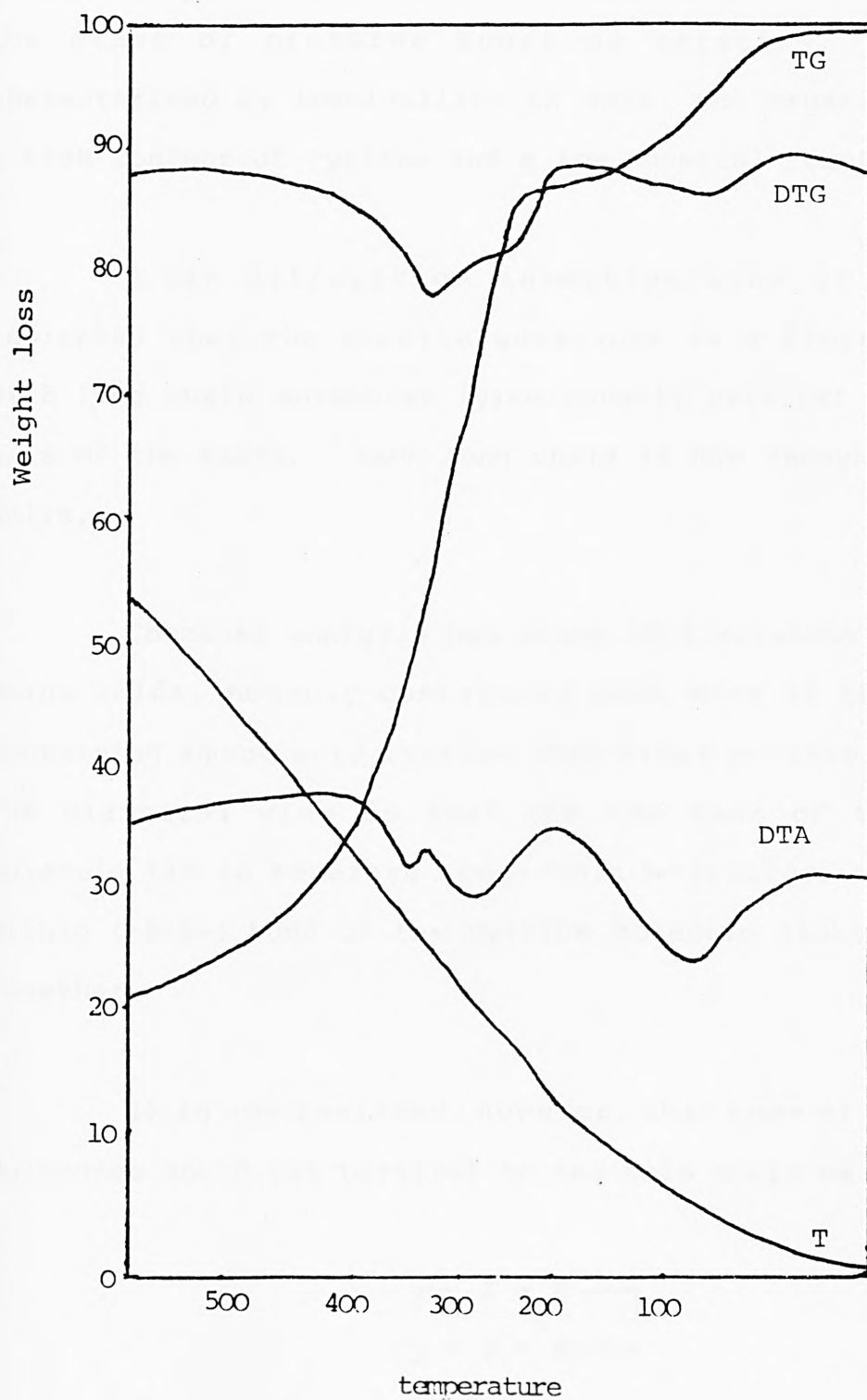
using hair as a reinforcement. Three properties of the reinforcing polymer are considered, namely, the modulus of elasticity (Young's Modulus), the ultimate tensile strength and the elongation to failure.

The polymers considered in this work are polyvinyl chloride and polyethene. These polymers are available commercially as fine powders. The hair used in this work was supplied by Ferrocom Ltd., and was used in the form of either chopped or powdered hair.

Attempts to powder normal hair failed to give a powder in a reasonable time scale, but hair dried at 130°C could be powdered with ease, although hair cut to short lengths and dried could be reduced to powder more easily than samples of long hair dried at 130°C. The thermogram of hair supplied Figure (33) shows that the weight loss at 130°C is 11%.

The hair was cut to approximately 3cm lengths and oven dried at 130°C for an hour. The dried hair was then ball milled for three hours to give a grey material of small particle size (53-87 $\mu$ ). While 2mm lengths of hair were prepared by cutting.

Figure (33) DTA trace of the hair fibre



#### 4.2 The chemical composition of keratins<sup>2,3</sup>

Wool, horn, hoof, feathers and hair all belong to the class of proteins known as keratins. They are characterised by insolubility in water and organic solvents, a high content of cystine and a low chemical reactivity.

X-ray diffraction investigations of hair have indicated that the keratin substance is a fibrous protein with long chain molecules lying roughly parallel to the main axis of the fibre. Each long chain is now thought to form a helix.

Chemical analysis has shown that keratine contains 18 amino acids, notably containing much more of the sulphur-containing amino acid cystine than other proteins Table(26). The classical view is that the two ends of the cystine molecule lie in separate long-chain molecules, and that the dithio (-S-S-) bond of the cystine molecule links the chains together.

It is now realised, however, that some of the cystine molecules could lie parallel to the main chain as follows:

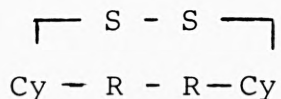


Table (26)

Approximate percentage by weight of the different amino acids in human hair

Alanine	2.8
Arginine	8.9
Aspartic acid	3.9
Cystine	18.0
Glutamic acid	13.6
Glycine	4.1
Histidine	1.2
Isoleucine	4.8
Leucine	6.4
Lysine	1.9
Methionine	0.7
Phenylalanine	2.4
Proline	4.3
Serine	10.6
Threonine	8.5
Tryptophan	1.0
Tyrosine	2.2
Valine	5.5

Additional linkages between the long chains are brought about by the ionization of COOH and NH<sub>2</sub> groups to form salt links:



A third method of linkage is provided by hydrogen bonds.

#### 4.3 Strength and the stress-strain curve<sup>4</sup>

Deformation occurs when forces are applied to a material. Strain is the amount of deformation per unit length, while stress is the force per unit area.

If this tensile stress induces a stretch to length ( $l_1$ ) then the tensile strain  $\epsilon_1$  is defined as:

$$\epsilon_1 = \frac{l_1 - l_0}{l_0}$$

Taking the stressing operation to the ultimate, that is increasing the force until the material breaks, tensile strength (ultimate tensile stress):

$$\sigma = \frac{F}{A}$$

where  $\sigma$  = tensile strength (Kgf/cm<sup>2</sup>)

F = force at failure

A = area of cross-section at failure

Most tensile strengths are based on the original cross-section ( $A_0$ ) since this is easily measured, before the test is started. As the material stretches under the load, the area of cross-section will decrease. Ultimate elongation, or elongation at break, equals:

$$l - l_0$$

where  $l$  is the length at failure

This is usually expressed as a percentage of original length:

$$\frac{l - l_0}{l_0} \times 100\%$$

According to Hooke's law, for an ideal elastic solid stress is proportional to strain Figure (34a). But in fact no plastic material comes very close to this ideal. Expressed in the form of stress-strain diagrams, plastics exhibit five possibilities as shown in Figure(34b).

A general plot of stress-strain is shown in Figure (35).

where  $\sigma_y$  = yield stress

$\epsilon_y$  = elongation at yield

$\sigma_B$  = ultimate tensile strength

$\epsilon_B$  = ultimate elongation or  
elongation at break

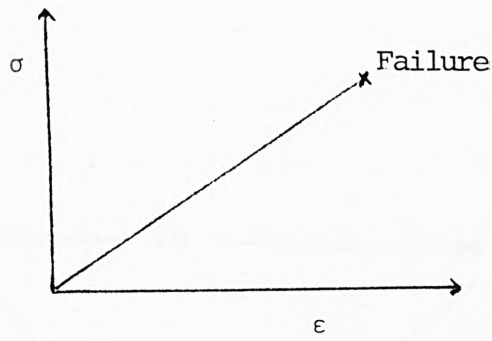
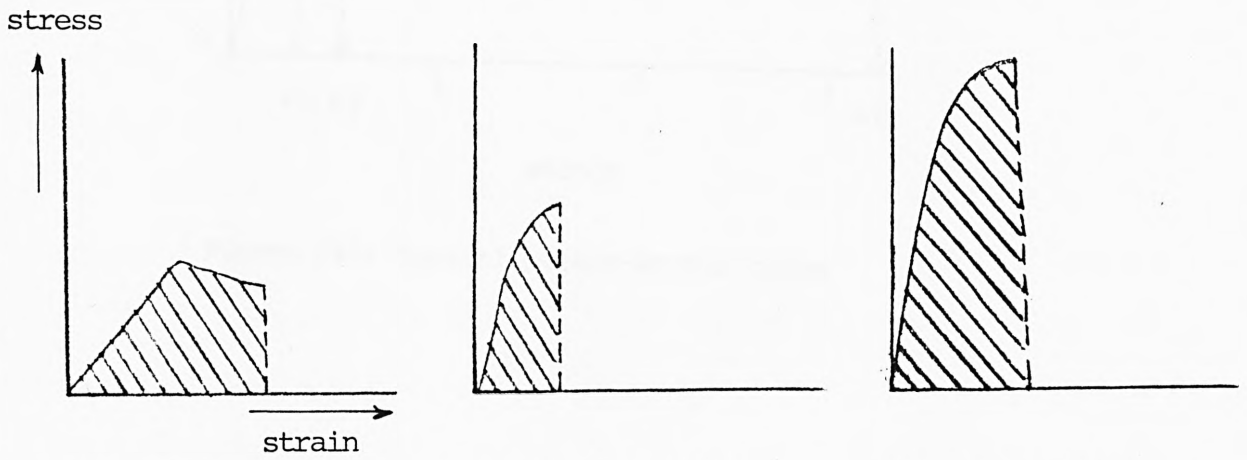


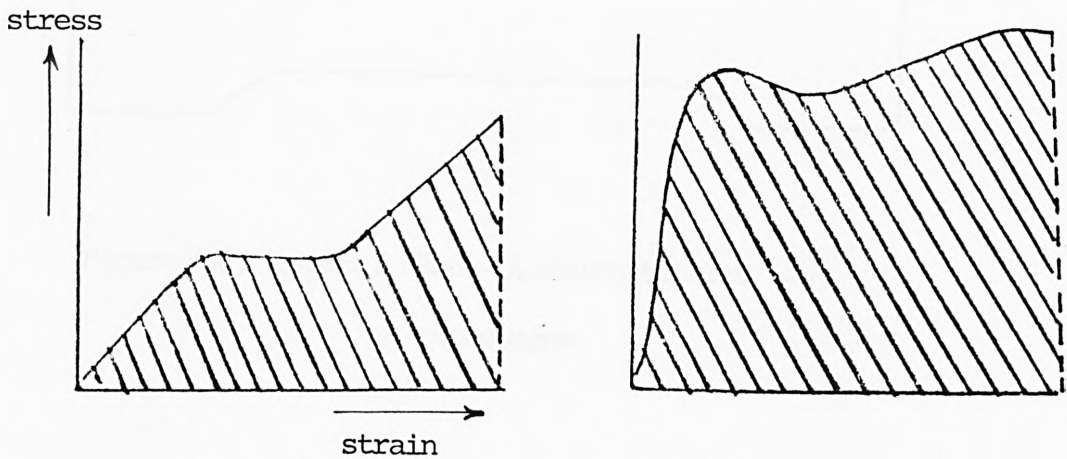
Fig. (34a) Hookean behaviour



(a) soft, weak

(b) hard, brittle

(c) hard, strong



(d) soft, tough

(e) hard, tough

Fig.(34b) Stress - strain behaviour of various types of plastics

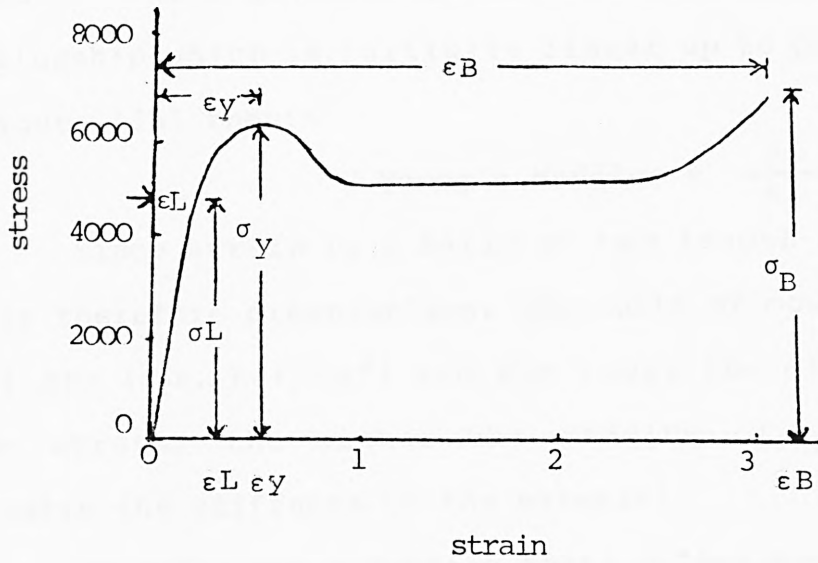


Figure (35) Typical stress-strain curve

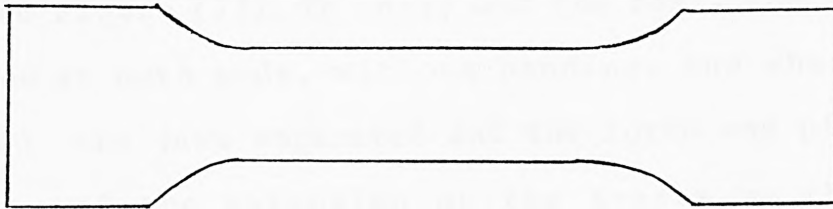


Figure (36) Typical sheet plastics tensile test

specimens

A Hookean material Figure (34a) has already been defined and the constant ratio  $\frac{\sigma}{\epsilon}$  is called the "Young's Modulus". If a given plastic material has a stress-strain relationship which is initially linear up to position (L) as in Figure (35) then:-

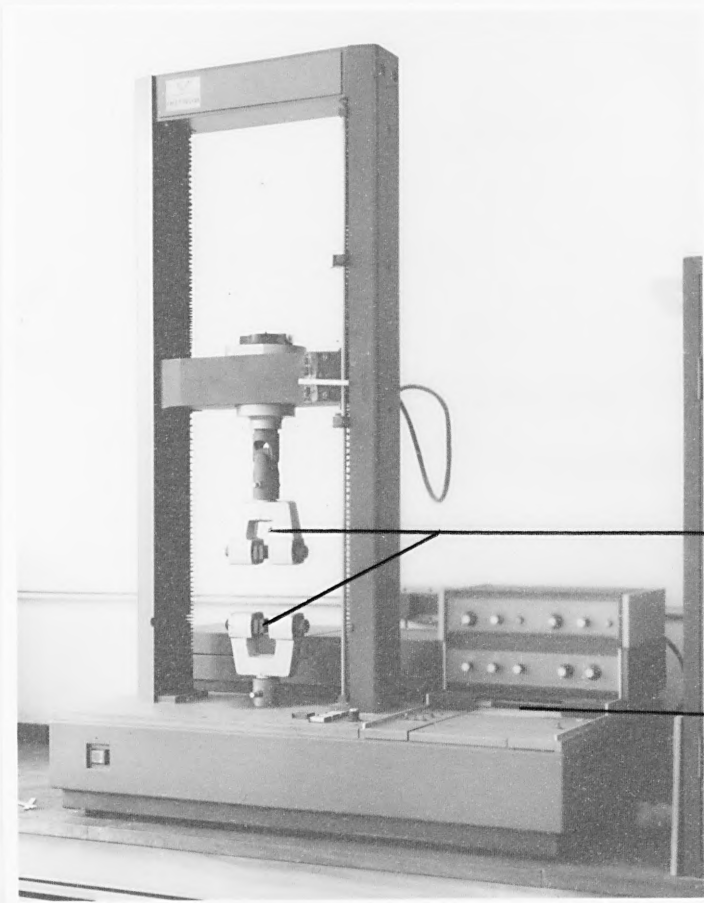
$$\text{Young's Modulus} = \frac{\sigma L}{\epsilon L}$$

Since strain is a ratio of two length measurements, and is therefore dimensionless, the units of modulus are those of stress (i.e. Kg/cm<sup>2</sup>) and the lower the extension for a given stress, the higher the modulus, i.e. the modulus indicates the stiffness of the material.

To carry out a tensile test, a "dog bone" specimen is normally employed Figure (36) and stress applied until failure takes place to obtain a breaking load on a measured cross-sectional area.

The tensile strength, Young's modulus and elongation were measured on an Instron machine which is a self-aligning grip system Figure (37). To carry out the test, the specimen was gripped at both ends, without bending, and when stress was applied, the jaws separated and the force was plotted on the Y-axis and the extension on the X-axis by the chart recorder.

Most plastics tests are conducted on constant rate of transverse machines and thus low speeds are used for virtually inextensible materials, i.e. rigid PVC (25±6mm/min) and high speeds for highly extensible materials, i.e. flexible PVC sheet (280±25mm/min), polyethene (460±75mm/min).



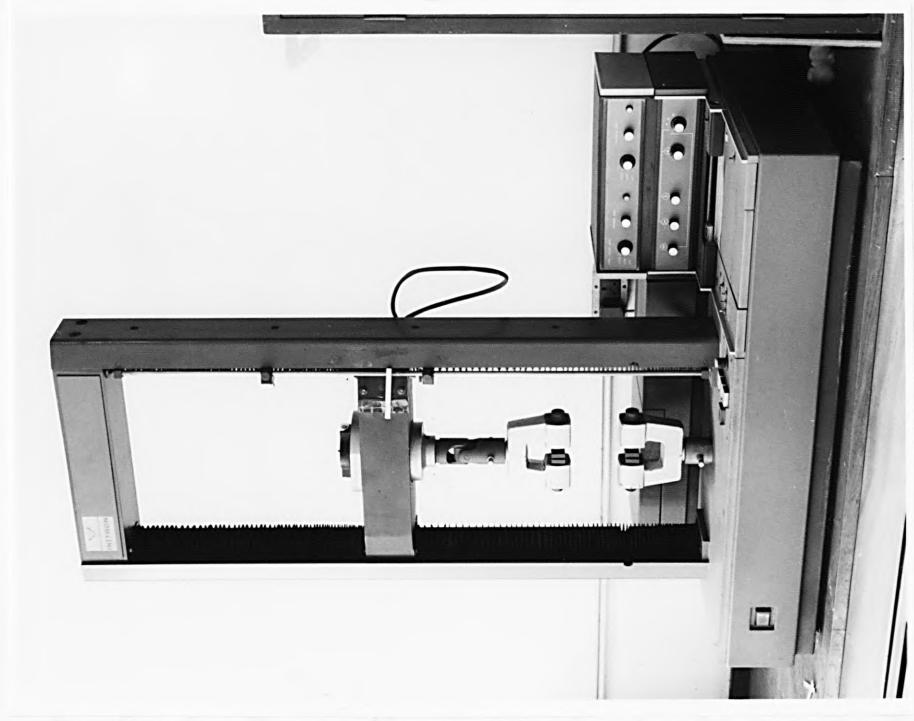
Jaws

Chart recorder

Figure (37) Instron machine

## Experimental

### 3.1 Preparation of the system



Construction of the rheometer system

A rheometer of the appropriate weight ratio of polyethylene and polypropylene was used. The rheometer was then blended on the two rollers. The rheometer was then blended on the two rollers. The rheometer was then blended on the two rollers.

#### 4.4 Experimental

##### 4.4.1 Preparation of Composites

The aims of this work are to study the methods of dispersion of hair in various types of polymer and to ascertain the effects of the dispersion of hair on the properties of the polymers.

The mechanical properties considered in this work are:-

- The modulus of elasticity (Young's modulus)
- The ultimate tensile strength
- The elongation to failure

Composites of the hair and selected polymer systems were prepared by the following method.

##### (a) Composites of hair with polyethene systems:-

A mixture of the appropriate weight ratio of polyethene and powdered hair or 2mm length hair was ball-milled for five minutes to achieve a homogeneous mix. The mixture was then blended on the two roll mill Figure (5). The front and rear rollers of the

mill were set at 95°C and 100°C respectively and the mixture was milled until a homogeneous crepe was formed. This crepe was then removed from the mill and sandwiched between two "Milinex" sheets and placed in a stainless steel mould of dimensions 0.3 x 15.2 x 15.2 cm. The mould was then placed in a press Figure (6) and heated to 130°C for two minutes at ambient pressure before being pressed at  $5.5 \times 10^6 \text{ Pa}$  for a further two minutes. The mould was then removed and placed in a fly press Figure (7) to keep the polymer flat as it cooled.

b) Composites of hair with polyvinyl chloride systems:

The mixture of PVC and powdered or 2mm lengths of hair and 1 phr stabilizer (basic lead carbonate) was ball-milled for five minutes to achieve a homogenous mix. The plasticiser di-iso-octyl-phthalate was added to the mixture and then blended on the two roll mill Figure (5). The front and rear rollers of the mill were set at 120°C and 125°C respectively and the mixture was milled until a homogeneous crepe was formed. This was then removed from the mill and sandwiched between two "Milinex" sheets and placed in a stainless steel mould of dimensions 0.3 x 15.2 x 15.2 cm. The mould was then placed in a press Figure (6) and heated to 150°C for two minutes at ambient pressure before being pressed at  $5.5 \times 10^6 \text{ Pa}$  for a further two minutes. The mould was then removed and placed in a fly press Figure (7) to keep the polymer flat as it cooled.

## 4.5 Results and discussion

### 4.5.1 Study of the effect of dispersing natural fibre on the physical properties of polymer systems

This Section deals with the results obtained from the study of the physical properties of composites of polyethene and polyvinyl chloride with natural fibre.

#### Polyethene systems

It is evident from Table (27) and Figures ( 38,39) that the tensile strengths and Young's moduli of the composites containing powdered hair increase with increasing fibre load up to the limits investigated (i.e. 0-20% wt fibre). While the elongation of the composites decreases with increasing fibre load.

A tensile strength of 124 Kgf/cm<sup>2</sup> was achieved with 20% wt powdered hair compared with 105 Kgf/cm<sup>2</sup> for unreinforced polyethene. A Young's modulus of 4900 Kgf/cm<sup>2</sup> was achieved with 20% wt powdered hair compared with 2600 Kgf/cm<sup>2</sup> for unreinforced polyethene.

The tensile strengths and the Young's moduli of the composites containing 2mm length hair increase with increasing fibre load up to the limits investigated (i.e. 0-25% wt fibre) except with 5% wt fibre, a decrease in tensile

Figure (38) Tensile strength vs. composition of polyethene/powdered hair phases

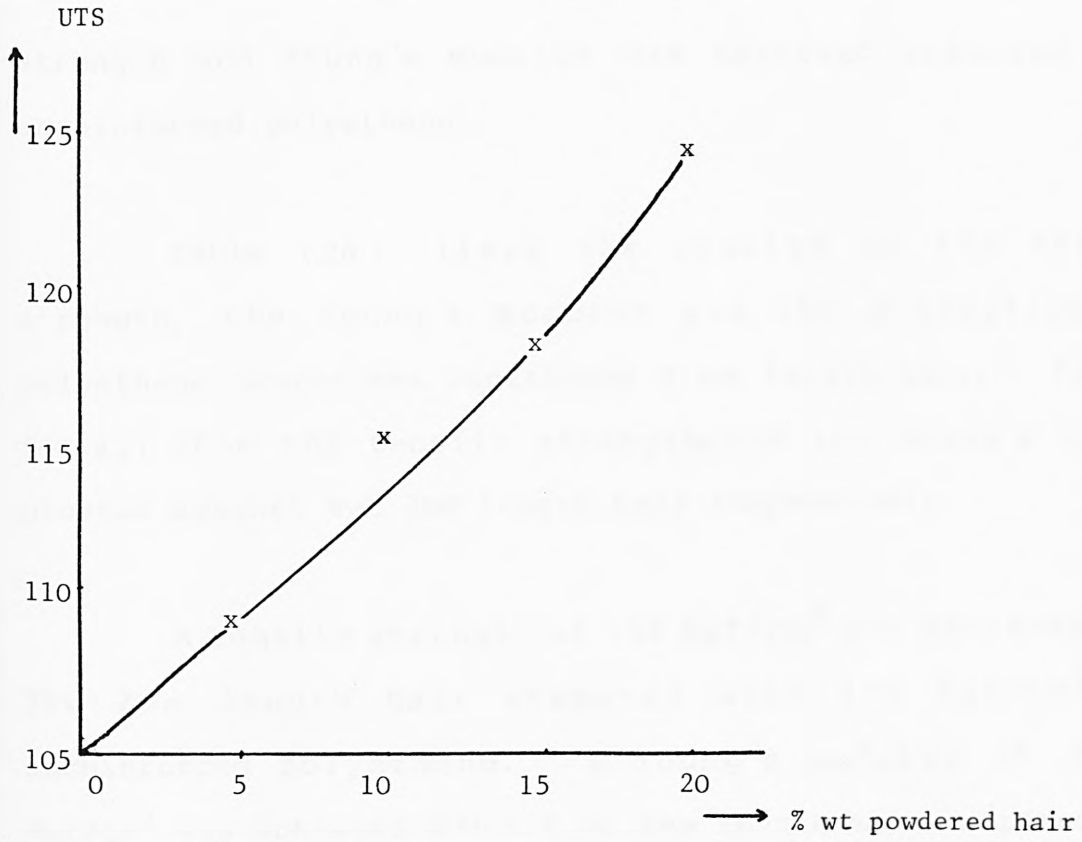
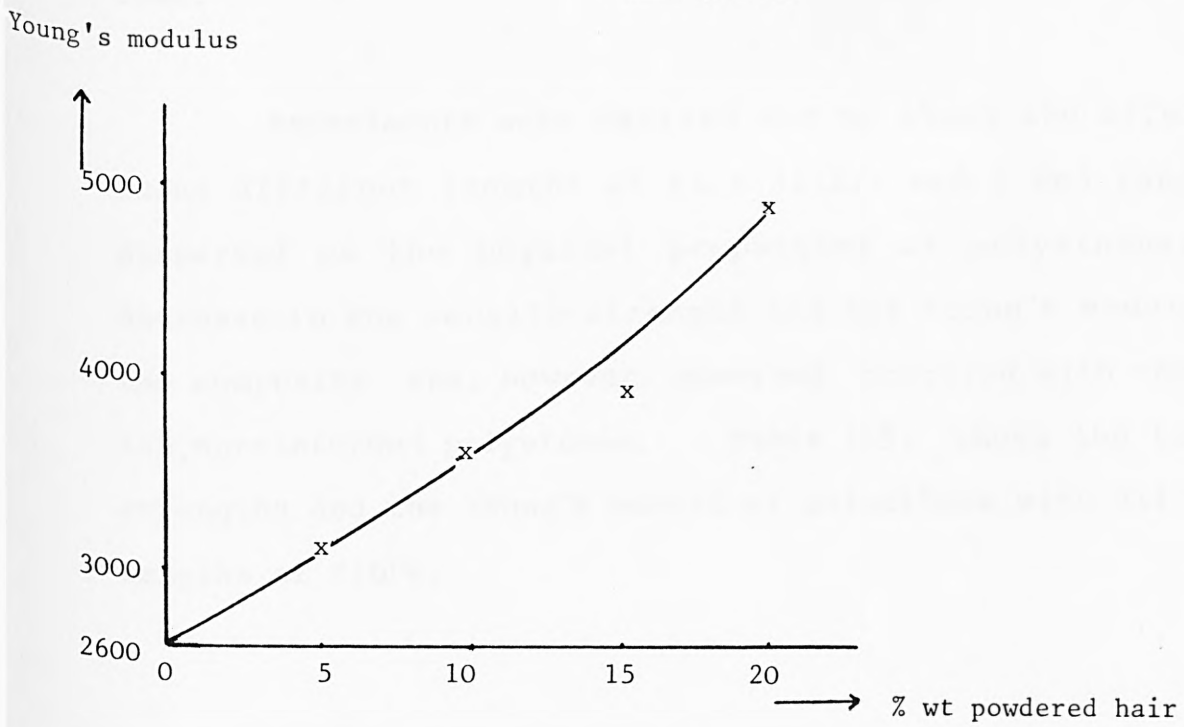


Figure (39) Young's modulus vs. composition of polyethene/powdered hair phases



strength and Young's modulus was observed compared with unreinforced polyethene.

Table (28) lists the results of the tensile strength, the Young's modulus and the elongation for polyethene composites containing 2 mm length hair. Figures (40,41) show the tensile strengths and the Young's moduli plotted against %wt 2mm length hair respectively.

A tensile strength of  $108 \text{ Kgf/cm}^2$  was achieved with 25% 2mm length hair compared with  $105 \text{ Kgf/cm}^2$  for unreinforced polyethene. A Young's modulus of  $4320 \text{ Kgf/cm}^2$  was achieved with 25% wt 2mm length hair compared with  $2600 \text{ Kgf/cm}^2$  for unreinforced polyethene. While the elongation of the composites decreases with increasing fibre load.

Experiments were carried out to study the effect of using different lengths of hair (1,2,3 and 5 cm) randomly dispersed on the physical properties of polyethene. A decrease in the tensile strength and the Young's modulus of the composite was, however, observed compared with those of the unreinforced polyethene. Table (29) shows the tensile strengths and the Young's moduli of polyethene with different lengths of fibre.

Figure (40) Tensile strength vs. composition of polyethene/  
2mm length hair phases

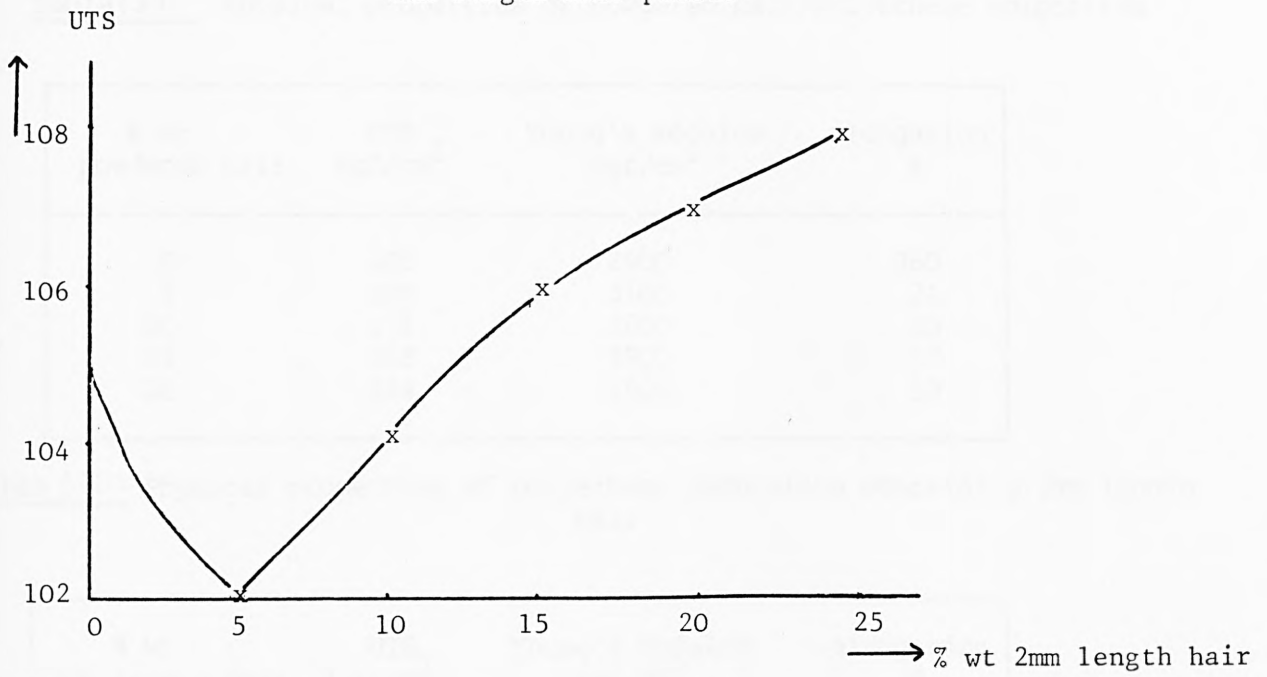


Figure (41) Young's modulus vs. composition of polyethene/  
2mm length hair phases

Young's modulus

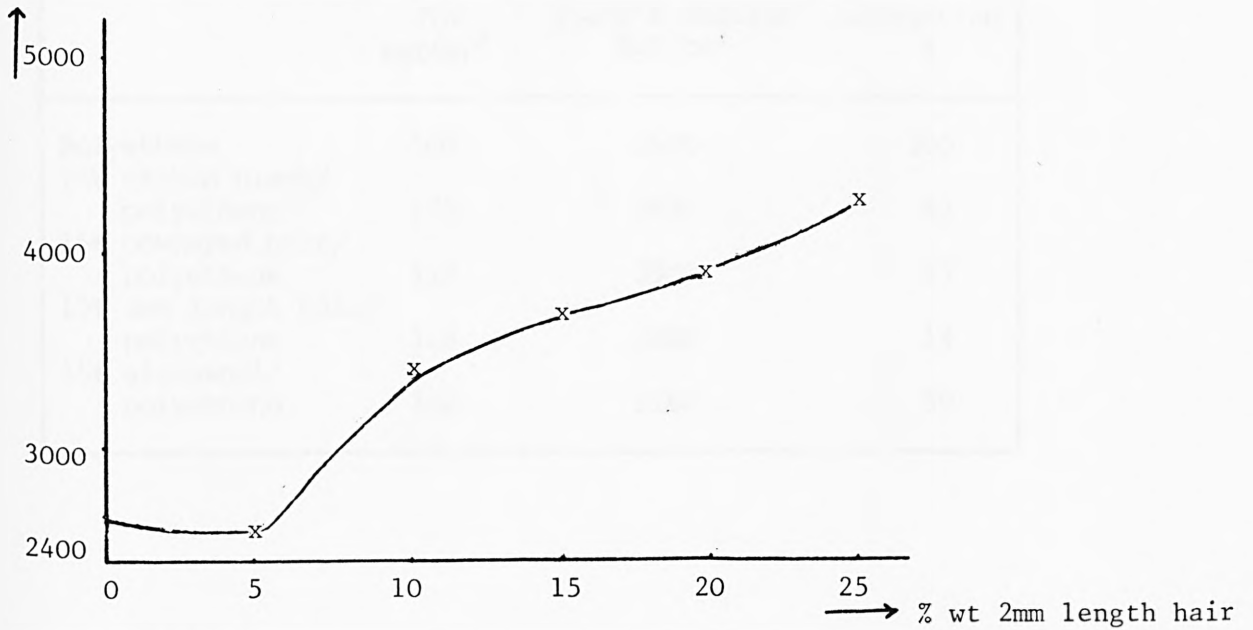


Table (27) Physical properties of powdered hair/polyethene composites

% wt powdered hair	UTS Kg/cm <sup>2</sup>	Young's modulus Kg/cm <sup>2</sup>	elongation %
0	105	2600	360
5	109	3100	24
10	115	3600	20
15	118	3900	17
20	124	4900	10

Table (28) Physical properties of polyethene composites containing 2mm length hair

% wt 2mm length hair	UTS Kg/cm <sup>2</sup>	Young's modulus Kg/cm <sup>2</sup>	elongation %
0	105	2600	360
5	102	2550	60
10	104	3420	20
15	106	3680	14
20	107	3870	16
25	108	4320	22

Table (30) Physical properties of various polyethene composites

	UTS Kg/cm <sup>2</sup>	Young's modulus Kg/cm <sup>2</sup>	elongation %
Polyethene	105	2600	360
15% carbon black/ polyethene	132	3680	42
15% powdered hair/ polyethene	118	3900	17
15% 2mm length hair/ polyethene	106	3680	14
15% glasswool/ polyethene	102	3160	59

Table (29) Physical properties of polyethene composites containing different lengths of hair

% wt hair	Polyethene composites containing							
	1 cm length hair		2 cm length hair		3 cm length hair		5 cm length hair	
	Tensile strength Kgf/cm <sup>2</sup>	Young's modulus Kgf/cm <sup>2</sup>						
5	81.2	2680	69.6	2200	70.2	1850	65	2290
10	62.5	2700	61.7	2100	69.9	2350	58.3	2280
15	56.6	2920	49.2	2600	74.4	2130	64.2	2260
20	63.5	2790	52	2600	73.5	2500	71.7	2300

In order to compare the physical properties of polyethene composites containing hair with the physical properties of polyethene containing other fillers, composites of polyethene with 15% wt carbon black and glasswool were prepared. Table (30) shows the results of the tensile strengths, the Young's moduli and the elongation of polyethene composites with 15% wt of various fillers. The results show that the tensile strength of the polyethene composite containing 15% wt carbon black ( $132 \text{ Kgf/cm}^2$ ) is the best compared with  $105 \text{ Kgf/cm}^2$  and  $118 \text{ Kgf/cm}^2$  for unreinforced polyethene and polyethene composite containing 15% powdered hair respectively, and the Young's modulus of the composite containing 15% powdered hair ( $3900 \text{ Kgf/cm}^2$ ) is the best and higher than  $2600 \text{ Kgf/cm}^2$  for unreinforced polyethene and  $3680 \text{ Kgf/cm}^2$  for the composite containing 15% carbon black. The elongation of the composites prepared, however, is lower than that for unreinforced polyethene.

#### Polyvinyl chloride system

It is evident from Table (31) and Figure (42) that the tensile strengths of the composites containing powdered hair increase with increasing fibre load up to the limits investigated (i.e. 0-20% wt fibre).

A tensile strength of  $220 \text{ Kgf/cm}^2$  was achieved with

Table (31) Physical properties of powdered hair/  
PVC composites

% wt powdered hair	UTS Kgf/cm <sup>2</sup>	Young's modulus Kgf/cm <sup>2</sup>	elongation %
0	215	2820	110
5	220	3400	103
10	217	3550	98
15	218	3600	81
20	220	3500	40

Table (32) Physical properties of 2mm length hair/PVC composites

% wt 2mm length hair	UTS Kgf/cm <sup>2</sup>	Young's modulus Kgf/cm <sup>2</sup>	elongation %
0	215	2820	110
5	202	3640	44
10	208	4400	72
15	217	5740	32
20	235	6130	14

Figure (42) Tensile strength vs. composition of PVC/powdered hair phases

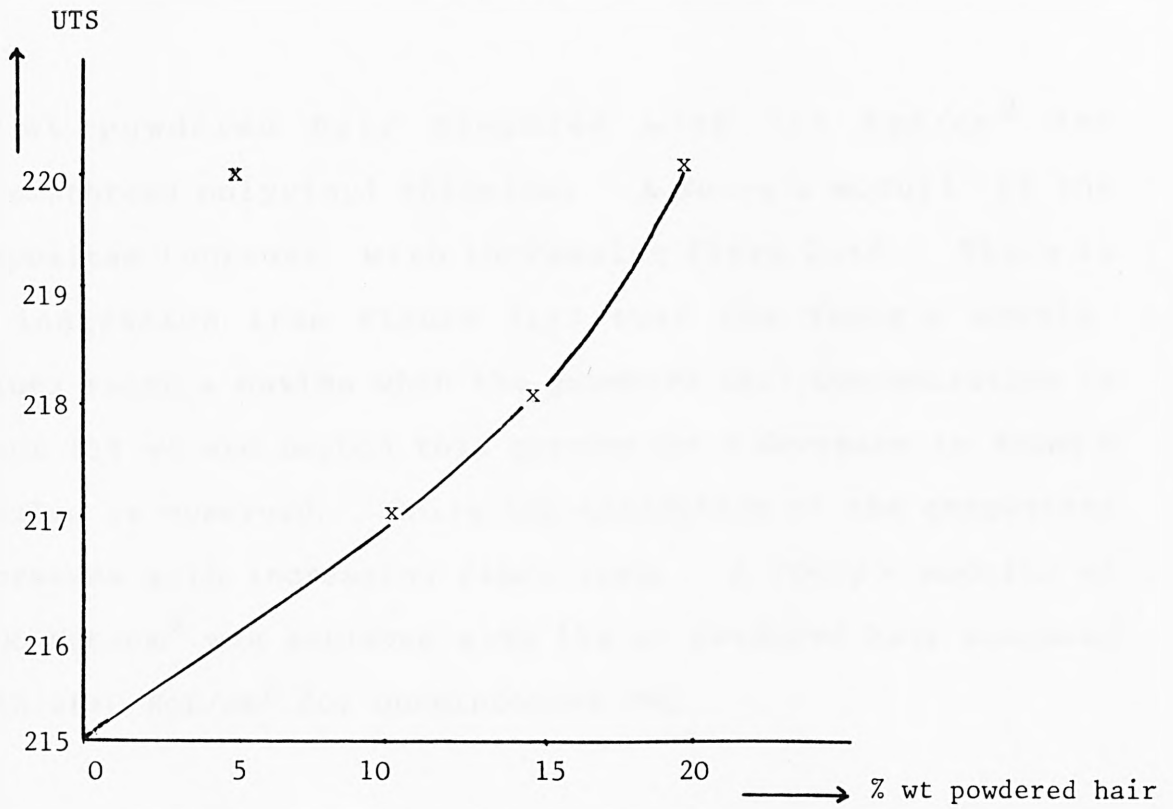
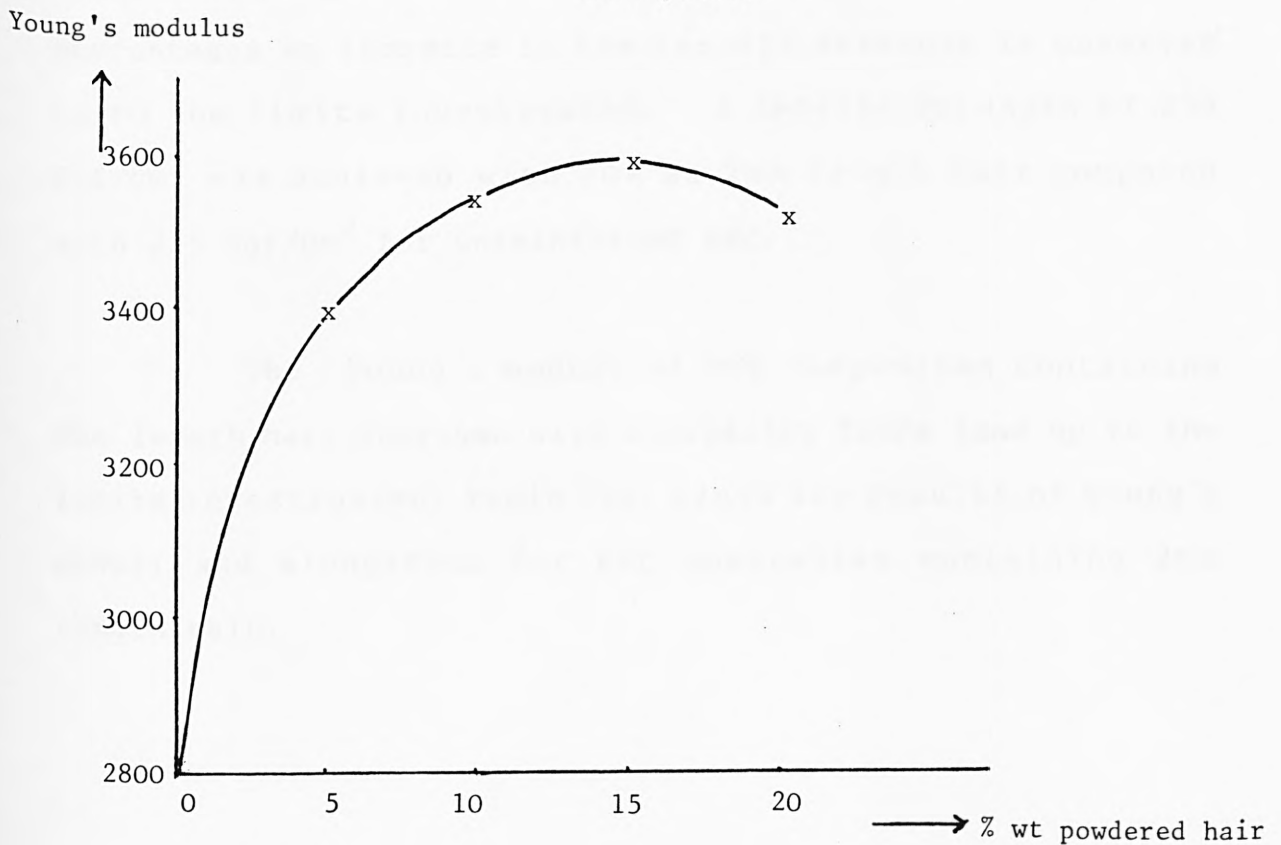


Figure (43) Young's modulus vs. composition of PVC/powdered hair phases



20% wt powdered hair compared with 215 Kgf/cm<sup>2</sup> for unreinforced polyvinyl chloride. A Young's moduli of the composites increase with increasing fibre load. There is an indication from Figure (42) that the Young's moduli values reach a maxima when the powdered hair concentration is about 15% wt and beyond this percentage a decrease in Young's modulus is observed. While the elongation of the composites decreases with increasing fibre load. A Young's modulus of 3600 Kgf/cm<sup>2</sup> was achieved with 15% wt powdered hair compared with 2820 Kgf/cm<sup>2</sup> for unreinforced PVC.

There is an indication from Table (32) and Figure (44) that the tensile strengths of PVC composites decrease with 5% wt and 10% wt 2mm length hair compared with the tensile strength of unreinforced PVC and beyond these percentages an increase in the tensile strength is observed up to the limits investigated. A tensile strength of 235 Kgf/cm<sup>2</sup> was achieved with 20% wt 2mm length hair compared with 215 Kgf/cm<sup>2</sup> for unreinforced PVC.

The Young's moduli of PVC composites containing 2mm length hair increase with increasing fibre load up to the limits investigated, Table (32) lists the results of Young's moduli and elongation for PVC composites containing 2mm length hair.

Figure (44) Tensile strength vs. composition of PVC/2mm length hair phases

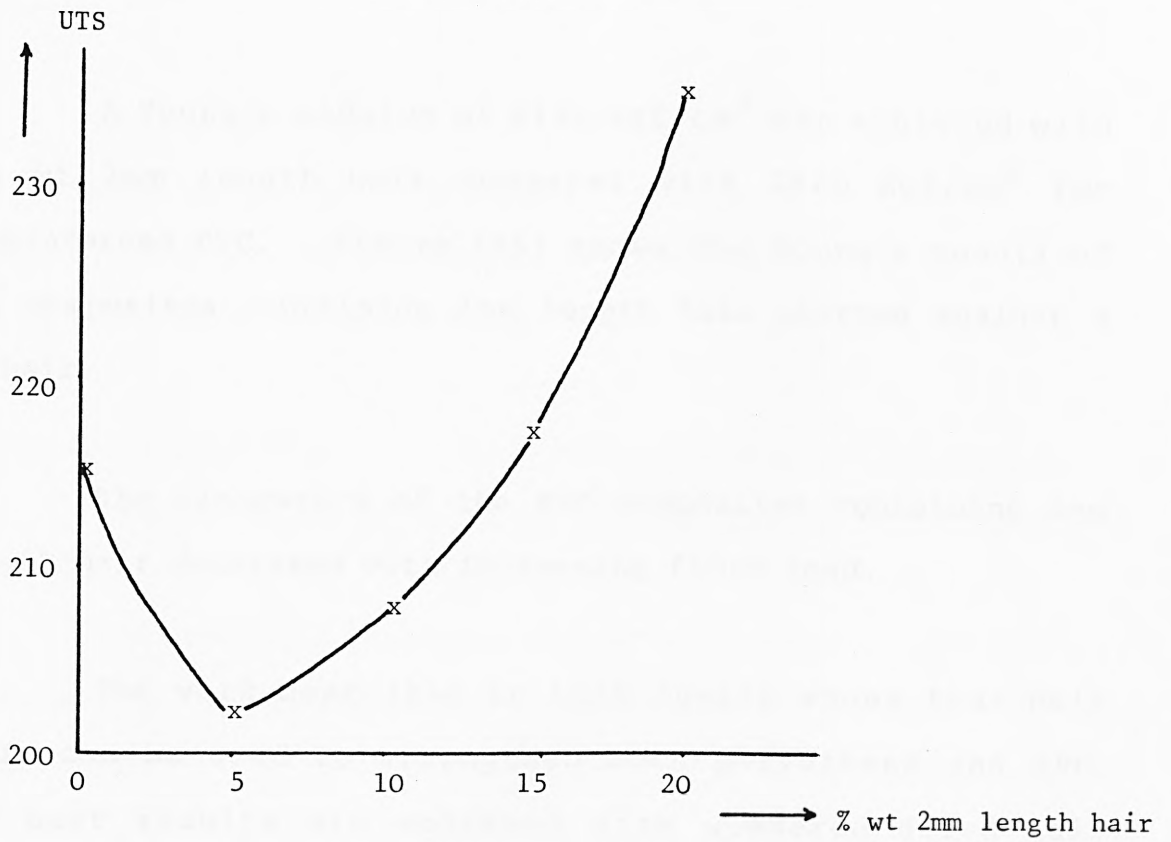
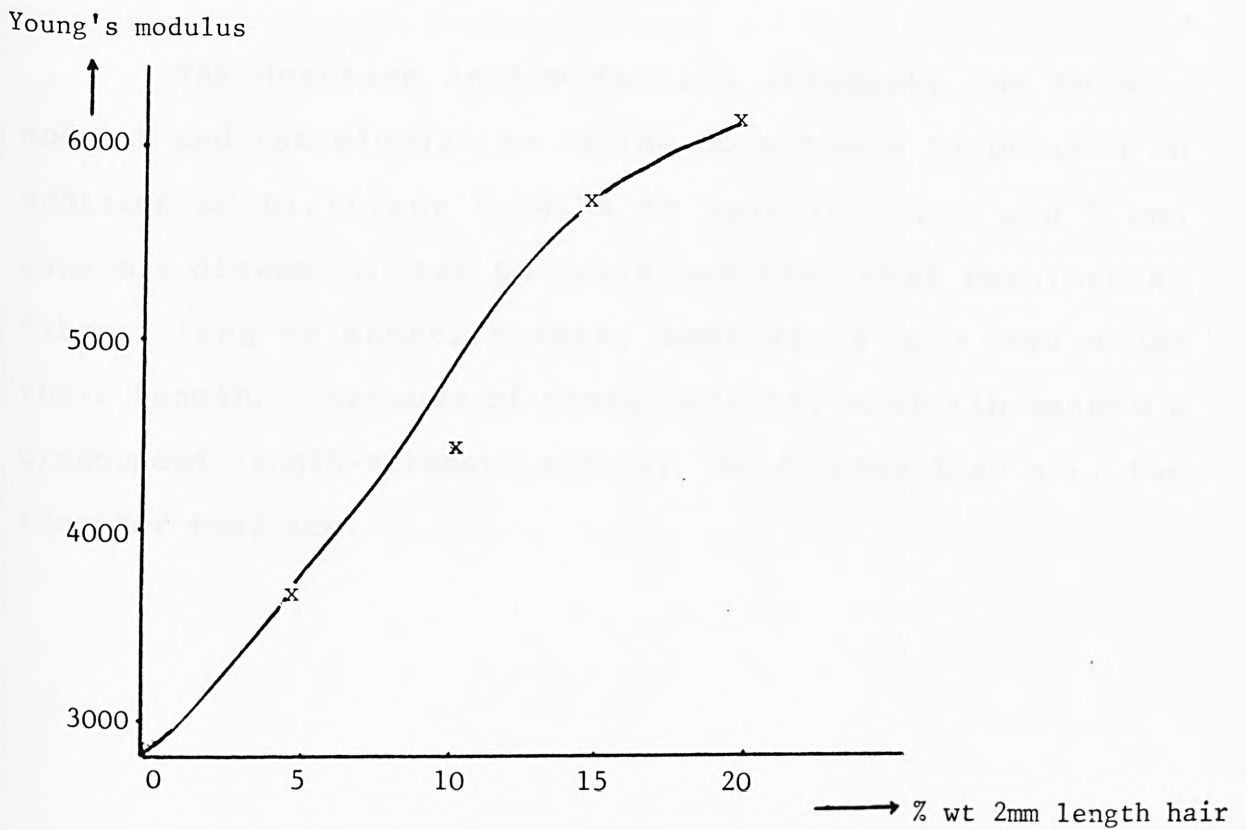


Figure (45) Young's modulus vs. composition of PVC/2mm length hair phases



A Young's modulus of 6130 Kgf/cm<sup>2</sup> was achieved with 20% wt 2mm length hair compared with 2820 Kgf/cm<sup>2</sup> for unreinforced PVC. Figure (45) shows the Young's moduli of PVC composites containing 2mm length hair plotted against % wt hair.

The elongation of the PVC composites containing 2mm length hair decreased with increasing fibre load.

The work described in this thesis shows that hair fibre can be used to strengthen both polyethene and PVC. The best results are achieved with powdered dried hair samples but improvements are also found when 2mm length natural hair fibre is used as a reinforcement. Use of longer fibre length hair is disadvantageous.

The decrease in the tensile strength, the Young's modulus and the elongation of the polyethene composites on addition of different lengths of hair (1, 2, 3 and 5 cm) randomly dispersed, can be explained that most reinforcing fibres, long or short, possess weak spots or flaws along their length. Because of these defects, most fibres show a pronounced length-strength effect; the shorter they are, the stronger they are.

The work described so far deals with dispersion in the absence of a coupling agent. The next Section of this chapter considers the effect of the addition of stearic acid and of HALLCOMIDS as coupling agents.

#### 4.5.2 Study of the effects of dispersing coupling agent additives on the physical properties of the composites

The physical properties of the composites can be improved by the addition of coupling agents (i.e. stearic acid, HALLCOMID M-10-OL and HALLCOMID M-8-10). The coupling agents<sup>5</sup> are designed to link with the oxide, hydroxide, sulphide or other charged surface groups on fibres and to provide a new surface of organic groups to combine with the resin and thus to more easily transfer stress within the composite. Coupling agents need only to be added in small quantities to provide an improvement and have been shown to have three main effects in polymer composites:-

1. Longer retention of strength
2. Increased flexural strength
3. Increased tensile strength

## Polyethene composites

In the present work, attempts to improve the physical properties (i.e. tensile strength and Young's modulus) of polyethene composites containing 15% wt powdered hair were carried out by adding the following coupling agents (stearic acid, HALLCOMID M-8-10 and HALLCOMID M-10-OL). (See Section 2.9 in this thesis). Stearic acid limits (0.24-2.4% wt) were used and Table (33) shows that the tensile strengths of the composites increase with increasing % wt stearic acid up to the limits used. While the Young's moduli of the composites increase with increasing % wt stearic acid to maxima when the stearic acid is present at about 0.72% wt. Beyond this percentage the Young's moduli values remained stable. The elongation of the composites decreases with increasing % wt stearic acid.

A tensile strength of 138 Kgf/cm<sup>2</sup> was achieved with 2.4% wt stearic acid compared with 118 Kgf/cm<sup>2</sup> for the same composites without stearic acid.

A Young's modulus of 5600 Kgf/cm<sup>2</sup> was achieved with 0.72% wt stearic acid compared with 3900 Kgf/cm<sup>2</sup> for the same composite without stearic acid. Figures (46,47) show the tensile strength and the Young's modulus of polyethene composites containing 15% wt powdered hair plotted against %wt

Figure (46) Tensile strength vs. composition of 15% powdered hair/  
polyethene/stearic acid phases

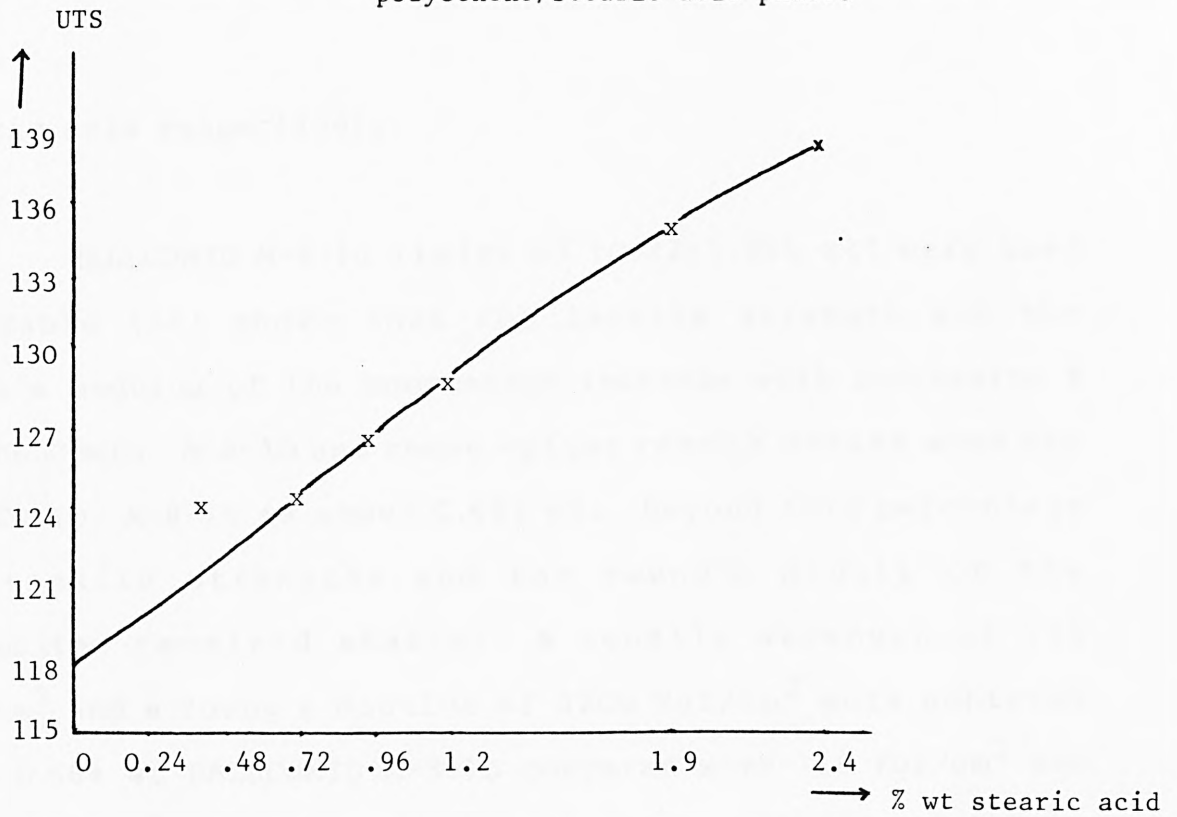
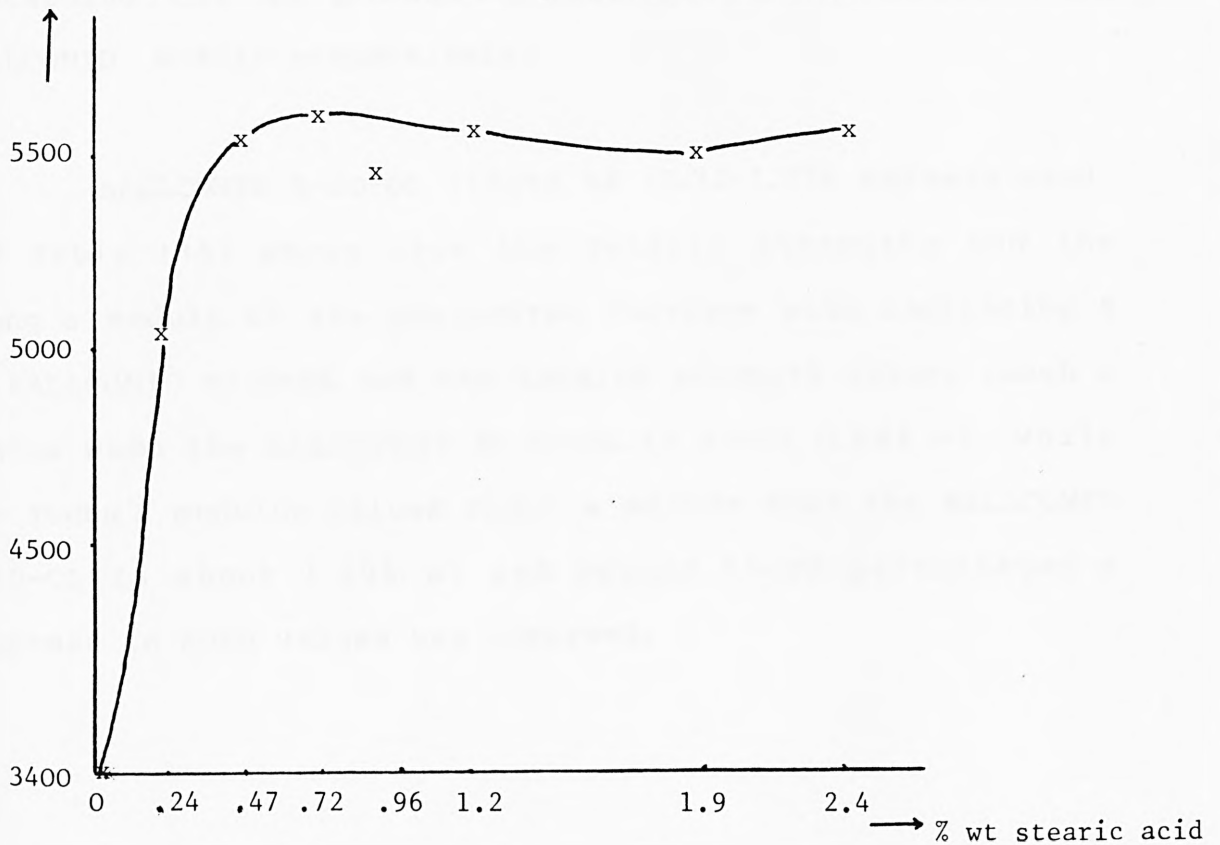


Figure (47) Young's modulus vs. composition of 15% powdered hair/  
polyethene/stearic acid phases



stearic acid respectively.

HALLCOMID M-8-10 limits of (0.22-1.98% wt) were used and Table (34) shows that the tensile strength and the Young's modulus of the composites increase with increasing % wt HALLCOMID M-8-10 and these values reach a maxima when the HALLCOMID M-8-10 is about 0.66% wt. Beyond this percentage the tensile strengths and the Young's moduli of the composites remained stable. A tensile strength of 131 Kg/cm<sup>2</sup> and a Young's modulus of 5200 Kg/cm<sup>2</sup> were achieved with 0.66% wt HALLCOMID M-8-10 compared with 118 Kg/cm<sup>2</sup> and 3900 Kg/cm<sup>2</sup> respectively for the same composite without HALLCOMID M-8-10. Figures (48,49) show the tensile strengths and the Young's moduli of polyethene composites containing 15% wt powdered hair plotted against % wt HALLCOMID M-8-10 respectively.

HALLCOMID M-10-OL limits of (0.22-1.72% wt) were used and Table (35) shows that the tensile strengths and the Young's moduli of the composites increase with increasing % wt HALLCOMID M-10-OL and the tensile strength values reach a maxima when the HALLCOMID M-10-OL is about 0.86% wt, while the Young's modulus values reach a maxima when the HALLCOMID M-10-OL is about 1.29% wt and beyond these percentages a decrease in both values was observed.

Figure (48) Tensile strength vs. composition of 15% powdered hair/  
polyethene/HALLCOMID M-8-10 phases

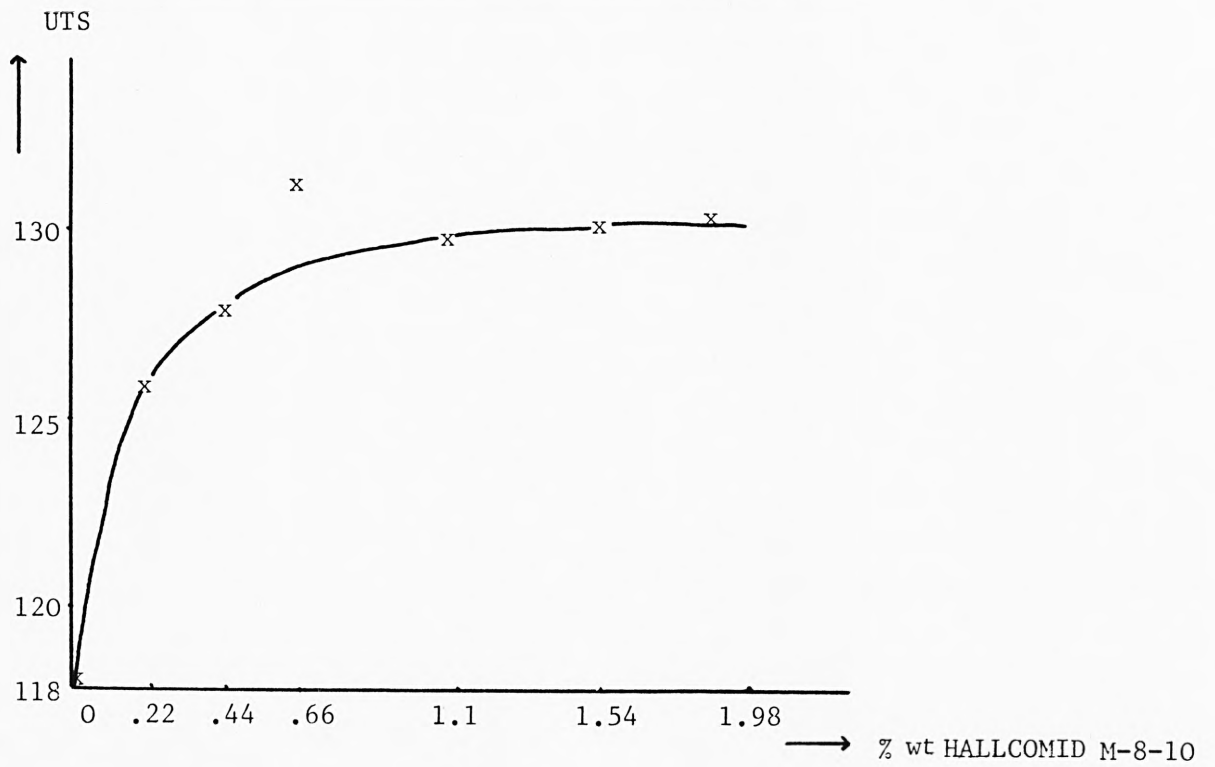
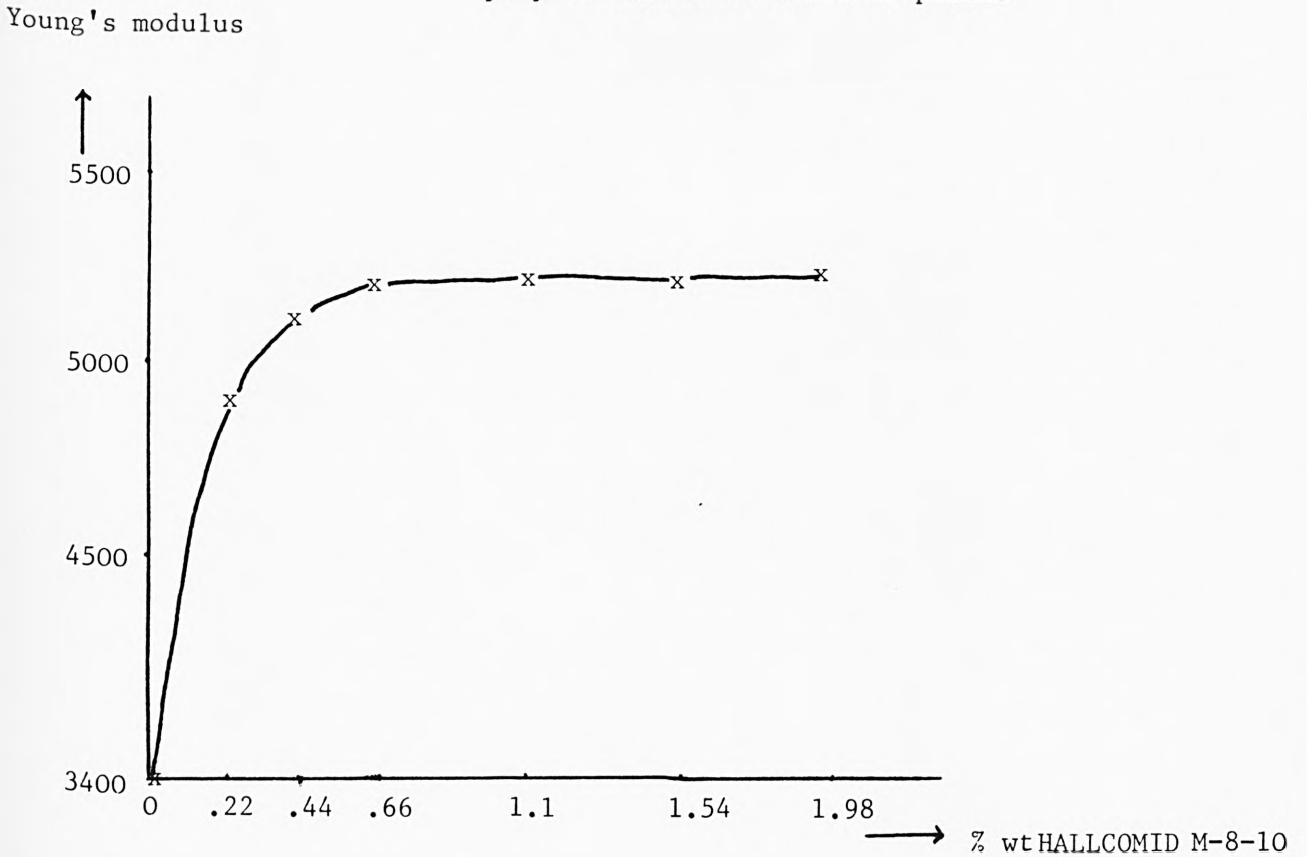


Figure (49) Young's modulus vs. composition of 15% powdered hair/  
polyethene/HALLCOMID M-8-10 phases



**Table (33)** Physical properties of 15% powdered hair/polyethene/  
stearic acid composites

% wt stearic acid	UTS Kgf/cm <sup>2</sup>	Young's modulus Kgf/cm <sup>2</sup>	elongation %
0	118	3900	17
0.24	116	5050	11
0.48	124	5550	10
0.72	125	5600	12
0.96	127	5450	12
1.2	129	5550	11
1.9	135	5500	9
2.4	138	5550	9

**Table (34)** Physical properties of 15% powdered hair/polyethene/HALLCOMID M-8-10  
composites

% wt HALLCOMID M-8-10	UTS Kgf/cm <sup>2</sup>	Young's modulus Kgf/cm <sup>2</sup>	elongation %
0	118	3900	17
0.22	126	4900	11
0.44	128	5100	13
0.66	131	5200	14
1.1	129.5	5200	10
1.54	130	5200	13
1.98	130	5200	13

**Table (35)** Physical properties of 15% powdered hair/polyethene/  
HALLCOMID M-10-OL composites

% wt HALLCOMID M-10-OL	UTS Kgf/cm <sup>2</sup>	Young's modulus Kgf/cm <sup>2</sup>	elongation %
0	118	3900	17
0.22	123	4750	14
0.43	129	5000	11
0.86	129	5100	14
1.29	128	5350	12
1.72	127	5100	13

Figure (50) Tensile strength vs. composition of 15% powdered hair/  
polyethylene/HALLCOMID M-10-OL phases

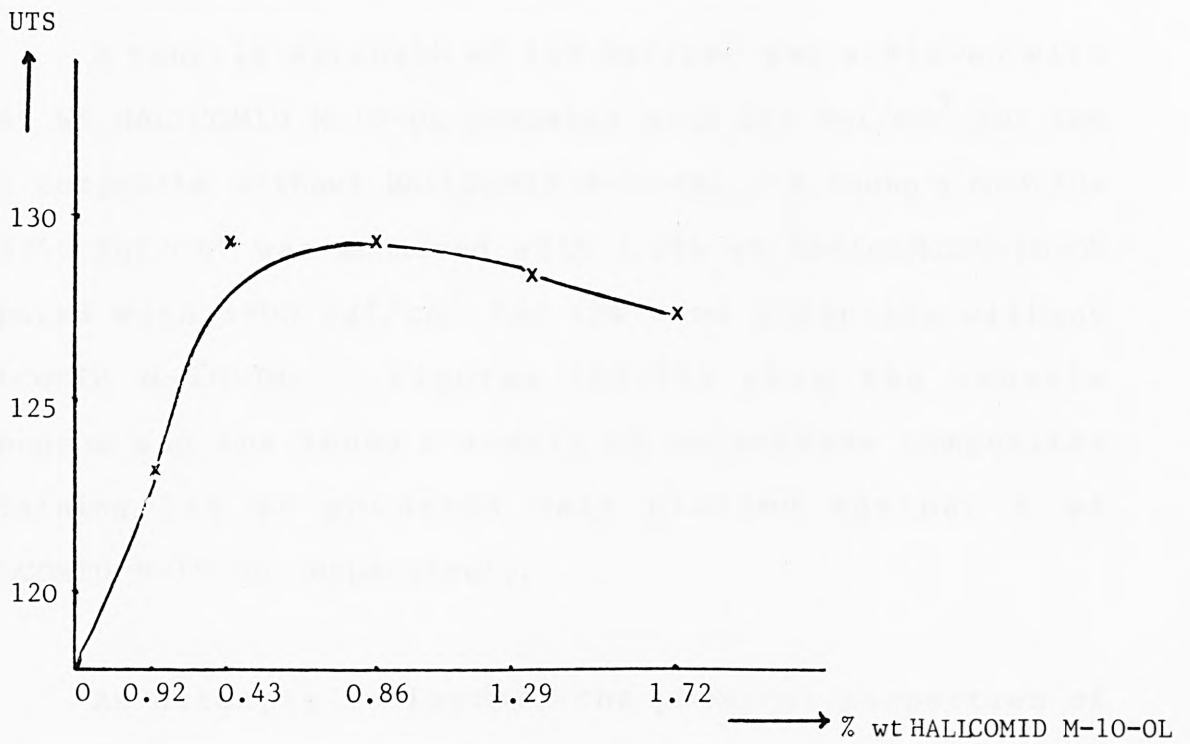
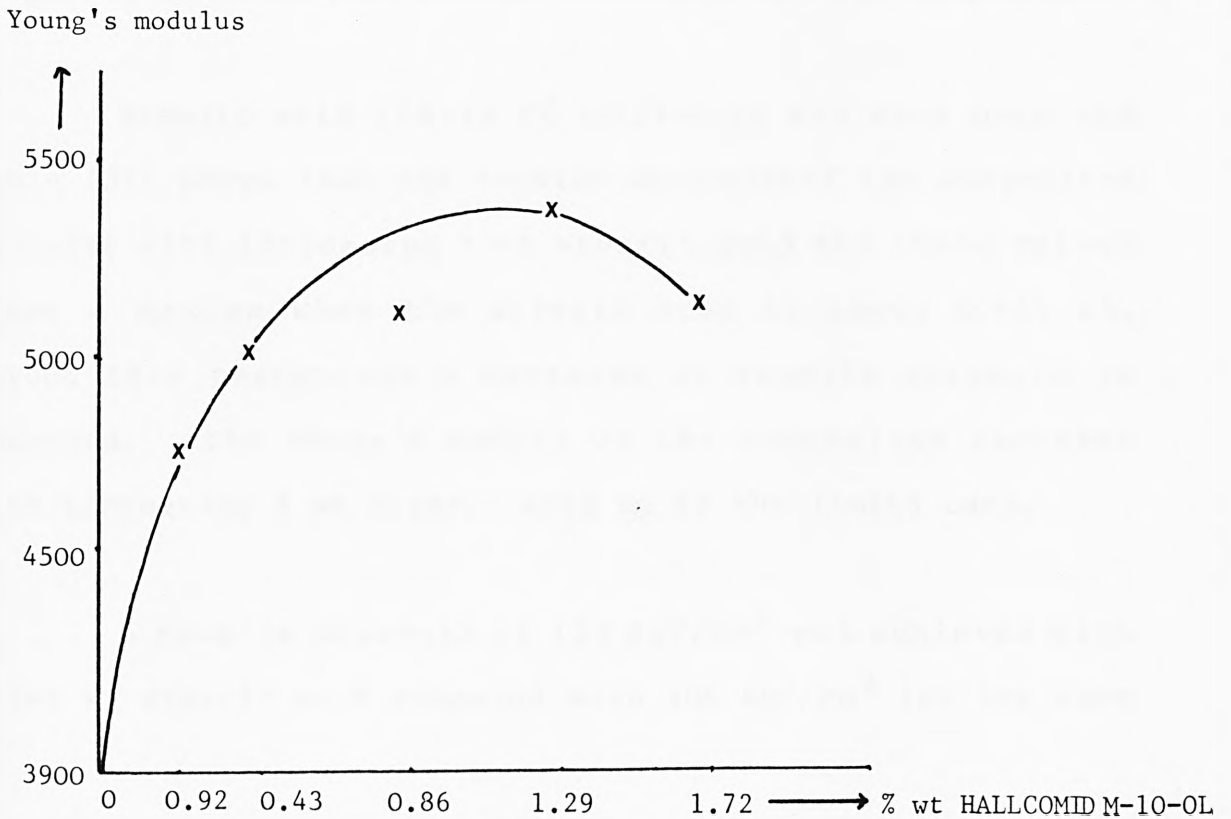


Figure (51) Young's modulus vs. composition of 15% powdered hair/  
polyethylene/HALLCOMID M-10-OL phases



A tensile strength of 129 Kgf/cm<sup>2</sup> was achieved with 0.86% wt HALLCOMID M-10-OL compared with 118 Kgf/cm<sup>2</sup> for the same composite without HALLCOMID M-10-OL. A Young's modulus of 5350 Kgf/cm<sup>2</sup> was achieved with 1.29% wt HALLCOMIDM-10-OL compared with 3900 Kgf/cm<sup>2</sup> for the same composite without HALLCOMID M-10-OL. Figures (50,51) show the tensile strengths and the Young's moduli of polyethene composites containing 15% wt powdered hair plotted against % wt HALLCOMID M-10-OL respectively.

As attempts to improve the physical properties of polyethene composites containing powdered hair by adding the coupling agents proved successful, the work was repeated using polyethene composites containing 2 mm length hair. The composite used was polyethene containing 15% 2mm length hair.

Stearic acid limits of (0.24-1.2% wt) were used and Table (36) shows that the tensile strengths of the composites increase with increasing % wt stearic acid and these values reach a maxima when the stearic acid is about 0.96% wt. Beyond this percentage a decrease in tensile strength is observed. The Young's moduli of the composites increase with increasing % wt stearic acid up to the limits used.

A tensile strength of 123 Kgf/cm<sup>2</sup> was achieved with 0.96% wt stearic acid compared with 106 Kgf/cm<sup>2</sup> for the same

composite without stearic acid. A Young's modulus of 4640 Kgf/cm<sup>2</sup> was achieved with 1.2% stearic acid compared with 3680 Kgf/cm<sup>2</sup> for the same composite without stearic acid.

Figures (52,53) show the tensile strengths and the Young's moduli of polyethene composites containing 15% wt 2 mm length hair plotted against % wt stearic acid respectively.

HALLCOMID M-8-10 limits of (0.44-2.2% wt) were used and Table (37) shows that the tensile strengths of the composites increase with increasing % wt HALLCOMID M-8-10 and these values reach a maxima when the HALLCOMID M-8-10 is about 0.88% wt. Beyond this percentage a decrease in tensile strength is observed. While the Young's moduli of the composites increase with increasing % wt HALLCOMID M-8-10 up to the limits used. A tensile strength of 117 Kgf/cm<sup>2</sup> was achieved with a 0.88% wt HALLCOMID M-8-10 compared with 106 Kgf/cm<sup>2</sup> for the same composite without HALLCOMID M-8-10. A Young's modulus of 4370 Kgf/cm<sup>2</sup> was achieved with 2.2% wt HALLCOMID M-8-10 compared with 3680 Kgf/cm<sup>2</sup> for the same composite without HALLCOMID M-8-10. Figures (54,55) show the tensile strengths and the Young's moduli of polyethene composites containing 15% 2mm length hair plotted against % wt HALLCOMID M-8-10 respectively.

**Table (36)** Physical properties of 15% 2mm length hair/  
polyethene/stearic acid composites

% wt stearic acid	UTS Kgf/cm <sup>2</sup>	Young's modulus Kgf/cm <sup>2</sup>	elongation %
0	106	3680	14
0.24	113	4180	16
0.72	122	4550	14
0.96	123	4630	18
1.2	118	4640	15

**Table (37)** Physical properties of 15% 2mm length hair/  
polyethene/HALLCOMID M-8-10 composites

% wt HALLCOMID M-8-10	UTS Kgf/cm <sup>2</sup>	Young's modulus Kgf/cm <sup>2</sup>	elongation %
0	106	3680	14
0.44	114	4190	12
0.88	117	4310	19
1.76	116	4360	15
2.2	108	4370	18

**Table (38)** Physical properties of 15% 2mm length hair/  
polyethene/HALLCOMID M-10-OL composites

% wt HALLCOMID M-10-OL	UTS Kgf/cm <sup>2</sup>	Young's modulus Kgf/cm <sup>2</sup>	elongation %
0	106	3680	14
0.43	110	4000	17
0.86	109	4190	18
1.29	108	4100	21
1.72	108	4300	21

Figure (52) Tensile strength vs. composition of 15% 2mm length hair/  
polyethene/stearic acid phases

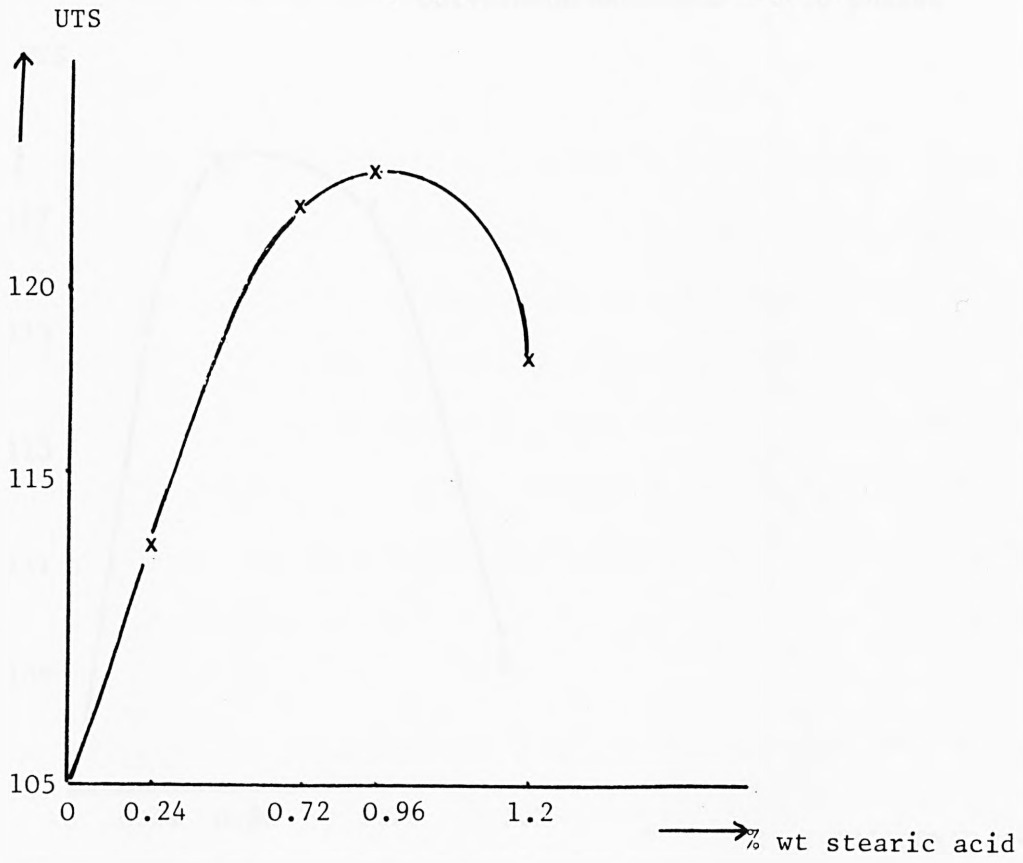


Figure (53) Young's modulus vs. composition of 15% 2mm length hair/  
polyethene/stearic acid phases

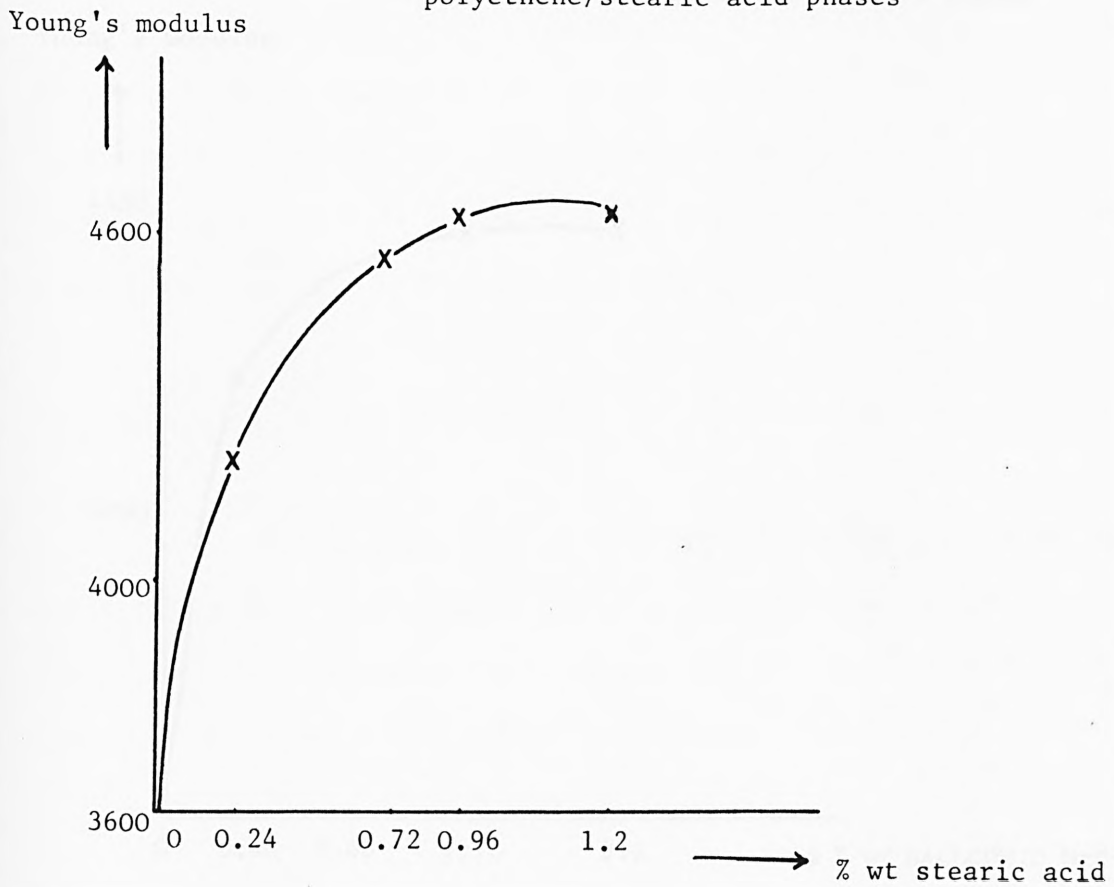


Figure (54) Tensile strength vs. composition of 15% 2mm length hair/  
polyethene/HALLCOMID M-8-10 phases

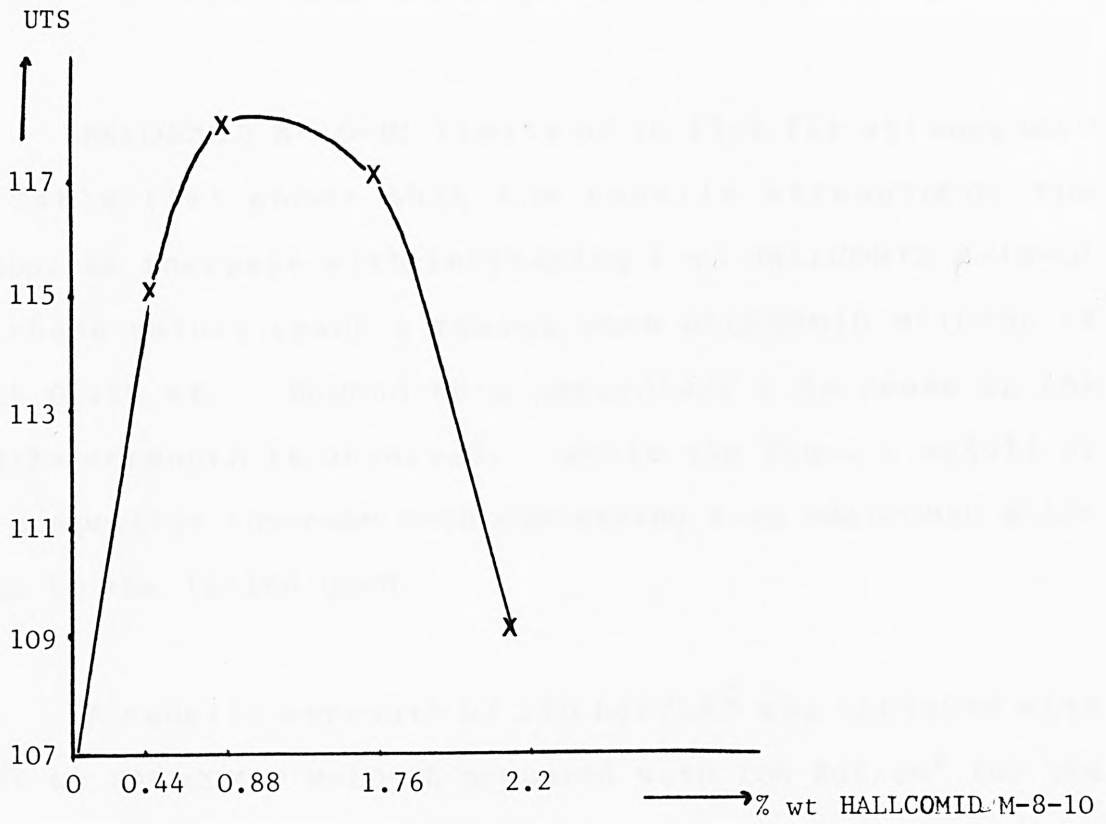
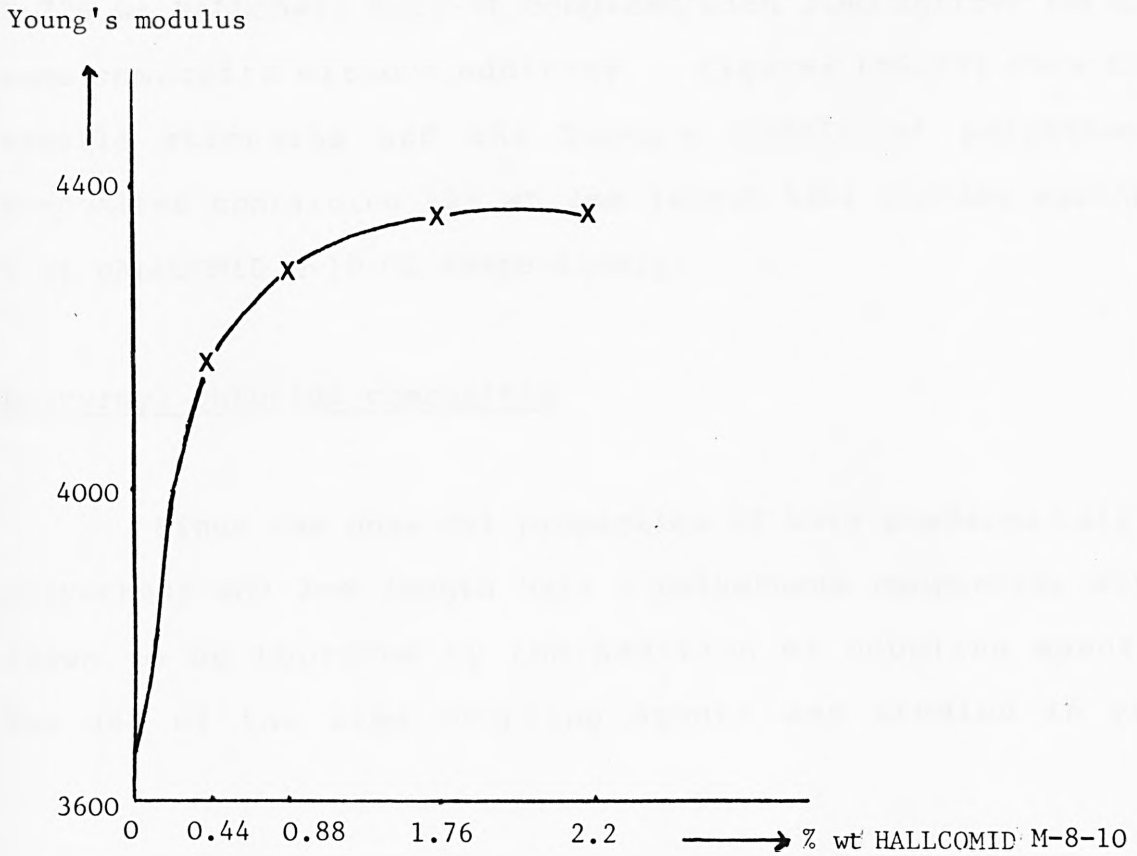


Figure (55) Tensile strength vs. composition of 15% 2mm length hair/  
polyethene/HALLCOMID M-8-10 phases



HALLCOMID M-10-OL limits of (0.43-1.72% wt) were used and Table (38) shows that the tensile strengths of the composites increase with increasing % wt HALLCOMID M-10-OL and these values reach a maxima when HALLCOMID M-10-OL is about 0.43% wt. Beyond this percentage a decrease in the tensile strength is observed. While the Young's moduli of the composites increase with increasing % wt HALLCOMID M-10-OL up to the limits used.

A tensile strength of  $110 \text{ Kgf/cm}^2$  was achieved with 0.43% wt HALLCOMID M-10-OL compared with  $106 \text{ Kgf/cm}^2$  for the same composite without additive.

A Young's modulus of  $4300 \text{ Kgf/cm}^2$  was achieved with 1.72% wt HALLCOMID M-10-OL compared with  $3680 \text{ Kgf/cm}^2$  for the same composite without additive. Figures (56,57) show the tensile strengths and the Young's moduli of polyethene composites containing 15% wt 2mm length hair plotted against % wt HALLCOMID M-10-OL respectively.

#### Polyvinyl chloride composites

Since the physical properties of both powdered hair - polyethene and 2mm length hair - polyethene composites were shown to be improved by the addition of coupling agents. The use of the same coupling agents was studied in PVC

Figure (56) Tensile strength vs. composition of 15% 2mm length hair/  
polyethene/HALLCOMID M-10-OL phases

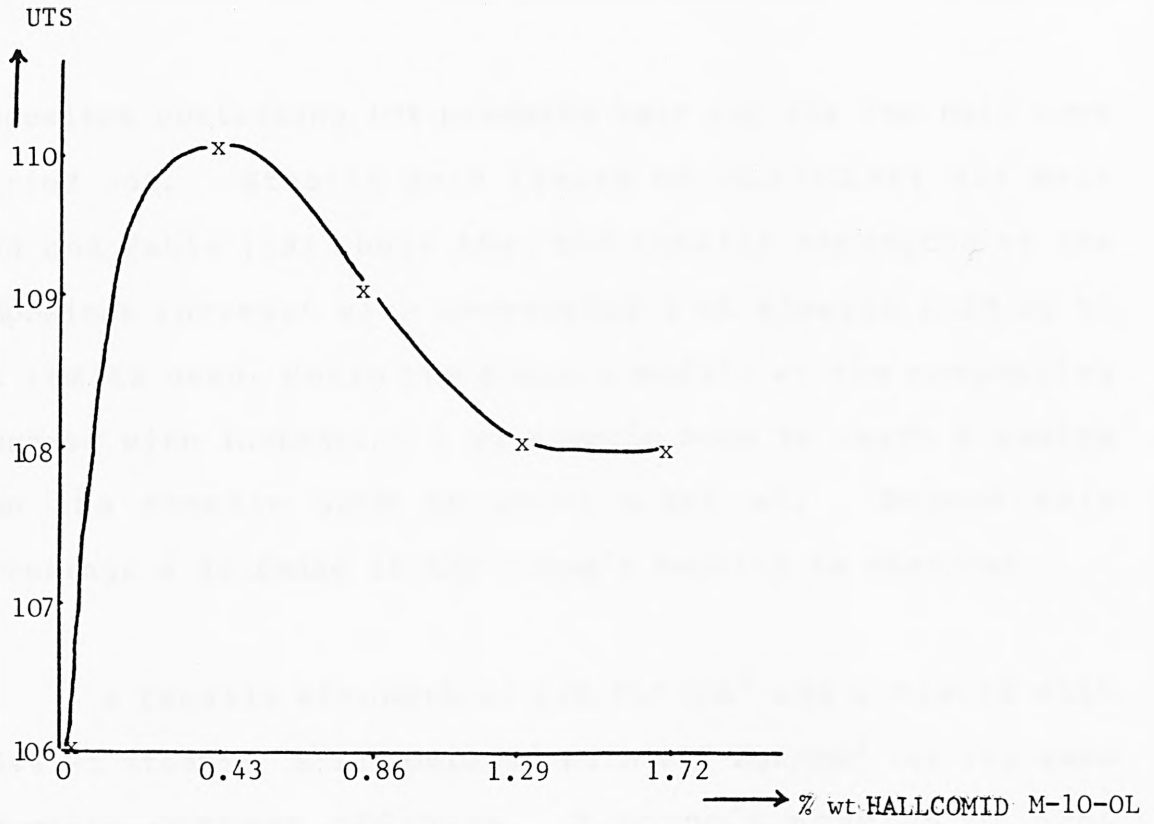
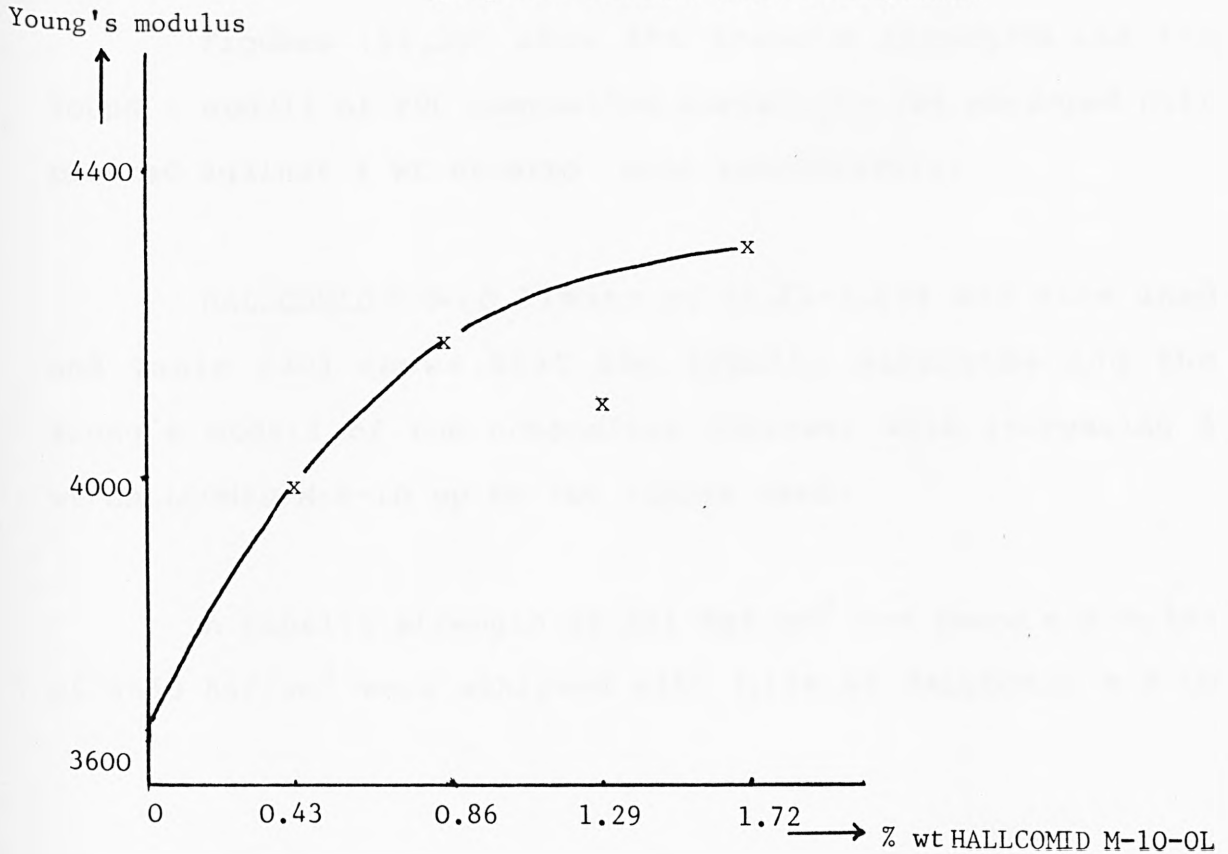


Figure (57) Young's modulus vs. composition of 15% 2mm length hair/  
polyethene/HALLCOMID M-10-OL phases



composites containing 10% powdered hair and 10% 2mm hair were carried out. Stearic acid limits of (0.13-0.44% wt) were used and Table (39) shows that the tensile strengths of the composites increase with increasing % wt stearic acid up to the limits used, while the Young's moduli of the composites increase with increasing % wt stearic acid to reach a maxima when the stearic acid is about 0.26% wt. Beyond this percentage a decrease in the Young's modulus is observed.

A tensile strength of 248 Kgf/cm<sup>2</sup> was achieved with 0.44% wt stearic acid compared with 217 Kgf/cm<sup>2</sup> for the same composite without additive. A Young's modulus of 5260 Kgf/cm<sup>2</sup> was achieved with 0.26% wt stearic acid compared with 3550 Kgf/cm<sup>2</sup> for the same composite without additive.

Figures (58,59) show the tensile strengths and the Young's moduli of PVC composites containing 10% powdered hair plotted against % wt stearic acid respectively.

HALLCOMID M-8-10 limits of (0.23-1.13% wt) were used and Table (40) shows that the tensile strengths and the Young's moduli of the composites increase with increasing % wt HALLCOMID M-8-10 up to the limits used.

A tensile strength of 251 Kgf/cm<sup>2</sup> and Young's modulus of 5660 Kgf/cm<sup>2</sup> were achieved with 1.13% wt HALLCOMID M-8-10

**Table (39)** Physical properties of 10% powdered hair/PVC/  
stearic acid composites

% wt stearic acid	UTS Kgf/cm <sup>2</sup>	Young's modulus Kgf/cm <sup>2</sup>	elongation %
0	217	3550	98
0.13	218	3660	124
0.19	220	5100	87
0.26	243	5260	92
0.32	244	4900	115
0.38	247	4800	111
0.44	248	4800	114

**Table (40)** Physical properties of 10% powdered hair/PVC/  
HALLCOMID M-8-10 composites

% wt HALLCOMID M-8-10	UTS Kgf/cm <sup>2</sup>	Young's modulus Kgf/cm <sup>2</sup>	elongation %
0	217	3550	98
0.23	218	4380	70
0.45	219	4450	83
0.68	223	5260	75
0.9	228	5380	93
1.13	251	5660	107

**Table (41.)** Physical properties of 10% powdered hair/PVC/  
HALLCOMID M-10-OL composites

% wt HALLCOMID M-10-OL	UTS Kgf/cm <sup>2</sup>	Young's modulus Kgf/cm <sup>2</sup>	elongation %
0	217	3550	98
0.23	216	4715	101
0.45	223	4700	109
0.56	240	4800	110
0.68	249	4700	122
0.79	241	4550	108
0.9	228	4430	110
1.13	222	3700	105

Figure (58) Tensile strength vs. composition of 10% powdered hair/  
PVC/stearic acid phases

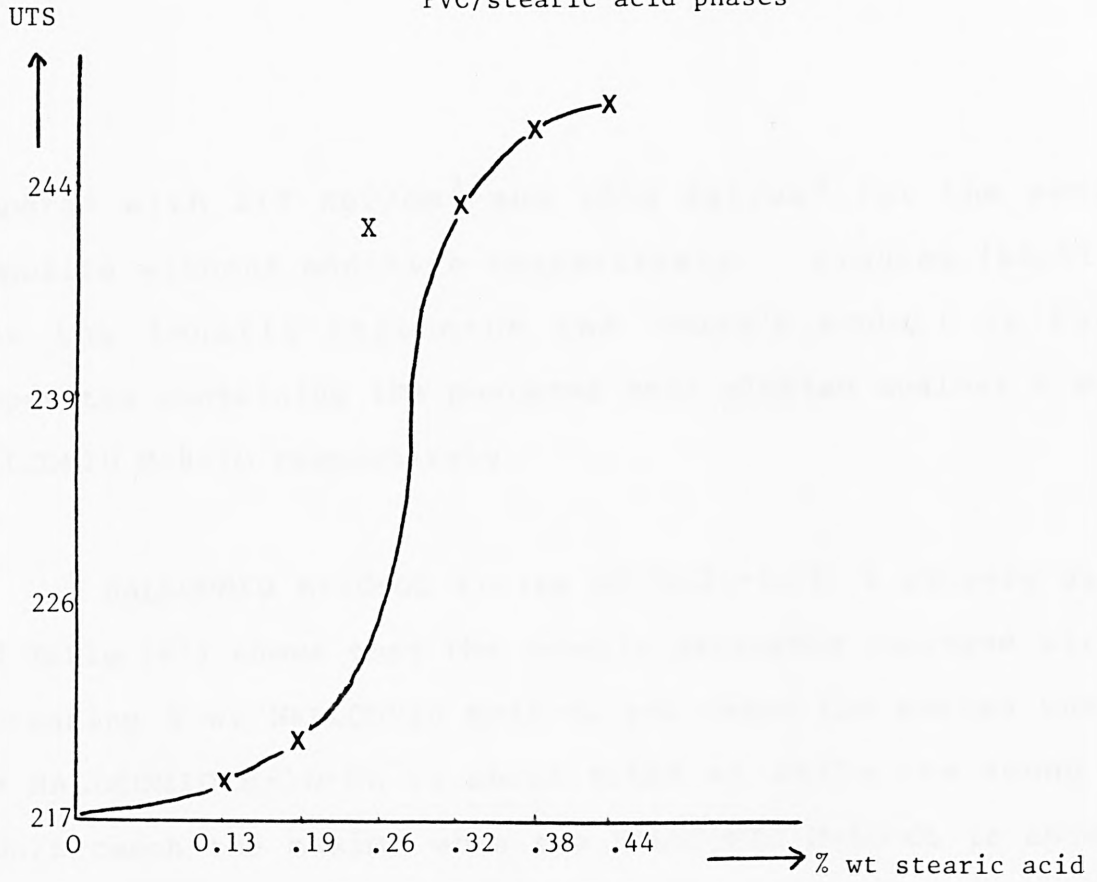
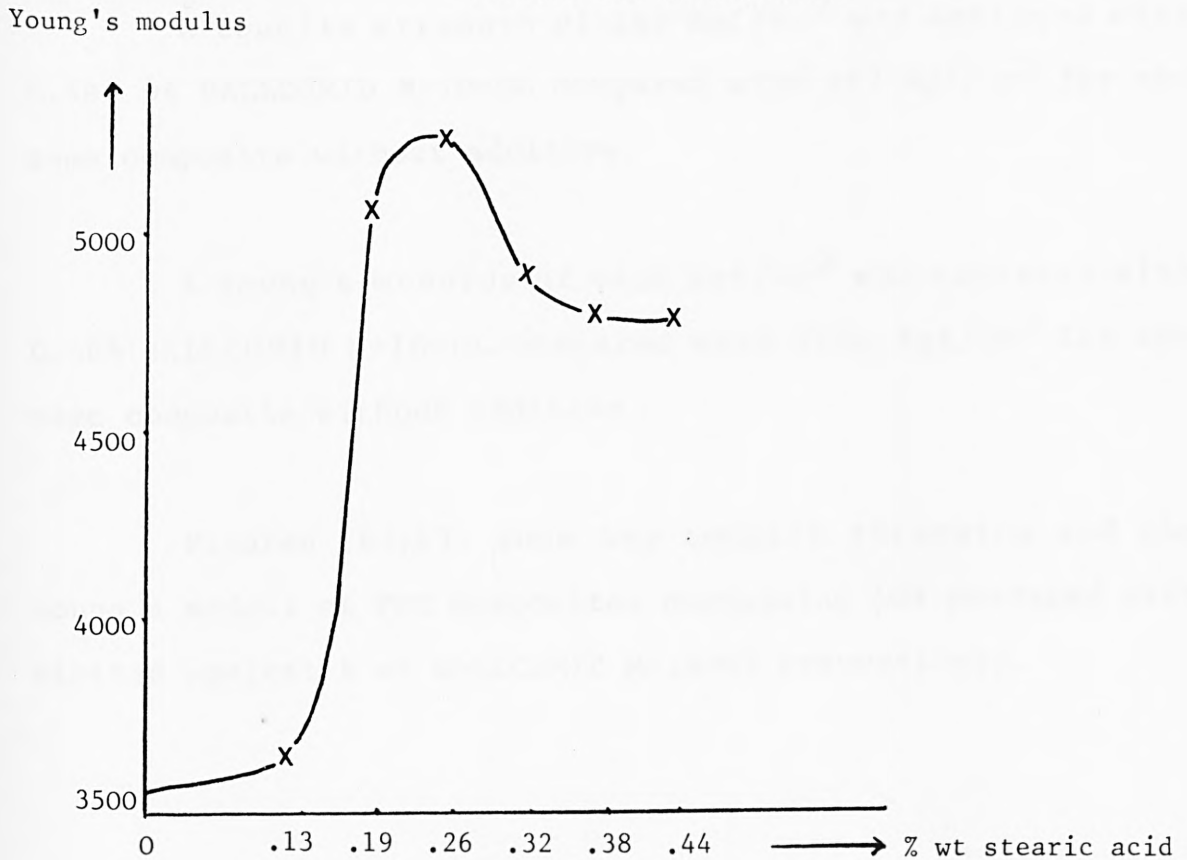


Figure (59) Young's modulus vs. composition of 10% powdered hair/  
PVC/stearic acid phases



compared with 217 Kgf/cm<sup>2</sup> and 3550 Kgf/cm<sup>2</sup> for the same composite without additive respectively. Figures (60,61) show the tensile strengths and Young's moduli of PVC composites containing 10% powdered hair plotted against % wt HALLCOMID M-8-10 respectively.

HALLCOMID M-10-OL limits of (0.23-1.13 % wt) were used and Table (41) shows that the tensile strengths increase with increasing % wt HALLCOMID M-10-OL and reach the maxima when the HALLCOMID M-10-OL is about 0.68% wt while the Young's moduli reach the maxima when the HALLCOMID M-10-OL is about 0.56% wt. Beyond these percentages a decrease in both values is observed.

A tensile strength of 249 Kgf/cm<sup>2</sup> was achieved with 0.68% wt HALLCOMID M-10-OL compared with 217 Kgf/cm<sup>2</sup> for the same composite without additive.

A Young's modulus of 4800 Kgf/cm<sup>2</sup> was achieved with 0.56% HALLCOMID M-10-OL compared with 3550 Kgf/cm<sup>2</sup> for the same composite without additive.

Figures (62,63) show the tensile strengths and the Young's moduli of PVC composites containing 10% powdered hair plotted against % wt HALLCOMID M-10-OL respectively.

Figure (60) Tensile strength vs. composition of 10% powdered hair/  
PVC/HALLCOMID M-8-10 phases

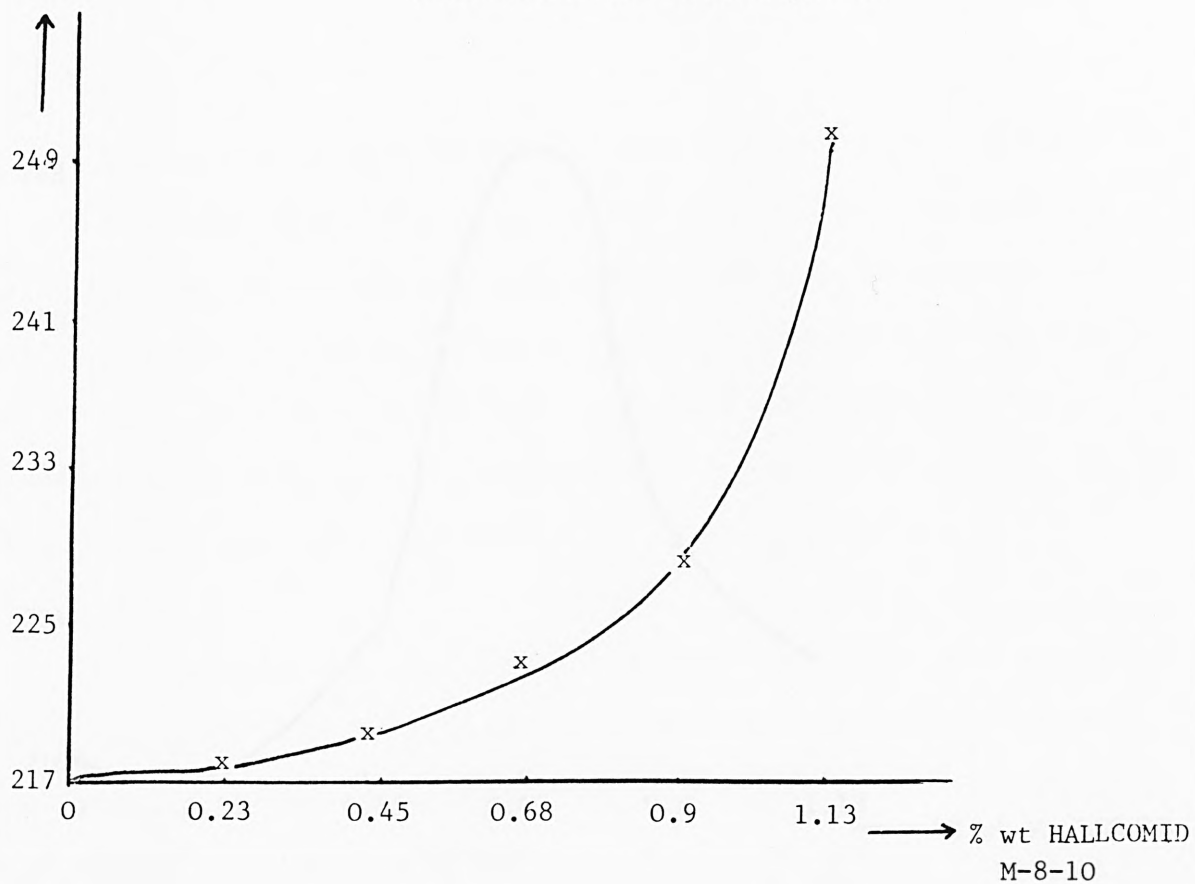


Figure (61) Young's modulus vs. composition of 10% powdered hair/  
PVC/HALLCOMID M-8-10 phases

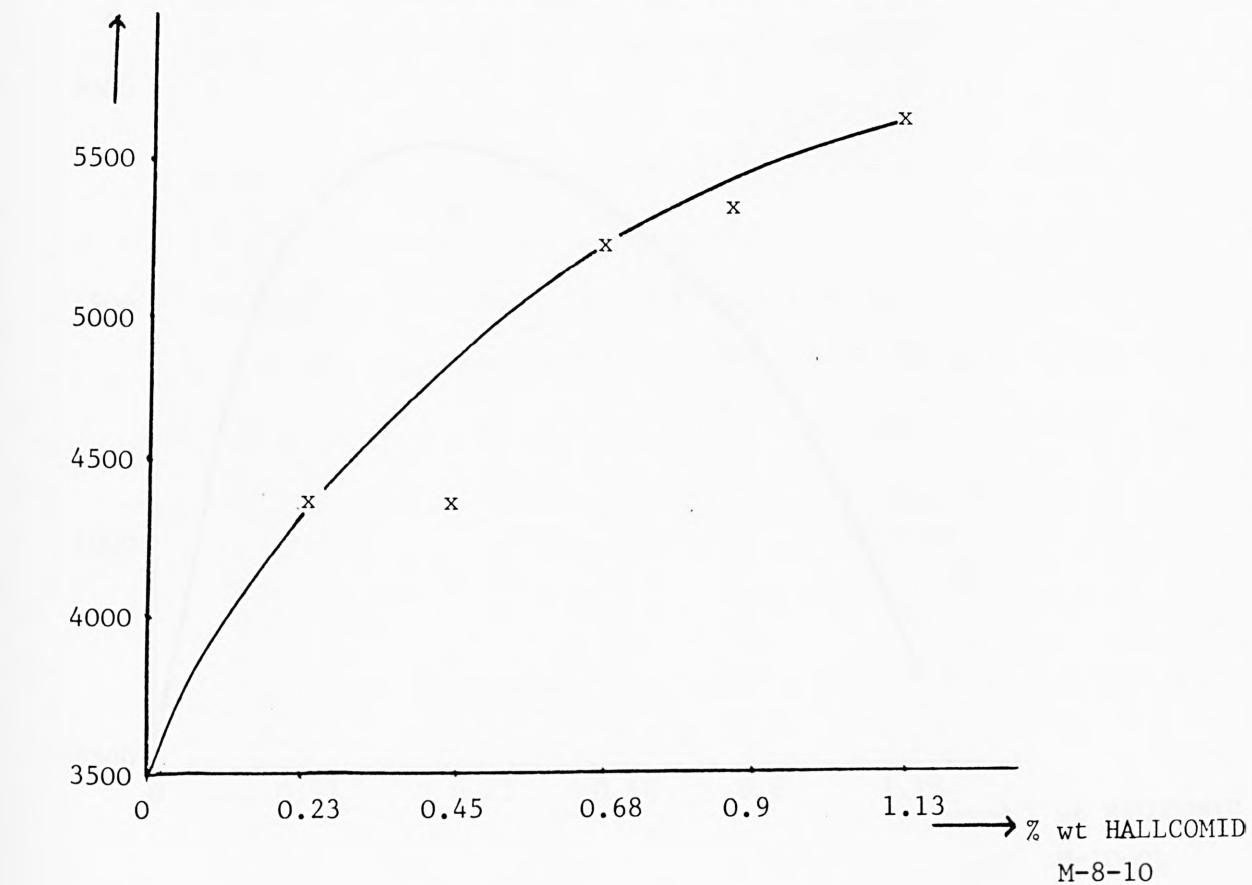


Figure (62) Tensile strength vs. composition of 10% powdered hair/  
PVC/HALLCOMID M-10-OL phases

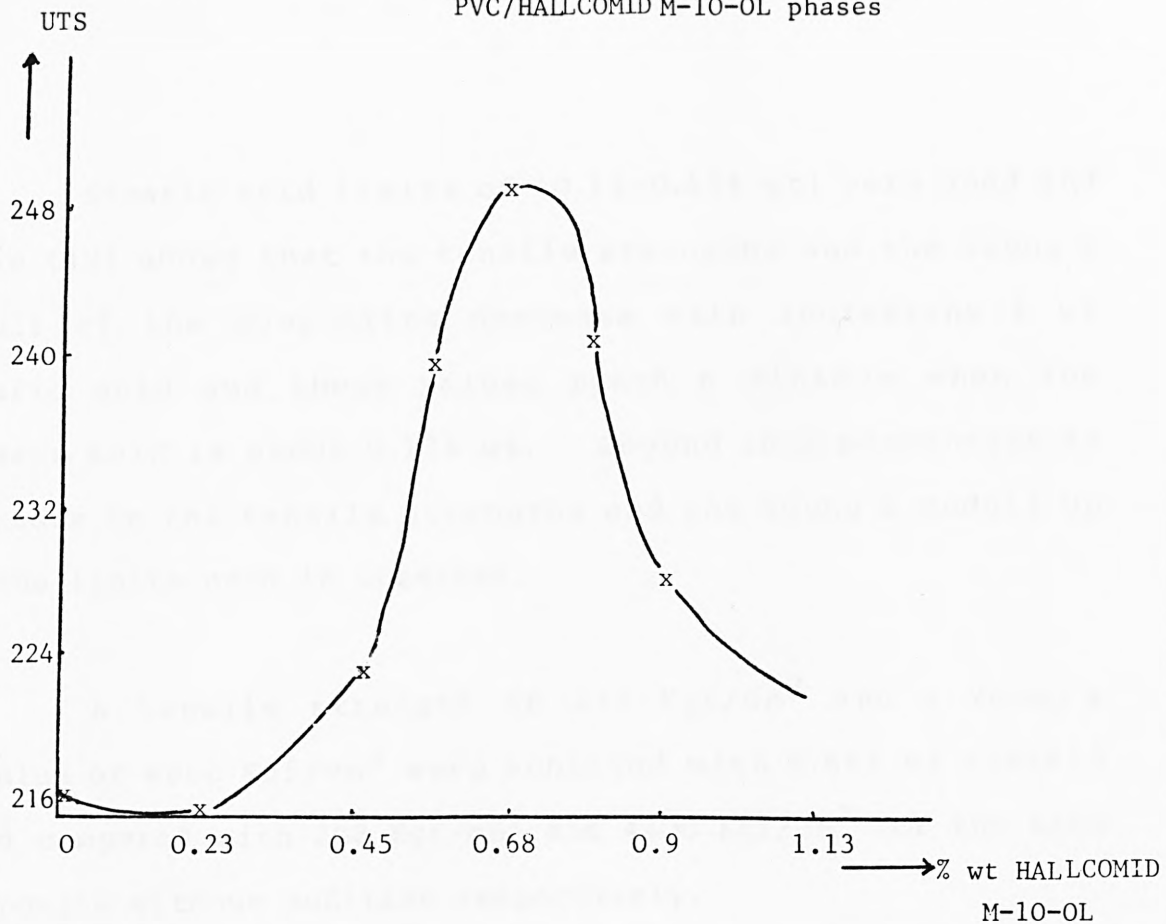
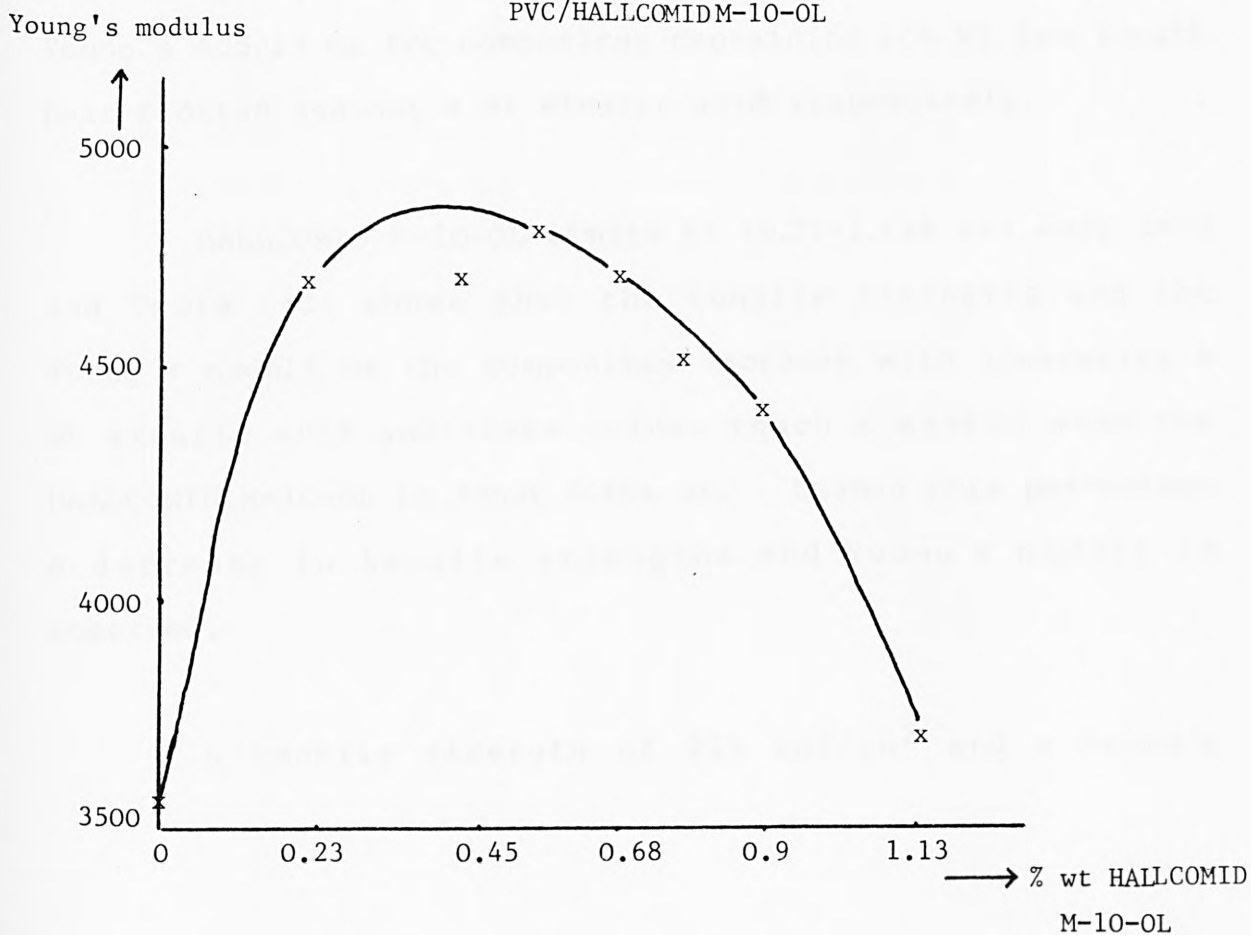


Figure (63) Young's modulus vs. composition of 10% powdered hair/  
PVC/HALLCOMID M-10-OL



Stearic acid limits of (0.13-0.65% wt) were used and Table (42) shows that the tensile strengths and the Young's moduli of the composites decrease with increasing % wt stearic acid and these values reach a minimum when the stearic acid is about 0.13% wt. Beyond this percentage an increase in the tensile strengths and the Young's moduli up to the limits used is observed.

A tensile strength of 215 Kgf/cm<sup>2</sup> and a Young's modulus of 4800 Kgf/cm<sup>2</sup> were achieved with 0.65% wt stearic acid compared with 208 Kgf/cm<sup>2</sup> and 4400 Kgf/cm<sup>2</sup> for the same composite without additive respectively.

Figures (64,65) show the tensile strengths and the Young's moduli of PVC composites containing 10% wt 2mm length hair plotted against % wt stearic acid respectively.

HALLCOMID M-10-OL limits of (0.23-1.13% wt) were used and Table (43) shows that the tensile strengths and the Young's moduli of the composites increase with increasing % wt stearic acid and these values reach a maxima when the HALLCOMID M-10-OL is about 0.45% wt. Beyond this percentage a decrease in tensile strengths and Young's moduli is observed.

A tensile strength of 225 Kgf/cm<sup>2</sup> and a Young's

**Table (42)** Physical properties of 10% 2mm length hair/PVC/  
stearic acid composites

% wt stearic acid	UTS Kgf/cm <sup>2</sup>	Young's modulus Kgf/cm <sup>2</sup>	elongation %
0	208	4400	72
0.13	180	3900	94
0.26	184	4270	73
0.38	188	4300	73
0.65	215	4800	88

**Table (43)** Physical properties of 10% 2mm length hair/PVC/  
HALLCOMID M-10-OL composites

% wt HALLCOMID M-10-OL	UTS Kgf/cm <sup>2</sup>	Young's modulus Kgf/cm <sup>2</sup>	elongation %
0	208	4400	72
0.23	211	4468	93
0.45	225	4690	88
0.68	214	4620	83
0.9	212	4180	114
1.13	180	3920	79

Figure (64) Tensile strength vs. composition of 10% 2mm length hair/  
PVC/stearic acid phases

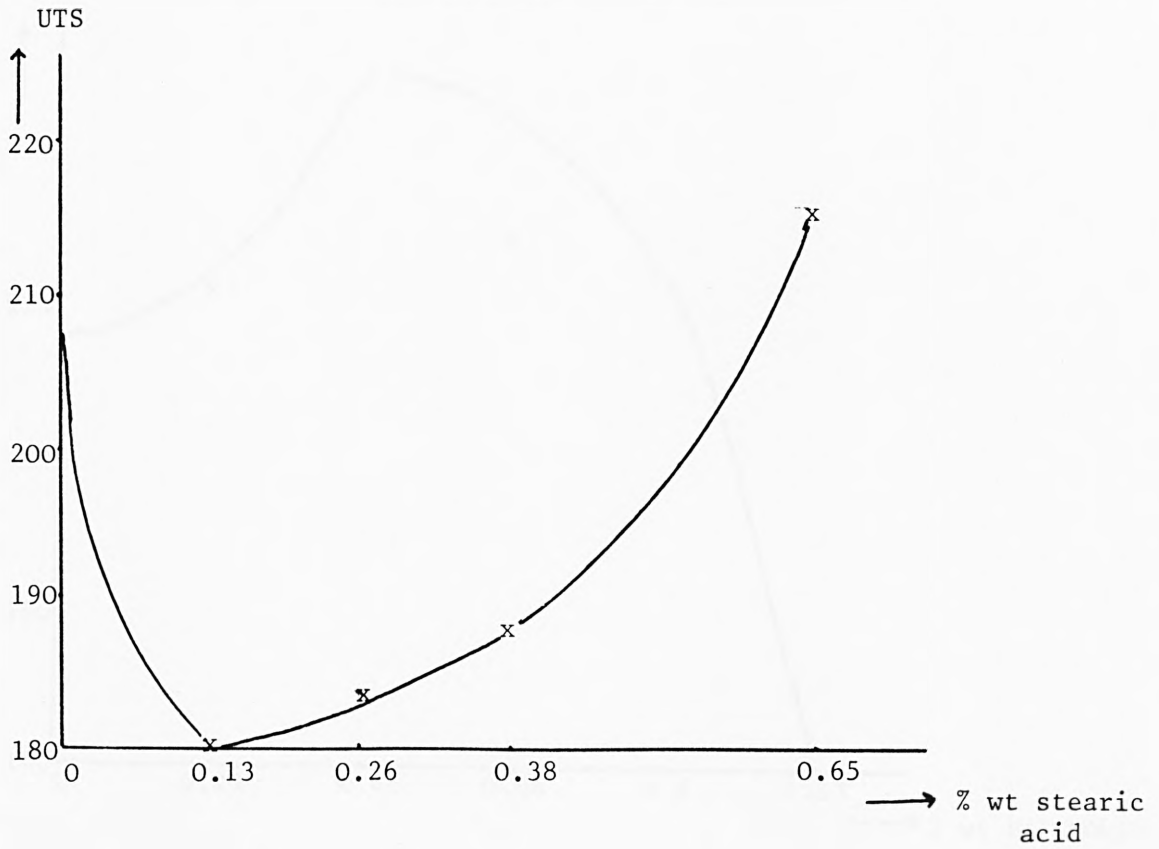


Figure (65) Young's modulus vs. composition of 10% 2mm length hair/  
PVC/stearic acid phases

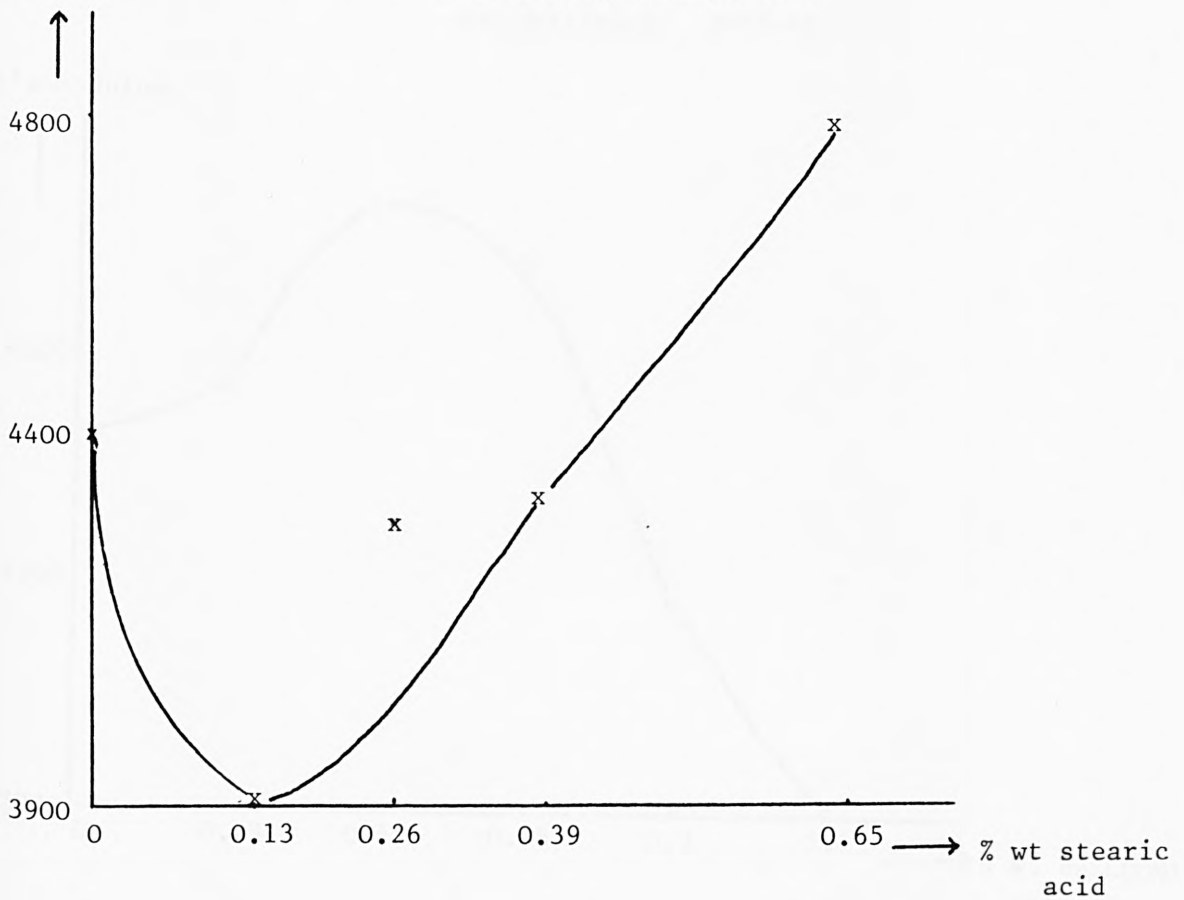


Figure (66) Tensile strength vs. composition of 10% 2mm length hair/

PVC/HALLCOMID M-10-OL phases

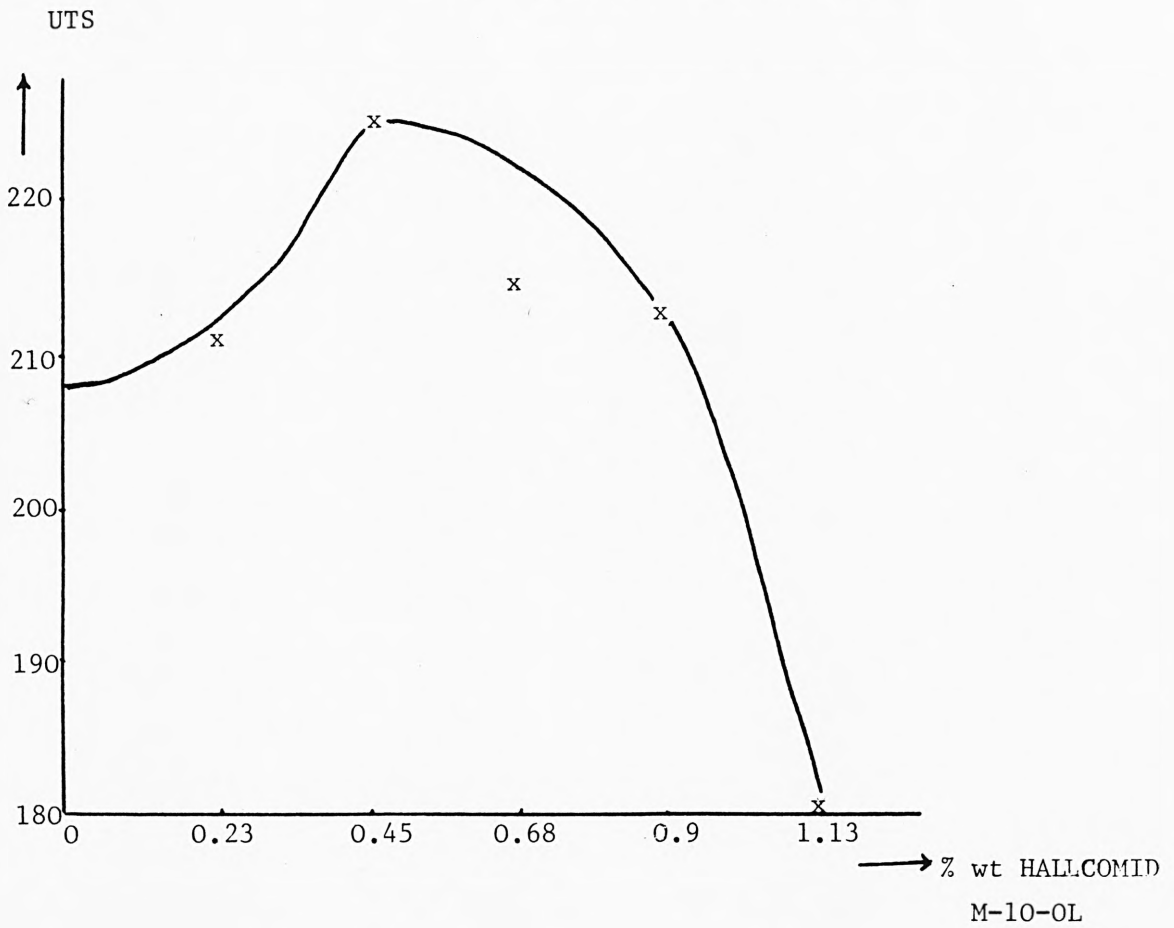
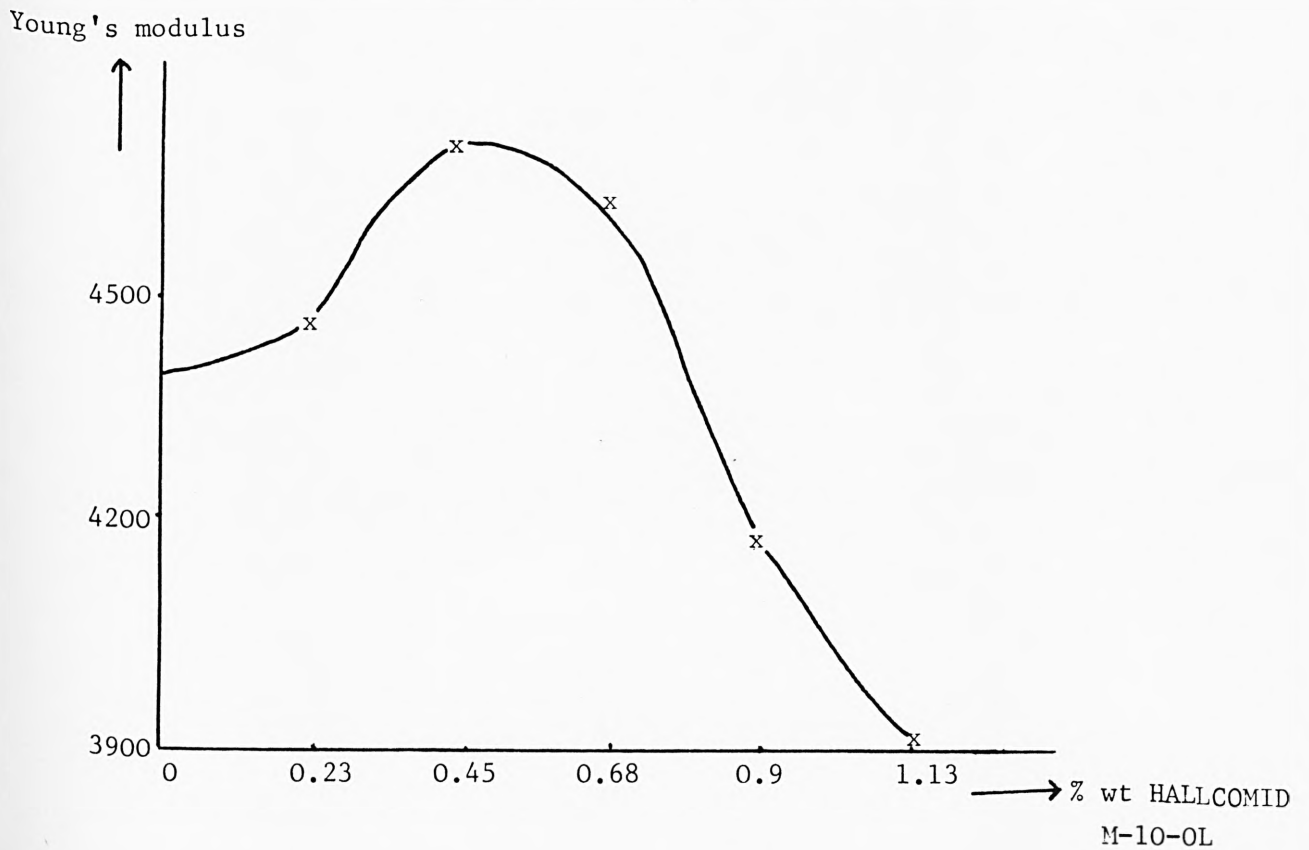


Figure (67) Young's modulus vs. composition of 10% 2mm length hair/

PVC/HALLCOMID M-10-OL



modulus of  $4690 \text{ Kgf/cm}^2$  were achieved with 0.45% wt HALLCOMID M-10-OL compared with  $208 \text{ Kgf/cm}^2$  and  $4400 \text{ Kgf/cm}^2$  for the same composite without additive respectively. Figures (66-67) show the tensile strengths and Young's moduli of the PVC composites containing 10% wt 2mm length hair plotted against % wt HALLCOMID M-10-OL respectively.

#### 4.6 Conclusion

The use of natural hair fibres as reinforcing materials for polyethene and PVC has been studied by the measuring of tensile strengths and Young's moduli of the composites. The results obtained show that:-

1. The tensile strengths and Young's moduli of the composites increase with increasing the load of the fibre for dried powdered hair and for 2mm natural hair.
2. For polyethene use of hair of longer lengths (1-5 cm) decreased the tensile strength and Young's modulus.
3. With polyethene, powdered fibre used in the dispersion gives a higher tensile strength and Young's modulus than 2mm cut fibre.
4. With PVC, 2mm cut hair used in the dispersion gives a higher tensile strength and Young's modulus than powdered hair.
5. The tensile strength and Young's modulus of the composites can be improved by the addition of small quantities of coupling agents.

#### 4.7 References

1. G. Lubin, "Handbook of fibreglass and advanced plastics composites", 1969.
2. M.L. Ryder, "Hair", 1973.
3. C. Long, "Biochemists' handbook", 1961.
4. G.C. Ives, J.A. Mead and M.M. Riley, "Handbook of plastics test methods", 1971.
5. N.J. Parratt, "Fibre reinforced materials technology", 1972.

## CONTENTS

### CHAPTER FIVE: Natural fibre reinforced Cement and Ceramics materials PAGE

#### Section 1

5.1	Introduction	157
5.2	Materials	159
5.3	Experimental	162
5.3.1	Fabrication of the specimens	162
5.3.2	Test methods	167
5.4	Results and discussion	168
5.5	Conclusion	175

#### Section 2

5.6	Introduction	177
5.7	Experimental	179
5.7.1	Fabrication of the specimens	179
5.7.2	Test methods	180
5.8	Results and discussion	180
5.9	Conclusion	184
5.10	References	186

## CHAPTER FIVE

Natural fibre reinforced cement and ceramics materials

### SECTION 1

Natural fibre reinforced cement

#### 5.1 Introduction

Cement is the cheapest building material available to man at present, except for those materials taken directly from their natural state such as mud, clay, stone and timber. Cement has great natural strength in compression, but unfortunately it is weak in tension and in shear. For this reason, various materials have been incorporated into it to make good its deficiencies. However, the incorporation of fibre into a cement matrix to form a composite is a very old technique. Records show that over 2,000 years ago, dwellings were constructed in some regions of the Middle East in which elements of straw were randomly distributed in a paste of silty clay. Significant structures like the 57m hill near Baghdad, built 3500 years ago, were reinforced with reed matting and bundle reinforcement.<sup>1</sup> This was followed by hair in plaster and in more modern times by steel to form reinforced concrete and asbestos to form asbestos cement products.

In recent years, a great deal of attention has been

directed towards improving the mechanical properties of cement and concrete by fibrous reinforcement.<sup>2,3</sup> Commercial products incorporating steel wire, fibrillated polypropylene and glass fibre in various forms are being introduced into the construction industry. However, none of these materials are ideal for strengthening a matrix based on ordinary Portland Cement. Steel is heavy and prone to corrosion if not protected by an adequate covering. Polymers have very low elastic modulus and are, in general, flammable. Glass fibres are generally not stable in the alkaline environment of the hydrated cement, although a degree of success has been achieved with special glass fibres. Carbon fibre has high specific strength and elastic modulus, and chemical inertness at normal temperatures, but because of its high cost, carbon fibre reinforced concrete has not received much attention.

It has proved difficult in the past to produce a thin concrete membrane principally because of its weakness in tension and shear. The need to incorporate steel reinforcement has resulted in the membrane thickness being increased as additional concrete has had to be provided to prevent corrosion. Most fibres, however, do not corrode in a normal environment and they can therefore be dispersed throughout the section of the cement composite without requiring additional protective material. This allows very thin composites of only a few millimetres thickness to be produced. Essentially the fibres act as crack arrestors,

restricting the growth of cracks and thereby transforming an inherently brittle material, with low tensile strength and impact resistance, into a composite with superior crack resistance, greater ductility and a distinctive post-cracking behaviour prior to failure.

Great success in terms of improvements in tensile strength have already resulted from experimental projects which have been carried out using fibre reinforced cement or concrete. There remain, however, problems of flexibility, flammability and expense. It is evident that in this work, the properties of the hair fibre described in the previous chapter (high specific strength, stability in alkaline environments at normal temperatures and very low cost) look particularly attractive.

## 5.2 Materials

Hair fibre reinforced cement composites made by the following materials:-

### 1. Hair fibre

The hair fibre samples used in this work both in cut or powdered form were prepared by the method described in Chapter 4.

## 2. Ordinary Portland Cement (OPC)<sup>4</sup>

The cement used in this work is ordinary Portland Cement. Portland Cement is made by heating a mixture of limestone and clay or other raw materials of equivalent bulk composition and sufficient reactivity, to a maximum temperature of about 1400°C, normally in rotary kiln. Various reactions occur, and the product emerges as hard lumps called clinker. These are mixed with a few per cent of gypsum, and ground to make the cement. The gypsum controls the rate of setting.

The clinker is a mixture of four principal compounds viz:

- (i) Tricalcium silicate ( $3\text{CaO} \cdot \text{SiO}_2$ , 50-70%)
- (ii)  $\beta$ -Dicalcium silicate ( $2\text{CaO} \cdot \text{SiO}_2$ , 20-30%)
- (iii) Tricalcium aluminate ( $3\text{CaO} \cdot \text{Al}_2\text{O}_3$ , 5-12%)
- (iv) Tetracalcium aluminoferrite ( $4\text{CaO} \cdot \text{Al}_2\text{O}_3 \cdot \text{Fe}_2\text{O}_3$ ,  
5-12%)

## Hydration reactions

As cement is a relatively complex mixture, many studies have employed the pure clinker compounds and treated under comparable conditions. Tricalcium silicate develops a high strength, relatively quickly.  $\beta$ -Dicalcium silicate develops a similar strength, though more slowly. The other two phases develop little strength. To a rough approximation, Portland Cements behave as the sums of their constituents, so that an increase in the proportion of tricalcium silicate causes more rapid development of strength. The ability of a substance to set and harden when mixed with water is governed by two factors. The first is its reactivity; tricalcium silicate develops strength more rapidly than does  $\beta$ -dicalcium silicate because it reacts more rapidly. The reactivity is in turn controlled by such factors as crystal structure, nature and the number of defects and particle size. The second is the microstructure of the products; tricalcium aluminate reacts rapidly with water, but the products formed under normal conditions have a poor microstructure and little strength is developed.

The hydration of tricalcium silicate gives calcium hydroxide and a hydrated calcium silicate.  $\beta$ -Dicalcium silicate paste gives closely similar results, but the reaction is much slower and less calcium hydroxide is formed.

### 5.3 Experimental

#### 5.3.1 Fabrication of specimens

A mixture of the appropriate weight ratio of cement and hair fibre was ball milled for five minutes to achieve a homogeneous mix. The mixture was then placed in a pan mixer model [Hobart SE-302] Figure (68) and water was then added. The water/cement ratio used in this work was 0.3 except for experiments with powdered hair where it had to be increased with increasing fibre loading.

In the first stage of mixing about three-quarters of the water was added and the pan was revolved several times until mixing had been achieved. The remainder of the water was then added, mixed in and the resultant slurry was poured into the moulds, trowelled flat and dewatered. To assist dewatering and compaction, the moulds were shaken on a vibrating table until no air was seen to bubble out of the mix. Each mould was lubricated with mould oil before use. Ten specimens were cast from each composition, six specimens were cubes having dimensions of 50 x 50 mm and four were cylinders having dimensions of 37 dia x 74 mm. The moulds were then kept at room temperature for twenty four hours before curing under water until tested.

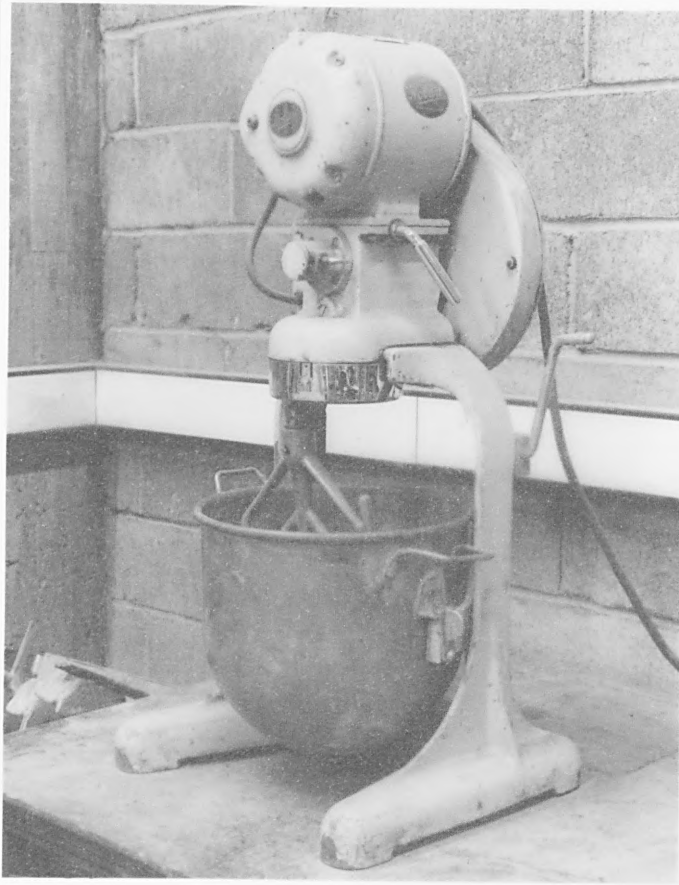


Figure (68) Mixer model (Hobart SE-302)

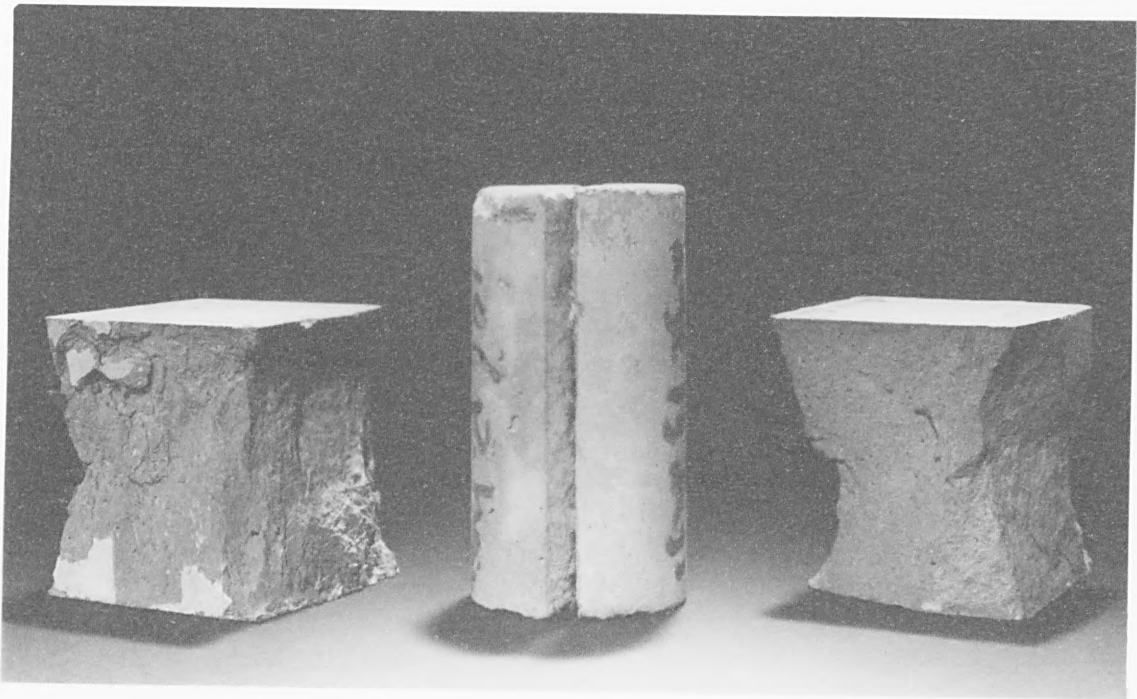
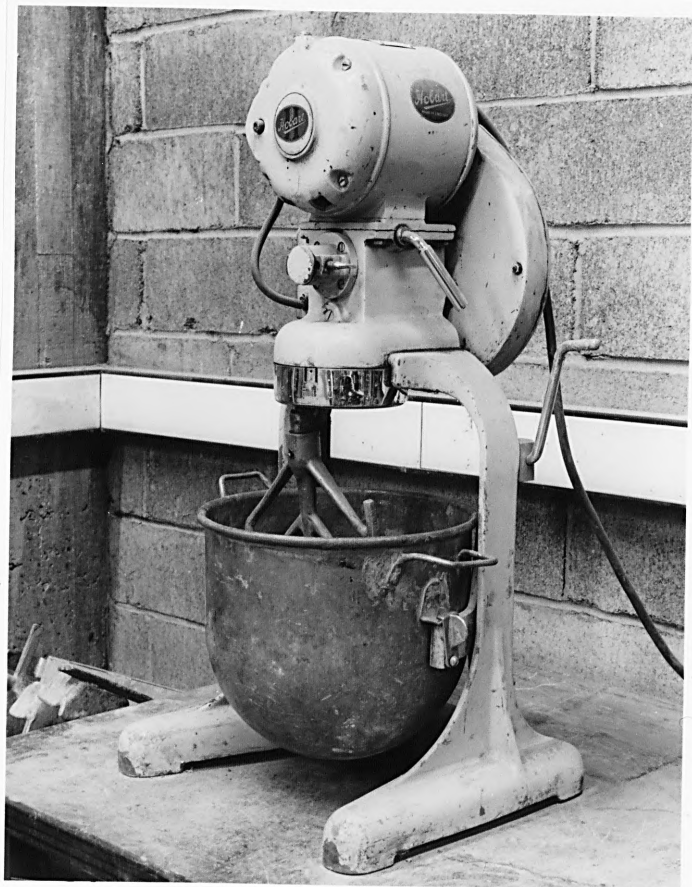


Figure (69) Shows cylinder splitting for measuring the tensile strength and undamaged faces cubes for measuring the compressive strength



### 5.3.2 Test Methods<sup>5</sup>

Two main test methods were used on the composite materials to determine their tensile strength and their compressive strength. The tests should be performed on a duly checked and calibrated testing machine, continuously and without shock.

The testing machine should be equipped with a ball-mounted platen the centre of which should approximately coincide with the centre of the upper loaded face of the specimen. The other platen on which the specimen rests should consist of a very rigid solid block. If the accuracy of the moulds is not satisfactory, the dimensions of all specimens made in them should be measured with an accuracy of within 1mm.

#### Tensile strength measurement by cylinder splitting method

The specimen to be tested should be placed between the platens of the press so that force is applied to two diametrically opposite generating lines. The load may be applied quickly up to 50% of the anticipated failure load, thereafter it should be increased more slowly.

Plywood or cardboard strips should be inserted

between the platens of the press and the generating lines to which the loading is applied. The tensile strength of the composite was determined by the split cylinder test Figure (69) as detailed in B.S. 1881.<sup>6</sup>

All specimens were tested after 7 days, 14 days, 21 days and 28 days of storage in water in the Avery testing machine Figure (70). If the failure load is (P) in Newtons, then the tensile strength (ft) is given by:-

$$f_t = \frac{2P}{\pi d I}$$

where:- d is diameter in mm

I is length in mm

### Compressive strength

The specimen should be well centred between the platens of the press, and loading should be applied at a constant rate. Cubes should be tested preferably by placing the lateral faces (which were in contact with the mould) in contact with the platens.

During the first half of the loading operation a higher loading rate can permissibly be applied, however, loading should continue until failure of the specimen occurs.

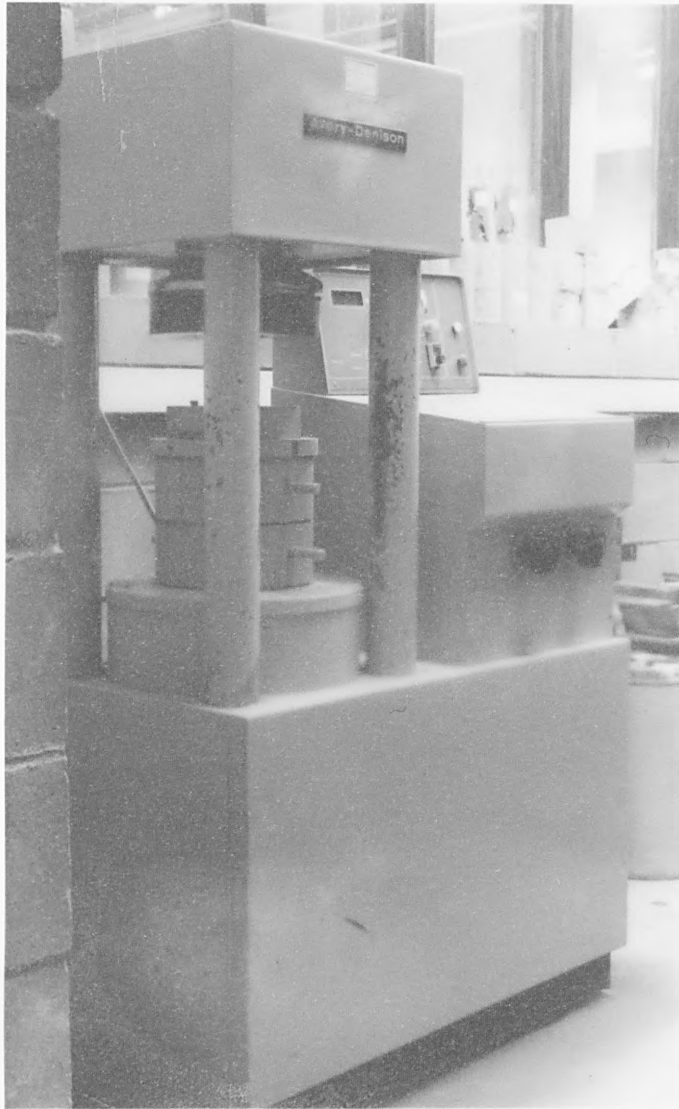
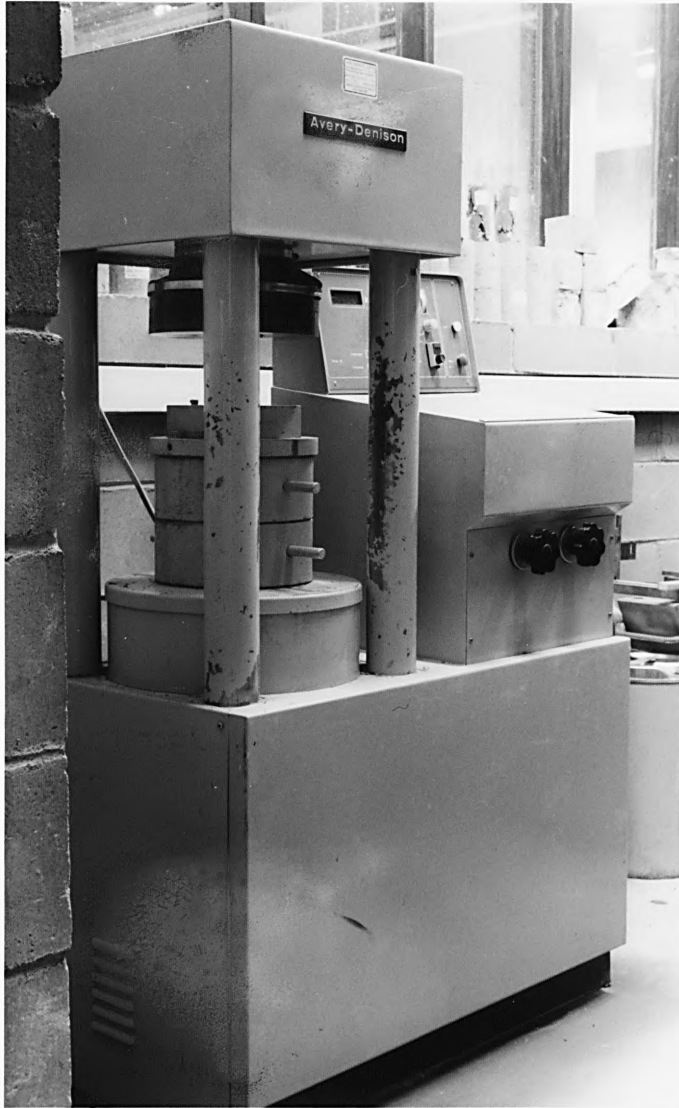


Figure (70) Avery testing machine



The maximum load reached should be recorded.

The cubes were tested for compressive strength after 7 days, 14 days, 21 days and 28 days of storage in water in an Avery testing machine. After failure the cubes showed slight spalling at the corner and edges, but the faces were generally undamaged Figure (69). The compressive strength was calculated using the nominal cross-sectional area as detailed in B.S.1881.

#### 5.4 Results and discussion

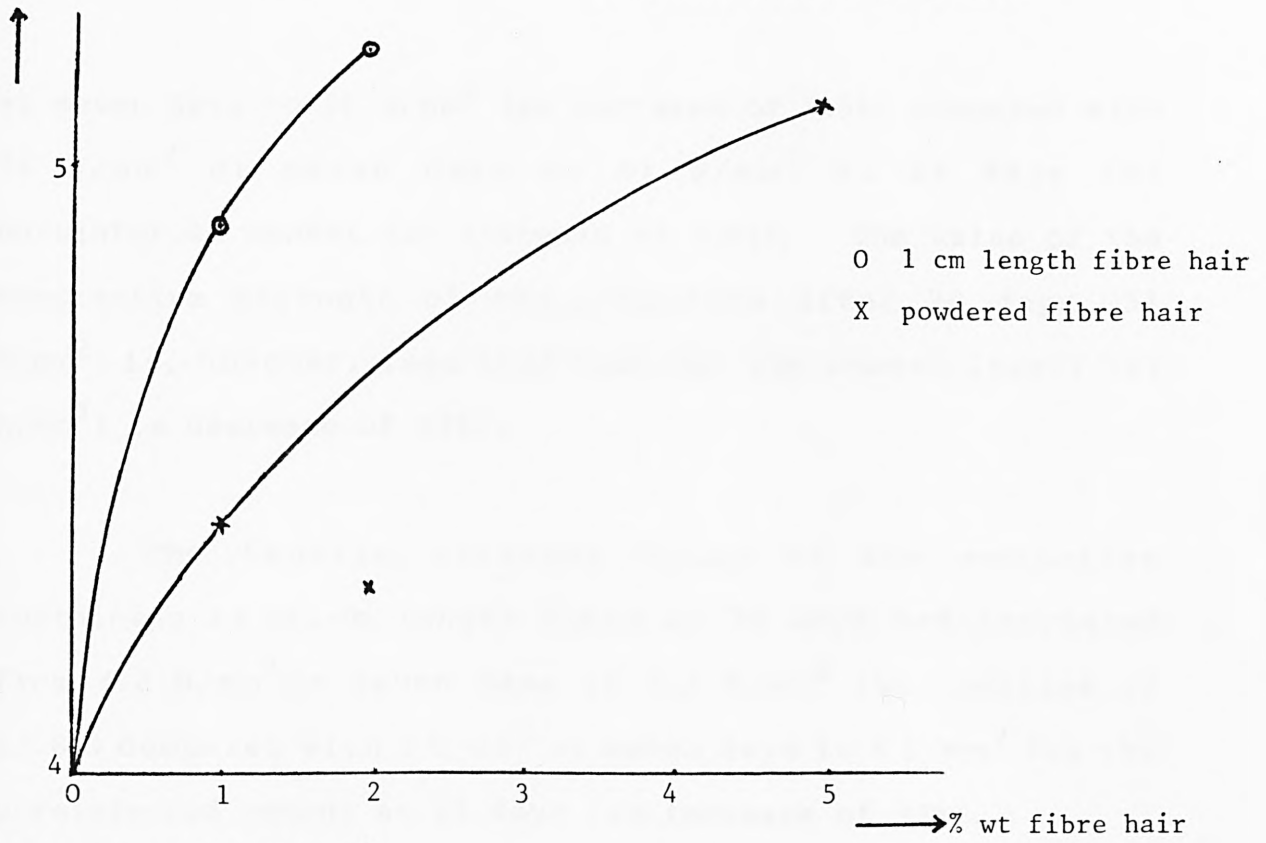
It is evident from Table (44) and Figure (71) that for all fibre types used the tensile strengths of the composites increase with increasing fibre proportions during the curing period, while the compressive strengths decrease with increasing fibre load. Both tensile strength and compressive strength of the composites increased with time during the curing period Figure (72) and (73).

There is an indication that the tensile strength values reach a maxima when the powdered fibre concentration is about 5% wt and beyond this percentage a decrease in tensile strength is observed. It is also noticed that the tendency of 1 cm length of fibre to tangle and ball up increases with increasing fibre loading and for this reason it was more difficult to achieve uniform dispersion when the proportion of 1 cm length fibre was greater than 2% wt. At the optimum level of powdered fibre addition (5% wt) the tensile strength values of the composites at 28 days had increased from 3 N/mm<sup>2</sup> at seven days to 5.1 N/mm<sup>2</sup> (an increase of 70%) compared with 3 N/mm<sup>2</sup> at seven days to 4 N/mm<sup>2</sup> for the unreinforced cement at 28 days (an increase of 33%).

The compressive strength of the composite containing 5% wt powdered fibre at 28 days had increased from 46.6 N/mm<sup>2</sup>

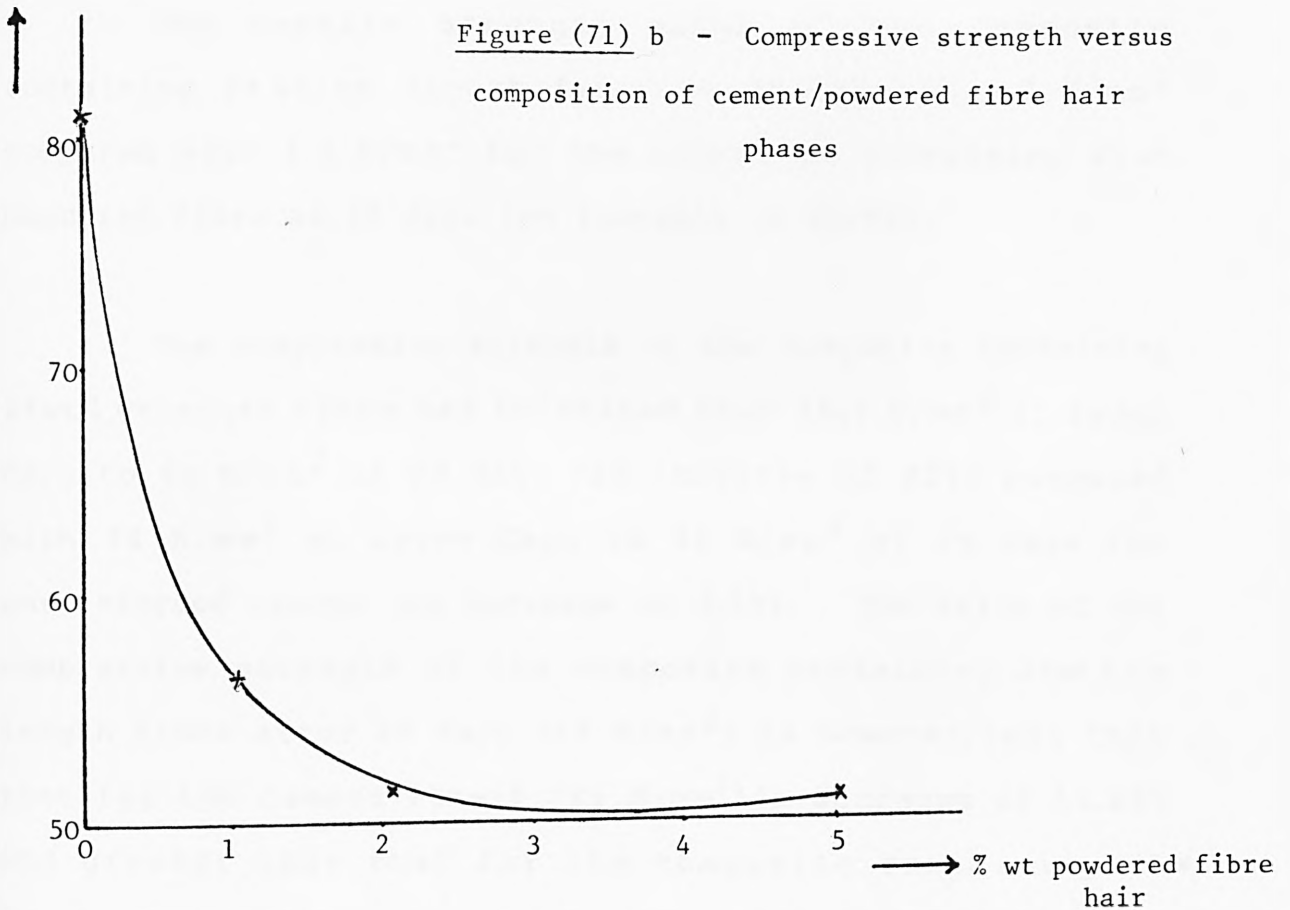
Figure (71) a - Tensile strength versus composition of cement/fibre hair phases

Tensile strength  $N/mm^2$



Compressive strength  $N/mm^2$

Figure (71) b - Compressive strength versus composition of cement/powdered fibre hair phases



at seven days to  $51 \text{ N/mm}^2$  (an increase of 9.5%) compared with  $74 \text{ N/mm}^2$  at seven days to  $81 \text{ N/mm}^2$  at 28 days for unreinforced cement (an increase of 9.5%). The value of the compressive strength of the composite after 28 days ( $51 \text{ N/mm}^2$ ) is, however, less than that for the cement itself ( $81 \text{ N/mm}^2$ ) (a decrease of 37%).

The tensile strength value of the composite containing 2% wt 1cm length fibre at 28 days had increased from  $4.2 \text{ N/mm}^2$  at seven days to  $5.2 \text{ N/mm}^2$  (an increase of 23.8%) compared with  $3 \text{ N/mm}^2$  at seven days to  $4 \text{ N/mm}^2$  for the unreinforced cement at 28 days (an increase of 33%).

The tensile strength value of the composite containing 2% wt 1cm length fibre at 28 days is  $5.2 \text{ N/mm}^2$  compared with  $4.3 \text{ N/mm}^2$  for the composite containing 2% wt powdered fibre at 28 days (an increase of 20.9%).

The compressive strength of the composite containing 2% wt 1cm length fibre had increased from  $56.5 \text{ N/mm}^2$  at seven days to  $69 \text{ N/mm}^2$  at 28 days (an increase of 22%) compared with  $74 \text{ N/mm}^2$  at seven days to  $81 \text{ N/mm}^2$  at 28 days for unreinforced cement (an increase of 9.5%). The value of the compressive strength of the composite containing 2% wt 1cm length fibre after 28 days ( $69 \text{ N/mm}^2$ ) is, however, less than that for the cement itself ( $81 \text{ N/mm}^2$ ) (a decrease of 14.8%) and greater than that for the composite containing 2% wt

powdered fibre after 28 days ( $51 \text{ N/mm}^2$ ) (an increase of 35.3%).

In order to study the effects of the alkaline environment of the cement on the physical properties of the fibre used, the 1 cm length fibre was treated with 1M NaOH for 15 minutes and then washed with water by decantation to pH7. The fibre was then dried at room temperature. The dried fibre was incorporated into the cement using the same method described in Section 5.3.1.

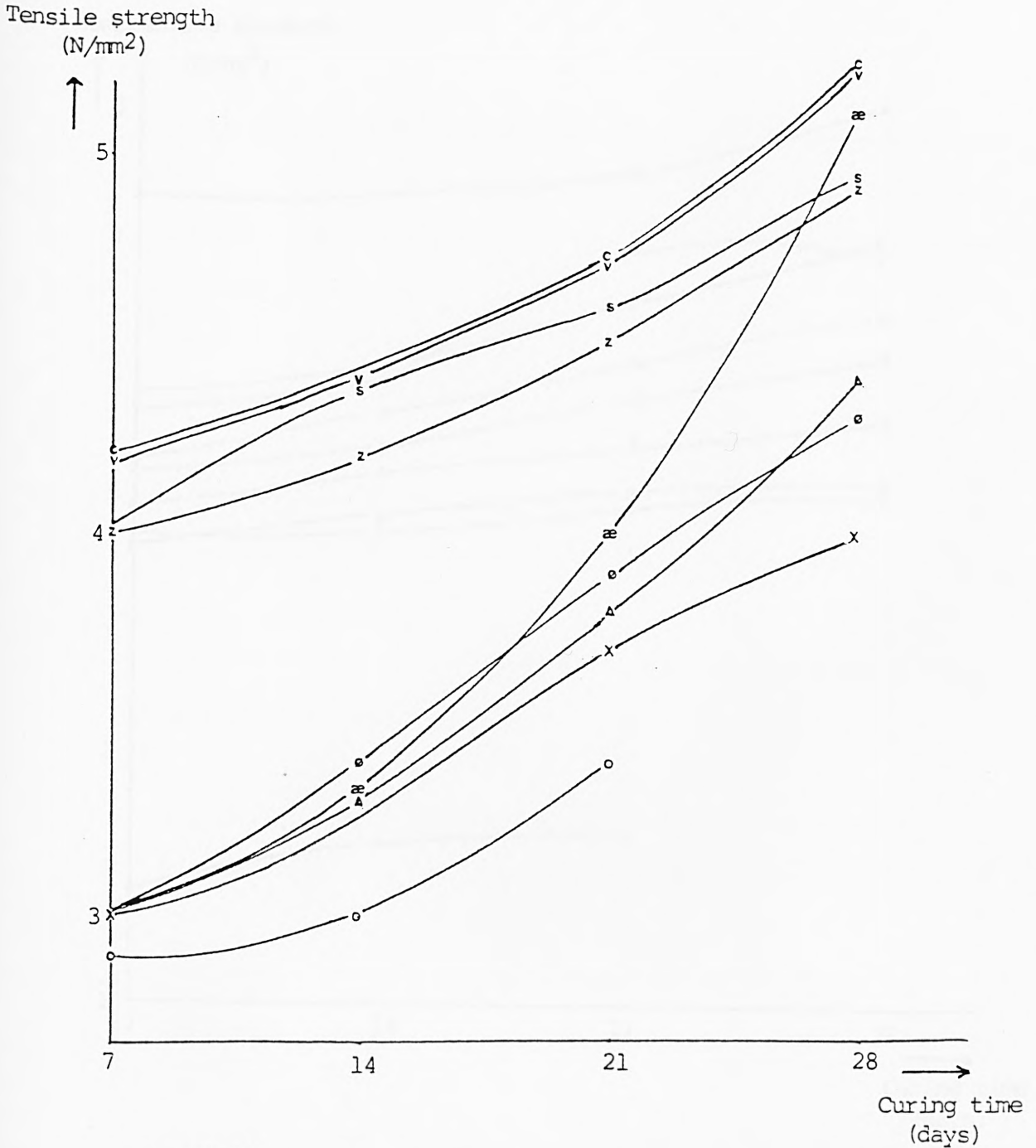
The tensile strength and compressive strength values showed little or no difference compared with the values obtained for untreated fibre (see Table 44).

**Table (44)**

Tensile strength and compressive strength measurements of  
hair:cement composites

	water:cement ratio	Tensile strength N/mm <sup>2</sup>				Compressive strength N/mm <sup>2</sup>			
		7 days	14 days	21 days	28 days	7 days	14 days	21 days	28 days
Cement	0.3	3		3.7	4	74		76	81
1:99 powdered hair:cement	0.3	3	3.3	3.8	4.4	49.5	52	54	56
2:98 powdered hair:cement	0.3	3	3.4	3.9	4.3	46	48	50	51
5:95 powdered hair:cement	0.34	3	3.3	4.0	5.1	46.6	47.2	49	51
10:90 powdered hair:cement	0.39	2.9	3	3.4		19	22.4	23.6	
1:99 1 cm length hair:cement	0.3	4	4.2	4.5	4.9	52	54	58	61
2:98 1 cm length hair:cement	0.3	4.2	4.4	4.7	5.2	56.5	59	69.5	69
1:99 1 cm length treated hair:cement	0.3	4	4.4	4.6	4.9	52	57	61	65
2:98 1 cm length treated hair:cement	0.3	4.2	3	4.7	5.2	58	60	65.4	70

Figure (72) Tensile strength vs. composition of cement/  
natural fibre phases



- x - cement
- Δ - 1:99 powdered hair : cement
- o - 2:98 " " "
- æ - 5:95 " " "
- o - 10:90 " " "
- z - 1:99 1 cm length hair : cement
- v - 2:98 " " " " "
- s - 1:99 " " " treated hair : cement
- c - 2:98 " " " " " "



## 5.5 Conclusion

Dispersion of fibre in ordinary Portland Cement has been investigated using a natural fibre as a reinforcement. The natural fibre was used in the form of either powdered fibre or chopped fibre.

The results obtained show that:-

1. The tensile strength of the cement composite increases with increasing fibre proportions.
2. Cut fibre gives a higher tensile strength than powdered fibre.
3. The compressive strength of the cement composite decreases with increasing fibre proportions.
4. Cut fibre gives a higher compressive strength than powdered fibre.
5. The tensile strength and the compressive strength of the cement composite increases with increased curing time in water because Portland Cement and other hydraulic cements expand if allowed to set and harden while stored in water.

6. The results obtained from the tensile strength and compressive strength of the composite containing natural fibre treated with 1M NaOH showed little or no difference compared with the results obtained for the composite containing untreated fibre.

The increase in the tensile strength of the cement on addition of the fibre must owe its origin to the fact<sup>7</sup> that the short fibres can transfer stress from one fibre to another resulting in reinforcement. It is interesting that the 1 cm cut fibres give higher tensile strength composites than the cement containing powdered fibre composites and this is consistent with more effective stress transfer in the longer untreated fibres.

## SECTION II

Natural fibre reinforced ceramic materials.

### 5.6 Introduction<sup>8,9,10</sup>

Traditional ceramic techniques consist in the main of working and heating china clay, ball clay, calcined flint and a feldspathic mineral. After firing, the clay becomes microporous and consists of crystalline phases bonded by a complex glassy phase. The mechanical strength and physical properties of the ceramics are reduced as their porosity increases.

The porosity is controlled to a degree by adding up to 50% of animal bone to produce domestic items and by adding feldspar as the flux in place of bone to produce porcelain goods for electrical insulators.

A second major branch of the ceramics industry uses clay minerals without additions, to produce building materials such as bricks, tiles, pipes and floor quarries. In general, bulk ceramics tend to exhibit low tensile strength and poor resistance to thermal and mechanical shock.

The brittle behaviour of ceramics has been discussed extensively in the literature.<sup>11,12</sup> It occurs because ceramics do not undergo extensive plastic deformation prior to fracture, which is thus a measure of toughness (the work of fracture for most ceramics  $10\text{J m}^{-2}$  and for ductile metals  $10^4\text{-}10^6\text{J m}^{-2}$ ). Considerable attention in recent years has been paid to the reinforcement of materials with fibres and whiskers. Great success has already resulted from experimental projects which have been carried out using carbon fibre, zirconia fibre, steel fibre, copper fibre and nickel fibre to reinforce ceramics.

The main aim of the work carried out in this thesis is to improve the physical properties of ceramic materials by using a natural fibre as a reinforcement. Tests of the success of the natural fibres as reinforcing agents are based on tensile and compressive strength measurements.

The natural fibre was supplied by Ferrocom Ltd. and used in either powdered fibre or chopped fibre (i.e. 1 cm length). The clay used in this work as a raw material to fabricate the ceramic samples was "ball clay" which is supplied by Fulham Pottery Ltd. as a fine creamy powder.

## 5.7 Experimental

### 5.7.1 Fabrication of the specimens

A mixture of the appropriate weight ratio of ball clay and natural fibre was ball milled for five minutes to achieve a homogeneous mix. The mixture was then placed in a bowl. Water (23%-26%) was then added and mixed by hand until a nonsticky dough was formed. The dough was then pressed by hand into an oiled mould to expel any air bubbles which might cause explosion in the firing and then flattened using a wire.

From each composition, four cylinders having dimensions of 37 dia x 74 mm and two cubes having dimensions of 50 x 50 mm were made. The samples were then kept at room temperature for 72 hrs before being oven dried at 110°C for 48 hrs then the dried samples were placed in a furnace and fired with the temperature being slowly increased to 1100°C over about 6-7 hrs. Once at maximum temperature the furnace was turned off and the moulded clay allowed to cool over night.

### 5.7.2 Test Methods

Two main test methods were carried out on the composite materials viz. to determine their tensile strength and their compressive strength. The measurements made were those described in Section 5.3.2.

### 5.8 Results and Discussion

It is evident from Table (45) and Figure (74) that for all fibre types (i.e. powdered fibre and 1 cm length fibre) the tensile strengths of the composites increase with increasing fibre proportions and reach their maxima when the powdered fibre concentration was about 1% wt. Beyond this percentage a decrease in tensile strength was observed although the value is still higher than the tensile strength value of unreinforced ball clay. The tensile strength values of  $4.2 \text{ N/mm}^2$  and  $3.3 \text{ N/mm}^2$  were achieved with 1%wt and 5% wt powdered fibre respectively compared with  $3.1 \text{ N/mm}^2$  for the unreinforced ball clay.

The compressive strength of the composites increased with increasing fibre proportions Figure (75). A compressive strength of  $20.9 \text{ N/mm}^2$  was achieved with 5%wt powdered hair compared with  $18.5 \text{ N/mm}^2$  for the unreinforced ball clay. The tensile strength of the composites containing 1 cm length fibre increased with increasing the

fibre proportions and reached their maxima when the fibre concentration was about 1%wt but beyond this percentage a decrease in the tensile strength occurred. A tensile strength of  $3.5 \text{ N/mm}^2$  was achieved with 1%wt 1 cm length fibre compared with  $3.1 \text{ N/mm}^2$  for the unreinforced ball clay. A tensile strength of  $4.7 \text{ N/mm}^2$  was achieved with 2%wt 1 cm length fibre treated with 1M NaOH for 15 minutes compared with  $3.1 \text{ N/mm}^2$  and  $3.5 \text{ N/mm}^2$  for the unreinforced ball clay and 1%wt 1 cm length untreated fibre respectively.

When clay dough samples dry, a decrease in volume is observed. This is called shrinkage, (shrinkage of 4-10% occurs depending on the type of clay used). This may give rise to cracks, particularly when the firing rate is high and the heating nonuniform.

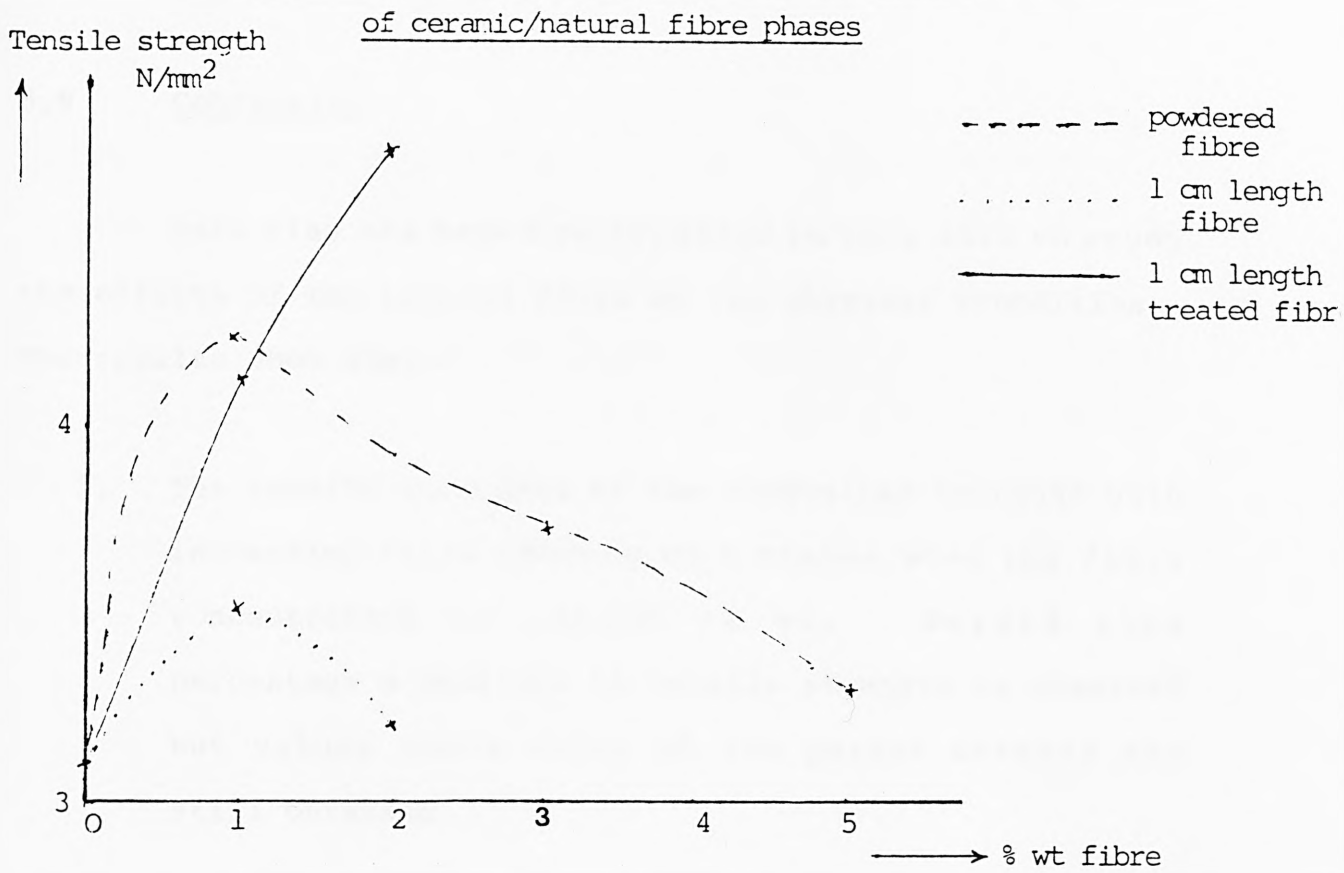
In this work the shrinkage was found to decrease with increasing fibre proportions. A volumetric shrinkage of 4% was achieved with 5%wt powdered fibre compared with 9.8% for the unreinforced ball clay.

Table (45)

Tensile strength and compressive strength measurements of  
hair:ceramic composition

	water:clay ratio	Tensile strength N/mm <sup>2</sup>	Compressive strength N/mm <sup>2</sup>
Ball clay	0.23	3.1	18.5
1:99 powdered hair:clay	0.23	4.2	
2:98 powdered hair:clay	0.25	3.9	
3:97 powdered hair:clay	0.26	3.7	19.9
5:95 powdered hair:clay	0.26	3.3	20.9
1:99 1 cm length hair:clay	0.23	3.5	
2.98 1 cm length hair:clay	0.23	3.2	
1.99 1 cm length treated hair:clay	0.23	4.1	
2:98 1 cm length treated hair:clay	0.23	4.7	

Figure (74) Tensile strength vs composition



Compressive strength  
N/mm<sup>2</sup>

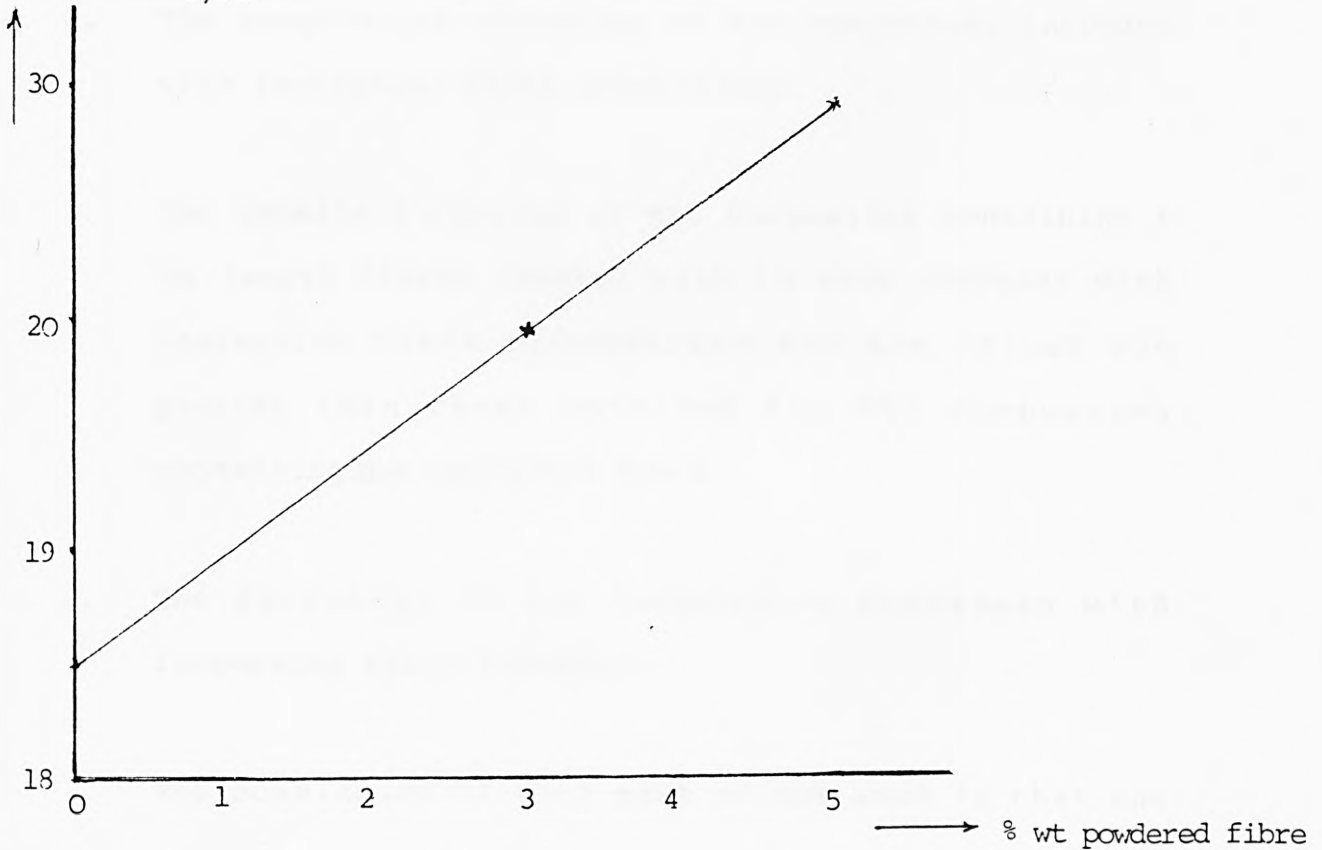


Figure (75) Compressive strength vs composition  
of ceramic/powdered fibre phases

## 5.9 Conclusion

Ball clay has been investigated in this work to study the effects of the natural fibre on its physical properties.

The results show that:-

1. The tensile strengths of the composites increase with increasing fibre loading to a maxima when the fibre concentration is about 1% wt. Beyond this percentage a decrease in tensile strength is observed but values above those of the parent ceramic are still obtained.
2. The compressive strengths of the composites increase with increasing fibre proportions.
3. The tensile strengths of the composites containing 1 cm length fibres treated with 1M NaOH increase with increasing fibre proportions and the values are greater than those obtained for the composites containing 1%wt untreated fibre.
4. The shrinkage of the composites decreases with increasing fibre loadings.

The conclusion of this part of the work is that the

addition of natural fibres to ceramic materials can improve the tensile and compressive strength of the composite materials even though the firing temperature is above the temperature of decomposition of the fibre itself. The results, particularly those for alkali treated fibres suggest that a reaction does occur between the ceramic and the fibre during the firing process.

5.10 References

1. N.R. Swamy, "Current status of research, development and applications of fibre reinforced cement and concrete", contemporary European concrete research, pp. 245-263, Stockholm, June 1981.
2. Partical studies from the Building Research Establishment, "Fibre reinforced materials", Vol. 2, 1978.
3. A. Neville, "Fibre reinforced cement and concrete", 1975.
4. Chemistry and Industry, 19th September 1981, No. 18, pages 620-625.
5. UNESCO, "Reinforced Concrete", 1971.
6. B.S. 1881 Part 4, Methods of testing concrete for strength, 1970.
7. N.J. Parratt, "Fibre reinforced materials technology", 1972.
8. P.P. Budnikov, "The technology of ceramics and refractories", 1964.
9. L.A. Lay, "Corrosion resistance of technical ceramics", 1983.
10. I.J. McColm, "Ceramic science for materials technologists", 1983.
11. D.C. Phillips, J. Mater. Sci., 9, 1847, 1974.
12. R.A.J. Sambell, D.H. Bowen and D.C. Phillips, J. Mater. Sci., 7, 663, 1972.

## CONTENTS

<u>CHAPTER SIX</u>	<u>Tin (II) methane sulphonate, Tin (II) <math>\rho</math>-toluene sulphonate and dispersion of Tin (II) sulphate in benzene sulphonic acid, <math>\rho</math>-toluene sulphonic acid and methane sulphonic acid</u>	<u>Page</u>
6.1	Introduction	183
6.2	Principles of anodising	188
6.3	Electrolytic colouring	191
6.4	Analytical techniques	192
6.4.1	Elemental analysis	192
6.4.2	Tin analysis (Donaldson and Möser's method)	193
6.4.3	Thermal analysis	194
6.4.4	Mössbauer spectroscopy	198
6.5	Experimental	209
6.5.1	Preparation of tin (II) sulphate	209
6.5.2	Preparation of tin (II) sulphate dispersion in benzene sulphonic acid and $\rho$ -toluene sulphonic acid	209
6.5.3	Preparation of tin (II) methane sulphonate and tin (II) $\rho$ -toluene sulphonate	210
6.6	Results and discussion	211
6.6.1	Element analysis	211
6.6.2	X-ray diffraction	212
6.6.3	Mössbauer data	215
6.6.4	Thermal analysis	218
6.7	Conclusion	221
6.8	References	222

## CHAPTER SIX

Tin (II) methane sulphonate, Tin (II) p-toluene sulphonate and dispersion of Tin (II) sulphate in benzene sulphonic acid, p-toluene sulphonic acid methane sulphonic acid

### 6.1 Introduction

Tin (II) methane sulphonate and tin(II) p-toluene sulphonate are used in the production of grey coloration in anodised aluminium coating. Both of these tin (II) derivatives could have a short shelf life because of their ease of oxidation in air. The purpose of this work was to determine whether dispersion of tin (II) materials in p-toluene sulphonic acid would lead to reduction in the rate of their oxidation and to longer useful working lifetimes.

### 6.2 Principles of anodising<sup>1,2</sup>

In anodising process aluminium components are made with the anode (A) in a dilute electrolyte containing suitable cathodes (C) and on passage of current, oxygen is liberated at the anode face to form an adherent, transparent oxide film. Hydrogen is liberated at the cathode. Various electrolytes can be employed for anodising, but sulphuric acid electrolyte produces a colourless transparent oxide film and is much used in architectural anodising and during the passage of current, sulphate ions are attracted towards the

anode. Part of aluminium which does not combine with oxygen dissolves in the electrolyte. Sulphate ions combine with the aluminium and assist the movement of protons in the electrolyte, hence reducing the voltage required for the process.

During the first minute of the passage of current, a thin film is formed whose thickness is directly proportional to the current density and time (i.e. to the quantity of electrical current used); this is known as the "barrier layer". Once this limiting thickness is reached, the sulphuric acid electrolyte begins dissolving the aluminium oxide, then a porous film is formed and the oxidation process can continue leading to the production of relatively thick films. Eventually the rate of film formation is balanced by the rate of solvent attack. Figure (76) shows microcellular structure of anodic film.

The diameter of the pores and the thickness of the barrier layer for any given electrolyte and temperature are proportional to the applied voltage. Thus by varying the anodising conditions it is possible to alter the physical properties of the coating, such as the hardness, abrasion resistance and the density.

The colouring process is carried out after anodising.

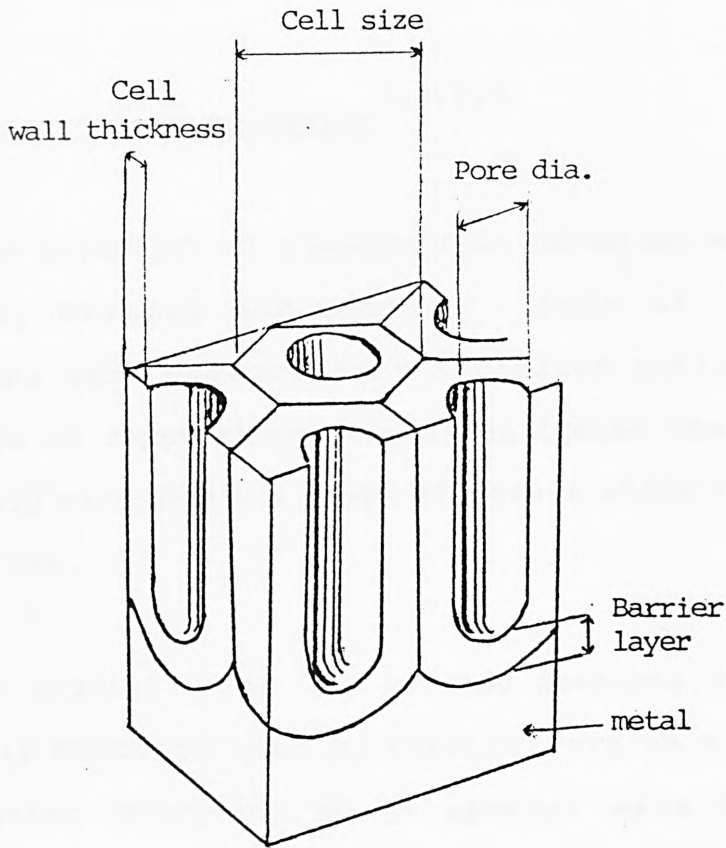


Figure (76) Microstructure of anodic film

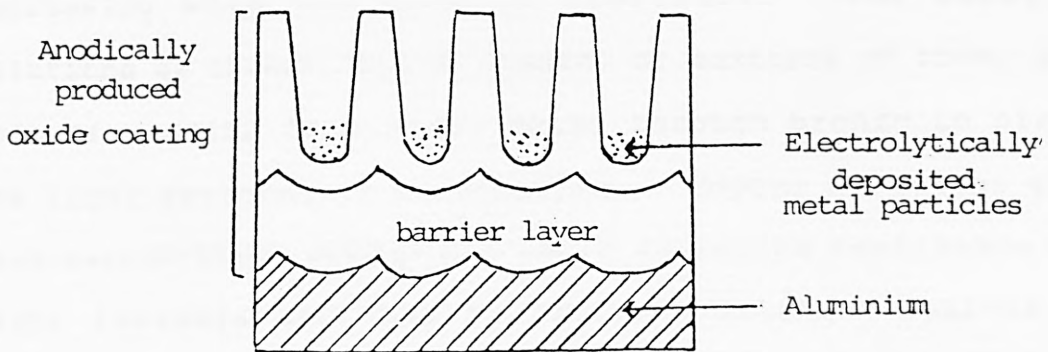


Figure (77) Colour produced by deposition of metallic particles at the base of pores in the oxide

### 6.3 Electrolytic colouring<sup>3,4,5,6</sup>

The principle of electrolytic colouring was described in 1936 by Carboni and others. None of these early observations were commercially exploited until 1960, when Tahei Asada of Japan thoroughly investigated the process and considerably extended the range of metals which could be used for colouring.

In general terms the process consists of submitting the freshly anodised work to electrolysis in a heavy metal salt solution using AC, DC or special wave forms. The anodic coating acts as the cathode whilst the anode is usually made of stainless steel. At the cathode, metal is deposited in a finely-divided form at the bottom of the pores of the coating Figure (77). Depending on the metal in the electrolyte a variety of colour can be developed, their depth increasing with the time of treatment. For example, solutions of nickel, tin or cobalt, or mixtures of them, give colours ranging from light beige through bronze to black. The light fastness is outstanding. Copper solutions give pink-maroon-black colour but their corrosion resistance and light fastness are less reliable. Dilute solutions of silver salts give gold and bronze colours.

Electrolytes based on tin salts are an excellent

means of producing coloured architectural finishes on anodised aluminium; these finishes are lightfast and corrosion resistant. This process is used in Europe and the United States of America.

Tin electrolytes are based on stannous sulphate. The addition of sulphophthalic acid, phenosulphonic acid or cresol sulphonic acid greatly improves the stability of stannous salts which have a tendency to oxidise to insoluble stannic salts.

In this work benzenesulphonic acid and  $\rho$ -toluene sulphonic acid were used and experiments were carried out to measure the stability of stannous sulphate.

#### 6.4 Analytical techniques

Stability of tin (II) sulphate dispersion in  $\rho$ -toluene sulphonic acid studied by chemical analysis, thermal analysis, and Mössbauer spectroscopy. The results obtained compared with those for tin (II)  $\rho$ -toluene sulphonate.

##### 6.4.1 Elemental Analysis

Carbon, hydrogen and sulphur analysis were carried out on a Carlo Erba Model 1106 Elemental Analyser.

#### 6.4.2 Tin analysis (Donaldson and Moser's method)<sup>7</sup>

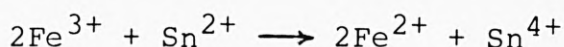
Tin compound (3g) was dissolved in dilute sulphuric acid and was then made up to 250 mls.

To 25 ml of aliquot, 0.2M ferric chloride (25 mls) was added. In order to decolorise the ferric chloride solution, orthophosphoric acid was added to the solution before being titrated against 0.1M ceric sulphate solution in the presence of phenanthroline iron sulphate complex-red as indicator. The end point was indicated by a blue-green colour change.

This method is not only accurate but also efficient.

This method involved the oxidation of tin (II) with excess ferric chloride acting as an oxidant. From titration with ceric sulphate, the amount of ferrous chloride which was reduced could be determined. The titration was not performed in an oxygen-free atmosphere, therefore, oxidation in ferric chloride overcomes the error caused by atmospheric oxidation.

Ferric chloride is reduced to ferrous in the oxidation of tin (II) to tin (IV):



The ferrous ion is oxidised back to ferric ion using ceric sulphate.



overall reaction: 1 mole of  $\text{Sn}^{2+}$  gives 2 moles of  $\text{Fe}^{2+}$  which requires 2 moles of  $\text{Ce}^{4+}$  for oxidation.

Therefore, 1 litre of 1M ceric sulphate =  $\frac{118.69}{2}$  g of tin.

#### 6.4.3 Thermal analysis<sup>8</sup>

Thermal analysis (TG, DTG and DTA) were used in this study to compare the decomposition behaviour of aged tin (II) sulphonate and tin (II) sulphate dispersion in sulphonic acid. This study was carried out using a Standon Redcroft STA 780 simultaneous thermal analyser.

DTA is a technique which involves the heating and cooling of a test material and an inert reference sample under identical conditions and recording any temperature differences that arise between them. The differential temperature is then plotted against either the temperature at some fixed point within the apparatus or time.

Any physical or chemical change which occurs within

the test sample which involves the evolution of heat will cause its temperature to rise temporarily above that of the reference sample, giving rise to an exothermic peak on the DTA plot. Conversely a process which is accompanied by the absorption of heat will cause the temperature of the sample to lag behind that of the reference material leading to an endothermic peak. Figure (78) shows an idealised DTA curve and Table (46) shows various processes which are characteristic as being either endothermic or exothermic. Transitions in which no heat is evolved or absorbed by the sample e.g. certain solid-state phase changes, can also be studied by DTA. Since, even if no physical or chemical processes are occurring, a small and steady differential temperature normally develops between test and reference material. This is due primarily to differences in the heat capacity and thermal conductivity of the two materials.

The difference in the heat capacity of the sample before and after the transition has occurred will be reflected in a new steady differential temperature being established between the test and reference sample. Figure (79) shows a simplified diagram of the DTA apparatus.

- 1) Sample holder-measuring system. Samples are contained in crucibles which make contact with thermocouple junctions.

Figure (78) Idealised DTA trace showing exothermic (A) and endothermic (B) processes

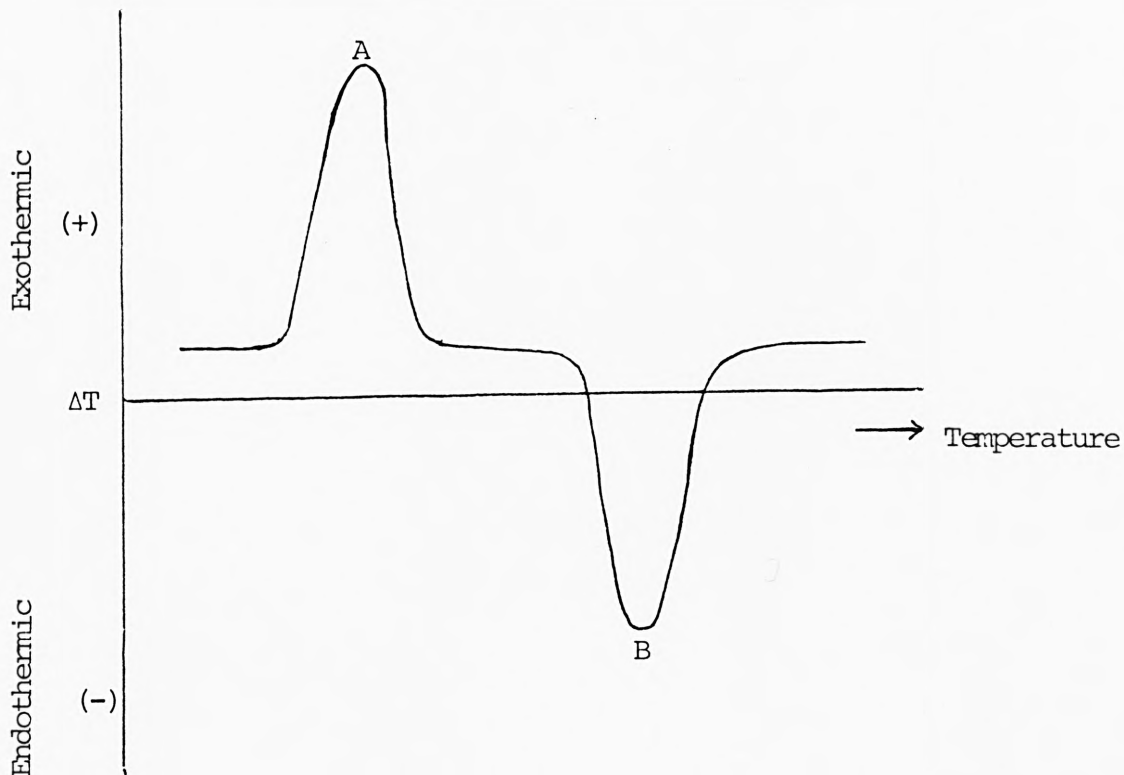
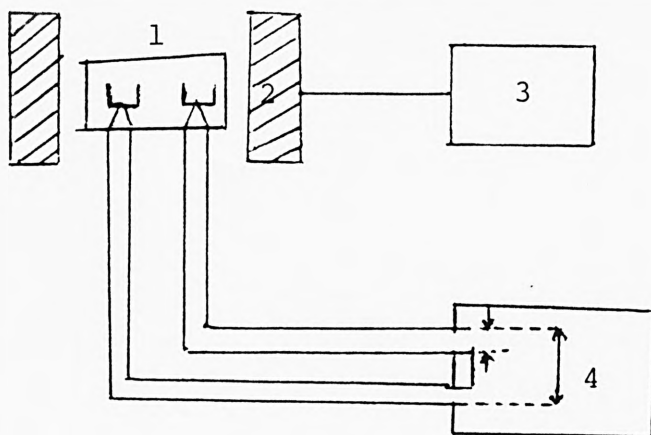


Figure (79) Simplified block diagram of DTA apparatus



- 2) Furnace-heat source having a large temperature zone.
- 3) Temperature programmer-supplies energy to the furnace in such a manner so as to ensure a reproducible rate of change of temperature.
- 4) Recording systems. For STA 780 this is a 4-pen chart recorder which records temperature, DTA, thermogravimetry (TG-weight of sample versus temperature) and differential thermogravimetry (DTG)

**Table (46)** Endothermic and Exothermic Processes

Process	Type of Reaction
Melting point	Endothermic
Boiling point	Endothermic
Decomposition	Endothermic or Exothermic
Solid-state phase transition	Endothermic or Exothermic

#### 6.4.4 Mössbauer spectroscopy<sup>9</sup>

The Mössbauer effect has proved to be one of the most powerful tools for investigating the behaviour of tin electrons in bonding and for observing the symmetry of their environment.

The Mössbauer effect is defined as the recoilless emission and resonant reabsorption of nuclear gamma radiation between the ground and usually the first excited state of the nucleus. The technique was discovered in 1958 by Rudolf Mössbauer.

#### Theory

The emission of  $\gamma$ -radiation results from the decay of an excited spin state of a nucleus to the ground state. In vapour phase the emitting nucleus recoils in the opposite direction (which means no energy is being given out) in the same way with the absorber. In this case no  $\gamma$ -radiation is absorbed. In a solid state the recoil of the emitting nucleus is taken up by the whole crystalline lattice and the  $\gamma$ -ray quantum may be resonantly reabsorbed by another identical nucleus.

If the difference in energy between the ground state

and excited state of the absorber nucleus is the same as that of the emitter, the  $\gamma$ -ray will be absorbed, if not, it will pass through and be detected.

Since the changes in the energy gap brought about by changes in the electronic environment of the nucleus are small ( $5 \times 10^{-8}$  eV for  $^{119}\text{Sn}$ ), the frequency of the emitted  $\gamma$ -rays may be modulated by supplying a small relative motion between the source and the absorber - the Doppler Velocity. Therefore when the modulated  $\gamma$ -ray has the exact energy to match the energy gap of the nuclei in the absorber, the  $\gamma$ -ray is absorbed as shown in Figure (80).

The effect of this Doppler motion, is to vary the  $\gamma$ -ray energy relative to the absorber, and to produce a  $\gamma$ -ray energy shift  $\Delta E$ , which is given by the expression below:

$$\Delta E = \frac{V}{C} E_{\gamma}$$

where  $C$  = velocity of light

when both the emitting and absorbing nuclei are in the same chemical environment, the energy of the emitted  $\gamma$ -ray is the same as the energy separation between the ground state and the first excited state of the absorbing nuclei.

Maximum resonance reabsorption occurs at  $V = 0$ , but

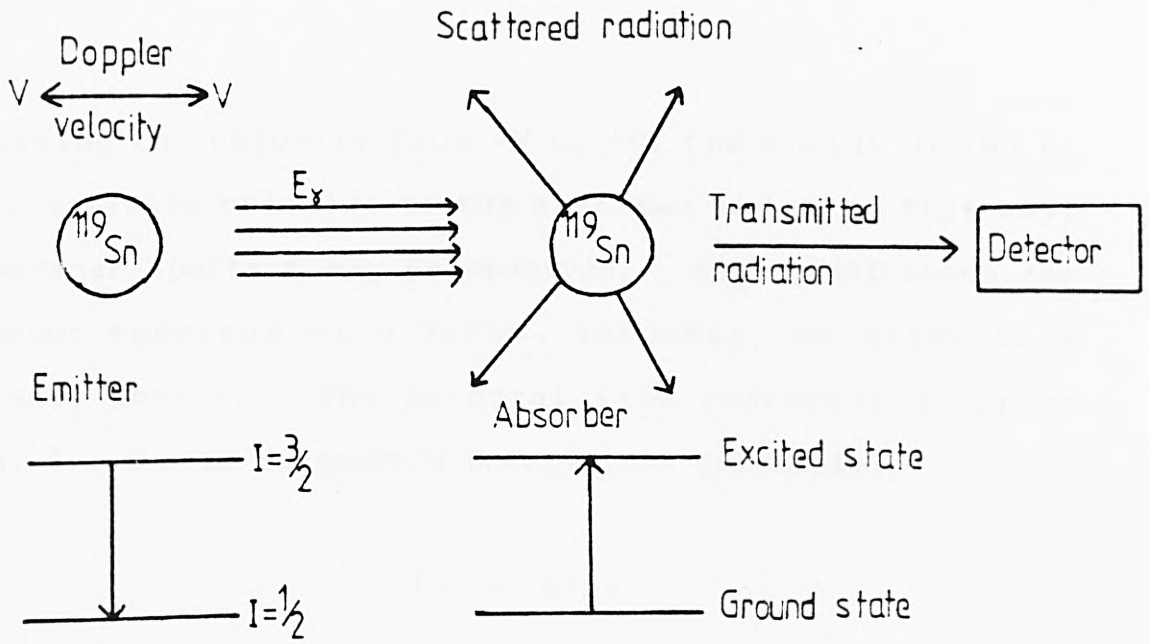


Figure (80)

Fundamental features of the Mössbauer effect

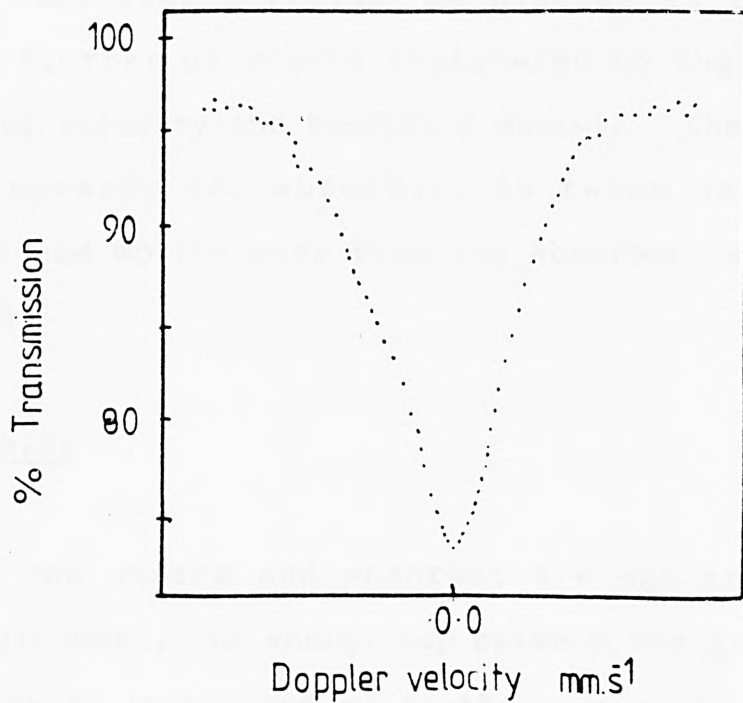


Figure (81)

Mössbauer spectrum of  $\text{BaSnO}_3$  using a  $\text{Ba}^{119}\text{SnO}_3$  source

by varying the velocity from  $-V$  to  $+V$ , the energy of the  $\gamma$ -rays are varied relative to the absorber and so in this way, a Mössbauer spectrum may be observed. Figure (81) shows the Mössbauer spectrum of a  $\text{BaSnO}_3$  absorber, relative to a  $\text{Ba}^{119}\text{SnO}_3$  source. The spectral line possesses a finite width,  $\Gamma$ , due to Heisenberg Uncertainty principle:

$$\Gamma\zeta = h/2\pi$$

where ( $\zeta$ ) is the mean lifetime of the excited state and ( $h$ ) is Planck's constant.

The Mössbauer spectrum is plotted as percentage transmission (number of counts registered by the detector) versus Doppler velocity and therefore energy. The motion of the source towards the absorber, is taken as positive velocity ( $+V$ ) and motion away from the absorber, as negative velocity ( $-V$ ).

### The Isomer Shift

When the source and absorber are not in the same chemical environment, the energy gap between the ground state and excited state in the nuclei of the source, is different to that in the absorber. Under these circumstances, the energy of the  $\gamma$ -radiation must be modulated by the Doppler

motion applied to the source to bring it into resonance with the absorber [ $E_S = E_A$ ]. Thus, it can be seen that this leads to a shift from zero in the Mössbauer line which provides information about the S-electron density of the nucleus. This shift in the resonance maximum is called the chemical or isomer shift ( $\delta$ ). Figure (82) shows the alteration in energy levels of the source and the absorber, which leads to an isomer shift.

The chemical shift is expressed by the following equation:

$$\delta = K \cdot \frac{\Delta R}{R} \cdot \left\{ \left| \psi_0 \right|_A^2 - \left| \psi_0 \right|_S^2 \right\}$$

where  $K$  = constant

$R$  = radius of the nucleus in the ground state

$\Delta R$  = change in the radius of the nucleus on going from the ground state to the excited state

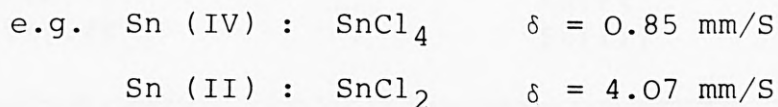
$\left| \psi_0 \right|^2$  = wave function defining the S-electron density at the nucleus

$\Delta R/R$  arises because of nucleus factors and the term associated with the S-electron density at the nucleus is due to electronic factors.

When  $\gamma$ -radiation is emitted, the radius of the nucleus changes, it can increase or decrease, depending upon the energy of the  $\gamma$ -radiation involved.  $\Delta R/R$  may be positive or negative, its sign varying with the Mössbauer isotope used.

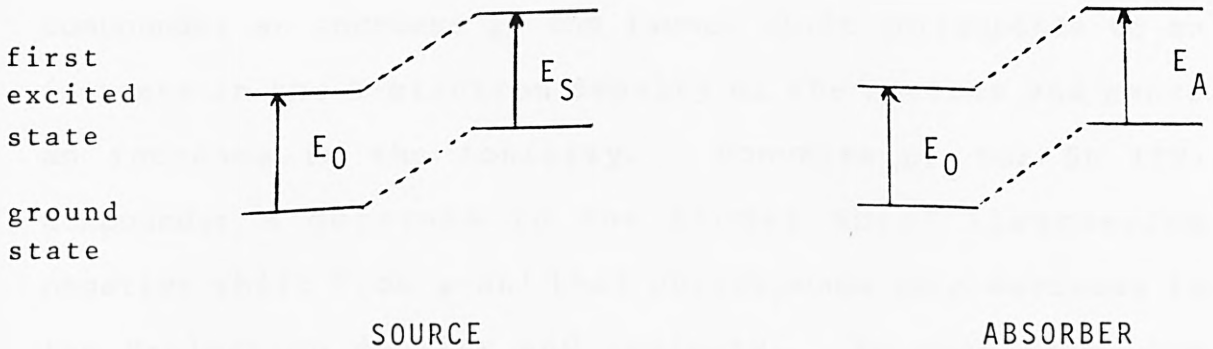
When  $\Delta R/R$  is positive, an increase in the S-electron density at the nucleus corresponds to an increase in the isomer shift and when  $\Delta R/R$  is negative, an increase in S-electron density results in a decrease in the isomer shift.

For  $^{119}\text{Sn}$ ,  $\Delta R/R$  is positive, therefore an increase in the S-electron density at the nucleus gives rise to an increase in the isomer shift. Since  $\text{Sn}^{4+}$  compounds typically have the electronic configuration  $4d^{10}5s^0$  and  $\text{Sn}^{2+}$  compounds the configuration  $4d^{10}5s^2$ , a change in valency from +4 to +2 is associated with an increase in the S-electron density and consequently an increase in the isomer shift values occurs:



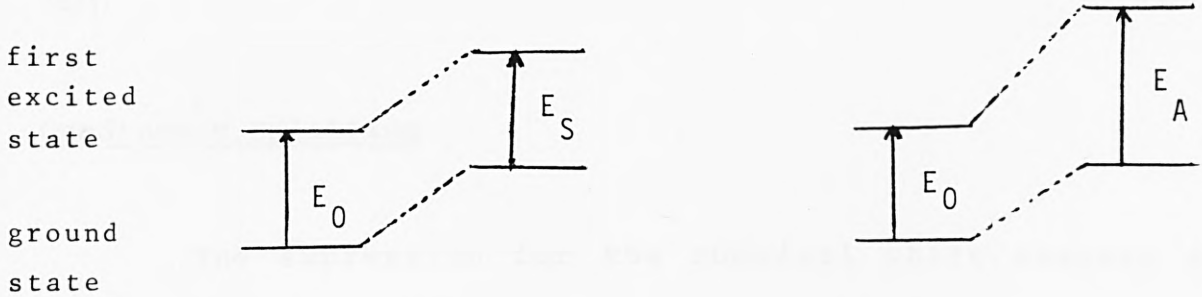
Mössbauer spectroscopy can also give an indication of the bonding to the tin nucleus, (i.e. it is ionic or covalent). Taking  $\alpha$ -Sn as the reference point, for Sn (II)

Figure (82) Energy Level Diagram Showing the Occurrence of the Isomer Shift



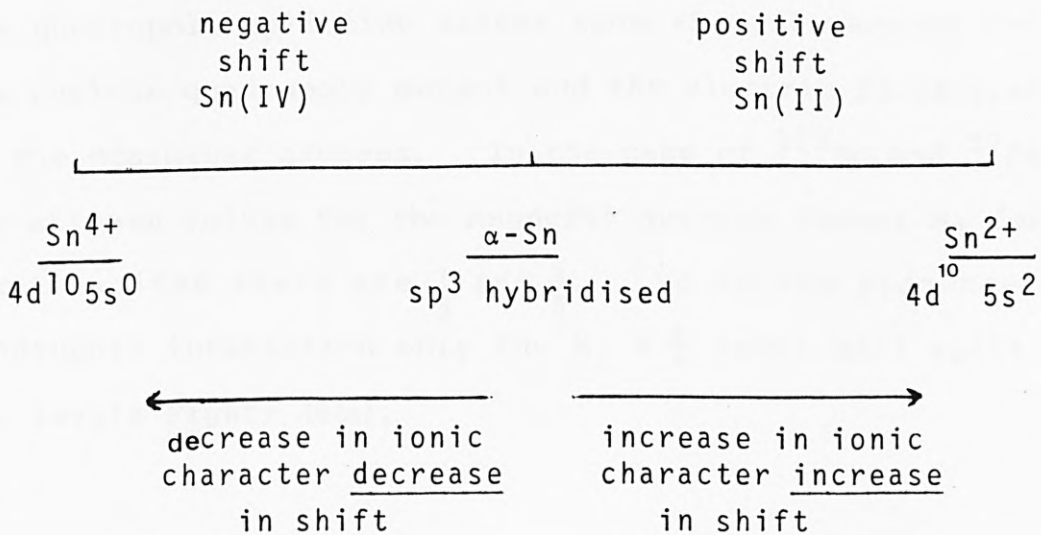
$$E_S = E_A$$

$$\delta = 0$$



$$\delta = E_A - E_S$$

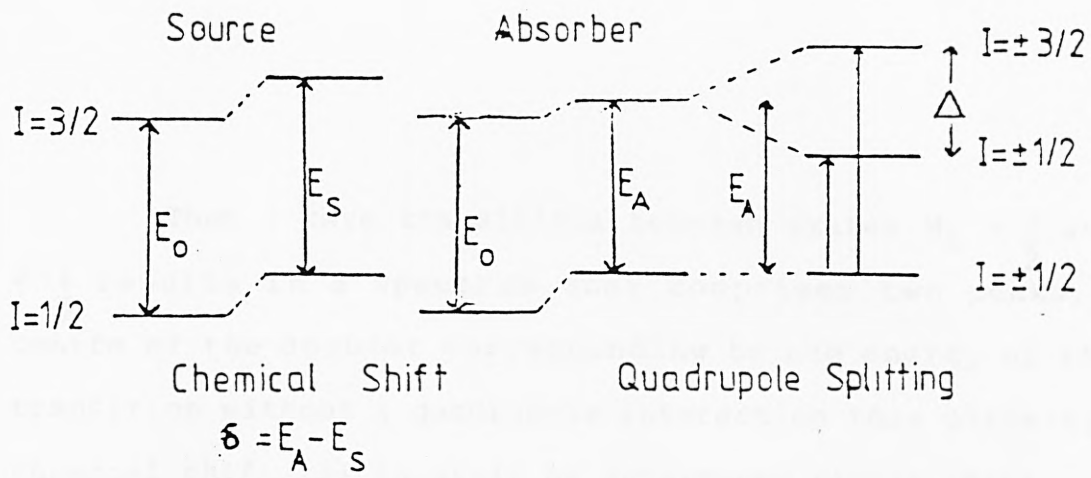
Figure (83) Schematic Representation of the Effect of the s-electron Density on the Mössbauer Isomer Shift for  $^{119}\text{Sn}$  Nuclei



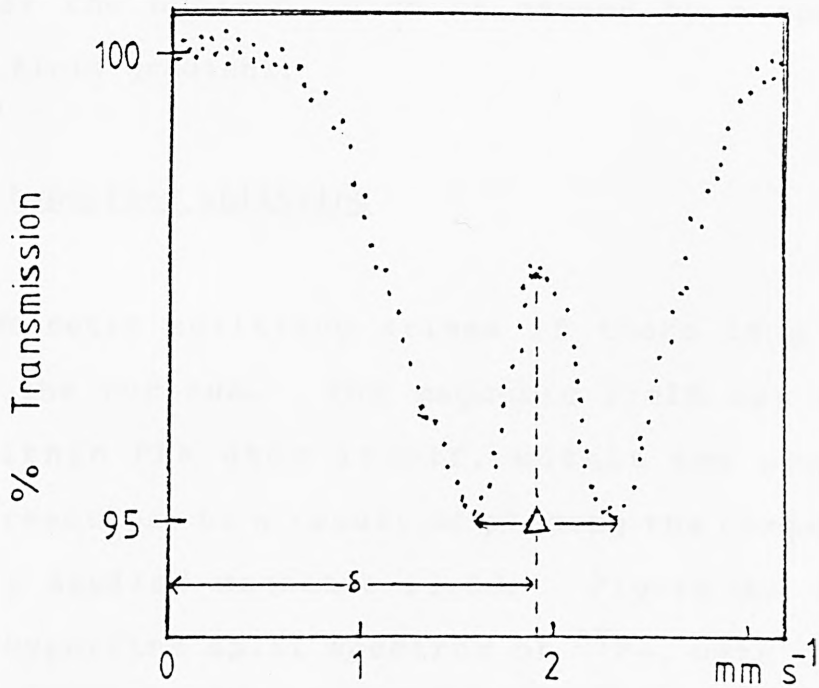
compounds, an increase in the isomer shift corresponds to an increase in the S-electron density of the nucleus and hence an increase in the ionicity. Conversely, for Sn (IV) compounds; a decrease in the isomer shift (increasing negative shift from  $\alpha$ -Sn) that corresponds to a decrease in the S-electron density and ionicity. In each case, the actual value for the isomer shift will give an indication of the ionicity or covalency in the bond to the tin. Figure (83).

#### Quadrupole splitting

The expression for the chemical shift assumes a spherical nucleus with a uniform charge distribution, but any nucleus with a spin quantum number of greater than  $I = \frac{1}{2}$  has a non-spherical charge distribution and hence a nuclear quadrupole moment. The various allowed orientation of the nuclear quadrupole moment in an electrical field gradient leads to differences in the energy with orientation. Thus the quadrupole splitting arises from the interaction between the nuclear quadrupole moment and the electric field gradient at the Mössbauer nucleus. In the case of  $^{119}\text{Sn}$  and  $^{57}\text{Fe}$  the two allowed values for the magnetic quantum number  $M_I$  for the first excited state are  $\frac{1}{2}$  and  $\frac{3}{2}$ . So in the presence of a quadrupole interaction only the  $M_I = \frac{3}{2}$  level will split into two levels Figure (84a).



(a)



(b)

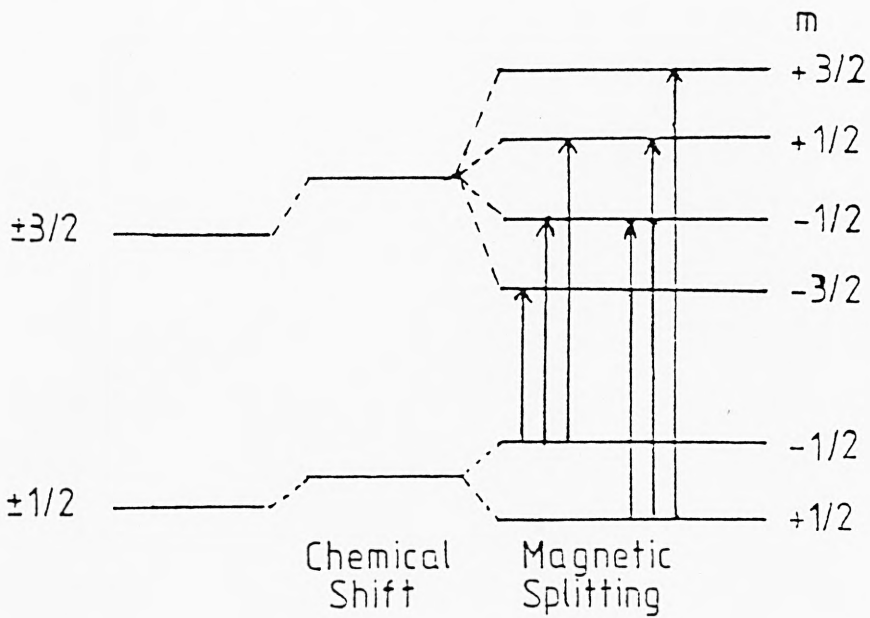
Figure (84) a, Origin of the chemical shift and quadrupole splitting; b, Mössbauer spectrum of  $\alpha\text{-SnF}_2$  using a  $\text{BaSnO}_3$  source showing chemical shift and quadrupole splitting.

Thus  $\gamma$ -rays transitions between states  $M_I = \frac{3}{2}$  and  $M_I = \frac{1}{2}$  results in a spectrum that comprises two peaks, the centre of the doublet corresponding to the energy of the  $\gamma$ -transition without a quadrupole interaction thus allowing the chemical shift ( $\delta$ ) to still be determined Figure (84b).

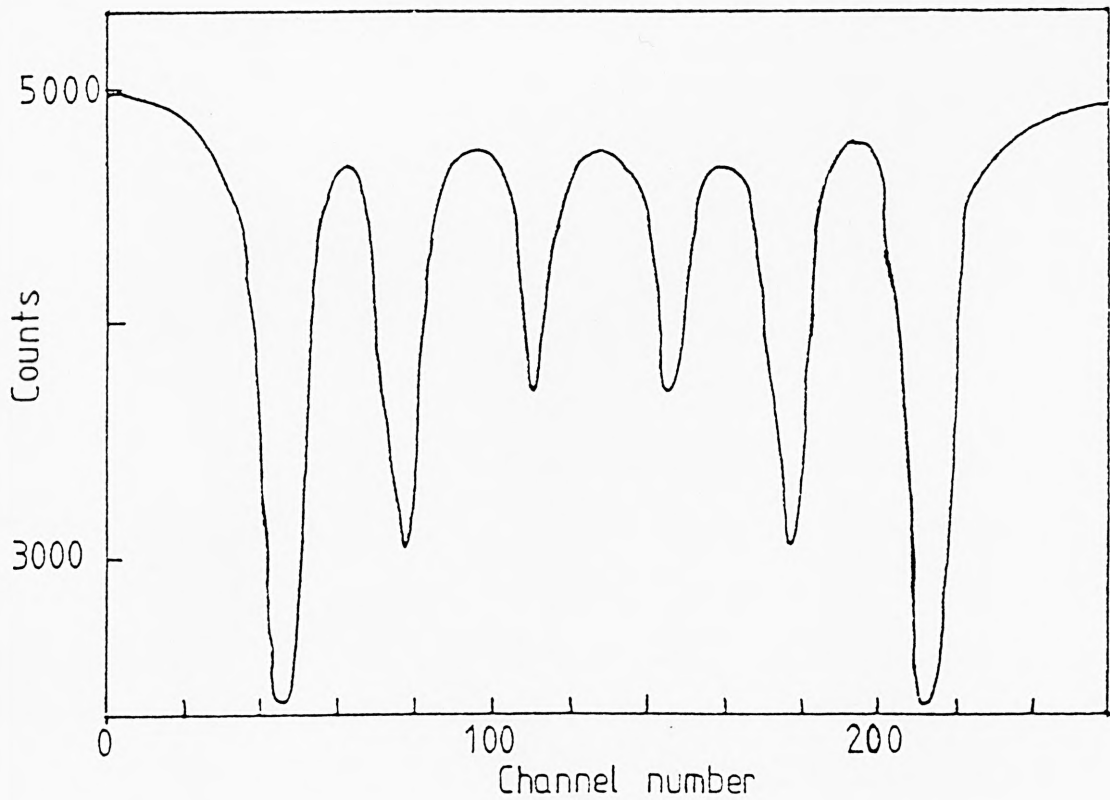
The extent of the quadrupole splitting ( $\Delta$ ) is therefore a measure of the symmetry of the p-or-d-electron density at the nucleus which is caused by a non-uniform electric field gradient.

#### Magnetic hyperfine splitting

Magnetic splitting arises if there is a magnetic field at the nucleus. The magnetic field may originate either within the atom itself, within the crystal via exchange reaction, or a result of placing the compound in an externally applied magnetic field. Figure (85) shows the magnetic hyperfine split spectrum of  $^{57}\text{Fe}$ , with the energy level diagram showing how these splittings arise.



(a)



(b)

Figure (85) a, Origin of magnetic hyperfine splitting; b, Mössbauer spectrum of natural iron.

## 6.5 Experimental

### 6.5.1 Preparation of tin (II) sulphate<sup>10</sup>

Copper (II) sulphate (37g) and [300 ml water + 15 ml sulphuric acid] was refluxed with (37g) of granulated tin. The solution was boiled under oxygen-free nitrogen. The copper in the solution was replaced by tin and the solution eventually became colourless and the deposit of copper turned grey, due to the re-deposition of tin on its surface. At this point the solution was filtered rapidly under oxygen-free nitrogen, concentrated to about 50 ml on a rotary evaporator and allowed to cool. The mother liquor was filtered off, and the crystalline product of tin (II) sulphate (25g) washed with alcohol and ether and oven dried at 100°C.

### 6.5.2 Preparation of tin (II) sulphate dispersion in benzene sulphonic acid and $\rho$ -toluene sulphonic acid

A mixture of the appropriate weight ratio of stannous sulphate and benzenesulphonic acid or  $\rho$ -toluene sulphonic acid was ball-milled for five minutes to achieve a homogeneous mix. Two dispersions were prepared viz: 30:70 wt% acid :  $\text{SnSO}_4$  and 35:65 wt% acid: $\text{SnSO}_4$  respectively. Tin analysis was carried out and the remainder of the sample was then kept in a closed bottle at room conditions until tested.

6.5.3 Preparation of tin (II) methane sulphate and tin (II) p-toluene sulphate

Blue-black stannous oxide (5g) was dissolved by refluxing it for 90 minutes under an oxygen-free nitrogen atmosphere in 25 g methane sulphonic acid or p-toluene sulphonic acid and 50 ml water until all stannous oxide had reacted.

The resulting mixture was filtered hot, concentrated to about 30 ml on a rotary evaporator and allowed to cool. The crystalline products obtained were washed with ether and dried in vacuo over potassium hydroxide pellets.

## 6.6 Results and discussion

This Section deals with the results obtained from analytical analysis, X-ray diffraction, thermal analysis and Mössbauer spectroscopy for fresh and aged tin (II) methane sulphonate and tin (II)  $\rho$ -toluene sulphonate. The results obtained for aged tin (II)  $\rho$ -toluene sulphonate are compared with those for aged tin (II) sulphate dispersion in  $\rho$ -toluene sulphonic acid.

### 6.6.1 Element analysis

The analytical data for tin (II) methane sulphonate and tin (II)  $\rho$ -toluene sulphonate are presented in Table (47). Tin analysis results for  $\text{SnSO}_4$  dispersion in benzene sulphonic acid and  $\rho$ -toluene sulphonic acid are given in Table (48).

Table (48) shows that the percentage of tin (II) in the aged  $\text{SnSO}_4$  dispersion in benzene sulphonic acid and  $\rho$ -toluene sulphonic acid prepared in this work remained similar to that calculated during the analysis period. There was no evidence for a substantial amount of oxidation of tin in the samples.

Table (47) Analytical data for tin (II) methane sulphonate  
and tin (II) *p*-toluene sulphonate

	% C	% H	% S	% Sn
$(\text{CH}_3\text{SO}_3)_2\text{Sn}\cdot\text{H}_2\text{O}$				
observed	7.60	2.58	20.57	37.90
calculated	7.30	2.40	19.60	36.30
$(\text{CH}_3\text{C}_6\text{H}_4\text{SO}_3)_2\text{Sn}\cdot\text{H}_2\text{O}$				
observed	35.42	3.37	13.50	24.90
calculated	35.10	3.34	13.40	24.80

### 6.6.2 X-ray Diffraction

X-ray powder diffractograms were recorded for tin (II) *p*-toluene sulphonate and tin (II) methane sulphonate, the data obtained are listed in Table (49).

Table (48) Tin analysis for SnSO<sub>4</sub> dispersion in benzene  
sulphonic acid and *p*-toluene sulphonic acid

	Sn%							
	7.3.84	9.3.84	16.3.84	30.3.84	9.4.84	2.5.84	22.5.84	Jly 86
30C <sub>6</sub> H <sub>5</sub> SO <sub>3</sub> H: 70SnSO <sub>4</sub> (Sn = 38.7%)	38.5	38.6	38.5	38.5	38.5	38.5	38.4	-
35C <sub>6</sub> H <sub>5</sub> SO <sub>3</sub> H: 65SnSO <sub>4</sub> (Sn = 35.9%)	35.6	35.5	35.5	35.5	35.4	35.4	35.5	33.8
30CH <sub>3</sub> C <sub>6</sub> H <sub>4</sub> SO <sub>3</sub> H.H <sub>2</sub> O: 70SnSO <sub>4</sub> (Sn = 38.7%)	-	-	-	-	38.7	38.6	38.8	38.6
35CH <sub>3</sub> C <sub>6</sub> H <sub>4</sub> SO <sub>3</sub> H.H <sub>2</sub> O: 65SnSO <sub>4</sub> (Sn = 35.9%)	-	-	-	-	35.9	35.7	36.0	33.4

Table (49) X-ray powder diffraction data for tin (II)  
p-toluene sulphonate and tin (II) methane  
sulphonate

$(\text{CH}_3\text{C}_6\text{H}_4\text{SO}_3)_2\text{Sn}\cdot\text{H}_2\text{O}$		$(\text{CH}_3\text{SO}_3)_2\text{Sn}\cdot\text{H}_2\text{O}$	
d spacing ( $\text{A}^\circ$ )	R.I	d spacing ( $\text{A}^\circ$ )	R.I
10.16	23.1	14.49	3.1
8.93	42.3	13.60	7.8
7.76	7.7	11.48	12.5
7.62	7.7	10.28	9.4
6.46	100	9.12	4.7
5.44	15.4	7.63	29.7
5.07	30.8	6.61	7.8
4.46	26.9	5.72	4.7
4.13	57.7	4.82	100
3.75	38.5	4.48	10.9
3.68	15.4	3.83	9.4
3.49	11.5	3.79	6.3
3.45	19.2	3.65	4.7
3.38	11.5	3.53	7.8
3.34	11.5	3.51	3.1
3.27	19.2	3.36	7.8
3.11	19.2	3.28	6.3
2.97	15.4	3.15	28.1
2.62	61.5	2.86	35.9
2.32	30.8	2.48	14.1
2.26	23.1	2.41	20.3
2.19	15.4	2.22	59.4
2.14	30.8	2.08	40.6
2.13	11.5	1.91	12.5
2.03	23.1	1.86	32.8
		1.64	28.1
		1.61	17.2
		1.59	37.5
		1.58	10.9
		1.51	50

### 6.6.3 Mössbauer Data

As part of the study of the stability of the compounds prepared in this work, the Mössbauer spectra of both freshly-prepared and aged samples of the tin (II) derivatives of methane sulphonic acid and *p*-toluene sulphonic acid were recorded. Their data are given in Table (50).  
<sup>11</sup> It was proved that there is a close connection between the Mössbauer chemical shift and the Sn-O bond distances. It was found that the chemical shift increases with increasing the average bond length.

<u>Compound</u> <sup>12</sup>	<u>Average b.I.</u> <sup>0</sup> <u>Å</u>	<u>δ mm/s</u>
CaSn(CH <sub>3</sub> CO <sub>2</sub> ) <sub>3</sub>	2.14	2.90
KSn(CH <sub>2</sub> ClCO <sub>2</sub> ) <sub>3</sub>	2.16	2.96
KSn(HCO <sub>2</sub> ) <sub>3</sub>	2.16	3.08
SnHPO <sub>3</sub>	2.17	3.15
SnSO <sub>4</sub>	2.26	3.95

Chemical isomer shifts for tin (II) methane sulphonate (3.65 mm s<sup>-1</sup>) and for tin (II) *p*-toluene sulphonate (3.64 mm s<sup>-1</sup>) are lower than that for tin (II) sulphate (3.95 mm s<sup>-1</sup>) which suggests that the Sn-O bond distances of tin (II) methane sulphonate and tin

(II) *p*-toluene sulphate would be shorter than those found in  $\text{SnSO}_4$ .

All fresh samples exhibit 2-line tin (II) spectra with no evidence for tin (IV). The aged samples, aged over a period of 12 months show no evidence for oxidation in either tin (II) sulphate dispersion in *p*-toluene sulphonic acid or tin (II) *p*-toluene sulphate, indicating that the Sn (II)-O interactions in these samples are stable to oxidation.

In aged tin (II) methane sulphate there is evidence for oxidation but the Sn (IV) peak is much less intense than the tin (II) peak ( $\delta = -0.09$  mm/s,  $\delta = 3.60$  mm/s) which is confirmed by the area ratio of Sn (IV) to Sn (II) = 0.34. The amount of tin (IV) in aged tin (II) methane sulphate is however small as can be seen from a comparison of its spectra with that of aged tin (II) methane sulphate doped with 5%  $\text{SnO}_2$ . The much higher Mössbauer fraction for the tin (IV) moiety is shown by the fact that the area ratio of tin (IV):tin (II) (0.34:1) is smaller than that in the doped sample (0.83:1). However, the area ratio will not represent the mole ratios of tin (IV) and tin (II) species because the Mössbauer fraction of tin (IV) oxide phases is much higher than that of tin (II) oxide phases.

It is interesting to note that on dispersion of  $\text{SnSO}_4$  into *p*-toluene sulphonic acid, the  $\text{SnSO}_4$  remains unchanged

Table (50) Mössbauer parameters of freshly-prepared and aged samples of the tin(II) derivatives of methane sulphonic acid and  $\rho$ -toluene sulphonic acid

<u>Compounds</u>	<u><math>\delta</math> mm s<sup>-1</sup></u>	<u><math>\Delta</math> mm s<sup>-1</sup></u>
fresh (CH <sub>3</sub> SO <sub>3</sub> ) <sub>2</sub> Sn.H <sub>2</sub> O	3.65	1.36
aged "	(-0.09 : 3.60)	1.46
fresh (CH <sub>3</sub> C <sub>6</sub> H <sub>4</sub> SO <sub>3</sub> ) <sub>2</sub> .H <sub>2</sub> O	3.64	1.39
aged "	3.61	1.40
aged 30 CH <sub>3</sub> C <sub>6</sub> H <sub>4</sub> SO <sub>3</sub> H.H <sub>2</sub> O:70 SnSO <sub>4</sub>	3.94	1.02
aged 35 CH <sub>3</sub> C <sub>6</sub> H <sub>4</sub> SO <sub>3</sub> H.H <sub>2</sub> O:65 SnSO <sub>4</sub>	3.91	1.06
SnSO <sub>4</sub>	3.95	1.00

because the Mössbauer parameters of the dispersed material and  $\text{SnSO}_4$  are the same with no evidence for a decrease in shift or increase in splitting that would suggest the formation of Sn-sulphonic acid bonds.

Table (50) shows the Mössbauer parameters of freshly-prepared and aged samples of the tin (II) derivatives of methane sulphonic acid and *p*-toluene sulphonic acid.

#### 6.6.4 Thermal Analysis

The simultaneous differential thermal analysis (DTA) and thermogravimetric analysis (TG) of the compounds prepared were carried out on a Stanton Redcroft STA-780 Thermal Analyser.

The DTA/TG traces of tin (II) methane sulphonate freshly prepared show that the compound undergoes a two stage decomposition: the first stage at  $66^\circ\text{C}$ , resulted in the loss of about 5% wt which corresponds to the loss of water molecule by an endothermic reaction; the second stage occurred at  $362^\circ\text{C}$  with a loss of 41% wt which corresponds to the loss of sulphur as  $\text{SO}_2$  by an exothermic process, to leave a grey black residue of 54% wt of  $\text{SnO}_2$ . An endothermic process also occurred at about  $248^\circ\text{C}$  and is associated with melting of the sample.

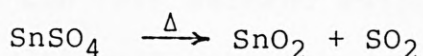
The decomposition of the aged tin (II) methane sulphonate differs from that of the freshly prepared material. The aged tin (II) methane sulphonate also undergoes a two stage decomposition: the first stage is again endothermic, resulting in a loss of about 5% wt at 40°C which corresponds to the loss of water molecule. This decomposition is followed by loss of a further 7% of the weight before the melting point at 235°C. The second stage occurred at 350°C with a loss of 38% wt which corresponds to the loss of sulphur as SO<sub>2</sub> by an exothermic process, to leave a grey black residue of 50% wt of SnO<sub>2</sub>.

In both cases, the second decomposition occurred in two stages.

The DTA/TG traces of tin (II) *p*-toluene sulphonate freshly prepared show that the compound undergoes a two stage decomposition: the first stage began at 73°C, resulted in the loss of 5% wt which corresponds to the loss of water molecule by an endothermic reaction. This decomposition occurred in two stages and was followed by a loss of a further 3% of the weight before the melting point at 300°C. The second stage occurred at about 382°C with a loss of 37% wt which corresponds to the loss of sulphur as SO<sub>2</sub> by an exothermic process, to leave a grey black residue of 55% of SnO<sub>2</sub>. This decomposition also occurred in two stages.

The decomposition of the aged tin (II) *p*-toluene sulphonate does differ from that of the freshly prepared material. The aged tin (II) *p*-toluene sulphonate also undergoes a two stage decomposition: the first stage at 94°C, resulted in the loss of 3% wt which corresponds to the loss of water molecule by an endothermic reaction followed by the melting point at 300°C. The second stage began at 346°C with a loss of 34% wt which corresponds to the loss of sulphur as SO<sub>2</sub> by an exothermic process, to leave a grey black residue of 63%. This decomposition occurred in two stages.

SnSO<sub>4</sub> decomposes at 379°C by the reaction:-<sup>13</sup>



DTA/TG traces of SnSO<sub>4</sub> dispersion in *p*-toluene sulphonic acid show that the decomposition of the SnSO<sub>4</sub> appears to be similar.

SnSO<sub>4</sub> dispersion in *p*-toluene sulphonic acid undergoes three stages of decomposition: the first stage at about 78°C, resulted in the loss of 3% wt which corresponds to the loss of water molecule by an endothermic reaction, followed by loss of a further 19% wt at 192°C (second stage) by an endothermic process. The third stage corresponds to the decomposition of SnSO<sub>4</sub>, resulted in the loss of about 32% wt which corresponds to the loss of sulphur as SO<sub>2</sub>, by an exothermic process, to leave a grey residue of SnO<sub>2</sub> (45% wt).

## 6.7 Conclusion

The aged samples of tin (II) methane sulphonate and tin (II)  $\rho$ -toluene sulphonate prepared in this work were compared with the aged tin (II) sulphate dispersion in methane sulphonic acid and  $\rho$ -toluene sulphonic acid.

This investigation has shown that:-

- (1) Tin (II) sulphate dispersion in methane sulphonic acid and  $\rho$ -toluene sulphonic acid has longer shelf life than tin (II) methane sulphonate and tin (II)  $\rho$ -toluene sulphonate (the samples aged over 12 months).
- (2) Mössbauer spectra of tin (II) sulphate dispersion in  $\rho$ -toluene sulphonic acid show that no reaction occurs between tin (II) sulphate and  $\rho$ -toluene sulphonic acid since no increase in shift or decrease in splitting compared with Mössbauer parameters of tin (II) sulphate.
- (3) Tin (II) sulphate dispersion in methane sulphonic acid and  $\rho$ -toluene sulphonic acid is simpler to manufacture than tin (II) methane sulphonate or tin (II)  $\rho$ -toluene sulphonate.

## 6.8 References

1. V.F. Henley, "Anodic oxidation of aluminium and its alloys", (1982), U.K.
2. "Anodic oxidation of aluminium and its alloys", The Aluminium Development Association, London, (1961).
3. Tin and its uses, (1982), No. 133, page (4-7).
4. Tahei Asada, Bri. Patent 1,022,927/(1966).
5. Tahei Asada, U.S. Patent 3,382,160/(1968).
6. O.C. Gedde, Bri. Patent 1,311,716/(1973).
7. J.D. Donaldson, W. Möser and W.B. Simpson, Analyst, (1961), (86), 619-21.
8. M.I. Pope and M.D. Judd, "Differential Thermal Analysis", (1977), U.K.
9. T.C. Gibb, "Principles of Mössbauer Spectroscopy", (1977).
10. D.G. Nicholson, Ph.D. thesis, University of London, (1969).
11. S.M. Grimes, Ph.D. thesis (1982), The City University, London.
12. J.D. Donaldson and A. Jelen, J.Chem.Soc., (A), (1968), 1448.
13. J.D. Donaldson, Ph.D. thesis, Aberdeen, (1959).